CHARLES UNIVERSITY

Second Faculty of Medicine

Doctoral study program: Doctoral Studies in Biomedicine

Rimjhim Tomar

Statistical models of information processing in neuronal systems

Doctoral Thesis

Supervisors of the doctoral thesis: Lubomír Košťál

Study branch: Biomedical informatics

Prague, May 2024

I declare hereby that I made this dissertation thesis by myself and that I mentioned and cited properly all the sources and literature. At the same time, I declare that this thesis was not used to obtain another or the same title.

I agree with the permanent deposition of an electronic version of my thesis in the system database of interuniversity project Thesis.cz for a permanent control of similarities of theses.

In ..... on ..... Name

Signature

TOMAR, Rimjhim. Statistical modelling of information processing in neuronal systems. Prague, 2024. 135 pages, 5 attachments. Dissertation thesis. Charles University, Second Faculty of Medicine and Czech Academy of Sciences, Institute of Physiology, Laboratory of Computational Neuroscience. Supervisor: KOŠŤÁL, Lubomír

Abstract: Understanding the mechanisms by which the brain processes and transmits information is a major goal of computational neuroscience. Neurons transform stimuli into sequences of action potentials, but the efficiency of this "neuronal code" is not fully understood. While spike count or temporal patterns alone may partially explain stimuli encoding, combining both features provides a more comprehensive representation.

In my thesis, I investigated information transmission in neuronal systems from the rate coding perspective by focusing on the instantaneous firing rate, which integrates rate coding and temporal coding features. Using classical statistical models of neural activity, I found that dispersion measures of the inter-spike intervals can differ significantly from the instantaneous rate dispersion measures in a model-dependent manner. Applying our findings to experimental data revealed that this approach offers deeper insights into the information-encoding mechanisms of neurons. Building on this foundation, I investigated the influence of biophysical properties on rate coding. Basic integrate-and-fire models lack firing rate and membrane voltage saturation, which is inconsistent with observed neural activity. Incorporating reversal potentials increased the slope of the "firing rate vs. input" curve, but did not achieve saturation. Extending the model to include two nodes (dendritic and somatic) effectively limited both voltage and firing rate, aligning the model more closely with biological observations.

In order to understand the rate coding principles that govern information transmission in neuronal systems, I studied how the olfactory receptor neurons (ORNs) of the male moth *Agrotis ipsilon* optimize information transmission under challenging sensory conditions. Analyzing responses to pheromones amid varying concentrations of volatile plant compounds (VPCs) showed that these backgrounds can suppress neural responses in pheromone-responsive ORNs but also increase the information transmitted per spike. This study highlights ORNs' optimization mechanisms for navigating complex olfactory landscapes, enabling insects to detect crucial pheromonal cues despite environmental interference.
Extending my research from neuron populations to neural networks, I investigated the effect of spike frequency adaptation (SFA) on neural variability quenching in cortical networks. Using a model with excitatory and inhibitory subpopulations, I demonstrated that SFA mechanisms significantly influence trial-to-trial variability, crucial for efficient information transmission.

Overall, my work provides a comprehensive analysis of information transmission from the perspective of rate coding, progressing from single neuron to complex neural networks. These findings enhance our understanding of the underlying mechanisms of neural coding, offering refined models that better reflect biological realities.

Keywords: Neural coding, variability, randomness, olfaction, rate coding

First and foremost, I would like to thank my thesis supervisor Lubomír Košťál who has patiently guided me as I made my transition from mathematics to the field of computational neuroscience. His unending patience and support meant a lot more whenever I ran into challenges that inevitably come with moving to a different country and culture.

I want to thank my colleagues from the Department of Computational Neuroscience, specifically Tomáš Bárta, as well as the collaborators I have worked with over the years. Special thanks to Philippe Lucas and Charles Smith, who have been very helpful and have always made themselves available with their scientific input. I also want to thank my family and my partner for being a constant source of support and encouragement when I needed it the most, and for making this life worth going through.

My most heartfelt thanks goes to the friends I have made in my years in Prague. Without them, this path would have been much more challenging. I would like to thank Matěj Štěpán (again), Aleksandra Marković, Gurbet Karayel, Tomáš Bárta (again), and Shah Rukh Khan. Finally, I would like to thank the friends and scientists who are too many to name but have been a constant presence in computational neuroscience conferences throughout the years. I have gained a lot through those conference discussions and they deserve a mention.

Contents

1. Introduction

Neurons, the fundamental units of the nervous system, exhibit a specialized structure tailored to transmit information throughout the body. A typical neuron consists of a cell body (soma), dendrites, and an axon. The soma houses the nucleus and metabolic machinery necessary for the neuron's survival and function. Dendrites extend from the soma-like branches, receiving signals from other neurons and conducting them towards the cell body. The axon, a long, slender projection, carries electrical impulses away from the soma to other neurons, muscles, or glands. At the axon terminals, neurotransmitters are released to communicate with target cells across synapses. Action potentials, or spikes, are the fundamental mechanisms through which neurons send signals. These are sudden changes in the electrical charge of the neuron's membrane, initiated by the influx of sodium ions when the membrane potential reaches a certain threshold (Fig. 1A). This creates a rapid depolarization, followed by a repolarization phase, where potassium ions exit the cell, restoring the resting membrane potential. This process propagates along the axon, enabling the neuron to transmit information rapidly and efficiently over long distances. Action potentials are all-or-none events, ensuring clear, consistent signal transmission regardless of the stimulus intensity, once the threshold is surpassed (Fig. 1B).

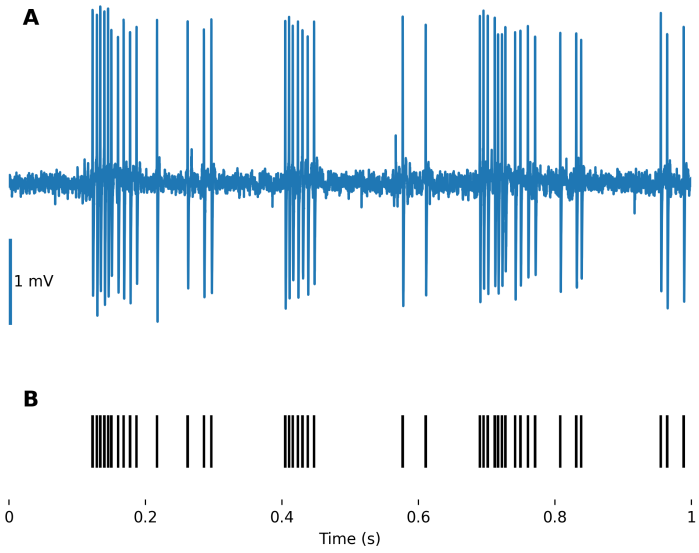

Figure 1: Neuronal action potentials and spike train visualization. A This plot illustrates the extracellular recording of the membrane potential of the olfactory receptor neuron of the noctuid moth *Agrotis ipsilon*. Each peak represents the influx of sodium ions triggering an action potential, followed by the efflux of potassium ions to restore the resting membrane potential. **B** Displayed below the membrane potential plot, the raster plot highlights the occurrence times of action potentials, or spikes, confirming the all-or-none nature of these events. Each vertical line corresponds to a single spiking event, showcasing the spike train. The data used in the figures in this section were obtained courtesy of our colleagues at INRAE, France.

The shape of the action potentials typically does not differ much (Dayan and Abbott, 2005). Moreover, their duration is relatively short compared to other timescales of the system. Therefore, in order to analyze the information that the neuron is sending further on, it is sufficient to look at the occurrence times of action potentials as their defining quality. A sequence of action potentials generated by a single neuron is called a "spike train". A spike train can be recorded by placing an electrode in the soma or close to it (Safronov et al., 2000). It remains a subject of research how specific and varied information is encoded within sequences of these seemingly indistinguishable spikes. Measures to quantify neural data from different perspectives are an active area of research (Perkel, 1968; Victor and Purpura, 1997; Rieke et al., 1996; Buracas and Albright, 1999; Nemenman et al., 2004), however, most of the proposed encoding schemes can be grouped into the following two categories: whether the information is embedded in the precise timing of the spikes (temporal code) or in their frequency (rate code).

The classic rate coding paradigm suggests that the neurons encode information through the average number of spikes sent along the axon per observation time window (also called the firing rate) (Dayan and Abbott, 2005). The description of the neuronal activity through the rate coding scheme is relatively straightforward and is characterized by the firing rate. Early studies demonstrated that the firing rate of neurons could vary significantly in response to the changes in sensory inputs. One of the foundational studies in neuroscience, conducted by Adrian and Zotterman (1926), demonstrated that the firing rate of sensory neurons in a frog changes in direct proportion to the intensity of the stimulus. However, subsequent research reveals that this relationship is generally non-linear (Kandel et al., 1991). Hubel and Wiesel (1962) found that the neurons in the visual cortex encode various stimulus features like orientation, direction, and spatial frequency through modulations in their firing rate. In a pivotal study, Georgopoulos et al. (1986) established that the firing rate of the motor cortex neurons of rhesus monkeys varied predictably with the direction of arm movement. These findings support the rate coding hypothesis that neurons could encode various aspects of different stimuli through a variation in their firing rate.
Subsequent research has demonstrated that neurons can encode information without necessarily altering the mean firing rate in response to a stimulus (Perkel, 1968; Gerstner and Kistler, 2002; Rigotti et al., 2013; Dettner et al., 2016). This has prompted further exploration into other coding schemes, such as temporal coding.

The temporal coding hypothesis states that the timing of individual spikes relative to each other and to external events is also employed in the embedding of neural information in the spike train (Theunissen and Miller, 1995). Perkel (1968) gives a classic overview of temporal coding. One example of temporal coding is seen in the phase locking observed in the auditory system, where neurons fire at a particular phase of a sound wave, thus encoding its frequency without necessarily changing the overall firing rate (Köppl, 1997). Another example is spike timing-dependent plasticity (STDP), where the precise timing of spikes between two neurons can lead to the strengthening or weakening of synapses, thereby encoding information through changes in synaptic strength rather than through changes in firing rate (Dan and Poo, 2006). Temporal pairwise spike correlation has been re-

ported to capture information transmission in single neurons (Dettner et al., 2016).

Over the last century, the attempts to accurately measure and interpret firing rates have led to the development of numerous methods, reflecting advances in both theoretical frameworks and experimental techniques. These methods range from simple counting of spikes within a fixed window (Gerstein and Kiang, 1960) to more complex approaches that consider the temporal dynamics of firing (Omi and Shinomoto, 2011; Shimazaki and Shinomoto, 2010), accommodating the often non-stationary nature of neural activity.

It is challenging to determine the time-dependent firing rate from a few spike trains, therefore most of the established methods use trial averaging (Fig. 3), however, averaging might phase out some of the important temporal features (Nawrot et al., 1999; Baker et al., 2001; Yu et al., 2005), thus extracting the time-dependent firing rate from limited data remains a persistent problem. We briefly review the established methods of firing rate estimation developed over the years, from classical to more recent ones in Attachment I.

Significant advances have been made in understanding and estimating the firing rate in non-stationary processes, where neural firing patterns change over time. However, challenges in neural coding persist. Transitioning to stationary processes, where the statistical properties of the firing rate are assumed to remain constant over time (Moore et al., 1966), presents its own set of difficulties. Despite the apparent simplicity of stationary processes, accurately estimating the firing

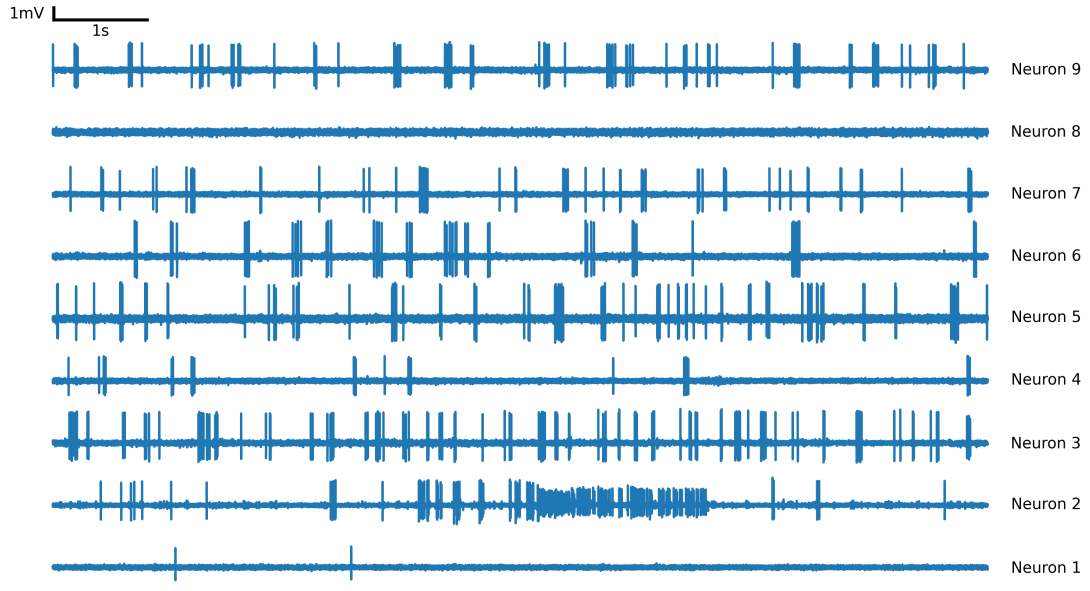

Figure 2: Response variability in spontaneously active neuron population. The traces represent the spontaneous electrical activity recorded from the nine separate olfactory receptor neurons of the noctuid moth *Agrotis ipsilon* over 10 seconds. This spontaneous activity reflects the inherent heterogeneity in neuronal activity, demonstrating a range of firing patterns and membrane potential oscillations that occur even in the absence of olfactory input.

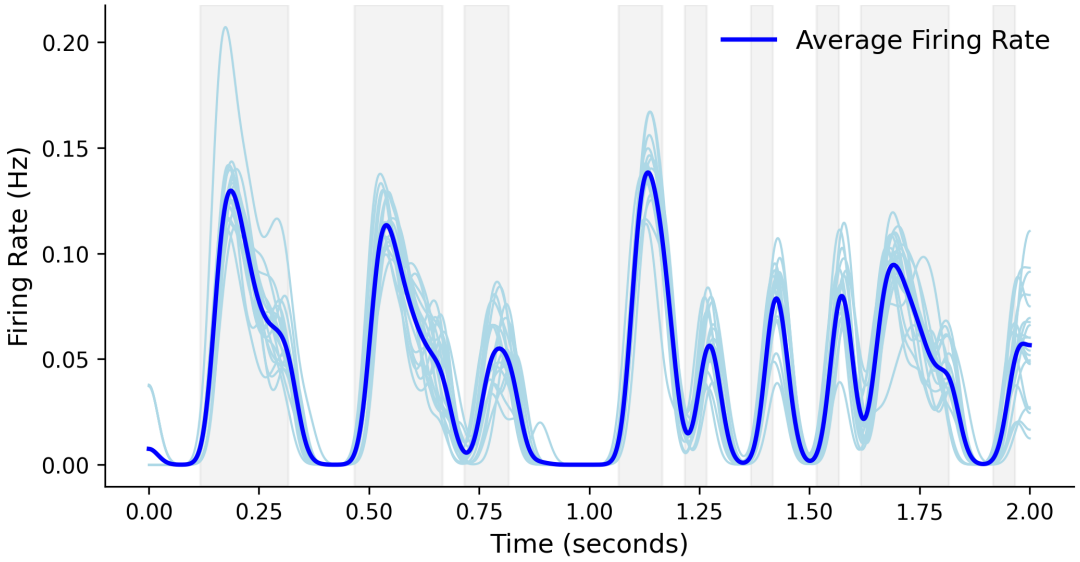

Figure 3: Neuronal response variability to identical stimulus. Olfactory receptor neurons of noctuid moth *Agrotis ipsilon* exhibit variable responses to the identical stimulus profile (shown with a grey background). Individual responses are depicted in light blue, illustrating the range of firing rates across trials, whereas aggregate behavior is highlighted in dark blue.

rate requires careful consideration of various factors, such as the selection of appropriate time windows for spike counting and the resolution of temporal binning, which can substantially influence the perceived firing rate (Shimazaki and Shinomoto, 2007). Moreover, the inherent variability in neuronal firing—even within what is considered stationary activity—necessitates robust statistical methods for signal discrimination from background noise (Stein, 1965; Kostal et al., 2007; Nawrot, 2010). This complexity is increased by the physiological realities of neuronal behavior, where even supposedly steady-state firing rates are subject to underlying fluctuations driven by various factors, from synaptic inputs to intrinsic cellular mechanisms (Tomko and Crapper, 1974).

To overcome some of these challenges the concept of instantaneous firing rate has gained popularity as an alternative to the classically defined firing rate (Longtin and St-Hilaire, 2000; Rospars et al., 2003; Lemon and Smith, 2006; Chacron et al., 2007; Miller et al., 2014; Sinha et al., 2021). Instantaneous firing rate, defined as the reciprocal value of the duration of the interval between two spikes, can offer a more detailed and dynamic account of neural activity (Kostal et al., 2018). Despite being used in many studies as the alternative to firing rate, there are several differences between the "instantaneous firing rate" and "firing rate", the key difference being that the mean instantaneous firing rate is typically higher than the mean firing rate. In Kostal et al. (2018), the authors demonstrate that the statistical properties of the instantaneous firing rate vary significantly depending on the timing of observation relative to neuronal spikes. Under the specific framework of *equilibrium renewal processes*, the mean instantaneous firing rate is equal to the mean firing rate. Our work in Attachment II builds on this by exploring the stochastic characteristics of the instantaneous firing rate,

revealing that it can uncover aspects of neural data that may not be evident from inter-spike interval (ISI) analysis alone. Furthermore, the instantaneous firing rate is instrumental in bridging the conceptual gap between rate coding and temporal coding paradigms, offering a more comprehensive understanding of neural information processing.

While the rate coding paradigm has dominated the field, enabling significant advancements in understanding neural communication, it is critical to address the complexity and limitations of current models in capturing the true essence of neuronal behavior. The original Hodgkin-Huxley model (Hodgkin and Huxley, 1952) neglects the stochastic nature of ion channel gating or the anatomical structure of the neuron. Subsequent studies have tried to fill these gaps (Fox, 1997; Schneidman et al., 1998; Li et al., 2010). Models like the FitzHugh-Nagumo model (Fitzhugh, 1961) and the Rall model (Rall, 1962) have each tried to focus on different aspects of neuronal dynamics, the former focuses on the generation and propagation of action potential while the latter focuses on the properties of dendrites. These basic models also do not consider the effect of synaptic input on neuronal dynamics, a limitation that was addressed in Destexhe et al. (1994). The integrate-and-fire (IF) model proposed by Lapicque (2007) focuses on the integration of synaptic inputs and the generation of action potentials once a threshold is exceeded. Over time various versions of the IF model have been developed, that included stochastic activity in the input current (Gerstein and Mandelbrot, 1964; Stein, 1965, 1967), incorporation of the dependence of excitatory and inhibitory postsynaptic potential amplitudes on the membrane potential relative to their respective reversal potentials (Tuckwell, 1978). Many of these basic models often assume neurons can fire at infinitely high rates in response to increasing stimulus intensity. However, this assumption does not align with observed biological constraints, such as the absolute refractory period, which imposes a natural limit on the firing frequency of neurons. These limitations highlight the necessity for models that can inherently incorporate mechanisms for saturation of the firing frequency, reflecting more accurately the physiological constraints observed in real neuronal systems. The research presented in Attachment III addresses this gap by introducing and comparing four simple neural models, including both single-point and two-point versions of the leaky integrate-and-fire (LIF) model, with and without consideration of reversal potentials.

Substantial progress has been made in understanding neuronal coding through the analysis of action potentials and firing rates in neurons. These principles also apply to more specialized contexts, such as olfactory receptor neurons (ORNs) in insects. ORNs are essential in processing odor signals, with their diverse sensitivities and complex response properties forming the basis of odor coding (Yao et al., 2005). Insects rely on these cues for locating food sources, mates, and suitable habitats, making the study of ORNs essential for understanding insect behavior and ecology.
The complexity of neuronal coding in ORNs becomes particularly apparent when considering the role of volatile plant compounds (VPCs) in the environment. These compounds can significantly influence the firing patterns of ORNs, thus affecting

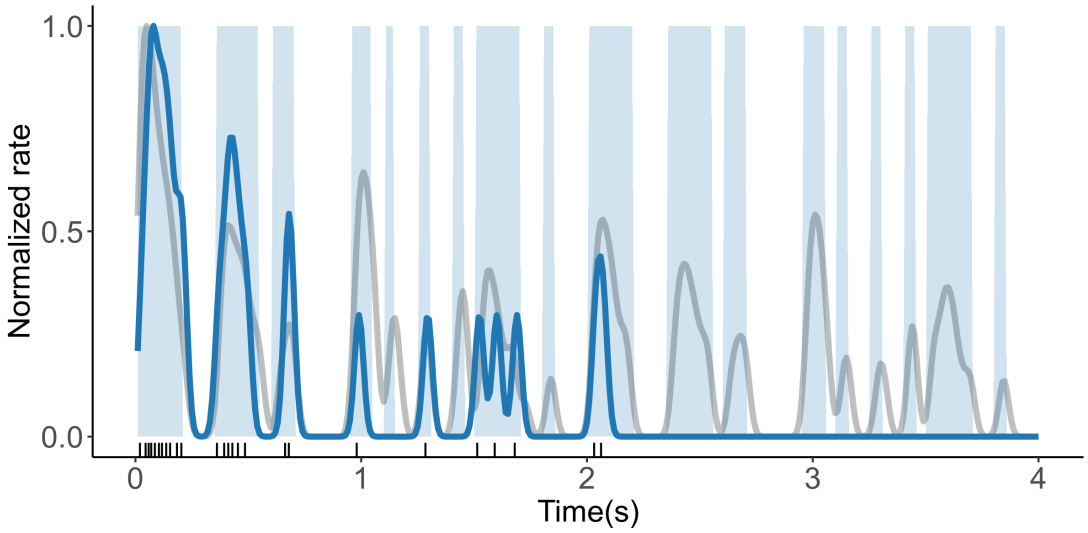

Figure 4: Inhibitory effect of volatile plant compounds (VPCs) on the firing rate of olfactory receptor neurons (ORNs) in *Agrotis ipsilon* moths. This graph illustrates the modulatory influence of (Z)-3-hexenyl acetate, a common VPC, on the firing patterns of ORNs sensitive to sex pheromones in *Agrotis ipsilon* moths. The control (grey line) demonstrates the baseline firing rate of the ORNs in the absence of VPCs, while the presence of VPCs (blue line) shows a notable suppression in neuronal activity. The shaded areas indicate the periods during which the pheromone stimulus is applied. Below, the corresponding raster plot provides a spike train representation under the VPC background.

an insect's ability to detect and respond to crucial olfactory signals. Studies have demonstrated that VPC backgrounds can alter the response to pheromones in ORNs (Conchou et al., 2020, 2021; Rangan, 2012), affecting both qualitative and quantitative coding, as well as increasing response variability (Dupuy et al., 2017). The addition of VPCs has been observed to suppress response in pheromone-responsive ORNs, suggesting a complex interaction between VPCs and pheromone signaling (Rouyar et al., 2015). Furthermore, VPCs like linalool, geraniol, or (Z)-3-hexenyl acetate have been found to suppress the response of specific ORNs, indicating a suppressive effect at the level of the pheromone receptor protein (Vandroux et al., 2022), as shown in Fig. 4. Nonetheless, there is a significant gap in understanding how VPCs may influence the information transmission capabilities of these neurons. Our work in Attachment IV examines how different concentrations of VPCs affect the coding efficiency of pheromone-responsive ORNs in male moths of the *Agrotis ipsilon* species. Through a series of experiments, we demonstrate that higher concentrations of specific VPCs can facilitate the encoding efficiency of pheromone signals by ORNs, in terms of information per evoked spike.

Another aspect of rate coding, that has been the subject of intensive research is the concept of variability. Studies have shown that neural variability can be categorized into stimulus-evoked variability, reflecting trial-to-trial fluctuations in response characteristics (Fig. 3), and ongoing variability, representing spontaneous fluctuations in neural activity (Arazi et al., 2017). Furthermore, prestimulus

neural variability is shown to be higher compared to poststimulus variability, suggesting that sensory input reduces ongoing neural variability, a phenomenon known as variability quenching (Monier et al., 2003; Churchland et al., 2006, 2010). In our article in Attachment V, we investigate the mechanisms underlying neural variability quenching. Spike frequency adaptation (SFA), which refers to the decrease of the firing rate of a neuron in response to sustained input, has been used to create more realistic neural networks. We investigate how different mechanisms of SFA influence the quenching of neural response variability. Using a cortical model with excitatory and inhibitory neuron subpopulations, we demonstrate that SFA implemented through dynamic firing threshold decreases trial-to-trial variability, whereas SFA through after-hyperpolarization currents increases variability.

In the following chapters, I provide an introduction to the theoretical framework for the neural coding problem, point process models of neural activity, biophysical models of neural activity, insect olfaction, and information-theoretical methods used to study it. More detailed information is provided in the attached manuscripts. In chapter 3, I provide a summary of the main results and a discussion of the attached work.

2. Theory and methods

2.1 Firing rate and efficient coding

The concept of firing rate has been central to the field of computational neuroscience, however, determining the firing rate from neuronal spike data introduces several challenges. The most commonly accepted definition of firing rate is based on counting the number of spikes in a given time interval and dividing it by the duration of the time interval, however, this approach assumes the stationarity of the underlying counting process of spikes. This assumption is rarely met in dynamic experimental environments (Rieke et al., 1996; Fenton and Muller, 1998). The task of accurately determining time-dependent firing rates becomes significantly more complex with limited data, a common scenario in neuroscience research. Sparse or incomplete spike records can result in unreliable estimates of firing rate, therefore most of the established methods use trial averaging, however, averaging might phase out some of the important temporal features (Dayan and Abbott, 2005; Kostal et al., 2007). Furthermore, the temporal dynamics of neural activity, characterized by bursts of rapid firing interspersed with periods of silence or low activity, add another layer of complexity to firing rate analysis. Traditional methods that average spikes over extended intervals may overlook these nuanced patterns, potentially omitting crucial information encoded in the temporal structure of the spike train (Keat et al., 2001; Fairhall et al., 2001). Thus extracting the time-dependent firing rate from limited data remains a persistent problem.

Another critical challenge arises from the heterogeneity of neuronal populations. Neurons within a network can exhibit a wide range of firing behaviors, influenced by their intrinsic properties and the complex dynamics of synaptic inputs (van Vreeswijk and Sompolinsky, 1996; Sekirnjak and du Lac, 2002). This diversity means that a single analytical approach to determine the firing rate may not be universally applicable across different neuron types or functional states, highlighting the need for more sophisticated, adaptable methods to accurately capture the dynamics of neuronal communication (Paninski, 2004).

The concept of the instantaneous firing rate addresses some of these challenges by offering a refined analysis tool that provides an instantaneous view of neuronal activity. The definition of instantaneous firing rate is based on the calculation of the inverse of the average inter-spike interval (ISI). Firing rate defined this way is used both in experimental and theoretical studies (Burkitt and Clark, 2000; Van Rullen and Thorpe, 2001) and it is identical to count-based firing rate under certain conditions. Since the instantaneous firing rate is derived from the inverse of the ISI, it is sensitive to the time-dependent changes in neural activity and captures the underlying fluctuations well. This approach allows for a more detailed examination of the dynamics of neural firing, accommodating the variability, and complexity inherent in neuronal processes. By focusing on the probability distribution of spikes at each moment, the instantaneous firing rate method offers a way to navigate these challenges.

2.1.1 Classical firing rate

Spike trains can be modeled as stochastic processes. The class of stochastic processes whose realization consists of a sequence of point events in time is called *stochastic point process* (Cox and Miller, 1965). A spike train, in the context of neural activity, can be described as a series of discrete events (spikes) that indicate when a neuron fires. In general, there are two ways of describing a spike train:

- **Spike time representation:** A spike train can be depicted by the specific times at which each individual spike occurs, typically denoted as $X_1, X_2, \ldots$. This representation provides a sequence of spikes based on the exact moment of neuronal firing.

- **ISI representation:** Alternatively, a spike train can be described through the ISIs, defined as $T_i = X_{i+1} - X_i$. This approach focuses on the time elapsed between consecutive spikes, which is crucial for understanding the temporal dynamics of the spike train.

A process is termed *stationary* when its statistical properties, such as the probability distributions of spike counts in various intervals, remain constant over time. A specific class of stationary point processes is the renewal point process, where the intervals between spikes (T_i) are modeled as independent and identically distributed (i.i.d.) variables. Renewal processes, with their probability distribution function f_T are commonly used to model spontaneously active cells, emphasizing the independence of successive spikes (Tuckwell, 2010).
In renewal processes, the firing rate can be estimated by dividing the number of spikes $N(w)$ in a time window $[0, w]$ by the width of the window w. The intensity λ of the point process, which represents the expected rate of spikes per unit time, is defined as:

$$\lim_{w \to \infty} \frac{\mathbb{E}(N(w))}{w} = \frac{1}{\mathbb{E}(T)} = \lambda. \tag{2.1}$$

When w is finite, the above equation holds true for renewal processes only if the origin time t_0 is not related to the point process realization. The corresponding renewal process is referred to as *equilibrium renewal process*, as opposed to the *ordinary renewal process* which starts from an arbitrary spiking event (Cox and Miller, 1965).
When the firing rate varies with time or depends on the history of the process, the process becomes non-stationary. This complicates the analysis but often provides richer insights into the dynamic nature of neural activity (Johnson, 1996). Below are some well-established methods to estimate the firing rate for non-stationary processes:

Frequencygram method uses the reciprocal values of ISIs to calculate the instantaneous firing rate, assuming that the spike rate varies significantly over short periods. This method is exemplified by its application in studies such as Bessou et al. (1968), who initially applied these principles in their experiments.

Time histograms segment the observation period into bins, averaging the spikes within each bin to approximate the firing rate (Johnson, 1978). This

method's efficiency in capturing the temporal variations of the firing rate is heavily dependent on choosing an appropriate bin size (Shinomoto, 2010).

Kernel smoothing techniques provide a continuous estimate of firing rates by convolving spike train data with a kernel function, such as Gaussian, to better handle variations compared to simple binning (Parzen, 1962; Silverman, 1986).

Optimized kernel smoothing refines this approach by adjusting the kernel's bandwidth, either globally or locally, enhancing the fit to data characteristics and minimizing estimation errors. Nawrot et al. (1999) and Cherif et al. (2008) contribute significantly to this method, focusing on the optimization of bandwidth to improve the accuracy of firing rate estimates.

Gaussian process firing rate models the firing rate as a Gaussian process, providing a robust framework for handling variability in firing rates over time and across trials by employing inhomogeneous gamma interval processes Barbieri et al. (2001). This probabilistic approach is supported by Cunningham et al. (2007), who apply it within the context of neural prosthetic decoding.

Bayesian adaptive regression splines fit a spline model to spike data using a Bayesian approach to determine the number and positions of knots optimally. Dimatteo et al. (2001) demonstrate the application of BARS, showing its effectiveness in capturing rapid changes in firing rate while smoothing out noise.

Bayesian binning combines features of binning and smoothing by using variable bin widths, adapted based on the data (Endres et al., 2007). This method balances flexibility in capturing the dynamics of firing rates with computational simplicity.

Bayesian adaptive kernel smoothing (BAKS) integrates kernel smoothing with adaptive techniques to dynamically optimize bandwidth based on the observed data (Ahmadi et al., 2018). This sophisticated method treats bandwidth as a random variable, continually updating its distribution based on the observed spikes to capture true firing rates accurately. Ahmadi et al. (2018) demonstrate the application of BAKS in both simulated and real neural data scenarios.

A more detailed overview of these methods is given in Tomar (2019).

2.1.2 Instantaneous firing rate

Instead of using the classically defined firing rate, researchers have often used "instantaneous firing rate" which is typically defined as the inverse of the ISIs $(1/T)$ (Pauluis and Baker, 2000). Examples of this can be found in theoretical studies like Burkitt and Clark (2000), Van Rullen and Thorpe (2001) and Harris and Waddington (2012) and in experimental studies like Martinez-Conde et al. (2000), Rospars et al. (2003) and Lemon and Smith (2006).
The advantage in using instantaneous rate over the count-based defined firing rate

lies in the fact that instantaneous rate is based on ISIs and ISI statistics is easily available as compared to count-based statistics, however, as proven in Lánský et al. (2004), the mean instantaneous firing rate is higher than or equal to the mean firing rate,

$$\mathbb{E}\left(\frac{1}{T}\right) \geq \frac{1}{\mathbb{E}(T)}, \tag{2.2}$$

with equality if all the ISIs are of the same length. This scenario is rare in actual neuronal data, where variability in ISI length is the norm due to the stochastic nature of neuronal firing.
The discrepancy noted in Eq. (2.2) actually achieves equality under a specific condition when the "time instant" at which the instantaneous rate is assessed does not typically align with the occurrence of a spike. As detailed in Kostal et al. (2018), the selection of the time instant for measuring the instantaneous rate is determined in relation to an "external" time frame, which is consistent across different trials and asynchronous with respect to individual spike train realizations. Consequently, this results in the probabilities of observed ISIs, denoted as $\tilde{T}$, being proportional to their lengths, expressed as $\tilde{T} \sim \lambda \tilde{t} f_T(\tilde{t})$. Here, λ represents the mean firing rate calculated as the mean inverse of these length-biased ISIs. Furthermore, in this setup, the instantaneous rate $R = 1/\tilde{T}$ is treated as a random variable with its probability density function (pdf) described by:

$$f_R(r) = \frac{1}{\mathbb{E}(T)} \frac{f_T(1/r)}{r^3}. \tag{2.3}$$

For a comprehensive breakdown of the mathematical derivations and assumptions leading to this formulation, please refer to Kostal et al. (2018). From the above equation, we can conclude that

$$\mathbb{E}\left(\frac{1}{\tilde{T}}\right) = \mathbb{E}(R) = \frac{1}{\mathbb{E}(T)} = \lambda. \tag{2.4}$$

We focused on the case of the equilibrium renewal process and analyzed the variability and randomness of the instantaneous rate for commonly used renewal point process models of stationary neural activity (Tomar and Kostal, 2021).

2.2 Variability and randomness quantification

2.2.1 Variability quantification

Understanding the variability in neural activity is essential for comprehending the complexities of neural codes and the mechanisms underlying brain function. Whether it be the variability of ISIs or firing rate, this variability is not necessarily noise or a secondary effect of neural processing, rather it is integral to the encoding and transmission of information within brain regions (Perkel, 1968).

The factors influencing the variability in ISIs can be several, like intrinsic properties of neurons, synaptic inputs, and the dynamics of the neural network. Intrinsic neuronal properties, such as the distribution of ion channels and firing thresholds, contribute to the variability in firing patterns (Hodgkin and Huxley, 1952). Synaptic inputs from other neurons, which can be either excitatory or

inhibitory, introduce another layer of complexity and variability to the timing of action potentials (Shadlen and Newsome, 1998). The state of the neural networks and the connection between the neurons also significantly impact the variability in neural activity (Amit and Brunel, 1997).
Decoding and understanding the nature and source of variability in neural activity is an important aspect of understanding the information transmission among neurons. To quantitatively assess the variability in neural firing patterns, especially the variability in ISIs, researchers utilize various measures. In the analysis of ISIs, described by a continuous positive random variable T, one of the primary statistical measures used is the standard deviation $\sigma(T)$. This measure is defined mathematically as:

$$\sigma(T) = \sqrt{\mathbb{E}([T - \mathbb{E}(T)]^2)}, \tag{2.5}$$

where $\mathbb{E}(T)$ represents the expected value of T. To provide a relative measure of dispersion that is independent of the units of T, the coefficient of variation $C_V(T)$ is employed,

$$C_V(T) = \frac{\sigma(T)}{\mathbb{E}(T)} = \lambda\sigma(T) \tag{2.6}$$

with $\lambda = 1/\mathbb{E}(T)$. The coefficient of variation $C_V(T)$ is a dimensionless quantity, making it particularly useful for comparing the variability of ISI distributions that have different means, unlike the standard deviation which is unit-dependent. Expanding on the concept of variability, the standard deviation for the instantaneous rate R can be derived from the pdf given earlier:

$$\sigma(R) = \sqrt{\lambda\mathbb{E}(1/T) - \lambda^2}, \tag{2.7}$$

where λ represents the mean firing rate. The corresponding relative dispersion measure for the instantaneous rate, known as the coefficient of variation of the instantaneous rate $C_V(R)$ is calculated as:

$$C_V(R) = \sqrt{\frac{\mathbb{E}(1/T)}{\lambda} - 1}. \tag{2.8}$$

These formulations of $C_V(T)$ and $C_V(R)$ are useful in quantifying how dispersed the values are around the mean of a distribution, offering a normalized perspective that is particularly advantageous when comparing distributions with different mean values. However, it is crucial to acknowledge that while σ or C_V effectively capture the spread of a distribution, they do not encompass all aspects of variability. Specifically, they do not provide information on the randomness or predictability of outcomes, nor do they reflect differences in distributions beyond the second moment, such as skewness and kurtosis. Thus, while these metrics are informative for assessing variability and dispersion, they may not fully characterize the complex behavior observed in neuronal spike trains, where higher moments and non-linear dynamics can also be significant (Kostal et al., 2007).

Trial-to-trial variability quantification

To compare the trial-to-trial variability of two neurons with the same mean spike count $\mathrm{E}[N(w)]$, we can use the variance of the observed spikes $\mathrm{Var}[N(w)]$. A

relative dispersion measure, called the Fano factor, for trial-to-trial variability can be obtained by scaling the variance with the mean of the spike counts:

$$\mathrm{FF} = \frac{\mathrm{Var}[N(w)]}{\mathrm{E}[N(w)]}. \tag{2.9}$$

A Fano Factor of one indicates that the spike counts follow a Poisson distribution (the variance equals the mean), typical of random processes. Trial-to-trial variability can also be estimated using $C_V(T)$ for a steady-state spike train, in which case,

$$FF_0 = CV^2 \tag{2.10}$$

where FF_0 is the Fano factor calculated from the infinite length time window ($w \to +\infty$).

2.2.2 Randomness quantification

To further understand the concept of randomness within spike trains, the field of computational neuroscience has turned to entropy-based measures, specifically differential entropy, as described by Shannon (1948). Differential entropy h for a continuous random variable X with pdf f_X is defined by the equation:

$$h(f_X) = -\int f_X(x) \ln f_X(x) \mathrm{d}x. \tag{2.11}$$

This measure quantifies the uncertainty or randomness inherent in the outcomes of the variable. However, $h(f_X)$ on its own cannot serve as a comprehensive measure of randomness, as it can yield both positive and negative values depending on the scale of the random variable X. To address this limitation, Kostal and Lansky (2015) introduced an entropy-based dispersion coefficient (σ_h), which normalizes the entropy value to create a more stable and interpretable metric:

$$\sigma_h = \exp(h(f_X) - 1). \tag{2.12}$$

This coefficient utilizes the asymptotic equipartition property, which suggests that for a large number of independent and identically distributed random variables, the mean of their natural logarithms approaches the differential entropy (Kostal et al., 2013).

Building upon these entropy measures, the relative entropy-based measure of dispersion C_h, analogously to the coefficient of variation C_V for standard deviation, is given by

$$C_h = \lambda \sigma_h. \tag{2.13}$$

A significant attribute of C_h is that its maximum value is 1. This occurs specifically when the pdf f_T is an exponential distribution, reflecting the maximum entropy state among all distributions with a given mean, thus representing the highest degree of randomness possible under those conditions.

2.3 Renewal point process models of steady state neuronal activity

2.3.1 Gamma distribution

The gamma distribution is commonly used in experimental data analysis, particularly in neuroscience, to describe the distribution of inter-spike intervals (ISIs) (Baker and Lemon, 2000; Shimokawa et al., 2010; Chen and Nitz, 2011; Xue et al., 2013; Li et al., 2015). This distribution has been found to be a suitable descriptor for the stochastic nature of ISIs in spike data analysis (Ikeda and Manton, 2009). The pdf of the Gamma distribution is mathematically defined as follows:

$$f_T(t) = \frac{b^a t^{a-1} e^{-bt}}{\Gamma(a)}, \tag{2.14}$$

where $\Gamma(z) = \int_0^\infty x^{z-1} e^{-x} \mathrm{d}x$ denotes the gamma function, and $a > 0$, $b > 0$ serve as the shape and rate parameters respectively. These parameters are crucial as they determine the skewness and scale of the distribution, allowing it to accurately model a broad spectrum of ISI patterns observed in neural activities (Dayan and Abbott, 2005). The mean firing rate (λ) and the coefficient of variation ($C_V(T)$) of the gamma distribution are given by:

$$\lambda = \frac{b}{a}, \quad C_V(T) = \frac{1}{\sqrt{a}}. \tag{2.15}$$

Using these parameters, the entropy of the ISI distribution can be expressed as:

$$h(f_T) = \log\left(\frac{\Gamma(a)}{b} e^{a+(1-a)\psi(a)}\right), \tag{2.16}$$

where $\psi(x) = \Gamma'(x)/\Gamma(x)$ is the digamma function, representing the derivative of the logarithm of the gamma function. The dispersion coefficient of randomness is then derived by combining the entropy and the parameters of the gamma distribution:

$$C_h(T) = \frac{\Gamma(a)}{a} e^{a+(1-a)\psi(a)-1}. \tag{2.17}$$

The distribution also facilitates the derivation of the instantaneous rate distribution, which follows an inverted gamma distribution:

$$f_R(r) = \frac{b^{a+1} r^{-a-2} e^{-b/r}}{\Gamma(a+1)}. \tag{2.18}$$

From this, the coefficient of variation for the rate $C_V(R)$ is calculated as:

$$C_V(R) = \sqrt{\frac{1}{a-1}}, \quad a > 1. \tag{2.19}$$

Finally, the differential entropy for the rate distribution $f_R(r)$ is expressed as:

$$h(f_R) = \log(\Gamma(a+1) b e^{(a+1)-(a+2)\psi(a+1)}), \tag{2.20}$$

and the corresponding dispersion coefficient of randomness is:

$$C_h(R) = a\Gamma(a+1) e^{a-(a+2)\psi(a+1)}. \tag{2.21}$$

2.3.2 Lognormal distribution

The lognormal distribution is a probability distribution of a random variable whose logarithm is normally distributed. In the context of ISI analysis, it is a common descriptor in experimental data analysis (Burns and Webb, 1976; Bhumbra et al., 2004). Experimental data from neuronal firing often exhibit right-skewed, long-tailed distributions, which can be well-described by the lognormal distribution. Additionally, Buzsáki and Mizuseki (2014) demonstrate that lognormal distributions in neural activity, resulting from multiplicative biological processes, crucially influence brain dynamics and network functionality. These distributions provide a robust framework for modeling neural variability and understanding the disproportionate impact of highly active neurons on cognitive functions.
The pdf for a lognormal distribution is given by:

$$f_T(t) = \frac{1}{\sigma t\sqrt{2\pi}} \exp\left\{ -\frac{(\ln t - \ln m)^2}{2\sigma^2} \right\}, \tag{2.22}$$

where m is the scale parameter and $\sigma > 0$ is the shape parameter (Crow and Shimizu, 2018). This formulation highlights the lognormal's capacity to model distributions where the majority of the data is concentrated around a central value, with a long tail extending towards higher values. The mean firing rate and the coefficient of variation for the lognormal distribution are calculated as:

$$\lambda = \frac{1}{me^{\sigma^2/2}}, \quad C_V(T) = \sqrt{e^{\sigma^2} - 1}. \tag{2.23}$$

The differential entropy of the distribution is expressed as:

$$h(f_T) = \frac{1}{2}\log(2\pi e\sigma^2 m^2), \tag{2.24}$$

and the dispersion coefficient of randomness for the distribution is:

$$C_h(T) = \sigma\sqrt{2\pi}e^{-(\sigma^2+1)/2}. \tag{2.25}$$

The instantaneous rate distribution follows the pdf:

$$f_R(r) = \frac{1}{me^{\sigma^2/2}} \frac{1}{r^2\sigma\sqrt{2\pi}} \exp\left\{ -\frac{(\ln r + \ln m)^2}{2\sigma^2} \right\} \tag{2.26}$$

with the coefficient of variation for the rate given by:

$$C_V(R) = \sqrt{e^{\sigma^2} - 1}. \tag{2.27}$$

The differential entropy for the rate distribution is derived as:

$$h(f_R) = \frac{1}{2}\log\left(\frac{2\pi e\sigma^2}{m^2 e^{2\sigma^2}}\right). \tag{2.28}$$

The dispersion coefficient is evaluated as:

$$C_h(R) = \sigma\sqrt{2\pi}e^{-(\sigma^2+1)/2}. \tag{2.29}$$

2.3.3 Inverse Gaussian distribution

The inverse Gaussian distribution has been proposed as a suitable model for describing the temporal structure of point processes in neuroscience, particularly in the context of neural spike train data analysis. This distribution is adept at capturing the asymmetric behavior of tails and the early response times characteristic of neuronal firing patterns. Tejo and Niklitschek-Soto (2016) provided theoretical arguments supporting the use of the inverse Gaussian distribution for modeling ISIs, highlighting its suitability in the neural activity framework. Tsubo et al. (2012) also included the inverse Gaussian distribution as part of a wide class of distributions suitable for describing ISIs in cortical neurons. Moreover, Rossoni and Feng (2006) derived a renewal process model with an inverse Gaussian density as the ISI distribution from a stochastic integrate-and-fire (IF) model, further supporting its relevance in neuroscience. The distribution is defined with a mean $a > 0$ and a scale parameter $b > 0$ with its pdf defined as:

$$f_T(t) = \sqrt{\frac{a}{2\pi b t^3}} \exp\left\{ -\frac{1}{2b}\frac{(t-a)^2}{at} \right\}. \tag{2.30}$$

This formula highlights the distribution's capability to model time intervals where events, like neuronal spikes, exhibit variability that is not necessarily symmetric around the mean. The parameters a and b play critical roles, where a represents the mean ISI, and b adjusts the distribution's tail, influencing the skewness and kurtosis. The mean firing rate and coefficient of variation for the ISIs are given by:

$$\lambda = \frac{1}{a}, \quad C_V(T) = \sqrt{b}. \tag{2.31}$$

The differential entropy for this distribution is calculated as:

$$h(f_T) = \frac{1}{2}\log(2\pi a^2 be) + \frac{3e^{1/b}}{\sqrt{2\pi b}} K^{(1,0)}\left(-\frac{1}{2}, \frac{1}{b} \right), \tag{2.32}$$

where $K_\nu^{(1,0)}(z)$ is the derivative of the modified Bessel function of the second kind (Abramowitz and Stegun, 1948), which helps quantify the randomness or unpredictability inherent in the ISI distribution.,

$$K_\nu^{(1,0)}(z) = \frac{\partial}{\partial \nu} K_\nu(z). \tag{2.33}$$

The dispersion coefficient of randomness is:

$$C_h(T) = \sqrt{\frac{2\pi b}{e}} \exp\left\{ \frac{3e^{1/b}}{\sqrt{2\pi b}} K^{(1,0)}\left(-\frac{1}{2}, \frac{1}{b} \right) \right\}. \tag{2.34}$$

For the instantaneous firing rate, the corresponding distribution follows:

$$f_R(r) = \sqrt{\frac{1}{2\pi a b r^3}} \exp\left\{ -\frac{1}{2b}\frac{(1-ar)^2}{ar} \right\}. \tag{2.35}$$

This rate distribution retains the coefficient of variation:

$$C_V(R) = \sqrt{b}, \tag{2.36}$$

and its differential entropy is similarly derived as:

$$h(f_R) = \frac{1}{2}\log\left(\frac{2\pi be}{a^2}\right) + \frac{3e^{1/b}}{\sqrt{2\pi b}}K^{(1,0)}\left(-\frac{1}{2}, \frac{1}{b}\right). \tag{2.37}$$

Lastly, the dispersion coefficient for the rate distribution mirrors that of the ISIs:

$$C_h(R) = \sqrt{\frac{2\pi b}{e}}\exp\left\{\frac{3e^{1/b}}{\sqrt{2\pi b}}K^{(1,0)}\left(-\frac{1}{2}, \frac{1}{b}\right)\right\}. \tag{2.38}$$

2.3.4 Shifted exponential distribution

The shifted exponential distribution is another statistical model used to describe ISIs in neuroscience, particularly for neurons that display a distinct refractory period followed by a period of exponential-like firing rates. This model is an adaptation of the exponential distribution, modified to incorporate a shift parameter that accounts for the absolute refractory period during which no spike can occur regardless of input (Grollier et al., 2020). In the context of auditory nerve fibers, deviations from strictly exponential ISI distributions are commonly attributed to the refractoriness of these fibers (Heil et al., 2007). Additionally, in the study of interspike interval distributions in the barn owl, it was found that the ISI distributions are better explained as resulting from the action of a brief refractory period on excitatory events generated by a homogeneous stochastic process, where the distribution of interevent intervals is a mixture of an exponential and a gamma distribution with the same scaling parameter (Neubauer et al., 2009). The pdf for the shifted exponential distribution, characterized by a rate parameter $a > 0$ and a refractory period $\tau \geq 0$, is given by:

$$f_T(t) = \begin{cases} 0, & t \leq \tau, \\ ae^{-a(t-\tau)}, & t > \tau. \end{cases} \tag{2.39}$$

This results in a mean firing rate and coefficient of variation expressed by:

$$\lambda = \frac{a}{1+a\tau}, \quad C_V(T) = \frac{1}{1+a\tau}. \tag{2.40}$$

The differential entropy for this distribution is straightforwardly computed as:

$$h(f_T) = \log\left(\frac{e}{a}\right), \tag{2.41}$$

leading to a dispersion coefficient of randomness given by:

$$C_h(T) = \frac{1}{1+a\tau}. \tag{2.42}$$

For the instantaneous rate, the distribution is defined as:

$$f_R(r) = \begin{cases} 0, & r \geq 1/\tau, \\ \frac{a^2}{r^3(1+a\tau)}e^{-a(\frac{1}{r}-\tau)}, & r < 1/\tau, \end{cases} \tag{2.43}$$

with the coefficient of variation for the rate:

$$C_V(R) = \sqrt{(1+a\tau)e^{a\tau}\Gamma(0, a\tau) - 1}, \tag{2.44}$$

where $\Gamma(s,x) = \int_x^\infty t^{s-1}e^{-t}\mathrm{d}t$ is the upper incomplete gamma function (Abramowitz and Stegun, 1948). Finally, the differential entropy for the rate distribution and the dispersion coefficient are derived as:

$$h(f_R) = -\log\left(\frac{a^2}{1+a\tau}\right) - \frac{3(1+e^{a\tau}\Gamma(0,a\tau)+(1+a\tau)\log\tau)}{1+a\tau} + \frac{2+a\tau}{1+a\tau}. \quad (2.45)$$

Expression for the dispersion coefficient is derived through Eq. (2.13),

$$C_h(R) = \frac{1+a\tau}{a}\exp\left\{-\log\left(\frac{a^2}{1+a\tau}\right) - \frac{3(1+e^{a\tau}\Gamma(0,a\tau)+(1+a\tau)\log\tau)}{1+a\tau} + \frac{2+a\tau}{1+a\tau} - 1\right\}. \quad (2.46)$$

This model of the shifted exponential distribution provides an insightful framework for understanding how neurons manage their firing rates following a refractory period, incorporating the complexity of neural firing dynamics into a quantifiable mathematical model.

2.3.5 Mixture of two exponential distributions with refractory period

The mixture of exponential distributions assumes that the ISIs are generated from multiple underlying exponential processes, each with its own characteristic rate parameter (Obeso et al., 2000; Dorval et al., 2008). This model is particularly effective in scenarios where neurons exhibit multiple operational modes—such as different phases of activity or varying responses to stimuli. For instance, a neuron might display a fast-firing mode under certain conditions and switch to a slower firing mode under others. Each mode can be represented by an exponential distribution with a different rate, and the overall ISI distribution is modeled as a weighted sum of these exponentials (Bhumbra and Dyball, 2004; Heil et al., 2007). Okada et al. (2020) demonstrated the use of mixtures of exponential distributions to model long-tailed distributions of inter-event times, providing a statistical framework for analyzing ISIs. Trapani and Nicolson (2011) found that in the lateral line organs of a zebrafish when the depolarizing currents were blocked, the ISI data of afferent neurons was best described by a mixture of exponential distribution.
The pdf of the mixed exponential distribution with refractory period $\tau \geq 0$ and mixture components with parameter $a > 0, b > 0, a \neq b$ is given by

$$f_T(t) = \begin{cases} 0, & t \leq \tau, \\ pae^{-a(t-\tau)} + (1-p)be^{-b(t-\tau)}, & t > \tau, \end{cases} \quad (2.47)$$

where $p \in (0,1)$. In this case,

$$\lambda = \frac{ab}{pb(1+a\tau)+(1-p)a(1+b\tau)}. \quad (2.48)$$

The analytical expressions for the C_V and C_h are difficult to obtain although they can be calculated numerically.

2.4 Biophysical models of neuronal dynamics

Biophysical models of neuronal dynamics are essential for unraveling the complex mechanisms governing neuronal behavior. These models integrate various factors like ion channels, membrane properties, and external influences to simulate and predict neuronal activity accurately, aiding in understanding brain function and neurological disorders.

2.4.1 Leaky integrate-and-fire model

The leaky integrate-and-fire (LIF) model is a simplified, yet realistic, neuronal model that describes the fundamental principles governing the electrical behavior of neurons (Lapicque, 2007). It represents the neuron's membrane potential $V(t)$ as it integrates incoming signals and leaks charge over time until a threshold is reached, prompting an action potential (Gerstner and Kistler, 2002; Burkitt, 2006). The behavior of the depolarization $V(t)$ of the neuronal membrane is described by the differential equation

$$d\mathrm{V}(t) = \big(-\frac{V(t)}{\tau} + \mu \big) d\mathrm{t}, \quad V(t_j) = v_0, \tag{2.49}$$

where $\tau > 0$ is the membrane time constant ($\tau = RC$, where R is the membrane resistance and C is its capacitance) dictating the rate at which the membrane potential decays towards its resting potential in the absence of any input; $\mu \in \mathbb{R}$ is measured in mV per unit time, which reflects the input signal resulting from the dendritic currents generated by the sensory stimulation or action of other neurons; t_j is the moment of the last firing of an action potential with the condition $t > t_j$ ensuring that the equation describes the membrane potential after the last spike. The solution to this equation is:

$$V(t) = \exp\big(-\frac{1}{\tau}(t - t_j) \big) v_0 + \mu\tau \big[1 - \exp\big(-\frac{1}{\tau}(t - t_j) \big) \big], \tag{2.50}$$

with asymptotic voltage given by $V(\infty) = \mu\tau$. The model postulates that the firing of an action potential occurs when V first surpasses a firing threshold S, where $S > v_0$. Following a spike, the membrane potential resets to v_0, typically 0mV. If $s = t_{j+1} - t_j$ represents the ISI length, then the voltage at the next firing instant is:

$$V(t_{j+1}) = \exp\left(-\frac{s}{\tau} \right) v_0 + \mu\tau \left[1 - \exp\left(-\frac{s}{\tau} \right) \right]. \tag{2.51}$$

Given constant input μ, the ISIs are consistent, defining the firing frequency as:

$$f(\mu) = 1/s = \frac{1}{\tau \ln\left(\frac{\mu\tau}{\mu\tau - S} \right)}, \tag{2.52}$$

illustrating how the firing frequency increases with μ and approaches infinity as μ increases substantially. The relationship, known as the gain function or transfer function, shows how neuronal firing frequency adapts based on input intensity and the decay dynamics dictated by τ.

2.4.2 Leaky integrate-and-fire model with reversal potentials

The LIF model incorporating reversal potentials enhances the classical LIF framework by introducing reversal potentials, providing a more detailed representation of neuronal dynamics. This extension allows the model to capture the impact of excitatory and inhibitory inputs more accurately. Originally, Stein's stochastic neuronal model, which includes reversal potentials, provides an insight into neuronal behavior under stochastic conditions (Stein, 1970; Lánský and Lánská, 1987). The differential equation describing this model is:

$$d\mathrm{V(t)} = -\frac{V(t)}{\tau}d\mathrm{t} + a(V_E(t) - V(t))d\mathrm{N(t)} + i(V(t) - V_I(t))d\mathrm{M(t)}, \quad V(t_j) = v_0, \tag{2.53}$$

where $\tau > 0$ continues to signify the membrane time constant, and a and i are constants representing the strengths of excitatory and inhibitory inputs, respectively, with excitatory and inhibitory reversal potentials denoted by V_E and V_I.

The terms $N(t)$, $M(t)$ represent independent homogeneous Poisson processes with specific intensities, modeling the arrival of synaptic inputs. These processes underscore the inherent variability in neuronal firing, with a and i indicating the proportionate changes in membrane potential per input pulse. The depolarization decreases as the membrane potential approaches the excitatory reversal potential V_E, and hyperpolarization diminishes as it nears the inhibitory reversal potential V_I, keeping the potential within these limits.

To formulate a deterministic counterpart of model (2.53), a reconfiguration of the model parameters $\{\lambda_n^+, \lambda_n^-, a_n, i_n\}$ is needed such that $\lambda_n^+ \to +\infty$, $\lambda_n^- \to +\infty$, $a_n \to 0_+$, $i_n \to 0_-$, fulfilling the condition $\lambda_n^+ a_n \to \mu_E > 0$ and $\lambda_n^- i_n \to \mu_I < 0$. This adjustment ensures that while the rate of synaptic events escalates, their individual impact diminishes but in such a way that the overall impact of the excitatory and inhibitory input on the neuron, represented by μ_E and μ_I respectively, remain constant. The resulting deterministic model, reflecting the average effects of synaptic inputs, is represented by:

$$\mathrm{d}V(t) = \left(-(\frac{1}{\tau} + \mu_E - \mu_I)V(t) + \mu_E V_E(t) - \mu_I V_I(t)\right)\mathrm{d}t. \tag{2.54}$$

This model differs from the classical LIF model by considering the effects of excitatory and inhibitory inputs on the leakage time constant. The asymptotic voltage of this model is:

$$V(\infty) = \frac{\mu_E V_E - \mu_I V_I}{\frac{1}{\tau} + \mu_E - \mu_I}, \tag{2.55}$$

which, unlike the classical LIF model, remains finite even as excitation μ_E increases indefinitely. The effective time constant $\tau_{ef} = \tau/(1 + \tau\mu_E - \tau\mu_I)$ and the effective input $\mu_{ef} = \mu_E V_E - \mu_I V_I$ dictate the firing frequency as:

$$f_a = \frac{S(V_E - \tau\mu_I(V_E - V_I))}{\tau V_E(V_E - S)\ln^2(V_E/(V_E - S))} + \frac{(1/\tau - \mu_I)}{\ln(V_E/(V_E - S))} + \frac{\mu_E}{\ln(V_E/(V_E - S))}. \tag{2.56}$$

2.4.3 Two point leaky integrate-and-fire model

The two-point LIF model represents an advanced iteration of the classic LIF framework that can capture the dual-compartmental nature of neuronal dynamics. This model distinguishes itself by simulating the neuron as comprising two interconnected points or compartments: one representing the soma (cell body) and the other representing the dendritic structure.
The relevance of such a model is underscored by research that highlights the importance of dendritic processing in neural computation. Studies have shown that dendrites are not merely passive conduits for electrical signals but actively participate in neural computation, significantly influencing the output of the neuron (Häusser et al., 2000; Poirazi et al., 2003; London and Häusser, 2005; Ujfalussy et al., 2015). The two-point LIF model, by incorporating this dual-compartment approach, offers a framework to explore these complex interactions within neurons.

In Lánský and Rodriguez (1999) the coding properties of a two-point neuronal model based on two LIF models were studied. The governing equations for the membrane potentials $V_1(t)$ and $V_2(t)$ in the dendritic and somatic compartments, respectively, are given by:

$$\mathrm{d}V_1(t) = \left(-\frac{V_1(t)}{\tau} + \frac{V_2(t) - V_1(t)}{\tau_r} + \mu\right)\mathrm{d}t \tag{2.57}$$

and

$$\mathrm{d}V_2(t) = \left(-\frac{V_2(t)}{\tau} + \frac{V_1(t) - V_2(t)}{\tau_r}\right)\mathrm{d}t, \tag{2.58}$$

where $\tau > 0$ is the same time constant as in Eq. (2.49) and $\tau_r > 0$ is a junctional time constant representing the conductance between the compartments. These equations describe the leakage through the membrane, the electrical coupling between compartments, and the input received by the soma. The initial conditions for these dynamics specify that when the somatic $V_2(t)$ reaches the firing threshold S, $V_2(t)$ resets to 0, while the dendritic compartment $V_1(t)$ continues evolving without reset. This indicates no backward spike propagation into the dendrite. The asymptotic solutions for the dendritic and somatic potentials are:

$$V_1(\infty) = \frac{\tau(\tau + \tau_r)\mu}{2\tau + \tau_r} \tag{2.59}$$

and

$$V_2(\infty) = \frac{\tau^2\mu}{2\tau + \tau_r}. \tag{2.60}$$

Firing occurs when the stimulation μ is sufficient, i.e., the asymptotic depolarization at the somatic compartment $V_2(\infty)$ exceeds the firing threshold S. The condition for rheobase stimulation is derived from this requirement:

$$\mu_0 = \frac{S}{\tau}\frac{\tau_r + 2\tau}{\tau}. \tag{2.61}$$

The general solutions for the membrane potentials during suprathreshold stimulation are given by complex expressions that stabilize to constant interspike

intervals (ISIs) in a steady state:

$$\begin{aligned} V_1(t) =& V_1(\infty) + \frac{1}{2}\exp\left(-\frac{1}{\tau}(t-t_j)\right)(-\mu\tau + V_1(t_j)) \\ & - \frac{1}{2}\exp\left(-\frac{\tau_r+2\tau}{\tau_r\tau}(t-t_j)\right)\left(\frac{\tau_r\tau\mu}{\tau_r+2\tau} - V_1(t_j)\right) \end{aligned} \tag{2.62}$$

and

$$\begin{aligned} V_2(t) =& V_2(\infty) + \frac{1}{2}\exp\left(-\frac{1}{\tau}(t-t_j)\right)(-\mu\tau + V_1(t_j)) \\ & + \frac{1}{2}\exp\left(-\frac{\tau_r+2\tau}{\tau_r\tau}(t-t_j)\right)\left(\frac{\tau_r\tau\mu}{\tau_r+2\tau} - V_1(t_j)\right), \end{aligned} \tag{2.63}$$

where t_j is the time instant of the last spike emission, $t > t_j$. Solving these equations for long-lasting suprathreshold stimulation, the system achieves its steady-state characterized by a constant $V_1(t_j)$ for each j leading to constant ISIs.

Given the system reaches steady-state under long-lasting suprathreshold stimulation, and considering two consecutive spikes at times t_j and t_{j+1} with an ISI length $s = t_{j+1} - t_j$, the firing frequency f can be derived as,

$$1 - \frac{\mu}{\mu_0} = \left(e^{-\frac{1}{\tau f}} + e^{-\frac{\tau_r+2\tau}{\tau_r\tau f}}\right)\left(\frac{1}{2} - \frac{\mu}{\mu_0}\right) + \frac{\mu}{\mu_0}e^{-\frac{2(\tau_r+\tau)}{\tau_r\tau f}}, \tag{2.64}$$

This equation captures the dynamics of firing frequency as a function of the input μ and the threshold μ_0 defined by the minimum required stimulation to trigger firing. The input-output transfer function of the model, which describes how the firing frequency escalates with increasing stimulation μ, is represented by,

$$f_a = -\frac{1}{2\tau}\frac{\tau_r+2\tau}{\tau_r+\tau} + \frac{\tau}{S(\tau_r+\tau)}\mu. \tag{2.65}$$

This formulation provides a comprehensive understanding of how the dual-compartment nature of the neuron processes and responds to synaptic inputs, defining both the transient and steady-state behavior of the neuronal firing dynamics.

2.4.4 Two point leaky integrate-and-fire model with reversal potentials

To address the limitations encountered in previous neuronal models, particularly the issue of infinite firing rates, we can extend the two-point model by incorporating dynamics that include reversal potentials. This is achieved by integrating the modifications from the model (2.54) into the two-compartment framework of equations (2.57) and (2.58). The revised model equations are as follows:

$$\mathrm{d}V_1(t) = \left(-(\frac{1}{\tau} + \mu_E - \mu_I)V_1(t) + \frac{V_2(t) - V_1(t)}{\tau_r} + \mu_E V_E(t) - \mu_I V_I(t)\right)\mathrm{d}t \tag{2.66}$$

and

$$\mathrm{d}V_2(t) = \left(-\frac{V_2(t)}{\tau} + \frac{V_1(t) - V_2(t)}{\tau_r} \right) \mathrm{d}t. \tag{2.67}$$

In these equations, the inclusion of the effective time constant $\tau_{ef} = \tau/(1 + \tau\mu_E - \tau\mu_I)$ and the effective input $\mu_{ef} = \mu_E V_E - \mu_I V_I$ allows for a more realistic representation of synaptic dynamics. The asymptotic behavior of the model provides insights into the long-term dynamics of the membrane potentials in both compartments:

$$V_1(\infty) = \frac{\mu_{ef}(\tau_r + \tau)}{1 + \tau_{ef}(\tau_r + \tau)}, \tag{2.68}$$

$$V_2(\infty) = \frac{\mu_{ef}\tau}{1 + \tau_{ef}(\tau_r + \tau)}. \tag{2.69}$$

These expressions reveal how the equilibrium potentials are influenced by both the intrinsic properties of the neuron and the external inputs modulated through excitatory and inhibitory mechanisms.

Although an analytical expression for the firing rate is challenging to derive for this complex model, numerical methods can be employed to calculate the firing rates for given parameter sets. This approach allows for an exploration of the neuron's response under various physiological conditions, enhancing our understanding of neural responsiveness and stability in a biologically plausible framework.

2.5 Spiking neuron models

While the leaky integrate-and-fire models offer a simplified approach to understanding neuronal dynamics, capturing only the basic elements of membrane potential changes, they lack the physiological details necessary to accurately describe more complex behaviors seen in real neurons. Spiking models bridge this gap by providing detailed mechanisms of action potential generation and propagation, specifically through the use of voltage-dependent ion channels.

Exponential integrate-and-fire model

To address the limitations of traditional LIF models and add biophysical realism, conductance-based models like the Hodgkin-Huxley model were developed (Hodgkin and Huxley, 1952). These models include detailed representations of ionic currents and are capable of capturing the intricate dynamics of neuronal action potentials. However, the complexity of these models, which may involve tuning hundreds of parameters, makes them less practical for certain applications (Roth and Häusser, 2001; Bower and Beeman, 2012).

This complexity and the realization that some behaviors can be accurately modeled with fewer parameters led to the development of generalized integrate-and-fire models. These models, such as the quadratic (Ermentrout, 1996; Latham et al., 2000) and exponential integrate-and-fire models (Fourcaud-Trocmé et al., 2003), address the shortcomings of both the simple LIF and the complex

Hodgkin-Huxley models by introducing a smoother spike initiation zone, adding subthreshold dynamics or adaptation mechanisms (Izhikevich, 2003; Richardson et al., 2003), and varying the input simulation from current to conductance-based (Destexhe et al., 2003). These generalizations provide a more realistic approach to modeling neuronal behavior while maintaining computational simplicity.

The adaptive exponential integrate-and-fire (AdEx) model emerges as a synthesis of these efforts. It incorporates the exponential mechanism for spike initiation and an adaptation equation that allows it to capture a wide range of neuronal behaviors observed in biological systems. The equation describes the model:

$$C\frac{\mathrm{d}V}{\mathrm{d}t} = -g_L(V - E_L) + g_L k_a \exp\left(\frac{V - S}{k_a}\right) + w + I, \tag{2.70}$$

where g_L is the leak conductance, E_L is the resting potential, w is an adaptation variable, I is the injected current. The slope factor k_a and threshold potential V_T characterize the exponential function. When the voltage reaches a threshold (for e.g. 20mV), a spike is triggered and the voltage sets to a reset value V_r, with $V_r = E_L$. In the case that $k_a \to 0$ the model transforms into a standard integrate-and-fire model with firing threshold S (Lapicque, 2007). The adaptation current w is described by the following equation:

$$\tau_w \frac{\mathrm{d}w}{\mathrm{d}t} = a(V - E_L) - w, \tag{2.71}$$

where τ_w is a time constant and a is the sub-threshold adaptation. Every time a spike is triggered, the variable w increases by a fixed amount b. Hence, the adaptation variable w accumulates during a spike train, whereas voltage is reset to V_r.
The AdEx model can produce multiple firing patterns depending on the parameters, e.g. initial bursting, regularly bursting, tonic spiking, adapting, accelerating, irregular spiking, or delayed initiation. Additionally, this model is particularly notable for its ability to systematically extract model parameters from experimental data, enhancing its practical utility and relevance.

Spike frequency adaptation models

Another biological phenomenon that is not an inherent part of the above-described neuronal models is spike frequency adaptation (SFA). SFA is a phenomenon observed in many neurons where the firing rate decreases progressively during sustained input or after an initial burst of activity. SFA plays a crucial role in stabilizing neuronal network dynamics (Barranca et al., 2019). Different LIF models with SFA mechanisms have been shown to effectively replicate the activity of a variety of neurons (Rauch et al., 2003; Jolivet et al., 2008; Teeter et al., 2018). The biophysical mechanisms responsible for SFA can be grouped into two broad categories: inactivation of depolarizing currents or activation of hyperpolarizing currents (Gutkin and Zeldenrust, 2014). In integrate-and-fire models, SFA is implemented through either a dynamic firing threshold or hyperpolarizing currents.

Dynamic threshold models

This refers to the mechanisms by which the excitability threshold of a neuron changes dynamically, often in response to recent activity. Inactivation of sodium channels leads to a dynamic threshold in the LIF models where the equation for the membrane voltage remains exactly the same but another equation governing the spiking threshold is added to the dynamics (Benda et al., 2010). In models where threshold dynamics are integrated within the neuron's overall response properties, like the AdEx model, the dynamic threshold is modeled by introducing a slow-gating variable s that represents the inactivation of sodium channels during depolarization (Martina and Jonas, 1997; Benda and Herz, 2003; Benda et al., 2010). The variable $0 \leq s \leq 1$ that inactivates during depolarization, affects the exponential term which is linked to the spiking mechanism:

$$C\frac{\mathrm{d}V}{\mathrm{d}t} = -g_L(V - E_L) + g_L k_a \exp\left(\frac{V - S}{k_a}\right)(1 - s) + w + I, \tag{2.72}$$

$$\tau_w \frac{\mathrm{d}w}{\mathrm{d}t} = a(V - E_L) - w, \tag{2.73}$$

$$\frac{\mathrm{d}s}{\mathrm{d}t} = \alpha_s(V)(1 - s) - \beta_s(V)s, \tag{2.74}$$

where $\alpha_s(V)$ and $\beta_s(V)$ are the voltage-dependent rate functions for the activation and deactivation of the gating variable s.

Hyperpolarizing currents

Hyperpolarizing currents within a neuron make the membrane potential more negative relative to the resting potential. This current typically flows through specific ion channels and acts to decrease the likelihood of the neuron firing an action potential. Hyperpolarizing currents can be mediated by the influx of negatively charged ions (such as chloride ions) or the efflux of positively charged ions (such as potassium ions) from the neuron. After-hyperpolarization (AHP) currents are a specific type of hyperpolarizing current that occurs in neurons following the firing of an action potential, triggered by the influx of calcium ions. In integrate-and-fire models, this SFA mechanism is incorporated by adding potassium conductance that increases with each spike and decays exponentially to zero:

$$C\frac{\mathrm{d}V}{\mathrm{d}t} = -g_L(V - E_L) - g_L k_a \exp\left(\frac{V - S}{k_a}\right) - g_{\mathrm{AHP}}(t)(V - E_{\mathrm{K}}) + w + I, \tag{2.75}$$

$$\tau_w \frac{\mathrm{d}w}{\mathrm{d}t} = a(V - E_L) - w, \tag{2.76}$$

$$\frac{\mathrm{d}g_{\mathrm{AHP}}}{\mathrm{d}t} = -\frac{g_{\mathrm{AHP}}}{\tau_{\mathrm{AHP}}} + \sum_k \Delta_{\mathrm{AHP}}\delta(t - t_k), \tag{2.77}$$

where τ_{AHP} represents the time constant governing the decay of the hyperpolarizing conductance, Δ_{AHP} indicates the increment in conductance triggered by each action potential, and t_k denotes the times at which the neuron fires action potentials.

Spiking neural networks

Spiking neural networks (SNNs) are a class of artificial neural networks that more closely mimic the behavior of biological neural networks. These networks incorporate the precise timing of spikes to encode and process information, reflecting the dynamic nature of biological communication among neurons. The connectivity of neurons within an SNN can be described by a connectivity matrix $\mathbf{W}$ containing the synaptic weights. The membrane potential of the i-th neuron in a network of N neurons- where neurons $1, \ldots, N_{\text{exc}}$ are excitatory and neurons $N_{\text{exc}}, \ldots, N$ are inhibitory—is given by the following equations:

$$C\frac{\mathrm{d}V_i}{\mathrm{d}t} = -g_L(V_i - E_L) + I^i_{\text{ext}}, \tag{2.78}$$

$$I^i_{\text{ext}} = -g^i_{\text{exc}}(V_i - E^i_{\text{exc}}) - g^i_{\text{inh}}(V_i - E^i_{\text{inh}}), \tag{2.79}$$

$$\frac{\mathrm{d}g_{\text{exc}}}{\mathrm{d}t} = \frac{g_{\text{exc}}}{\tau_{\text{exc}}} + \sum_{j=1}^{N_{\text{exc}}} \sum_{t_s \in \mathcal{T}_j} w_{ji}\delta(t - t_s), \tag{2.80}$$

$$\frac{\mathrm{d}g_{\text{inh}}}{\mathrm{d}t} = \frac{g_{\text{inh}}}{\tau_{\text{inh}}} + \sum_{j=N_{\text{exc}}+1}^{N} \sum_{t_s \in \mathcal{T}_j} w_{ji}\delta(t - t_s), \tag{2.81}$$

where w_{ij} represents the synaptic strength from the j-th neuron to the i-th neuron, $\mathcal{T}_j$ are the times at which the j-th neuron fires action potentials.

2.6 Insect Olfactory System

Insects navigate their complex chemical environments primarily through an evolved olfactory system, with olfactory receptor neurons (ORNs) playing an important role in detecting a vast array of volatile compounds. These compounds, ranging from pheromones to diverse volatile plant compounds (VPCs), inform behaviors critical for survival and reproduction (Hansson and Stensmyr, 2011; Knudsen et al., 2006). Understanding the mechanisms of olfactory detection and processing in insects thus offers insights into fundamental principles of sensory neuroscience and ecological interactions (Conchou et al., 2019). In my thesis, I focus on principles of efficient information processing that these ORNs employ in complex environments (Conchou et al., 2020; Gupta and Stopfer, 2014).

2.6.1 Olfactory receptor neurons and the role of volatile plant compounds

ORNs are essential components of the insect olfactory system, specialized for the detection of odor molecules. Located predominantly on the antennae, these neurons are equipped with receptor proteins that bind specific volatile compounds, initiating a cascade of cellular events leading to the generation of neural signals (Hansson and Stensmyr, 2011). This specificity allows insects to detect and discriminate among a wide variety of olfactory cues, from pheromones crucial for reproductive communication to volatile plant compounds (VPCs) that indicate food sources or potential hazards (Knudsen et al., 2006). We focus on the moth ORNs that are tuned to sex pheromones for our study.

Historically, the interaction between ORNs and VPCs has been a subject of significant interest, particularly concerning how VPCs interfere with the detection of pheromones. Studies have shown that certain VPCs can modulate the activity of ORNs, affecting the firing rate and altering the neural representation of pheromone signals (Party, V et al., 2009). This modulation is not just about the competition for receptor sites but involves complex adjustments in the response properties of neurons. VPCs have been found to increase response variability in ORNs, besides altering qualitative and quantitative coding (Dupuy et al., 2017). The findings in Conchou et al. (2021) suggest that VPCs can impact the firing of MGC neurons, masking the response to pheromones.

While considerable research has focused on the impact of VPCs on the firing rates of ORNs, less attention has been given to how these interactions affect the overall information-processing capabilities of the olfactory system. Firing rate changes, while indicative of neural activity modulation, do not fully capture the nuances of information encoding and decoding within these sensory neurons. Our study aims to bridge this gap by examining not just how VPCs influence the firing rates of ORNs but more crucially, how they impact the processing and encoding of information. By focusing on the information-theoretic aspects of ORN responses, we aim to explore the deeper implications of VPC interference on olfactory signaling.
To this end, we stimulated the ORNs of male *Agrotis ipsilon* with intermittent puffs of pheromone against varying concentrations of VPC backgrounds to mimic the natural environment. Each pheromone-responsive ORN was recorded during an 8-minute sequence, consisting of two distinct 40-second stimulations separated by a 2-minute gap. Each 40-second stimulation involved repeating the same 2-second trial 20 times. This trial comprised a sequence of short pheromone puffs and blanks of random durations, generated using a white noise pattern, where the durations of puffs and blanks followed an exponential distribution. Meanwhile, the background was either (1) absent (control stimuli) or (2) delivered continuously. The background onset started 2 ms before the pheromone stimulation to assess the response of pheromone-responsive ORNs to individual VPCs. The order of presentation for the two distinct stimulations—pheromone with no background and pheromone with continuous background—was randomized. The analysis included 186 ORNs recorded over two distinct 40-second stimulations per ORN: one with pheromone and no background, and another with pheromone and a background of (Z)-3-hexenyl acetate or linalool. The minimum and maximum number of neurons per VPC concentration were 11 and 21, respectively. During high-concentration VPC backgrounds, some neurons stopped responding altogether; these neurons were excluded from the analysis.

This approach allows us to investigate the sophisticated mechanisms by which moths navigate their olfactory environment, providing insights into the resilience and adaptability of the olfactory system in a world of complex and dynamic chemical landscapes.

2.6.2 Firing Rate Estimation

The firing rate of ORN was estimated with kernel density estimation using a Gaussian kernel (Shimazaki and Shinomoto, 2010; Tomar, 2019)

$$\lambda_t = \sum_{i=1}^{N} K_w(t - t_i) \tag{2.82}$$

where t_i is the spike time and $K_w(s)$ is the normal distribution bandwidth $w = 20ms$, defined as

$$K_w(s) = \frac{1}{\sqrt{2\pi}w} \exp -\left(\frac{s^2}{2w^2}\right). \tag{2.83}$$

2.6.3 Neural response model fitting

To assess the impact of a VPC background on ORNs' ability to encode pheromone signals, we formulated two models. The first model quantifies the neuronal response solely to pheromones. It uses a Gaussian kernel for firing rate estimation and a weighted history function to incorporate the influence of firing rates from the preceding 200ms, diminishing progressively over 4 time bins. The probability of detecting a pheromone at a specific time bin j, denoted as prob_j, is modeled using the logistic function:

$$\text{prob}_j = \frac{e^{\beta_0 + \beta_1 * \lambda_j + \beta_2 * w_j}}{1 + e^{\beta_0 + \beta_1 * \lambda_j + \beta_2 * w_j}}, \tag{2.84}$$

where λ_j represents the firing rate at time bin j, w_j denotes the weighted history at time bin j, and β_0, β_1 and β_2 are regression coefficients derived from the model. The second model incorporates the VPC background to evaluate its modulatory effects on the neuronal encoding of pheromone signals. This approach allows us to compare how VPCs influence pheromone perception in a dynamic environmental context. We assess model performance using the Area Under the Receiver Operating Characteristic Curve (AUC-ROC), where high AUC values suggest effective differentiation between the presence and absence of pheromone signals. The average AUC value for trial k across all neurons, considering the VPC type and concentration, is given by:

$$a_k = \frac{1}{m} \sum_{i=1}^{m} a_{k,i}. \tag{2.85}$$

This metric facilitates a comprehensive analysis of the models under various VPC conditions, providing insights into the nuanced interactions between VPCs and pheromone signal processing.

2.6.4 Stimulus prediction model

To quantify the impact of a VPC background on the encoding efficiency of ORNs for pheromone signals, we employed logistic regression. Utilizing predictor variables of firing rate and weighted history, we initially trained the logistic model on three trials and then used it to predict pheromone presence across 16 subsequent trials

under each background condition. The first trial was excluded from training due to the high firing rates exhibited by ORNs, as they tend to adapt in the later trials. Trials of 2 seconds were subdivided into 200 bins of 10ms, during which firing rates were calculated under control (λ_{air}) and VPC-enhanced (λ_{VPC}) backgrounds. Model accuracy in predicting stimulus conditions was evaluated, with "prediction accuracy" reflecting the proportion of correct predictions:

$$p_k = \frac{1}{m} \sum_{i=1}^{m} p_{k,i} \tag{2.86}$$

where $p_{k,i}$ represents the accuracy for neuron i in trial k, and m is the number of neurons. To determine the efficiency of prediction relative to the neuron's spiking activity, we calculated the average prediction accuracy per spike, p_k^*, which adjusts for the number of spikes $a_{k,i}$ fired by neuron i:

$$p_k^* = \frac{1}{m} \sum_{i=1}^{m} \frac{p_{k,i}}{a_{k,i}} \tag{2.87}$$

This metric provides a normalized measure of model performance on a per-spike basis, enhancing our understanding of neuronal efficiency under varying sensory conditions.

2.6.5 Mutual Information

Information theory is crucial for quantifying neuronal information transfer, specifically how neuronal spike trains reflect external stimuli (Shannon, 1948; Quian Quiroga and Panzeri, 2009; Kostal et al., 2013).
Entropy measures the uncertainty of a random variable X as:

$$H(X) = \sum_x P(x) \log_2 P(x), \tag{2.88}$$

where X is distributed according to $P(X)$, measured in *bits* for logarithms base 2. *Conditional entropy*, for two variables X and Y, quantifies the uncertainty of X given Y:

$$H(X|Y) = \sum_y P(y) H(X|Y = y). \tag{2.89}$$

This metric assesses how Y influences the uncertainty in X.
Mutual information ($I(R, S)$) evaluates the reduction in uncertainty about a stimulus (S) given the neural response (R):

$$I(R, S) = H(S) - H(S|R). \tag{2.90}$$

In our analysis, we computed mutual information between the stimulus and the response for a particular trial k of a given concentration d, using spike data from neurons under different VPC concentrations, denoted by $I_{k,d}(R_{k,d}, S_{k,d})$. To assess efficiency, we derived mutual information per spike for each trial by:

$$I_k(R_k, S_k) = \frac{I_{k,d}(R_{k,d}, S_{k,d})}{a_{k,d}}, \tag{2.91}$$

where $a_{k,d}$ is the number of spikes in trial k under a given VPC background condition d. This approach quantifies the efficiency of information transfer per spike across different experimental conditions.

3. Results

3.1 Comprehensive overview of firing rate estimation methods

Attachment I

Neuronal firing rate estimation is an essential tool for interpreting neural activity and understanding the underlying mechanisms of information processing in the brain (Dayan and Abbott, 2005). The firing rate, generally defined as the number of action potentials per unit of time, is a fundamental metric for quantifying neuronal output. The problem of firing rate estimation, especially if the rate itself is not stable but evolves over time, has been a topic of significant interest for researchers (Cunningham et al., 2009; Davis et al., 2011). The methodologies for estimating this rate have evolved significantly, each with its own set of assumptions, advantages, and limitations. We wrote a comprehensive review of firing rate estimation methods, examining their theoretical foundations, application contexts, and implications for neural data analysis.

Early attempts at firing rate estimation relied heavily on simple time window averaging, where the count of spikes within predefined intervals was normalized by the duration of those intervals (Gerstein and Kiang, 1960; Johnson, 1978). This method, while straightforward, introduced variability related to the choice of window size, often requiring a balance between temporal resolution and statistical reliability.

Advancements in computational techniques led to the adoption of kernel-based methods, offering a more sophisticated approach to firing rate estimation (Nawrot et al., 1999; Shimazaki and Shinomoto, 2007; Cherif et al., 2008; Shimazaki and Shinomoto, 2010). By convolving spike trains with a predefined kernel function, these methods produce a continuous estimate of the firing rate over time. The choice of kernel, typically Gaussian or exponential, influences the smoothness and responsiveness of the rate estimate. Kernel-based methods highlight the importance of parameter selection, where kernel width plays a critical role in capturing the dynamics of neuronal firing patterns.

Further refinement of firing rate estimation methodologies introduced Bayesian frameworks, incorporating prior knowledge and probabilistic models to infer firing rates (Dimatteo et al., 2001; Cunningham et al., 2007; Endres et al., 2007; Mochizuki and Shinomoto, 2014; Ahmadi et al., 2018). These approaches allowed for the estimation of firing rates as probabilistic distributions, providing means to quantify uncertainty in the rate estimates. Additionally, adaptive methods emerged, capable of adjusting estimation parameters in real-time based on the characteristics of the spike train, thus enhancing the accuracy of firing rate reconstructions in varying neural activity regimes.

The evolution of firing rate estimation methods from simple averages to complex computational models reflects the growing understanding of neural coding mechanisms. Each method offers a unique lens through which neuronal activity can be interpreted, highlighting the diverse temporal and spatial scales at which neural information processing occurs. The choice of estimation method, therefore, is not merely a technical consideration but a reflection of the underlying hypotheses re-

garding neural function and information flow. This review of firing rate estimation methods was published in the journal *Biosystems* (Tomar, 2019).

3.2 Variability and randomness in instantaneous rate analysis

Attachment II

While the above section highlighted the firing rate estimation methods in non-stationary processes, in this study we focus on a specific class of stationary point processes called the renewal point process. Renewal processes are often used to model the activity of spontaneously active cells (Tuckwell, 1990). For a special subclass of renewal point processes, called the *equilibrium renewal processes*, the mean instantaneous firing rate is equal to the mean firing rate.
Our goal is to determine if analyzing the instantaneous firing rate within these processes offers any additional insight. To do this, we compared the dispersion coefficients for ISIs with those for the instantaneous rate.

For the gamma distribution, we find that the dispersion measures $C_V(T)$ and $C_V(R)$ are linked by the equation $C_V(R) = C_V(T)/\sqrt{1 - C_V(T)^2}$ (Fig. 5A). This result shows that the variability and randomness of the instantaneous firing rate can diverge significantly from those of the ISIs. It indicates that the instantaneous firing rate might reveal different aspects of neuronal dynamics that are not evident through ISI analysis alone.

For the lognormal distribution, there is a "symmetric" relationship between $f_T(t)$ and $f_R(r)$ (Kostal et al., 2018), $f_R(r; \lambda) = f_T(r; 1/\lambda)$, i.e. the shape of the probability distributions of ISI and instantaneous rates are the same for $\lambda = 1$. Furthermore, the relationship between $C_V(T)$ and $C_V(R)$ is that of an identity (Fig. 5A). The same holds for the relationship between $C_h(T)$ and $C_h(R)$ (Fig. 5B). Since the inverse Gaussian distribution also satisfies the "symmetrical" property, the relationship between the dispersion measures of ISI and the instantaneous rate is of identity for this distribution as well. This consistency across domains supports the idea that certain statistical properties of neuronal firing are invariant to the perspective from which they are analyzed, be it temporal or rate-based.

For shifted exponential distribution, since $C_V(T)$ depends on the firing rate and the refractory period through the equation $C_V(T) = 1 - \lambda\tau$, we varied the values of these parameters in order to analyze the relationship between $C_V(T)$ and $C_V(R)$ (Fig. 5A). This section highlights how physiological constraints, such as the inability of a neuron to fire immediately after an action potential, influence the statistical characteristics of neuronal activity.

For the mixed exponential distribution, since the analytical expressions are difficult to obtain we used a few different set of parameter values to look at the behavior of dispersion coefficients. To emphasize the significance of our findings, we applied our analysis to experimental data from the study of spontaneously active afferent neurons in the Zebrafish lateral line by Song et al. (2018). This

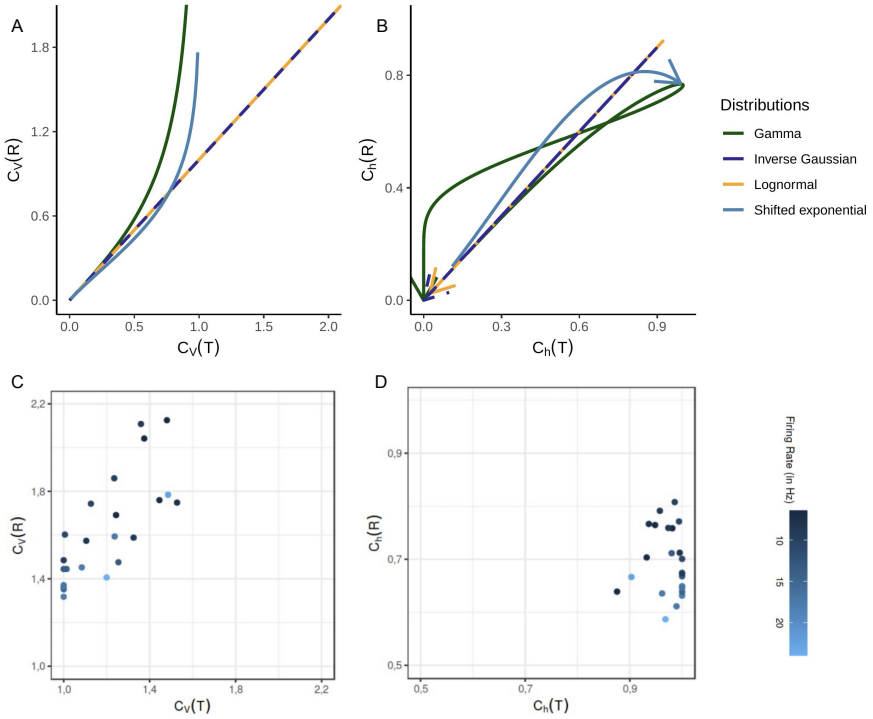

Figure 5: Exploring the relationship between statistical dispersion in interspike intervals (ISIs) and instantaneous rate across distributions and experimental data. A and **B** illustrate the relationship between the C_Vs C_hs of the interspike interval and instantaneous rate. The relationship is not straightforward due to the fact that rate distribution is obtained from length-biased sampling of ISIs. **C** $C_V(T)$ and $C_V(R)$ reveal separate aspects of the data sets. Overall $C_V(R)$ helps differentiate among the data sets with similar $C_V(T)$ values. **D** We can see that $C_h(R)$ further differentiates the data sets with equal $C_h(T)$. The data sets which might have similar randomness on the ISI scale, can be differentiated on the basis of their instantaneous rate randomness.

AA

application showed that instantaneous rate dispersion measures can offer a new perspective on the data, distinct from what is provided by ISI dispersion measures (Fig. 5C and 5D).

Our findings suggest that the instantaneous firing rate's variability and randomness are not merely reflections of ISI properties, this is due to the fact that the instantaneous rate distribution is obtained from a length-biased sampling of the ISIs (Eq. 2.3). Moreover, we illustrate that different models of neuronal firing can exhibit unique relationships between temporal variability and rate variability, offering new perspectives on how information may be encoded and processed in neural circuits. This study contributes to a comprehensive examination of the instantaneous firing rate. The results were published in the journal *Frontiers in Computational Neuroscience* (Tomar and Kostal, 2021).

3.3 Intrinsic firing rate saturation in neuronal models

Attachment III

In our published study, we concentrated on intrinsic firing rate saturation across four simplified neural models: the basic leaky integrate-and-fire (LIF) model, the LIF model with reversal potentials, a two-point LIF model, and a two-point LIF model incorporating reversal potentials. The term "two-point" refers to models that consider two nodes (representing dendritic and somatic compartments) instead of a singular (somatic) node, providing a more detailed simulation of neuronal behavior.

Our analysis primarily revealed that the inclusion of reversal potentials significantly influences the firing rate's response to input currents. While reversal potentials elevate the slope of the firing rate versus input curve by reducing the effective membrane time constant, they do not inherently lead to saturation of the firing rate. Interestingly, the two-point model without reversal potentials exhibited no limitations on voltage or firing rate, demonstrating that the model's structure alone does not guarantee a realistic saturation effect.

In contrast, the two-point model with reversal potentials marked a crucial finding of our study. This configuration not only limited the maximum attainable voltage but also limited the firing rate, showcasing a built-in saturation frequency. For increasing μ_E the depolarization V_1 at the dendritic compartment is limited by V_E. Using this with Eq. (2.67) yields the maximum firing frequency,

$$f_{max} = \frac{\tau + \tau_r}{\tau\tau_r \ln\left(\frac{V_E\tau}{V_E\tau - S(\tau+\tau_r)}\right)}, \tag{3.1}$$

where τ is the membrane time constant, τ_r is the junctional time constant and S is the firing threshold.
This is a significant departure from common neuronal models, which often require external mechanisms, such as absolute refractory periods, to impose a ceiling on firing rates. For a thorough analysis, we compared the transfer functions across models as seen in Fig. 6. These comparisons highlighted distinct behaviors in how each model approaches its firing rate limit, with the two-point model with reversal potentials demonstrating a clear saturation effect – a characteristic more aligned with observed neuronal behavior than unlimited firing rates suggested by simpler models.

Our findings underscore the importance of model selection in neuronal simulations. The intrinsic firing rate saturation observed in the two-point model with reversal potentials offers a closer approximation to biological neuron behavior, particularly under conditions of high input currents. This work contributes a crucial perspective to the understanding of neuronal firing mechanisms, suggesting that more complex models can provide insights into the limitations of neuronal firing rates that simpler models cannot. The outcomes of this investigation were detailed in our publication in the journal *Biosystems* (Tomar et al., 2022).

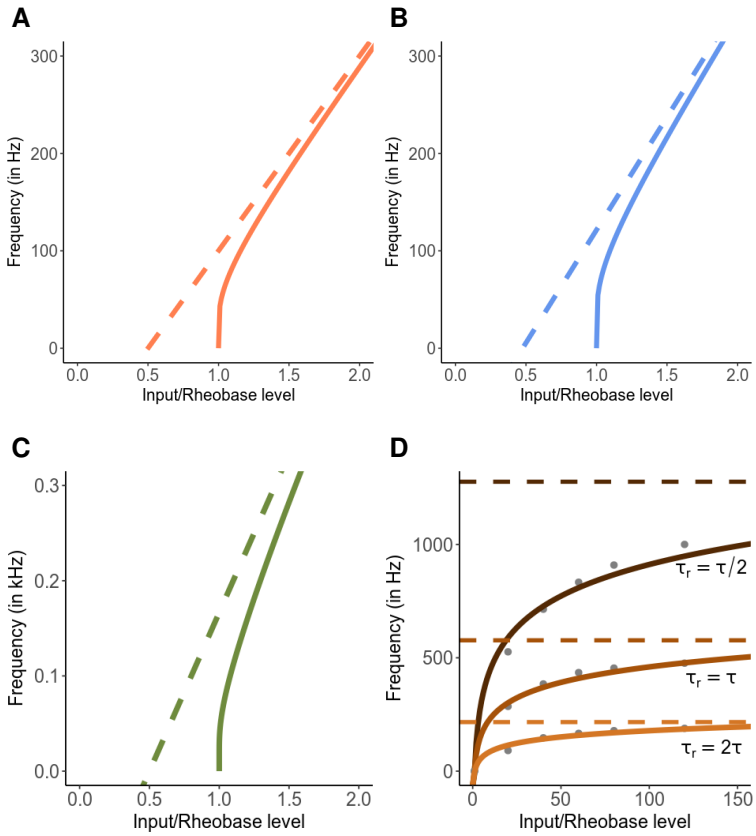

Figure 6: Transfer function plots for different leaky integrate-and-fire (LIF) neuron models with input normalized to rheobase. A Transfer function of a standard LIF neuron model. (B) LIF model with incorporation of a reversal potential with μ_I set to 0. (C) Two-point LIF model with parameter values set at $\tau = 5$ms, $\tau_r = 2.5$ms and $S = 15$mV. (D) Two-point LIF model with reversal potential, with parameter values set at $\tau = 5$ms, $S = 15$mV, $V_E = 60$mV, $V_I = -10$mV and τ_r is 2.5ms, 5ms and 10ms for the different cases. There is an intrinsic saturation of the firing frequency.

3.4 Efficient information transmission in moth olfactory receptor neurons

Attachment IV

In our investigation into the coding efficiency of moth pheromone receptor neurons (Phe-ORNs) against a backdrop of volatile plant compounds (VPCs), we aim to explore the impact of environmental odors on insect sensory processing. Utilizing the olfactory system of male *Agrotis ipsilon* moth as our model, we expose ORNs to intermittent puffs of pheromone amidst varying concentrations of VPCs, namely linalool and (Z)-3-hexenyl acetate, to simulate naturalistic olfactory scenes. Our findings reveal a complex relationship where high VPC concentrations significantly influence the ORN response to pheromone signals, ultimately affecting the moth's ability to navigate its olfactory landscape.

We found that (Z)-3-hexenyl acetate and linalool at high concentrations activate neuronal firing, leading to a suppression of the neuronal response to pheromones

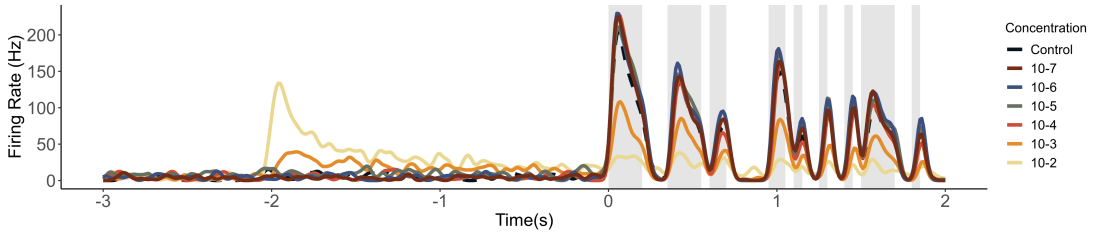

Figure 7: The inhibiting effect of various concentrations of (Z)-3-hexenyl acetate on the neural response in moth ORNs. Average firing rate of ORNs when exposed to (Z)-3-hexenyl acetate at -2s and pheromone introduced at 0s (indicated by the grey shaded area). The control is represented by the black dashed line.

as seen in Fig. 7. This effect suggests that the presence of VPCs at certain concentrations can interfere with the neurons' ability to respond to pheromones, potentially impacting the moth's olfactory navigation capabilities. This suppression was most pronounced at the highest tested concentrations of VPCs, suggesting a threshold beyond which the presence of environmental odors begins to interfere with pheromone detection. Through information theoretical methods, we quantify the impact of VPC background on the information transmission abilities of these ORNs.

The study examines the ORN's coding efficiency through logistic regression models, comparing the presence or absence of pheromones amidst varying odor backgrounds. Despite the overall suppression of neuronal firing rates by high VPC concentrations, the coding efficiency of ORNs—measured by prediction accuracy per spike—increases. Additionally, the mutual information per spike, which quantifies the amount of information a single spike conveys about the stimulus, was found to increase at higher VPC concentrations. This increase aligns with the previous observations. These findings suggest that while the neurons may fire less frequently in the presence of high VPC concentrations, each spike carries more information about the presence of pheromones, indicating an enhancement in signal encoding efficiency under these conditions.

To ensure that the improvement in coding efficiency at high VPC concentrations is not merely a result of neural adaptation to repetitive stimuli but is an independent effect of the VPC concentration levels themselves, we compared neurons with equal average firing rates exposed to varying concentrations of VPC. If the improved per-spike prediction accuracy was an effect of adaptation, then we would expect all neurons with similar firing rates to show similar prediction accuracies, regardless of the VPC concentration they were exposed to. However, we found that neurons exposed to higher concentrations of VPCs had better prediction accuracy per spike, even when their firing rates were comparable to those of neurons exposed to lower VPC concentrations. This finding suggests that the presence of high VPC concentrations itself, rather than any form of neural adaptation to repeated stimulus exposure, enhances the neuron's ability to encode pheromone signals.

Our results highlight a fascinating ecological interaction, where environmental odors, rather than merely obstructing pheromone detection, may play an important role in enhancing the coding efficiency of Phe-ORNs. This enhancement suggests

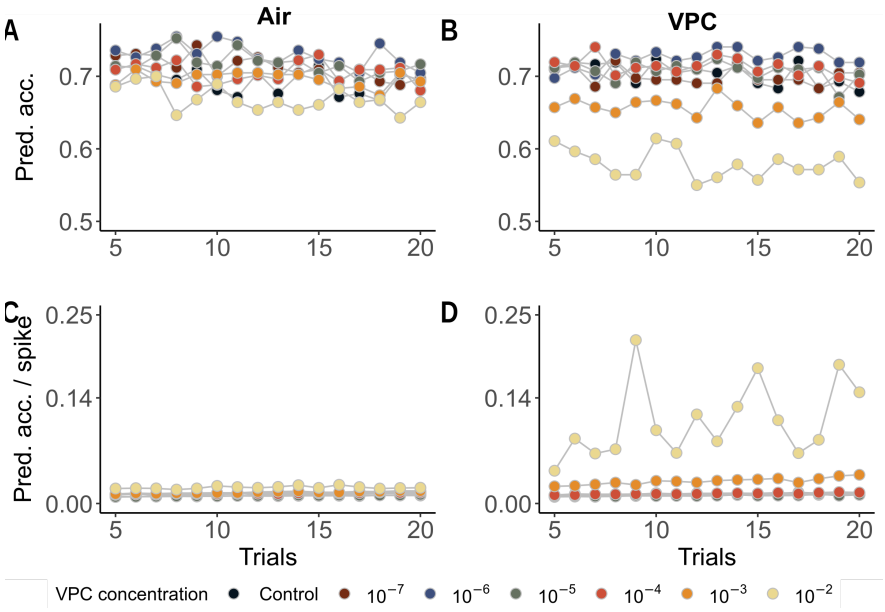

Figure 8: Stimulus prediction model has a high efficiency per spike under high concentrations of (Z)-3-hexenyl acetate. This figure demonstrates the predictive accuracies as well as the predictive accuracies per spike in Phe-ORNs exposed to intermittent pheromones amidst variable (Z)-3-hexenyl acetate concentrations. The x-axis represents the trial number, indicating repeated exposure, while the y-axis measures predictive accuracy in **A** and **B**, displaying a decrease in accuracy at higher concentrations. In contrast, y-axis measures predictive accuracies per spike in **C** and **D**, displaying an increase in efficiency per spike at higher concentrations of (Z)-3-hexenyl acetate. Each line corresponds to a different concentration of VPC, with the control group depicted as black dots. These results suggest an adaptive response in the ORNs' coding ability under high VPC conditions, potentially hinting at an evolutionary advantage in complex olfactory environments.

an adaptive advantage in complex olfactory environments, where the ability to discern mating signals amidst a plethora of plant odors is crucial for reproductive success.

In conclusion, our study contributes significantly to the field of sensory biology by revealing how high concentrations of VPCs can facilitate the coding efficiency of ORNs independently of spike-frequency adaptation. This investigation not only sheds light on the complex mechanisms of olfactory perception in moths, but also hints at the broader ecological and evolutionary strategies employed by these insects to thrive in complex chemical landscapes. This manuscript for this study is attached in Attachment IV.

3.5 Neural variability quenching in networks

Attachment V

Stimulus-evoked quenching of trial-to-trial variability of neural activity is a widely observed phenomenon across different brain areas (Goris et al., 2014; Chang et al., 2012). To understand the underlying mechanisms, we constructed a

recurrent neural network representing the sensory cortex with different neurons having different stimulus preferences, thus replicating the experimental conditions observed in studies like Monier et al. (2003) and Churchland et al. (2010). The stimulus was represented by an increased input intensity dependent on the preferred stimulus and the associated increase in inhibitory input given by the network properties. In this way, we could reproduce the variability quenching effect with stimulus onset.

We considered a recurrent neural network of 10000 neurons, with 7500 excitatory and 2500 inhibitory neurons. Each neuron was modeled as an exponential leaky integrated-and-fire neuron, and the probability of a connection from one neuron to another was set to 5% (Zerlaut et al., 2018). We also considered a proximity-based connection matrix, where neurons with peak response to similar stimuli had a stronger probability of connection, as is observed in cortical neurons (Ko et al., 2011). We compared two types of networks, specified by different spike frequency adaptation (SFA) of the neurons:

1. SFA through after-hyperpolarization currents (AHP),

2. SFA through dynamic firing threshold.

Every neuron received a background input until it was presented with an additional input. In the case of a fixed connection matrix, the neurons receiving strong input responded with an increased firing activity, and neurons receiving a weak input decreased their firing activity due to increased inhibitory input from the network activity, regardless of the SFA mechanism. In contrast, in the case of a proximity-based connection matrix, we observed that neurons on the edge of the network exhibit lower activity due to the lack of connections whereas neurons with an increased number of connections and significantly high stimuli show clusters of increased activity (Fig. 9A-B).

For both connectivity matrices, we ran the simulation 3600 times to obtain the trial-to-trial variability of each neuron before and after the stimulus. We plotted the variance of the response of each neuron against the mean response. Neurons with the AHP-mediated SFA increased their trial-to-trial variability after the stimulus onset. In contrast, neurons with the SFA mediated by a dynamic threshold decreased their trial-to-trial variability after the stimulus onset (Fig. 9).

This model describes a possible mechanism for the reduction in trial-to-trial variability with stimulus onset. To further develop this work, we will investigate the impact of varying the connection probabilities for excitatory-excitatory (EE), excitatory-inhibitory (EI), inhibitory-excitatory (IE), and inhibitory-inhibitory (II) connections on neural variability. Additionally, we aim to explore the functional role of excitatory and inhibitory neuron clusters within these diverse connectivity frameworks. The results of this study are enclosed with this thesis in the form of a manuscript (Attachment V).

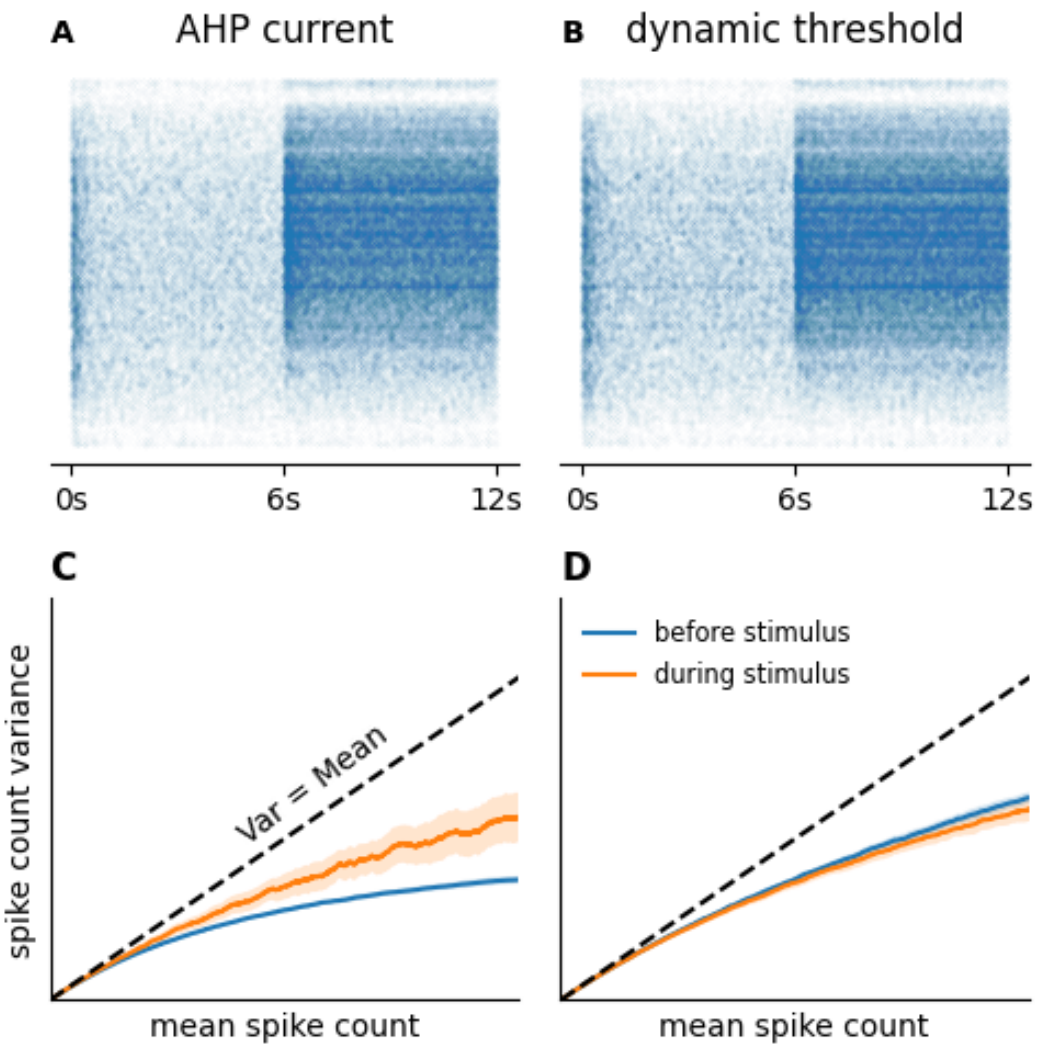

Figure 9: Neural variability quenching in recurrent neural networks with proximity-based connectivity. A-B: Throughout the 12 s simulation, all neurons receive a consistent background input. Starting at 6 s, each neuron receives an additional input that varies according to its specific stimulus preference. The vertical arrangement of neurons indicates the strength of additional input received, with neurons at the bottom receiving none and those at the top receiving the strongest input. The raster plots display the activity of the 7500 excitatory neurons under different spike frequency adaptation (SFA) mechanisms: after-hyperpolarization (AHP) current (**A**) and dynamic threshold (**B**). **C-D:** Using proximity-based connectivity, we conducted 3600 simulation repetitions. The plots show the variance of each neuron's response across these trials against its mean response. Neurons with AHP SFA (**C**) exhibited increased trial-to-trial variability following the stimulus onset. Conversely, neurons with dynamic threshold SFA (**D**) showed a reduction in trial-to-trial variability post-stimulus.

Conclusions

In this thesis, I examined the information transmission mechanisms in neuronal systems from the rate coding perspective. By incorporating measures such as the instantaneous firing rate, I provided a more nuanced understanding of neural encoding. Through detailed analysis and comparison of existing models, I evaluated how biophysical properties influence the dynamics of firing rate. My research demonstrated the significant impact of environmental stimuli on information transmission and highlighted the crucial role of adaptation mechanisms in maintaining efficient neural communication.

The neural coding problem is a key research area in neuroscience. To make further advances in this area, it is important to understand how neurons encode information and what principles they use to optimize this information transmission. Several studies have been done to determine which features of the spike train contain relevant information about the stimuli. Some of the candidates for these features over the year have been the average number of spikes per observation time window (Gerstner et al., 1997) or the occurrence frequency of a pair or trio of spikes (Oram et al., 1999) or the pairwise autocorrelation function along with the pairwise cross-correlation across noisy trials (Dettner et al., 2016). Fukushima et al. (2015) found that temporal coding carries more information than spike counts when discriminating between different versions of the bird's own song in the zebra finch auditory system. Foffani et al. (2009) showed that spike timing is more critical for discriminating between tactile stimuli when stimulus discriminability is low, while spike count becomes increasingly important as discriminability improves. These findings underscore that rate coding alone cannot capture the complexity of neuronal coding, highlighting the need to integrate metrics like the instantaneous firing rate that encapsulate both spike count and temporal properties of neural data. This approach allows for a more accurate representation of neural activity compared to averaging over longer time windows (Ostojic and Brunel, 2011). Furthermore, the instantaneous firing rate is directly proportional to input variance, highlighting its sensitivity to changes in stimulus statistics which makes it a valuable metric for understanding how neural populations encode information and respond to varying inputs (Fourcaud-Trocmé and Brunel, 2005).

Despite the advancements provided by metrics like the instantaneous firing rate, another significant obstacle in understanding information transmission mechanisms lies in the limitations of biophysical models. Brette (2015) argued that single-compartment integrate-and-fire (IF) models are more realistic than single-compartment Hodgkin-Huxley models. However, single-compartment IF models fail to capture several crucial features of neuronal behavior, like the effects of dendritic spikes (Górski et al., 2018) or the impact of multiplicative dendritic integration (An et al., 2019) and neither do they have an intrinsic saturation of the firing rate. More detailed models can address these limitations, sometimes at the cost of computational efficiency. The two-compartment IF models with reversal potentials have an intrinsic saturation of the firing rate. Additionally,

a two-dimensional integrate-and-fire model incorporating an exponential spike mechanism with an adaptation equation has been proposed to effectively describe neuronal activity (Brette and Gerstner, 2005). This model called the adaptive exponential IF (AdEx) model, can replicate various firing patterns observed in neurons (Naud et al., 2008; Górski et al., 2021). A spiking neural network, where single neuron dynamics is based on the AdEx model and the network dynamics consist of excitatory and inhibitory subpopulation with recurrent architecture and excitatory feedforward input captures the trial-to-trial variability typically observed in cortical neurons. This trial-to-trial variability of spiking activity in cortical neurons has been recognized as a source of information about the state of neurons and their involvement in behavioral tasks (Hussar and Pasternak, 2010). Using the SNN model, our research demonstrated that stimulus onset can lead to a quenching of neural variability, dependent on the spike frequency adaptation (SFA) mechanisms employed. These findings emphasize the importance of SFA mechanisms in shaping neural response dynamics and their critical role in accurately modeling neural variability in cortical networks.
Empirical research into the influence of environmental stimuli on olfactory receptor neurons (ORNs) provides new insights into how external factors modulate neural coding strategies. The study on volatile plant compounds (VPCs) and their effect on ORNs demonstrated that high concentrations of VPCs enhance information per spike despite reducing overall firing rates, suggesting an adaptive mechanism that optimizes information transmission in complex sensory environments.

The research presented offers a detailed exploration of information transmission in neuronal systems from the rate coding perspective. By integrating advanced models and empirical studies, and focusing on biophysical properties and adaptation mechanisms, new insights are provided into how neurons encode and adapt to varying inputs, enhancing our understanding of neural dynamics and information processing.

Bibliography

M Abramowitz and I A Stegun. *Handbook of Mathematical Functions with Formulas, Graphs, and Mathematical Tables*. U.S. Government Printing Office, 1948.

E D Adrian and Y Zotterman. The impulses produced by sensory nerve endings: Part 3. impulses set up by touch and pressure. *J. Physiol.*, 61(4):465–483, August 1926. ISSN 0022-3751. doi: 10.1113/jphysiol.1926.sp002308.

N Ahmadi, T G Constandinou, and C S Bouganis. Estimation of neuronal firing rate using bayesian adaptive kernel smoother (BAKS). *PLoS One*, 13(11): e0206794, November 2018. ISSN 1932-6203. doi: 10.1371/journal.pone.0206794.

D J Amit and N Brunel. Dynamics of a recurrent network of spiking neurons before and following learning. *Network: Computation in Neural Systems*, 8(4): 373–404, January 1997. ISSN 0954-898X. doi: 10.1088/0954-898X_8_4_003.

L An, Y Tang, Q Wang, Q Pei, R Wei, H Duan, and J K Liu. Coding capacity of purkinje cells with different schemes of morphological reduction. *Front. Comput. Neurosci.*, 13:29, May 2019. ISSN 1662-5188. doi: 10.3389/fncom.2019.00029.

A Arazi, N Censor, and I Dinstein. Neural variability quenching predicts individual perceptual abilities. *J. Neurosci.*, 37(1):97–109, January 2017. ISSN 0270-6474, 1529-2401. doi: 10.1523/JNEUROSCI.1671-16.2016.

S N Baker and R N Lemon. Precise spatiotemporal repeating patterns in monkey primary and supplementary motor areas occur at chance levels. *J. Neurophysiol.*, 84(4):1770–1780, October 2000. ISSN 0022-3077. doi: 10.1152/jn.2000.84.4.1770.

S N Baker, R Spinks, A Jackson, and R N Lemon. Synchronization in monkey motor cortex during a precision grip task. i. task-dependent modulation in single-unit synchrony. *J. Neurophysiol.*, 85(2):869–885, February 2001. ISSN 0022-3077. doi: 10.1152/jn.2001.85.2.869.

R Barbieri, M C Quirk, L M Frank, M A Wilson, and E N Brown. Construction and analysis of non-poisson stimulus-response models of neural spiking activity. *J. Neurosci. Methods*, 105(1):25–37, January 2001. ISSN 0165-0270. doi: 10.1016/s0165-0270(00)00344-7.

V J Barranca, H Huang, and S Li. The impact of spike-frequency adaptation on balanced network dynamics. *Cogn. Neurodyn.*, 13(1):105–120, February 2019. ISSN 1871-4080. doi: 10.1007/s11571-018-9504-2.

J Benda and A V M Herz. A universal model for spike-frequency adaptation. *Neural Comput.*, 15(11):2523–2564, November 2003. ISSN 0899-7667. doi: 10.1162/089976603322385063.

J Benda, L Maler, and A Longtin. Linear versus nonlinear signal transmission in neuron models with adaptation currents or dynamic thresholds. *J. Neurophysiol.*, 104(5):2806–2820, November 2010. ISSN 0022-3077, 1522-1598. doi: 10.1152/jn.00240.2010.

P Bessou, Y Laporte, and B Pagès. Frequencygrams of spindle primary endings elicited by stimulation of static and dynamic fusimotor fibres. *J. Physiol.*, 196 (1):47–63, May 1968. ISSN 0022-3751. doi: 10.1113/jphysiol.1968.sp008493.

G S Bhumbra and R E J Dyball. Measuring spike coding in the rat supraoptic nucleus. *J. Physiol.*, 555(Pt 1):281–296, February 2004. ISSN 0022-3751. doi: 10.1113/jphysiol.2003.053264.

G S Bhumbra, A N Inyushkin, and R E J Dyball. Assessment of spike activity in the supraoptic nucleus. *J. Neuroendocrinol.*, 16(4):390–397, April 2004. ISSN 0953-8194. doi: 10.1111/j.0953-8194.2004.01166.x.

J M Bower and D Beeman. *The Book of GENESIS: Exploring Realistic Neural Models with the GEneral NEural SImulation System*. Springer Science & Business Media, December 2012. ISBN 9781461216346.

R Brette. What is the most realistic single-compartment model of spike initiation? *PLoS Comput. Biol.*, 11(4):e1004114, April 2015. ISSN 1553-734X, 1553-7358. doi: 10.1371/journal.pcbi.1004114.

R Brette and W Gerstner. Adaptive exponential integrate-and-fire model as an effective description of neuronal activity. *J. Neurophysiol.*, 94(5):3637–3642, November 2005. ISSN 0022-3077. doi: 10.1152/jn.00686.2005.

G T Buracas and T D Albright. Gauging sensory representations in the brain. *Trends Neurosci.*, 22(7):303–309, July 1999. ISSN 0166-2236. doi: 10.1016/s0166-2236(98)01376-9.

A N Burkitt. A review of the integrate-and-fire neuron model: I. homogeneous synaptic input. *Biol. Cybern.*, 95(1):1–19, July 2006. ISSN 0340-1200. doi: 10.1007/s00422-006-0068-6.

A N Burkitt and G M Clark. Calculation of interspike intervals for integrate-and-fire neurons with poisson distribution of synaptic inputs. *Neural Comput.*, 12(8): 1789–1820, August 2000. ISSN 0899-7667. doi: 10.1162/089976600300015141.

B D Burns and A C Webb. The spontaneous activity of neurones in the cat's cerebral cortex. *Proc. R. Soc. Lond. B Biol. Sci.*, 194(1115):211–223, October 1976. ISSN 0080-4649, 0950-1193. doi: 10.1098/rspb.1976.0074.

G Buzsáki and K Mizuseki. The log-dynamic brain: how skewed distributions affect network operations. *Nat. Rev. Neurosci.*, 15(4):264–278, April 2014. ISSN 1471-003X, 1471-0048. doi: 10.1038/nrn3687.

M J Chacron, B Lindner, and A Longtin. Threshold fatigue and information transfer. *J. Comput. Neurosci.*, 23(3):301–311, December 2007. ISSN 0929-5313. doi: 10.1007/s10827-007-0033-y.

M H Chang, K M Armstrong, and T Moore. Dissociation of response variability from firing rate effects in frontal eye field neurons during visual stimulation, working memory, and attention. *J. Neurosci.*, 32(6):2204–2216, February 2012. ISSN 0270-6474, 1529-2401. doi: 10.1523/JNEUROSCI.2967-11.2012.

Y Chen and D A Nitz. A unified description of cerebellar inter-spike interval distributions and variabilities using summation of gaussians. *Network*, 22(1-4): 74–96, 2011. ISSN 0093-3341. doi: 10.3109/0954898X.2011.636860.

S Cherif, K E Cullen, and H L Galiana. An improved method for the estimation of firing rate dynamics using an optimal digital filter. *J. Neurosci. Methods*, 173(1): 165–181, August 2008. ISSN 0165-0270. doi: 10.1016/j.jneumeth.2008.05.021.

M M Churchland, B M Yu, S I Ryu, G Santhanam, and K V Shenoy. Neural variability in premotor cortex provides a signature of motor preparation. *J. Neurosci.*, 26(14):3697–3712, April 2006. ISSN 0270-6474, 1529-2401. doi: 10.1523/JNEUROSCI.3762-05.2006.

M M Churchland, B M Yu, J P Cunningham, L P Sugrue, M R Cohen, G S Corrado, W T Newsome, A M Clark, P Hosseini, B B Scott, D C Bradley, M A Smith, A Kohn, J A Movshon, K M Armstrong, T Moore, S W Chang, L H Snyder, S G Lisberger, N J Priebe, I M Finn, D Ferster, S I Ryu, G Santhanam, M Sahani, and K V Shenoy. Stimulus onset quenches neural variability: a widespread cortical phenomenon. *Nat. Neurosci.*, 13(3):369–378, March 2010. ISSN 1097-6256, 1546-1726. doi: 10.1038/nn.2501.

L Conchou, P Lucas, C Meslin, M Proffit, M Staudt, and M Renou. Insect odorscapes: From plant volatiles to natural olfactory scenes. *Front. Physiol.*, 10:972, August 2019. ISSN 1664-042X. doi: 10.3389/fphys.2019.00972.

L Conchou, P Lucas, N Deisig, E Demondion, and M Renou. Effects of an odor background on moth pheromone communication: constituent identity matters more than blend complexity. September 2020.

L Conchou, P Lucas, N Deisig, E Demondion, and M Renou. Effects of Multi-Component backgrounds of volatile plant compounds on moth pheromone perception. *Insects*, 12(5):409, May 2021. ISSN 2075-4450. doi: 10.3390/insects12050409.

D R Cox and H D Miller. *Theory of stochastic processes*. Chapman and Hall, London, England, October 1965. ISBN 9780412117206.

E L Crow and K Shimizu. *Lognormal Distributions: Theory and Applications*. Routledge, May 2018. ISBN 9781351434690.

J Cunningham, Byron M Yu, K Shenoy, and M Sahani. Inferring neural firing rates from spike trains using gaussian processes. *Adv. Neural Inf. Process. Syst.*, pages 329–336, December 2007. ISSN 1049-5258.

J P Cunningham, V Gilja, S I Ryu, and K V Shenoy. Methods for estimating neural firing rates, and their application to brain–machine interfaces. *Neural Netw.*, 22(9):1235–1246, November 2009. ISSN 0893-6080. doi: 10.1016/j.neunet.2009.02.004.

Y Dan and M M Poo. Spike timing-dependent plasticity: from synapse to perception. *Physiol. Rev.*, 86(3):1033–1048, July 2006. ISSN 0031-9333. doi: 10.1152/physrev.00030.2005.

R A Davis, K S Lii, and D N Politis. Remarks on some nonparametric estimates of a density function. In R A Davis, K S Lii, and D N Politis, editors, *Selected Works of Murray Rosenblatt*, pages 95–100. Springer New York, New York, NY, 2011. ISBN 9781441983398. doi: 10.1007/978-1-4419-8339-8_13.

P Dayan and L F Abbott. *Theoretical Neuroscience: Computational and Mathematical Modeling of Neural Systems*. MIT Press, August 2005. ISBN 9780262541855.

A Destexhe, Z F Mainen, and T J Sejnowski. Synthesis of models for excitable membranes, synaptic transmission and neuromodulation using a common kinetic formalism. *J. Comput. Neurosci.*, 1(3):195–230, August 1994. ISSN 0929-5313. doi: 10.1007/BF00961734.

A Destexhe, M Rudolph, and D Paré. The high-conductance state of neocortical neurons in vivo. *Nat. Rev. Neurosci.*, 4(9):739–751, September 2003. ISSN 1471-003X. doi: 10.1038/nrn1198.

A Dettner, S Münzberg, and T Tchumatchenko. Temporal pairwise spike correlations fully capture single-neuron information. *Nat. Commun.*, 7, 2016. doi: 10.1038/ncomms13805.

I Dimatteo, C R Genovese, and R E Kass. Bayesian curve-fitting with free-knot splines. *Biometrika*, 88(4):1055–1071, December 2001. ISSN 0006-3444. doi: 10.1093/biomet/88.4.1055.

A D Dorval, G S Russo, T Hashimoto, W Xu, W M Grill, and J L Vitek. Deep brain stimulation reduces neuronal entropy in the MPTP-primate model of parkinson's disease. *J. Neurophysiol.*, 100(5):2807–2818, November 2008. ISSN 0022-3077. doi: 10.1152/jn.90763.2008.

F Dupuy, A Rouyar, N Deisig, T Bourgeois, D Limousin, M A Wycke, S Anton, and M Renou. A background of a volatile plant compound alters neural and behavioral responses to the sex pheromone blend in a moth. *Front. Physiol.*, 8: 79, February 2017. ISSN 1664-042X. doi: 10.3389/fphys.2017.00079.

D M Endres, M Oram, J Schindelin, and P Földiák. Bayesian binning beats approximate alternatives: estimating peri-stimulus time histograms. *Adv. Neural Inf. Process. Syst.*, pages 393–400, December 2007. ISSN 1049-5258.

B Ermentrout. Type I membranes, phase resetting curves, and synchrony. *Neural Comput.*, 8(5):979–1001, July 1996. ISSN 0899-7667. doi: 10.1162/neco.1996.8.5.979.

A L Fairhall, G D Lewen, W Bialek, and R R de Ruyter Van Steveninck. Efficiency and ambiguity in an adaptive neural code. *Nature*, 412(6849):787–792, August 2001. ISSN 0028-0836. doi: 10.1038/35090500.

A A Fenton and R U Muller. Place cell discharge is extremely variable during individual passes of the rat through the firing field. *Proc. Natl. Acad. Sci. U. S. A.*, 95(6):3182–3187, March 1998. ISSN 0027-8424. doi: 10.1073/pnas.95.6.3182.

R Fitzhugh. Impulses and physiological states in theoretical models of nerve membrane. *Biophys. J.*, 1(6):445–466, July 1961. ISSN 0006-3495. doi: 10.1016/s0006-3495(61)86902-6.

G Foffani, M L Morales-Botello, and J Aguilar. Spike timing, spike count, and temporal information for the discrimination of tactile stimuli in the rat ventrobasal complex. *J. Neurosci.*, 29(18):5964–5973, May 2009. ISSN 0270-6474, 1529-2401. doi: 10.1523/JNEUROSCI.4416-08.2009.

N Fourcaud-Trocmé and N Brunel. Dynamics of the instantaneous firing rate in response to changes in input statistics. *J. Comput. Neurosci.*, 18(3):311–321, June 2005. ISSN 0929-5313, 1573-6873. doi: 10.1007/s10827-005-0337-8.

N Fourcaud-Trocmé, D Hansel, C van Vreeswijk, and N Brunel. How spike generation mechanisms determine the neuronal response to fluctuating inputs. *J. Neurosci.*, 23(37):11628–11640, December 2003. ISSN 0270-6474, 1529-2401. doi: 10.1523/JNEUROSCI.23-37-11628.2003.

R F Fox. Stochastic versions of the Hodgkin-Huxley equations. *Biophys. J.*, 72(5): 2068–2074, May 1997. ISSN 0006-3495. doi: 10.1016/S0006-3495(97)78850-7.

M Fukushima, P L Rauske, and D Margoliash. Temporal and rate code analysis of responses to low-frequency components in the bird's own song by song system neurons. *J. Comp. Physiol. A Neuroethol. Sens. Neural Behav. Physiol.*, 201 (12):1103–1114, December 2015. ISSN 0340-7594, 1432-1351. doi: 10.1007/s00359-015-1037-0.

A P Georgopoulos, A B Schwartz, and R E Kettner. Neuronal population coding of movement direction. *Science*, 233(4771):1416–1419, September 1986. ISSN 0036-8075. doi: 10.1126/science.3749885.

G L Gerstein and N Y Kiang. An approach to the quantitative analysis of electrophysiological data from single neurons. *Biophys. J.*, 1(1):15–28, September 1960. ISSN 0006-3495. doi: 10.1016/s0006-3495(60)86872-5.

G L Gerstein and B Mandelbrot. Random walk models for the spike activity of a single neuron. *Biophys. J.*, 4(1 Pt 1):41–68, January 1964. ISSN 0006-3495. doi: 10.1016/s0006-3495(64)86768-0.

W Gerstner and W M Kistler. *Spiking Neuron Models: Single Neurons, Populations, Plasticity*. Cambridge University Press, August 2002. ISBN 9780521890793.

W Gerstner, A K Kreiter, H Markram, and A V M Herz. Neural codes: Firing rates and beyond. *Proc. Natl. Acad. Sci. U. S. A.*, 94(24):12740–12741, November 1997. ISSN 0027-8424. doi: 10.1073/pnas.94.24.12740.

R L T Goris, J A Movshon, and E P Simoncelli. Partitioning neuronal variability. *Nat. Neurosci.*, 17(6):858–865, June 2014. ISSN 1097-6256, 1546-1726. doi: 10.1038/nn.3711.

T Górski, R Veltz, M Galtier, H Fragnaud, J S Goldman, B Teleńczuk, and A Destexhe. Dendritic sodium spikes endow neurons with inverse firing rate

response to correlated synaptic activity. *J. Comput. Neurosci.*, 45(3):223–234, December 2018. ISSN 0929-5313, 1573-6873. doi: 10.1007/s10827-018-0707-7.

T Górski, D Depannemaecker, and A Destexhe. Conductance-Based adaptive exponential Integrate-and-Fire model. *Neural Comput.*, 33(1):41–66, January 2021. ISSN 0899-7667, 1530-888X. doi: 10.1162/neco_a_01342.

J Grollier, D Querlioz, K Y Camsari, K Everschor-Sitte, S Fukami, and M D Stiles. Neuromorphic spintronics. *Nat Electron*, 3(7), 2020. ISSN 2520-1131. doi: 10.1038/s41928-019-0360-9.

N Gupta and M Stopfer. A temporal channel for information in sparse sensory coding. *Curr. Biol.*, 24(19):2247–2256, October 2014. ISSN 0960-9822, 1879-0445. doi: 10.1016/j.cub.2014.08.021.

B Gutkin and F Zeldenrust. Spike frequency adaptation. *Scholarpedia J.*, 9(2): 30643, 2014. ISSN 1941-6016. doi: 10.4249/scholarpedia.30643.

B S Hansson and M C Stensmyr. Evolution of insect olfaction. *Neuron*, 72(5): 698–711, December 2011. ISSN 0896-6273, 1097-4199. doi: 10.1016/j.neuron.2011.11.003.

C M Harris and J Waddington. On the convergence of time interval moments: caveat sciscitator. *J. Neurosci. Methods*, 205(2):345–356, April 2012. ISSN 0165-0270, 1872-678X. doi: 10.1016/j.jneumeth.2012.01.017.

M Häusser, N Spruston, and G J Stuart. Diversity and dynamics of dendritic signaling. *Science*, 290(5492):739–744, October 2000. ISSN 0036-8075. doi: 10.1126/science.290.5492.739.

P Heil, H Neubauer, D R F Irvine, and M Brown. Spontaneous activity of auditory-nerve fibers: insights into stochastic processes at ribbon synapses. *J. Neurosci.*, 27(31):8457–8474, August 2007. ISSN 0270-6474, 1529-2401. doi: 10.1523/JNEUROSCI.1512-07.2007.

A L Hodgkin and A F Huxley. A quantitative description of membrane current and its application to conduction and excitation in nerve. *J. Physiol.*, 117(4): 500–544, August 1952. ISSN 0022-3751. doi: 10.1113/jphysiol.1952.sp004764.

D H Hubel and T N Wiesel. Receptive fields, binocular interaction and functional architecture in the cat's visual cortex. *J. Physiol.*, 160(1):106–154, January 1962. ISSN 0022-3751. doi: 10.1113/jphysiol.1962.sp006837.

C Hussar and T Pasternak. Trial-to-trial variability of the prefrontal neurons reveals the nature of their engagement in a motion discrimination task. *Proceedings of the National Academy of Sciences*, 107(50):21842–21847, 2010. doi: 10.1073/pnas.1009956107.

S Ikeda and J H Manton. Spiking neuron channel. In *2009 IEEE International Symposium on Information Theory*, pages 1589–1593. IEEE, June 2009. ISBN 9781424443123, 9781424443130. doi: 10.1109/ISIT.2009.5205817.

E M Izhikevich. Simple model of spiking neurons. *IEEE Trans. Neural Netw.*, 14 (6):1569–1572, 2003. ISSN 1045-9227. doi: 10.1109/TNN.2003.820440.

D H Johnson. The relationship of post-stimulus time and interval histograms to the timming characteristics of spike trains. *Biophys. J.*, 22(3):413–430, 1978. ISSN 0006-3495.

D H Johnson. Point process models of single-neuron discharges. *J. Comput. Neurosci.*, 3(4):275–299, December 1996. ISSN 0929-5313. doi: 10.1007/BF00161089.

Renaud Jolivet, Ryota Kobayashi, Alexander Rauch, Richard Naud, Shigeru Shinomoto, and Wulfram Gerstner. A benchmark test for a quantitative assessment of simple neuron models. *J. Neurosci. Methods*, 169(2):417–424, April 2008. ISSN 0165-0270. doi: 10.1016/j.jneumeth.2007.11.006.

E R Kandel, J H Schwartz, and T M Jessell. *Principles of Neural Science*. Appleton & Lange, 1991. ISBN 9780838580349.

J Keat, P Reinagel, R C Reid, and M Meister. Predicting every spike: a model for the responses of visual neurons. *Neuron*, 30(3):803–817, June 2001. ISSN 0896-6273. doi: 10.1016/s0896-6273(01)00322-1.

J T Knudsen, R Eriksson, J Gershenzon, and B Ståhl. Diversity and distribution of floral scent. *Bot. Rev.*, 72(1):1, January 2006. ISSN 0006-8101, 1874-9372. doi: 10.1663/0006-8101(2006)72[1:DADOFS]2.0.CO;2.

H Ko, S B Hofer, B Pichler, K A Buchanan, P J Sjöström, and T D Mrsic-Flogel. Functional specificity of local synaptic connections in neocortical networks. *Nature*, 473(7345):87–91, May 2011. ISSN 0028-0836, 1476-4687. doi: 10.1038/nature09880.

C Köppl. Phase locking to high frequencies in the auditory nerve and cochlear nucleus magnocellularis of the barn owl, tyto alba. *J. Neurosci.*, 17(9):3312–3321, May 1997. ISSN 0270-6474. doi: 10.1523/JNEUROSCI.17-09-03312.1997.

L Kostal and P Lansky. Coding accuracy is not fully determined by the neuronal model. *Neural Comput.*, 27(5):1051–1057, May 2015. ISSN 0899-7667, 1530-888X. doi: 10.1162/NECO_a_00724.

L Kostal, P Lansky, and J P Rospars. Neuronal coding and spiking randomness. *Eur. J. Neurosci.*, 26(10):2693–2701, November 2007. ISSN 0953-816X. doi: 10.1111/j.1460-9568.2007.05880.x.

L Kostal, P Lansky, and M D McDonnell. Metabolic cost of neuronal information in an empirical stimulus-response model. *Biol. Cybern.*, 107(3):355–365, June 2013. ISSN 0340-1200, 1432-0770. doi: 10.1007/s00422-013-0554-6.

L Kostal, P Lansky, and M Stiber. Statistics of inverse interspike intervals: The instantaneous firing rate revisited. *Chaos*, 28(10):106305, October 2018. ISSN 1054-1500, 1089-7682. doi: 10.1063/1.5036831.

P Lánský and V Lánská. Diffusion approximation of the neuronal model with synaptic reversal potentials. *Biol. Cybern.*, 56(1):19–26, 1987. ISSN 0340-1200. doi: 10.1007/BF00333064.

P Lánský and R Rodriguez. The spatial properties of a model neuron increase its coding range. *Biol. Cybern.*, 81(2):161–167, August 1999. ISSN 0340-1200. doi: 10.1007/s004220050552.

P Lánský, R Rodriguez, and L Sacerdote. Mean instantaneous firing frequency is always higher than the firing rate. *Neural Comput.*, 16(3):477–489, March 2004. ISSN 0899-7667. doi: 10.1162/089976604772744875.

L Lapicque. Quantitative investigations of electrical nerve excitation treated as polarization. 1907. *Biol. Cybern.*, 97(5-6):341–349, December 2007. ISSN 0340-1200. doi: 10.1007/s00422-007-0189-6.

P E Latham, B J Richmond, P G Nelson, and S Nirenberg. Intrinsic dynamics in neuronal networks. i. theory. *J. Neurophysiol.*, 83(2):808–827, February 2000. ISSN 0022-3077. doi: 10.1152/jn.2000.83.2.808.

C H Lemon and D V Smith. Influence of response variability on the coding performance of central gustatory neurons. *J. Neurosci.*, 26(28):7433–7443, July 2006. ISSN 0270-6474, 1529-2401. doi: 10.1523/JNEUROSCI.0106-06.2006.

M Li, F Zhao, J Lee, D Wang, H Kuang, and J Z Tsien. Computational classification approach to profile neuron subtypes from brain activity mapping data. *Sci. Rep.*, 5:12474, July 2015. ISSN 2045-2322. doi: 10.1038/srep12474.

Y Li, G Schmid, P Hänggi, and L Schimansky-Geier. Spontaneous spiking in an autaptic Hodgkin-Huxley setup. *Phys. Rev. E Stat. Nonlin. Soft Matter Phys.*, 82(6 Pt 1):061907, December 2010. ISSN 1539-3755, 1550-2376. doi: 10.1103/PhysRevE.82.061907.

M London and M Häusser. Dendritic computation. *Annu. Rev. Neurosci.*, 28: 503–532, 2005. ISSN 0147-006X. doi: 10.1146/annurev.neuro.28.061604.135703.

A Longtin and M St-Hilaire. Encoding carrier amplitude modulations via stochastic phase synchronization. *Int. J. Bifurcat. Chaos*, 10(10):2447–2463, October 2000. ISSN 0218-1274. doi: 10.1142/S0218127400001596.

M Martina and P Jonas. Functional differences in na+ channel gating between fast-spiking interneurones and principal neurones of rat hippocampus. *J. Physiol.*, 505 (Pt 3)(Pt 3):593–603, December 1997. ISSN 0022-3751. doi: 10.1111/j.1469-7793.1997.593ba.x.

S Martinez-Conde, S L Macknik, and D H Hubel. Microsaccadic eye movements and firing of single cells in the striate cortex of macaque monkeys. *Nat. Neurosci.*, 3(4):409, April 2000. ISSN 1097-6256, 1546-1726. doi: 10.1038/73992.

L C Miller, C K Thompson, F Negro, C J Heckman, D Farina, and J P A Dewald. High-density surface EMG decomposition allows for recording of motor unit discharge from proximal and distal flexion synergy muscles simultaneously in

individuals with stroke. *Conf. Proc. IEEE Eng. Med. Biol. Soc.*, 2014:5340–5344, 2014. ISSN 1557-170X. doi: 10.1109/EMBC.2014.6944832.

Y Mochizuki and S Shinomoto. Analog and digital codes in the brain. *Phys. Rev. E Stat. Nonlin. Soft Matter Phys.*, 89(2):022705, February 2014. ISSN 1539-3755, 1550-2376. doi: 10.1103/PhysRevE.89.022705.

C Monier, F Chavane, P Baudot, L J Graham, and Y Frégnac. Orientation and direction selectivity of synaptic inputs in visual cortical neurons: a diversity of combinations produces spike tuning. *Neuron*, 37(4):663–680, February 2003. ISSN 0896-6273. doi: 10.1016/s0896-6273(03)00064-3.

G P Moore, D H Perkel, and J P Segundo. Statistical analysis and functional interpretation of neuronal spike data. *Annu. Rev. Physiol.*, 28:493–522, 1966. ISSN 0066-4278. doi: 10.1146/annurev.ph.28.030166.002425.

R Naud, N Marcille, C Clopath, and W Gerstner. Firing patterns in the adaptive exponential integrate-and-fire model. *Biol. Cybern.*, 99(4-5):335–347, November 2008. ISSN 0340-1200, 1432-0770. doi: 10.1007/s00422-008-0264-7.

M Nawrot. Analysis and interpretation of interval and count variability in neural spike trains. In Sonja Grün and Stefan Rotter, editors, *Analysis of Parallel Spike Trains*, pages 37–58. Springer US, Boston, MA, 2010. ISBN 9781441956750. doi: 10.1007/978-1-4419-5675-0_3.

M Nawrot, A Aertsen, and S Rotter. Single-trial estimation of neuronal firing rates: from single-neuron spike trains to population activity. *J. Neurosci. Methods*, 94 (1):81–92, December 1999. ISSN 0165-0270. doi: 10.1016/s0165-0270(99)00127-2.

I Nemenman, W Bialek, and R de Ruyter van Steveninck. Entropy and information in neural spike trains: progress on the sampling problem. *Phys. Rev. E Stat. Nonlin. Soft Matter Phys.*, 69(5 Pt 2):056111, May 2004. ISSN 1539-3755. doi: 10.1103/PhysRevE.69.056111.

Heinrich Neubauer, Christine Köppl, and Peter Heil. Spontaneous activity of auditory nerve fibers in the barn owl (tyto alba): analyses of interspike interval distributions. *J. Neurophysiol.*, 101(6):3169–3191, June 2009. ISSN 0022-3077. doi: 10.1152/jn.90779.2008.

J A Obeso, M C Rodríguez-Oroz, M Rodríguez, J L Lanciego, J Artieda, N Gonzalo, and C W Olanow. Pathophysiology of the basal ganglia in parkinson's disease. *Trends Neurosci.*, 23(10 Suppl):S8–19, October 2000. ISSN 0166-2236. doi: 10.1016/s1471-1931(00)00028-8.

M Okada, K Yamanishi, and N Masuda. Long-tailed distributions of inter-event times as mixtures of exponential distributions. *R Soc Open Sci*, 7(2):191643, February 2020. ISSN 2054-5703. doi: 10.1098/rsos.191643.

T Omi and S Shinomoto. Optimizing time histograms for non-poissonian spike trains. *Neural Comput.*, 23(12):3125–3144, December 2011. ISSN 0899-7667, 1530-888X. doi: 10.1162/NECO_a_00213.

M W Oram, M C Wiener, R Lestienne, and B J Richmond. Stochastic nature of precisely timed spike patterns in visual system neuronal responses. *J. Neurophysiol.*, 81(6):3021–3033, June 1999. ISSN 0022-3077. doi: 10.1152/jn.1999.81.6.3021.

S Ostojic and N Brunel. From spiking neuron models to linear-nonlinear models. *PLoS Comput. Biol.*, 7(1):e1001056, January 2011. ISSN 1553-734X, 1553-7358. doi: 10.1371/journal.pcbi.1001056.

L Paninski. Maximum likelihood estimation of cascade point-process neural encoding models. *Network*, 15(4):243–262, November 2004. ISSN 0093-3341, 0954-898X.

Party, V, C Hanot, I Said, D Rochat, and M Renou. Plant terpenes affect intensity and temporal parameters of pheromone detection in a moth. *Chem. Senses*, 34(9):763–774, November 2009. ISSN 0379-864X, 1464-3553. doi: 10.1093/chemse/bjp060.

E Parzen. On estimation of a probability density function and mode. *Ann. Math. Stat.*, 33(3):1065–1076, 1962. ISSN 0003-4851.

Q Pauluis and S N Baker. An accurate measure of the instantaneous discharge probability, with application to unitary joint-event analysis. *Neural Comput.*, 12(3):647–669, March 2000. ISSN 0899-7667, 1530-888X. doi: 10.1162/089976600300015736.

D H Perkel. *Neural Coding: A Report Based on an NRP Work Session Organized by Theodore Holmes Bullock and Held on January 21-23, 1968*. Neurosciences Research Program, 1968.

P Poirazi, T Brannon, and B W Mel. Pyramidal neuron as two-layer neural network. *Neuron*, 37(6):989–999, March 2003. ISSN 0896-6273. doi: 10.1016/s0896-6273(03)00149-1.

R Quian Quiroga and S Panzeri. Extracting information from neuronal populations: information theory and decoding approaches. *Nat. Rev. Neurosci.*, 10(3):173–185, March 2009. ISSN 1471-003X, 1471-0048. doi: 10.1038/nrn2578.

W Rall. Theory of physiological properties of dendrites. *Ann. N. Y. Acad. Sci.*, 96:1071–1092, March 1962. ISSN 0077-8923. doi: 10.1111/j.1749-6632.1962.tb54120.x.

A V Rangan. Functional roles for synaptic-depression within a model of the fly antennal lobe. *PLoS Comput. Biol.*, 8(8):e1002622, August 2012. ISSN 1553-734X, 1553-7358. doi: 10.1371/journal.pcbi.1002622.

A Rauch, G La Camera, H R Lüscher, W Senn, and S Fusi. Neocortical pyramidal cells respond as Integrate-and-Fire neurons to in Vivo–Like input currents. *J. Neurophysiol.*, 90(3):1598–1612, September 2003. ISSN 0022-3077. doi: 10.1152/jn.00293.2003.

M J E Richardson, N Brunel, and V Hakim. From subthreshold to firing-rate resonance. *J. Neurophysiol.*, 89(5):2538–2554, May 2003. ISSN 0022-3077. doi: 10.1152/jn.00955.2002.

F Rieke, D Warland, R D V Steveninck, and W Bialek. Spikes: Exploring the neural code. November 1996.

M Rigotti, O Barak, M R Warden, X J Wang, N D Daw, E K Miller, and S Fusi. The importance of mixed selectivity in complex cognitive tasks. *Nature*, 497(7451): 585–590, May 2013. ISSN 0028-0836, 1476-4687. doi: 10.1038/nature12160.

J P Rospars, P Lánský, A Duchamp, and P Duchamp-Viret. Relation between stimulus and response in frog olfactory receptor neurons in vivo. *Eur. J. Neurosci.*, 18(5):1135–1154, September 2003. ISSN 0953-816X. doi: 10.1046/j.1460-9568.2003.02766.x.

E Rossoni and J Feng. A nonparametric approach to extract information from interspike interval data. *J. Neurosci. Methods*, 150(1):30–40, January 2006. ISSN 0165-0270. doi: 10.1016/j.jneumeth.2005.05.021.

A Roth and M Häusser. Compartmental models of rat cerebellar purkinje cells based on simultaneous somatic and dendritic patch-clamp recordings. *J. Physiol.*, 535(Pt 2):445–472, September 2001. ISSN 0022-3751. doi: 10.1111/j.1469-7793.2001.00445.x.

A Rouyar, N Deisig, F Dupuy, D Limousin, M A Wycke, M Renou, and S Anton. Unexpected plant odor responses in a moth pheromone system. *Front. Physiol.*, 6:148, May 2015. ISSN 1664-042X. doi: 10.3389/fphys.2015.00148.

B V Safronov, M Wolff, and W Vogel. Excitability of the soma in central nervous system neurons. *Biophys. J.*, 78(6):2998–3010, June 2000. ISSN 0006-3495. doi: 10.1016/S0006-3495(00)76838-X.

E Schneidman, B Freedman, and I Segev. Ion channel stochasticity may be critical in determining the reliability and precision of spike timing. *Neural Comput.*, 10(7):1679–1703, October 1998. ISSN 0899-7667. doi: 10.1162/089976698300017089.

C Sekirnjak and S du Lac. Intrinsic firing dynamics of vestibular nucleus neurons. *J. Neurosci.*, 22(6):2083–2095, March 2002. ISSN 0270-6474, 1529-2401. doi: 10.1523/JNEUROSCI.22-06-02083.2002.

M N Shadlen and W T Newsome. The variable discharge of cortical neurons: implications for connectivity, computation, and information coding. *J. Neurosci.*, 18(10):3870–3896, May 1998. ISSN 0270-6474. doi: 10.1523/JNEUROSCI.18-10-03870.1998.

C E Shannon. A mathematical theory of communication. *The Bell System Technical Journal*, 27(3):379–423, July 1948. ISSN 0005-8580. doi: 10.1002/j.1538-7305.1948.tb01338.x.

H Shimazaki and S Shinomoto. A method for selecting the bin size of a time histogram. *Neural Comput.*, 19(6):1503–1527, June 2007. ISSN 0899-7667. doi: 10.1162/neco.2007.19.6.1503.

H Shimazaki and S Shinomoto. Kernel bandwidth optimization in spike rate estimation. *J. Comput. Neurosci.*, 29(1-2):171–182, August 2010. ISSN 0929-5313, 1573-6873. doi: 10.1007/s10827-009-0180-4.

T Shimokawa, S Koyama, and S Shinomoto. A characterization of the time-rescaled gamma process as a model for spike trains. *J. Comput. Neurosci.*, 29(1-2):183–191, August 2010. ISSN 0929-5313, 1573-6873. doi: 10.1007/s10827-009-0194-y.

S Shinomoto. Estimating the firing rate. In Sonja Grün and Stefan Rotter, editors, *Analysis of Parallel Spike Trains*, pages 21–35. Springer US, Boston, MA, 2010. ISBN 9781441956750. doi: 10.1007/978-1-4419-5675-0_2.

B W Silverman. *Density Estimation for Statistics and Data Analysis Estimation Density*. Kluwer Academic Publishers, 1986.

G P Sinha, P Prasoon, B N Smith, and B K Taylor. Fast a-type currents shape a rapidly adapting form of delayed short latency firing of excitatory superficial dorsal horn neurons that express the neuropeptide Y Y1 receptor. *J. Physiol.*, 599(10):2723–2750, May 2021. ISSN 0022-3751, 1469-7793. doi: 10.1113/JP281033.

S Song, J A Lee, I Kiselev, V Iyengar, J G Trapani, and N Tania. Mathematical modeling and analyses of Interspike-Intervals of spontaneous activity in afferent neurons of the zebrafish lateral line. *Sci. Rep.*, 8(1):14851, December 2018. ISSN 2045-2322. doi: 10.1038/s41598-018-33064-z.

R B Stein. A theoretical analysis of neural variability. *Biophys. J.*, 5(2):173–194, March 1965. ISSN 0006-3495. doi: 10.1016/s0006-3495(65)86709-1.

R B Stein. Some models of neuronal variability. *Biophys. J.*, 7(1):37–68, January 1967. ISSN 0006-3495. doi: 10.1016/S0006-3495(67)86574-3.

R B Stein. The role of spike trains in transmitting and distorting sensory signals; in 'the Neurosciences-Second study program'ed. FO schmitt. *Rockefeller Univ Press*, 1970.

C Teeter, R Iyer, V Menon, N Gouwens, D Feng, J Berg, A Szafer, N Cain, H Zeng, M Hawrylycz, C Koch, and S Mihalas. Generalized leaky integrate-and-fire models classify multiple neuron types. *Nat. Commun.*, 9(1):1–15, February 2018. ISSN 2041-1723, 2041-1723. doi: 10.1038/s41467-017-02717-4.

M Tejo and S Niklitschek-Soto. The membrane potential process of a single neuron seen as a cumulative damage process. *Cogn. Neurodyn.*, 10(6):593–595, December 2016. ISSN 1871-4080. doi: 10.1007/s11571-016-9400-6.

F Theunissen and J P Miller. Temporal encoding in nervous systems: a rigorous definition. *J. Comput. Neurosci.*, 2(2):149–162, June 1995. ISSN 0929-5313. doi: 10.1007/BF00961885.

R Tomar. Review: Methods of firing rate estimation. *Biosystems.*, 183:103980, September 2019. ISSN 0303-2647. doi: 10.1016/J.BIOSYSTEMS.2019.103980.

R Tomar and L Kostal. Variability and randomness of the instantaneous firing rate. *Front. Comput. Neurosci.*, 15:620410, June 2021. ISSN 1662-5188. doi: 10.3389/fncom.2021.620410.

R Tomar, C E Smith, and P Lansky. A simple neuronal model with intrinsic saturation of the firing frequency. *Biosystems.*, 222:104780, December 2022. ISSN 0303-2647, 1872-8324. doi: 10.1016/j.biosystems.2022.104780.

G J Tomko and D R Crapper. Neuronal variability: non-stationary responses to identical visual stimuli. *Brain Res.*, 79(3):405–418, October 1974. ISSN 0006-8993. doi: 10.1016/0006-8993(74)90438-7.

J G Trapani and T Nicolson. Mechanism of spontaneous activity in afferent neurons of the zebrafish lateral-line organ. *J. Neurosci.*, 31(5):1614–1623, February 2011. ISSN 0270-6474, 1529-2401. doi: 10.1523/JNEUROSCI.3369-10.2011.

Y Tsubo, Y Isomura, and T Fukai. Power-law inter-spike interval distributions infer a conditional maximization of entropy in cortical neurons. *PLoS Comput. Biol.*, 8(4):e1002461, April 2012. ISSN 1553-734X, 1553-7358. doi: 10.1371/journal.pcbi.1002461.

H C Tuckwell. Neuronal interspike time histograms for a random input model. *Biophys. J.*, 21(3):289–290, March 1978. ISSN 0006-3495. doi: 10.1016/S0006-3495(78)85527-1.

H C Tuckwell. Stochastic processes in the neurosciences. *Biometrics*, 46(2):544, June 1990. ISSN 0006-341X, 1541-0420. doi: 10.2307/2531467.

H C Tuckwell. *Introduction to Theoretical Neurobiology: Volume 2, Nonlinear and Stochastic Theories*. Cambridge University Press, January 2010. ISBN 9780511623202.

B B Ujfalussy, J K Makara, T Branco, and M Lengyel. Dendritic nonlinearities are tuned for efficient spike-based computations in cortical circuits. *Elife*, 4, December 2015. ISSN 2050-084X. doi: 10.7554/eLife.10056.

R Van Rullen and S J Thorpe. Rate coding versus temporal order coding: what the retinal ganglion cells tell the visual cortex. *Neural Comput.*, 13(6):1255–1283, June 2001. ISSN 0899-7667. doi: 10.1162/08997660152002852.

C van Vreeswijk and H Sompolinsky. Chaos in neuronal networks with balanced excitatory and inhibitory activity. *Science*, 274(5293):1724–1726, December 1996. ISSN 0036-8075. doi: 10.1126/science.274.5293.1724.

P Vandroux, Z Li, R Capoduro, M C François, M Renou, N Montagné, and E Jacquin-Joly. Activation of pheromone-sensitive olfactory neurons by plant volatiles in the moth agrotis ipsilon does not occur at the level of the pheromone receptor protein. *Front. Ecol. Evol.*, 10, November 2022. ISSN 2296-701X. doi: 10.3389/fevo.2022.1035252.

J D Victor and K P Purpura. Metric-space analysis of spike trains: theory, algorithms and application. *Network*, 8(2):127, May 1997. ISSN 0093-3341, 0954-898X. doi: 10.1088/0954-898X/8/2/003.

M Xue, J Wang, B Deng, X L Wei, H T Yu, and Y Y Chen. Characterizing neural activities evoked by manual acupuncture through spiking irregularity measures. *Chin. Physics B*, 22(9):098703, September 2013. ISSN 1674-1056. doi: 10.1088/1674-1056/22/9/098703.

C A Yao, R Ignell, and J R Carlson. Chemosensory coding by neurons in the coeloconic sensilla of the drosophila antenna. *J. Neurosci.*, 25(37):8359–8367, September 2005. ISSN 0270-6474, 1529-2401. doi: 10.1523/JNEUROSCI.2432-05.2005.

B M Yu, A Afshar, G Santhanam, S I Ryu, K V Shenoy, and M Sahani. Extracting dynamical structure embedded in neural activity. In *Proceedings of the 18th International Conference on Neural Information Processing Systems*, NIPS'05, pages 1545–1552, Cambridge, MA, USA, December 2005. MIT Press.

Y Zerlaut, S Chemla, F Chavane, and A Destexhe. Modeling mesoscopic cortical dynamics using a mean-field model of conductance-based networks of adaptive exponential integrate-and-fire neurons. *J. Comput. Neurosci.*, 44(1):45–61, February 2018. ISSN 0929-5313, 1573-6873. doi: 10.1007/s10827-017-0668-2.

Attachments

Attachment I Manuscript on comprehensive review of firing rate estimation methods published in *Biosystems* (Tomar, 2019)

Attachment II Manuscript on the variability and randomness of instantaneous rate published in *Frontiers in Computational Neuroscience* (Tomar and Kostal, 2021)

Attachment III Manuscript on intrinsic firing rate saturation in neuronal models published in *Biosystems* (Tomar et al., 2022)

Attachment IV Manuscript on efficient information transmission by moth olfactory receptor neurons

Attachment V Manuscript on trial-to-trial variability quenching in neural networks

Attachment I

Manuscript published in *Biosystems* **183**, 103980. Published on September, 2019
doi: 10.1016/J.BIOSYSTEMS.2019.103980

BioSystems 183 (2019) 103980

Contents lists available at ScienceDirect

BioSystems

journal homepage: www.elsevier.com/locate/biosystems

Review article

Review: Methods of firing rate estimation

Rimjhim Tomar

Institute of Physiology of the Czech Academy of Sciences, Videnska 1083, 14220 Prague 4, Czech Republic

ARTICLE INFO

Keywords:
Firing rate
Spike train
Bayesian rule
Kernel smoothing
Time histogram

ABSTRACT

Neuronal firing rate is traditionally defined as the number of spikes per time window. The concept is essential for the rate coding hypothesis, which is still the most commonly investigated scenario in neuronal activity analysis. The estimation of dynamically changing firing rate from neural data can be challenging due to the variability of spike times, even under identical external conditions; hence a wide range of statistical measures have been employed to solve this particular problem. In this paper, we review established firing rate estimation methods, briefly summarize the technical aspects of each approach and discuss their practical applications.

1. Introduction

Neuronal activity is composed of electric impulses called *action potentials* or *spikes*. Spikes are abrupt and transient changes in membrane voltage that travel to other neurons via axons, and are assumed to be the main channel of communication between neurons. It is a general assumption that spikes carry neural information through their occurrence times since their shape and duration are very similar (Dayan and Abbott, 2001). A set of spikes in time recorded from a single neuron is referred to as a spike train.

One of the most persistent problems in neuroscience has been the question of neuronal coding, i.e., the exact quantitative description of the way information is represented in a spike train: whether the information is embedded in the precise timing of the spikes (temporal code) or their frequency (rate code). As the interspike interval (ISI) between two successive spikes often vary, both within and across trials (Shadlen and Newsome, 1998; Stein et al., 2005; Gerstner and Kistler, 2002; Koyama and Kostal, 2014), there are two main ways of interpreting this irregularity (Shadlen and Newsome, 1994). The *rate coding hypothesis* (Adrian and Zotterman, 1926) suggests that it might be due to stochastic forces, then the irregular ISIs reflect a random process. Therefore, the pooled response from many neurons would be required for firing rate estimation. In this scenario, the exact temporal pattern of spikes contains little information. On the other hand, according to the *temporal coding hypothesis* the irregularity might be due to pre-synaptic events, in which case the timings of spikes and their patterns may carry important information (Perkel and Bullock, 1968; Shadlen and Newsome, 1994; Kostal et al., 2007; Kostal and Shinomoto, 2016). A wide range of methods from probability theory and stochastic point processes have been applied to obtain embedded information content in a neural spike train (Cox, 1966; Moore et al., 1966; Tuckwell, 2005; Kostal and Lansky, 2006).

The classic rate coding paradigm suggests that the communicated information is embedded in the spikes sent along the axon per observation time window (also called the firing rate) (Dayan and Abbott, 2001). In most sensory systems, the firing rate increases, generally nonlinearly, with increasing stimulus intensity (Kandel et al., 1991). In this paper, we focus on the problem of firing rate estimation, especially if the rate itself is not stable but evolves in time.

It is challenging to determine the time dependent firing rate from a few spike trains. Most of the established methods use trial averaging; however, averaging might phase out some of the critical temporal features (Nawrot et al., 1999; Baker et al., 2001; Byron et al., 2006), thus extracting the time dependent firing rate from limited data remains a persistent problem. We briefly review the established methods of firing rate estimation developed over the years, from classical to more recent approaches.

The paper is organized as follows: the concept of firing rate is explained in detail using point process theory in Section 2, whereas Section 3 presents a concise overview of stationary and non stationary neural activity, which is an important classification from a statistical point of view. Finally, in Section 4 a brief description of each method is presented.

2. Firing rate

Spike times $0 < s_1 < s_2 < \ldots$ are often modeled as a realization of a *stochastic point process* (Cox, 1966; Perkel et al., 1967; Tuckwell, 2005) i.e., the nth spike time is a random variable, denoted as S_n. It is assumed that the time instant $t = 0$ is not related to the actual spike times, i.e., it is fixed with respect to a *reference* (laboratory) time before the point process realization (Kostal et al., 2018; Cox, 1966). The

E-mail address: rimjhim.tomar@fgu.cas.cz.

https://doi.org/10.1016/j.biosystems.2019.103980
Received 10 April 2019; Received in revised form 27 May 2019; Accepted 30 May 2019
Available online 01 June 2019
0303-2647/

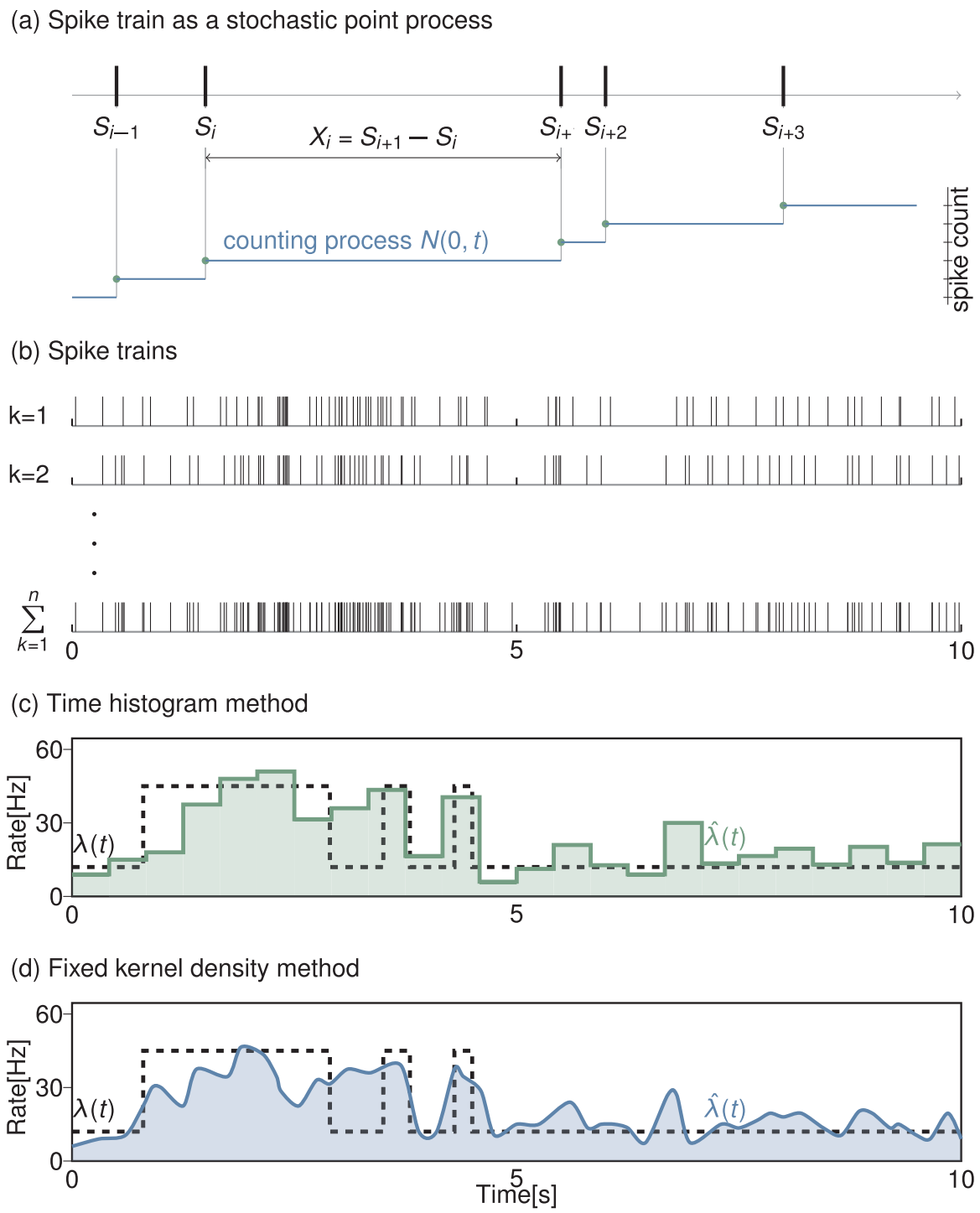

Fig. 1. Neuronal spiking activity and firing rate estimation. (a) Spikes occur at times S_i; the corresponding interspike intervals (ISIs) are denoted as X_i, and the associated counting process up to time instant t is $N(0, t)$. (b) Examples of spike trains simulated under identical statistical conditions. For most of the firing rate estimation methods, individual spike trains are superimposed but few methods, like Frequencygram (Section 4.1) and Bayesian Adaptive Kernel Smoothing (Section 4.8), work with individual recordings as well. (c) Estimation of underlying firing rate (green) from the spike train data, using the time histogram method, compared with the true underlying firing rate (dashed). (d) Firing rate estimation (blue) using the kernel smoothing method with Gaussian kernel, against the true underlying firing rate (dashed). (For interpretation of the references to color in this figure legend, the reader is referred to the web version of this article.)

interspike intervals (ISIs), X_i, are defined as $X_i = S_{i+1} - S_i$, $i = 1, 2, \ldots$. The associated *counting process*, $N(t_1, t_2)$, for any $t_2 > t_1$, is a random variable describing the number of spikes in the time interval $(t_1, t_2]$. The spike times S_i and the process $N(0, t)$ are related by $\{S_i \leq t\} = \{N(0, t) \geq i\}$.

The *firing rate* $\lambda(t)$ of the point process at some time t is the limit of the expected number of events in an interval beginning at t divided by the duration of the interval (Fig. 1) (Johnson, 1996),

$$\lambda(t) = \lim_{\epsilon \downarrow 0} \frac{\mathbb{E}[N(t, t+\epsilon)]}{\epsilon} \tag{1}$$

where the mean (expected) spike count in $(t_1, t_2]$ is denoted as $\mathbb{E}[N(t_1, t_2)]$.

Generally, the firing rate may depend on the time and history of the

point process. If the firing rate $\lambda(t)$ depends on time, then the process is non stationary. The part of the rate that depends on history takes into account the detailed interactions between past spike times and the current ones (Johnson, 1996). One example of such interactions is the refractory time, a period where the rate takes the value zero, right after a spike occurs.

The firing rate $\lambda(t)$ specifies the statistical structure of the process (Johnson, 1996). However, without any prior information about the point process, the experimental data might not be enough to determine the limit given in Eq. (1) uniquely. Alternatively, in such cases, the firing rate is often defined as the actual number of spikes in a sufficiently long (finite) time window of duration w, chosen by the experimenter. This term is called the *firing frequency* and it's defined as (Adrian, 1928; Dayan and Abbott, 2001)

$$v(t, w) = \frac{\mathbb{E}[N(t, t+w)]}{w}. \tag{2}$$

Formally, little can be said about the relationship between $\lambda(t)$ and $v(t, w)$ without knowing the exact probabilistic description of the underlying point process. From a practical point of view, assumptions are needed about the underlying statistical models of spike data used for the analysis. More details about the commonly used underlying stochastic processes are given in the following sections.

3. Stationary neural activity

A point process is stationary if the probability distribution of the number of events in an interval $(t_1, t_2]$ is invariant under translation, i.e., is the same for $(t_1 + h, t_2 + h]$ for all h (Cox, 1966). In a practical sense, stationarity implies that the firing rate of the point process does not display any trends or shift from one instant of time to the other:

$$\lambda(t) = C, \tag{3}$$

where C is constant. Cox (1965) addresses the issue of estimating the rate function for a large class of stationary point processes.

One class of stationary point process, known as *renewal processes* exhibits the property of independent and identically distributed intervals between events (Cox, 1962). In renewal processes, the time to the first spike after $t = 0$ does not follow the same probability distribution as the consequent ISIs. The sequence of random variables corresponding to the ISIs after time t is thus not stationary (Cox, 1962). Consider a spike train with an underlying renewal process conveniently characterized by the random variable X (the ISI length), then it follows from the "elementary renewal theorem" (Cox, 1966; Rudd and Brown, 1997; Kostal et al., 2018),

$$\lambda = \frac{1}{\mathbb{E}(X)} = \lim_{w \to \infty} v(t, w). \tag{4}$$

Stationary neural activity is typical in the case of spontaneous activity or steady-state stimulations (Moore et al., 1966). However, neural responses are often non-stationary (Perkel et al., 1967), hence the case of stationary neural activity is of limited interest for the purpose of this paper. In what follows, we generally focus on non-stationary processes that describe the behavior of the spike trains.

4. Methods for firing rate estimation

In the following sections, it is assumed that the data from n spike trains have been recorded under independent and statistically identical trials. Let $(0, T]$ denote the duration of trials and $0 \le s_1 < s_2 \ldots < s_n \le T$ be the spike times for a particular spike train. We denote the estimated underlying firing rate with $\hat{\lambda}(t)$.

4.1. Frequencygram

One of the oldest methods that deal with time-dependent changes in the firing rate employs the concept of "instantaneous firing rate", where the reciprocal values of ISIs are used to determine the firing rate. The instantaneous firing rate for a given spike train $s_1, s_2, \ldots$, at a time point t is estimated as

$$\hat{\lambda}(t) = \frac{1}{s_i - s_{i-1}}, \quad s_{i-1} \le t < s_i. \tag{5}$$

In an experiment conducted in Bessou et al. (1968), an 'instantaneous frequency meter' is used to record the discharges of spindle primary endings as a succession of points. The superposition of a large number of records of 'instantaneous' frequency, under certain conditions, lead to the construction of graphs called *frequencygrams*. Knight (1972) worked on the efficiency analysis of such methods for periodic signals. Following the analogy of frequencygram, under the renewal model, the instantaneous firing rate F is a random variable obtained from the ISI random variable X through the one to one transformation,

$$F = \frac{1}{X}. \tag{6}$$

There are several key differences between the classical firing rate and instantaneous firing rate, and the most important one is that the mean instantaneous firing rate is typically higher than the count-based firing rate (Lansky et al., 2004).

The concept of instantaneous firing rate has been applied in many situations. For example, Sawczuk et al. (1995) use the reciprocal of the first interspike interval as the magnitude of initial adaptation while investigating spike frequency adaptation in hypoglossal motoneurons of a rat. Martinez-Conde et al. (2000) define firing rate as the reciprocal of ISIs, in his paper where he studies microsaccadic eye movements and firing of neurons in striate cortex of macaque monkey. Rospars et al. (2003) and Lemon and Smith (2006) adopt the definition of instantaneous firing rate (Eq. (6)) in their respective papers. Val-Calvo et al. (2019) use the firing rate estimated from inverse ISIs in frequency variation analysis in neuronal cultures for stimulus-response characterization. Theoretical applications of instantaneous firing rate can for example be found in Pauluis and Baker (2000) in their presentation of the detailed study of the treatment of rapid change in frequencygrams, in Harris and Waddington (2012) in the investigation of the inverse distribution of common models of ISIs, in Kostal et al. (2018) where the authors revisit the main concepts involved in the method of estimating instantaneous firing rate and the impact of the inspection time on instantaneous firing rate statistics.

4.2. Time histograms

In order to obtain an approximate estimate of the firing rate from a few spike trains, time averaging over short time intervals is performed. This process is called *binning*, and it is used in various firing rate estimation methods. The most basic and frequently used tool for rate estimation is the time histogram method (Gerstein and Kiang, 1960), also referred to as the post-stimulus time histogram method (PSTH) (Johnson, 1978).

For this method, n spike trains observed under independent and identical statistical trials are taken and superimposed. Observation period T is divided into bins of duration Δ and the number of spikes in the ith bin, across all trials, is denoted by k_i. The firing rate $\hat{\lambda}(t)$ for the ith bin is estimated as (Shinomoto, 2010)

$$\hat{\lambda}(t) = \frac{k_i}{n\Delta} \tag{7}$$

for $t \in [(i-1)\Delta, i\Delta)$. This process is repeated for each of the $N_b = \lfloor T/\Delta \rfloor$ bins to compute a piece-wise constant function representing the firing rate value in that particular bin.

This method is very easy to implement; however, it might not represent the firing rate fluctuations accurately. In particular, the temporal resolution of the estimation critically depends on the bin size.

With a bin size too large, the time dependency of the firing rate is lost, and with a bin size too small, the fluctuations in the estimation might be too rapid (Hardle and Abbott, 1991).

Shimazaki and Shinomoto (2007) proposed a method to optimize the bin size of the time histogram method so that the mean integrated squared error (MISE) between the estimated rate and the unknown underlying rate is minimized,

$$\text{MISE} = \frac{1}{T}\int_0^T \mathbb{E}(\hat{\lambda}(t) - \lambda(t))^2 \,\mathrm{d}t \tag{8}$$

where $\mathbb{E}$ refers to the expectation over different trials, given the rate $\lambda(t)$. However, since the underlying firing rate is not known, Shimazaki and Shinomoto (2007) derive an optimization method to obtain the bin size. This method is derived rigorously using bias-variance decomposition to obtain the expected value of MISE in terms of observed spike count.

This approach was further improved in Omi and Shinomoto (2011) by the inclusion of non-Poissonian features such as the impact of the firing history on the occurrence of a spike (Kuffler et al., 1957; Baker and Lemon, 2000; Pillow et al., 2005; Kostal and Lansky, 2006). The bin width optimization for these spike trains is done with the aid of a *cost function*, which is derived by decomposing the MISE function with the help of a Fano-factor (ratio of variance of the spike count to the mean) like quantity $\hat{F}_i$. This quantity $\hat{F}_i$ is defined in terms of local variation L_V that measures the ISI variability (Omi and Shinomoto, 2011),

$$\hat{F}_i = \begin{cases} 1, & \text{if } k_i \le 2, \\ \dfrac{2L_V}{3 - L_V}, & \text{otherwise,} \end{cases} \tag{9}$$

where the local variation $L_V = \frac{3}{k_i - 2}\sum_{j=1}^{k_i-2}\left(\frac{x_j - x_{j+1}}{x_j + x_{j+1}}\right)^2$ is computed from the ISIs $\{x_j\}$ that fall into the bin. Using $\hat{F}_i$, average $\bar{h}$ of $\{\hat{F}_i k_i\}$ and variance $\bar{v}$ of $\{k_i\}$ is calculated for each bin i. Then the estimated cost function is

$$\hat{C}(\Delta) = \frac{2\bar{h} - \bar{v}}{\Delta^2}. \tag{10}$$

This procedure is repeated, while changing the value of Δ, to obtain the optimal bin size that minimizes the cost function. More details about this method are given in Omi and Shinomoto (2011) with application to simulated and biological data along with the discussion of potential limitations.

Gerstein and Mandelbrot (1964) use time histograms to show the activity of a cochlear nucleus in response to clicks at various rate in the description of a random walk model for the spike activity of a single neuron. Movshon et al. (1978) compile the neural responses to visual stimuli with time histograms while investigating the spatial summation in the receptive fields of simple cells in the cat's striate cortex. Berry and Meister (1998) calculate the firing rate of a salamander ganglion cell in response to a random flicker situation, employing this method. Lütkenhöner and Smith (1986)Lütkenhöner and Smith (1986) show the rapid adaptation properties associated with high or low spontaneous rate recorded from single auditory nerve fibers of a cat, using histograms. Ruskin et al. (1999) record variations in firing rate in response to event signals from a ventilator apparatus, with the help of time histograms. Mukamel et al. (2010) measure the firing rate with time histogram method, in their study of the single-neuron responses in humans during execution and observation of actions. Vizuete et al. (2014) use the MISE technique mentioned in Shimazaki and Shinomoto (2007) in computing the ISI histograms of data obtained from adult male Sprague-Dawley rats in their study of graded defragmentation of cortical neuronal firing during the recovery of consciousness in rats.

4.3. Kernel smoothing

This method is also known as the *fixed kernel estimation*. To address the issue of localized error around the bin edges, the window method was proposed (Rosenblatt, 1956; Parzen, 1962). Instead of dividing the time interval into N_b separate time windows of a certain duration, placed at pre-determined time points, a moving average is taken, which calculates the local average value in a window centered around each data point s_i. Mathematically, this is equivalent to convolving the data with a window function. Generally, the window function can be re-written using the kernel function $K_h(t)$ with bandwidth h. For spike time data $s_1, s_2, \ldots, s_N$ the fixed kernel estimator is given by

$$\hat{\lambda}(t) = \sum_{i=1}^{N} K_h(t - s_i), \tag{11}$$

where h is called the *smoothing parameter* or the *bandwidth*. Estimated rate $\hat{\lambda}(t)$ is also referred to as Spike Density Function (SDF). The smoothing parameter is held constant for all the data points (Silverman, 1986). The kernel function satisfies the natural conditions (Nawrot et al., 1999),

$$K_h(t) \ge 0, \tag{12a}$$

$$\int_{-\infty}^{\infty} K_h(t)\mathrm{d}t = 1, \tag{12b}$$

$$\int_{-\infty}^{\infty} \mathrm{t}K_h(t)\mathrm{d}t = 0. \tag{12c}$$

Smoothness of the estimated rate depends on the choice of the kernel. Desirable qualities of a good kernel function are discussed in Paulin (1992) with a comparison of some pre-established kernels. Nawrot et al. (1999) use numerical simulations to assess the effects of width and shape of the kernel functions and conclude that the choice of specific kernel shape does not have critical effects on the estimation error. These findings are in agreement with the results given in Silverman (1986) and Scott (1992). More details about kernel smoothing can be found in Silverman (1986), Scott (1992), Wand and Jones (1994) and Bowman and Azzalini (1997).

Sanderson (1980) uses spike density function and filtering techniques to study the relationship between spike firing of a single neuron and gross evoked potentials. Richmond et al. (1987) represent the firing rate of inferior temporal (IT) neurons of alert behaving monkeys with spike density function. Tovee and Rolls (1995) analyze the neural response using spike density function, from two alert macaque monkeys, to a different face stimulus in order to obtain different time series for principal component extraction. This data is used to conclude that short periods of firing may be sufficient to provide useful information as compared to longer periods of neuronal firing. Szucs (1998) uses the kernel smoothing method in the analysis of the firing patterns of Lymnaea neurons. Kohler et al. (2002) show the activity of neurons responding to the sound of different specific actions in the ventral premotor cortex of awake macaque monkeys, with spike density function. Yaksi and Friedrich (2006) obtain firing rate of sensory neurons via kernel smoothing method with Gaussian kernel to demonstrate that neuronal firing rate changes of many neurons can be reconstructed efficiently and robustly by temporally deconvolved Ca^{2+} imaging.

For a time-varying rate function, kernel smoothing might not be effective in capturing the temporal variations. Silverman (1986) discusses the over-smoothing effect of the fixed bandwidth in certain probability distributions. The next step is to find an optimum kernel bandwidth, which gives a smooth estimation irrespective of the dips in the time-dependent firing rate.

4.4. Optimized kernel smoothing

The choice of the free parameter h is a crucial problem with kernel smoothing method since it affects the smoothness of the firing rate estimate and highlights the temporal structure of the underlying spiking activity. There are multiple ways to infer the optimized kernel bandwidth, a few of which use the discrepancy between the estimate $\hat{\lambda}(t)$

and $\lambda(t)$ to define some error criterion. The optimized bandwidth will then be the bandwidth minimizing the error obtained through the defined error criterion. Alternatively, the concept of using a variable kernel bandwidth is studied in detail as well. We review the main methods of optimized kernel smoothing in this section.

4.4.1. Globally optimized kernel smoothing

The idea of bandwidth optimization was proposed by Loftsgaarden and Quesenberry (1965). It has been employed to obtain a smooth estimation of a rapidly changing firing rate $\lambda(t)$. Nawrot et al. (1999) propose a technique of optimizing bandwidth to get optimal results. The method starts with a wide kernel bandwidth, which is systematically reduced. Integrated Squared Error (ISE) is recorded after each step between the successive rate estimates associated with each bandwidth choice. Assuming that the bandwidth choice at certain step is h and for the succeeding step is h', the ISE for the pair of successive rate estimate is

$$\mathrm{ISE} = \int_0^T \left(\hat{\lambda}_h - \hat{\lambda}_{h'}\right)^2(t)\,\mathrm{d}t. \tag{13}$$

From observations, it is then concluded that at a particular kernel width, the ISE curve encounters a clear minimum which is close to the optimum kernel bandwidth.

Another method for bandwidth optimization is given in Cherif et al. (2008), which furthermore involves convolving the spike train with an *optimal kernel*. An optimally designed Kaiser window (Cherif et al., 2008) is used to define the Kaiser kernel which works as the kernel of choice, where the bandwidth selection is done with frequency analysis of the spike train. The Kaiser window function (Kaiser, 1974) is defined as,

$$w_\alpha(t) = \begin{cases} \dfrac{I_0(\beta\sqrt{1-((2t/M)-1)^2})}{I_0(\beta)}, & 0 \le t \le M \\ 0, & \text{otherwise} \end{cases} \tag{14}$$

where I_0 is the zero order modified Bessel function and M is the length of the window and β is the shape parameter. Kaiser filter design is based on the optimization of these parameters. The advantage of the Kaiser window is its flexibility due to the two independent variables M and β. The optimal values of M and β are given in Cherif et al. (2008). The authors have compared the performance of the Kaiser window method with other well-established methods.

Building up on the technique used to find an optimal bin width for time histograms (Eq. (10)), a similar optimization method is applied to find a fixed kernel bandwidth that fits the varying firing rate (Shinomoto, 2010). The modified cost function for n spike trains, with the kernel function $K_h(t)$ of bandwidth h, is

$$C_n(h) = \frac{1}{n^2}\sum_{i,j}\psi_h(s_i, s_j) - \frac{2}{n^2}\sum_{i\neq j}K_h(s_i - s_j), \tag{15}$$

where $\psi_h(s_i, s_j) = \int K_h(t - s_i)K_h(t - s_j)$, and similar to the method presented in Shimazaki and Shinomoto (2007), minimizing the cost function with respect to h yields the optimal kernel bandwidth.

Cunningham et al. (2009) use the method mentioned in Nawrot et al. (1999) for their study regarding the brain machine interface application of neural prosthetic decoding in arm-reaching setting and report that this method produces a wide range of different kernel bandwidth depending on the experimental data. Jamali et al. (2009) represent the neural discharge data obtained from analyzing the head movements of macaque monkeys with the Kaiser window method, which was further used in the analysis of response dynamics of utricular and saccular afferents. Kaiser window method is used in Van Horn et al. (2013) to determine the firing rate of neurons in the rostral superior colliculus (rSC), while investigating whether the rSC contributes to the development of neural signals that are suitable for controlling vergence eye movements. Tilunaite et al. (2017) apply the kernel bandwidth optimization method mentioned in Shinomoto (2010), to obtain optimized kernel smoothing estimate of the firing rate function describing the Ca^{2+} spike sequences. The paper focuses on proposing a modeling framework that allows a quantitative description of the timing of calcium spikes.

4.4.2. Locally adaptive kernel smoothing

Another way of improving kernel smoothing is to allow for a variable bandwidth, which can adapt to the local rate, instead of a fixed bandwidth throughout the whole duration of the trial. Typically, this method proceeds in two steps. The first step includes an initial estimation to get a rough idea of the density, which provides a pattern of the bandwidths based on the data and these bandwidths are used to develop the adaptive estimator (Silverman, 1986). The first estimate, called the *pilot estimate* can be done with the fixed-width kernel (Richmond et al., 1987), as there are no specific smoothness requirements for the first step estimation; however, choice of the fixed width of the pilot estimate does affect the adaptive estimate. Let $\hat{\lambda}_p(s_i)$ be the pilot estimate at the ith data point as described in Eq. (11), and let μ be the geometric mean of all pilot estimates at the N given data points,

$$\mu = \exp\left[\frac{1}{N}\sum \ln\hat{\lambda}_p(s_i)\right]. \tag{16}$$

Local bandwidth of the adaptive estimate is given by

$$\bar{h}_i = \left[\frac{\hat{\lambda}_p(s_i)}{\mu}\right]^{-\alpha}, \tag{17}$$

where α is called the *sensitivity parameter*, the value of which lies between 0 and 1. Adaptive kernel estimate is then given as a modification of Eq. (11) (Breiman et al., 1977; Sain and Scott, 1996),

$$\hat{\lambda}(t) = \sum_{i=1}^{N} K_{h_i}(t - s_i), \tag{18}$$

where h_i is a product of smoothing parameter from fixed-width method h and local bandwidth $\bar{h}_i$ obtained with the pilot estimate. This new estimate makes the kernel narrow when spikes are closer together (which implicates high firing rate, or spikes occurring at the same time across trials), and spreads the kernel whenspikes are isolated. Abramson (1982) proposes $\alpha = 1/2$ as a reasonable choice for the smoothing parameter under mild assumptions.

Another approach is to extend the fixed width optimization technique (Eq. (15)) by dividing the trial duration into local sub-intervals where the variable bandwidth is used. A local MISE function at time t is used to derive a local cost function at that instant. Through the local cost function, a locally optimal bandwidth h_t and suitable time window length are established. A new parameter γ is obtained to overlook the smoothness factor between the choice of window length and optimal bandwidth. The cost function derived using a kernel function K_t, accounting for variable bandwidth t with smoothing parameter γ (Shimazaki and Shinomoto, 2010), is

$$\hat{C}_n(\gamma) = \int \hat{\lambda}_t^{\,2} - \frac{2}{n^2}\sum_{i\neq j}K_t(s_i - s_j), \tag{19}$$

where $\hat{\lambda}_t = \sum_i K_t(t - s_i)$ is the estimated rate. Using the above equation, the cost function is minimized to obtain an optimal γ^*. The ideal bandwidth h_t^γ is calculated using γ^* and the cost function.

Shimazaki and Shinomoto (2010) compare the fixed and variable kernel methods to the other established methods with sample spike data from 10 superimposed spike trains on the basis of integrated squared error (ISE) and notice that variable kernel estimation is more efficient in capturing the abrupt changes in the rate. The authors also include the performance analysis of variable and fixed kernel bandwidth, with application to real biological spike data of an MT (visual area) neuron responding to a random dot stimulus (Britten et al., 2004).

Richmond et al. (1987) use both fixed and adaptive kernel methods

to study striate cortical neurons. Jones (1990) presents a thorough description of the differences between the two estimation methods. Waitzman et al. (1991) obtain the firing rate for single cell analysis, using the adaptive kernel method with neural data from two female rhesus monkeys. Additionally, a collicular feedback model of the saccadic system is proposed which accounts for the dynamic relationships of collicular firing to both saccadic amplitude and velocity. Terrell and Scott (1992) analyze all different variations of variable kernel estimation. Lee and Malpeli (1998) investigate the effects of saccades on the activity of neurons in the cat lateral geniculate nucleus (LGN) and use adaptive kernel smoothing on data obtained from seven LGN in four cats. Missal et al. (2000) conducted an experiment to investigate the activity of medium-lead burst neurons during saccade and smooth pursuit and to assess their possible roles in the control of the two types of movements. Here adaptive kernel smoothing is used to estimate the firing rate of spike trains obtained from two adult cats trained to perform a saccade and smooth pursuit task. Sheinberg and Logothetis (2001) estimate the firing rate of individual temporal cortical neurons with the aid of adaptive kernel smoothing, while monkeys looked for and identified familiar targets placed in isolation and embedded setting.

Bayesian methods

The problem of firing rate estimation is widely studied using the methods of Bayesian statistics as well. Bayesian methods typically start with assuming prior probability distribution $p(\lambda(t))$ on the firing rate function $\lambda(t)$ and a probability model describing how the spike train $\mathbf{s} = [s_0, s_1, \ldots, s_N]$ is generated, given the underlying firing rate, denoted by $p(\mathbf{s}|\lambda(t))$. Bayes' rule (Papoulis and Pillai, 2002) is used to infer the most likely firing rate function from the given spike trains (Mochizuki and Shinomoto, 2014)

$$\hat{\lambda}(t) = \underset{\lambda(t)>0}{\operatorname{argmax}} p[\lambda(t)|\mathbf{s}], \tag{20}$$

where

$$p[\lambda(t)|\mathbf{s}] = \frac{p[\mathbf{s}|\lambda(t)]p[\lambda(t)]}{p[\mathbf{s}]} \tag{21}$$

is the posterior distribution for $\lambda(t)$. These equations are easily modified accordingly for multiple spike trains. Variations of this general approach are seen in the methods in the following sections.

Method	Main characteristics	Notable references
Frequencygram	Uses the reciprocal values of ISIs to determine the firing rate.	Bessou et al. (1968)
Time Histogram (PSTH)	Trial duration is divided into bins and firing rate of a particular time bin is ratio of the number of spikes in the time bin and its duration.	Gerstein and Kiang (1960), Shimazaki and Shinomoto (2007)
Kernel Smoothing (KS)	Spike train is convolved with a kernel function to produce the firing rate as a weighted average of the spikes nearby at any given instant.	Rosenblatt (1956), Parzen (1962), Nawrot et al. (1999), Shinomoto (2010)
Globally Optimized Kernel Smoothing	Bandwidth parameter of the kernel function is optimized using a predefined error criterion to yield a fixed bandwidth.	Nawrot et al. (1999), Cherif et al. (2008), Shinomoto (2010)
Adaptive Kernel Smoothing	Non stationary kernel or local optimized bandwidth is incorporated to allow for a smoother firing rate estimation.	Silverman (1986), Shimazaki and Shinomoto (2010)
Gaussian Process Firing Rate (GPFR)	Firing rate is assumed to be drawn from Gaussian process, spike trains are generated according to IGIP. Bayes' rule is used to infer the most likely firing rate function.	Cunningham et al. (2008)
Bayesian Adaptive Regression Splines (BARS)	Spline basis with prior distribution is used to model the firing rate, spike trains are assumed to generated according to Poisson process. Reversible jump MCMC is used to estimate the underlying firing rate.	DiMatteo et al. (2001)
Bayesian Binning (BB)	Firing rate is modeled a priori by piecewise constant regions of varying width, the spike trains are assumed to be generated from inhomogeneous Bernoulli process. Firing rate is inferred using Bayes' rule.	Endres et al. (2008)
Bayesian Adaptive Kernel Smoothing (BAKS)	BAKS incorporates the Adaptive Kernel Smoothing technique and treats the adaptive bandwidth as a random variable which is constantly updated under a Bayesian framework to yield an adaptive bandwidth.	Ahmadi et al. (2018a)

4.5. Gaussian process firing rate (GPFR)

In this method, the firing rate $\lambda(t): t \in [0, T]$ is assumed to be drawn from a Gaussian process (GP) prior, and spike trains are modeled by inhomogeneous gamma interval process (IGIP) (Barbieri et al., 2001). Given the firing rate function $\lambda(t)$, the conditional probability $p(\mathbf{s}|\lambda(t))$, is given by

$$p(\mathbf{s}|\lambda(t)) = \prod^{N} p(s_i|s_{i-1}, \lambda(t)) p_0(s_0|\lambda(t)) p_T(T|s_N, \lambda(t)), \tag{22}$$

where p_0 is the density of the first spike occurring at time s_0 and p_T is the density of no spike occurring in the interval $(s_N, T]$; $p(s_i|s_{i-1}, \lambda(t))$ is the density of the IGIP intervals which can be written as (Barbieri et al., 2001),

$$p(s_i|s_{i-1}, \lambda(t)) = \frac{\nu\lambda(s_i)}{\Gamma(\nu)}\left(\nu\int_{s_{i-1}}^{s_i}\lambda(u)\mathrm{d}u\right)^{\nu-1}\exp\left\{-\nu\int_{s_{i-1}}^{s_i}\lambda(u)\right\}\mathrm{d}u, \tag{23}$$

where ν is the shape parameter and $\Gamma(\nu)$ is the gamma function (Johnson and Kotz, 1971). The true p_0 and p_T are not closed form in IGIP model, hence for tractability these distributions are simplified as the intervals of an inhomogeneous Poisson process. Furthermore, $\lambda(t)$, $t \in [0, T]$ is discretized by the time resolution of the experiment (say Δ) to yield a series of $N_b = T/\Delta$ evenly spaced samples $\boldsymbol{\lambda} = [\lambda_1, \lambda_2, \ldots, \lambda_{N_b}]'$. Modifying Eq. (22) according to the discretization produces an updated formula for $p(\mathbf{s}|\boldsymbol{\lambda})$ (Daley and Vere-Jones, 2002). The details of this derivation are given in Cunningham et al. (2008).

Another important factor is the choice of the covariance function used in the firing rate prior. Cunningham et al. (2008) use the standard squared exponential covariance function defined below and note that the other standard covariance functions behave similarly. Thus, $\boldsymbol{\lambda} \sim N(\mu, \Sigma)$, where the covariance matrix Σ is defined by,

$$\Sigma = K(t_i, t_j)_{i,j=1,\ldots,n}, \tag{24}$$

where $K(t_i, t_j) = \sigma_f^2 \exp\{-\frac{\kappa}{2}(t_i - t_j)^2\} + \sigma_v^2\delta_{ij}$; signal variance σ_f^2 and noise variance σ_v^2 are the parameters of Gaussian prior. For more information about the GP and covariance functions, see Williams and Rasmussen (2006).

For notational convenience, let the hyperparameter set for this model be denoted by $\theta = [\mu; \gamma; \kappa; \sigma_f^2; \sigma v^2]$. The problem of calculating the posterior on firing rate $p(\boldsymbol{\lambda}|\mathbf{s}) = \int_\theta p(\boldsymbol{\lambda}|\mathbf{s}, \theta)p(\theta)\mathrm{d}\theta$ is intractable, and it's approximated by either replacing the integral by evaluation at the modal θ

$$\theta^* = \underset{\theta}{\operatorname{argmax}} p(\theta|\mathbf{s}) = \underset{\theta}{\operatorname{argmax}} p(\theta)p(\mathbf{s}|\theta) = \underset{\theta}{\operatorname{argmax}} \int_\lambda p(\mathbf{s}|\lambda, \theta)p(\lambda|\theta)\mathrm{d}\lambda, \tag{25}$$

or replacing the integral with a sum over a discrete grid of θ values. To proceed with either of these methods, the modal firing rate estimate is needed, which is obtained using the maximum a posteriori (MAP) estimator (see Eq. (20)). Modal firing rate $\hat{\boldsymbol{\lambda}}^*$ is used for the Laplace approximation to determine the modal hyperparameter θ^*. The basic idea of Laplace approximation is to approximate the logarithm of the integrand in question by its second degree Taylor expansion about its

mode. The same Laplace approximation is used in approximating the integral over θ using a simple grid of θ values, to arrive at an approximate integrated posterior. For an in-depth description of this method, see Cunningham et al. (2009).

Since this method works in multiple iterative layers, Cunningham et al. (2008) give a brief outline of efficient algorithms to potentially alleviate the challenges associated with the computational cost of this method. Rad and Paninski (2010) use a similar technique to derive efficient estimates of two dimensional firing rate surfaces.

4.6. Bayesian Adaptive Regression Splines (BARS)

This technique uses the smoothing spline method of curve estimation to estimate the firing rate function. Splines are functions defined piece-wise by polynomials, connecting at time points called "knots". Similar to GPFR, BARS models the firing rate by assuming a prior distribution on the number and position of knots and other parameters of the spline function representing the firing rate. BARS uses standard cubic splines. Spline basis allows the estimator to capture the high frequency changes in the firing rate while removing the high frequency noise, which is an added advantage.

To make inference about the firing rate function $\lambda(t)$, BARS fits the generalized non-parametric regression model for the spike counts Y_i observed at the time points X_i's,

$$Y_i \sim p(y_i|\lambda(X_i), \zeta), \tag{26}$$

where $\lambda(t)$ is a spline with an unknown number of knots at unknown locations $\xi = (\xi_1, \ldots, \xi_k)$, ζ is an optional nuisance parameter and p is a specified distribution. With these assumptions, $\lambda(t)$ may be written in terms of the basis functions b_j, $j = 1, \ldots, k+2$ as $\lambda = \sum_{j=1}^{k+2} \beta_j b_j(x)$ for some vector $\beta = (\beta_1, \ldots, \beta_{k+2})$.

For a known knot set, Eq. (26) reduces to an easy estimation problem; however, determining ξ is the challenging part. BARS uses prior distribution on the number and location of the knots and then a reversible-jump MCMC algorithm, to generate draws from the posterior distribution and provide an optimally fitted curve based on drawn samples of the possible number of knots and their location. The original idea of using reversible-jump MCMC to select knots is given in Denison et al. (1998).

DiMatteo et al. (2001) show that BARS could reduce the MSE below other existing methods and use BARS to estimate the time-intensity function of neuronal firing in a monkey's brain. Kass et al. (2003) demonstrate the smoothing properties of BARS method when it comes to highly varying firing rate. Kaufman et al. (2005) use BARS as a basis to propose a new non-parametric regression method to fit neuronal data. BARS is used to calculate the firing rate function of simulated neurons in Ventura et al. (2005) when no trial-to-trial variation is assumed. This data is used to propose a statistical method to describe trial-to-trial variation or "excitability" effects. Wen et al. (2009) apply BARS to fit the firing rate function, of the inferior culliculus neuron and auditory nerve fiber of anesthetized cats in response to continuous, dynamic sound stimuli. In this paper, the authors investigate whether dynamic range adaptation to the sound level distribution first observed in the auditory midbrain also occurs in primary auditory neurons.

4.7. Bayesian binning

Endres et al. (2008) developed this Bayesian method of estimating the neural firing rate. It is a compromise between binning and smoothing in a way that the bins are kept to enable rapid changes in firing rate, but the bin duration is variable. Neural firing rate is modeled a priori by piecewise constant regions of varying width (Endres et al., 2008).

Given the underlying firing rate, let the ith spike train recorded between time 0 and T be represented by a binary vector $\mathbf{s}$. The trial duration T is discretized into Δ time bins, and thus the vector $\mathbf{s}$ has dimension $N_b = \lfloor T/\Delta \rfloor$. The time interval is divided into $M+1$ contiguous, non overlapping bins having inclusive upper boundaries k_m, within which the firing probability $f_m = P(spike|t \in (t_{min} + \Delta t(k_{m-1} + 1),\ t_{min} + \Delta t(k_m + 1))]$ is constant. The number of bin boundaries for the trial duration is M. Spike train $\mathbf{s}$ of independent spikes is modeled by an inhomogeneous Bernoulli process with piecewise constant probabilities, given the firing rate

$$P(\mathbf{s}|\{f_m\}, \{k_m\}, M) = \prod_{m=1}^{M} f_m^{z(\mathbf{s},m)} (1 - f_m)^{g(\mathbf{s},m)}, \tag{27}$$

where $z(\mathbf{s}, m)$ is the number of spikes and $g(\mathbf{s}, m)$ is the number of non spikes (gaps) in the spike train $\mathbf{s}$ in the bin m. The equation above is easily modified for multiple spike trains, denoted by $\{\mathbf{s}\}$.

The chosen prior on $f_m \in [0, 1]$ is a density since f_m is a continuous model parameter,

$$p(\{f_m\}|M) = \prod_{m=1}^{M} B(f_m; \sigma_m, \gamma_m), \tag{28}$$

where the Beta density $B(f_m; \sigma_m, \gamma_m)$ is defined in the usual way with shape parameters σ_m and γ_m. For k_m, there can only be finitely many configurations, and assuming that none of those configurations have any special preference, the prior for the bin boundary is

$$p(\{k_m\}|M) = \frac{1}{\binom{N_b - 1}{M}}, \tag{29}$$

where the denominator is the number of possibilities to choose M bin boundaries from $N_b - 1$ places. Prior for M is assumed to be uniform. This model is used to infer the predictive firing rate $\hat{\lambda}(t) = p(\text{spike}|\tilde{k}, \{\mathbf{s}\})$ using the posterior $p(\{f_m\}, \{k_m\}|M, \{\mathbf{s}\})$ and $p(M|\{\mathbf{s}\})$.

The authors obtained spike trains from superior temporal sulcus and the inferior temporal cortex of two monkeys performing a visual fixation task. This data was used in firing rate estimation and the comparison of the PSTH, obtained from Bayesian binning method, to the bar PSTH, line PSTH and SDF obtained with fixed kernel smoothing method using a Gaussian kernel. Endres and Oram (2010) adapt Bayesian binning method to extract other characteristic features of neural responses other than firing rate distribution, such as neural latencies.

4.8. Bayesian Adaptive Kernel Smoothing (BAKS)

BAKS addresses the particular problem of estimating the firing rate from a single trial. Single trial spike trains have been shown to reflect non Poissonian properties like refractory period and bursting (Barbieri et al., 2001; Kass et al., 2005), hence this method avoids using the Poisson process to describe the spike train. The authors (Ahmadi et al., 2018a) use spike trains described by inhomogeneous Gamma and inhomogeneous inverse Gaussian processes to represent non-stationary processes. BAKS uses the kernel smoothing technique with adaptive bandwidth at the estimation points. The adaptive bandwidth is considered as a random variable with prior distribution, which is updated under a Bayesian framework given the spiking data.

Among the several choices for the kernel function, the Gaussian is used quite frequently. Another reason for choosing Gaussian kernel is mathematical convenience since it enables the availability of several conjugate prior distributions which leads to a closed-form expression for the posterior distribution. A closed form expression simplifies the computational complexities by avoiding numerical approximation techniques (MCMC). A Gaussian kernel with adaptive bandwidth is defined as,

$$K_{h(t)}(t) = \frac{1}{\sqrt{2\pi}h(t)} \exp\left\{-\frac{t^2}{2h(t)^2}\right\}. \quad (30)$$

The parameter bandwidth $h(t)$ represents how the data is spread around the mean, and it can be parameterized in terms of precision $\sigma = 1/h(t)^2$, which represents the concentration of the data around the mean. For firing rate estimation, the ISIs are conveniently modeled by Gamma distribution (Kuffler et al., 1957; Stein, 1965; Sanderson et al., 1973; Seal et al., 1983; Levine, 1991; Mandl, 1992; Barbieri et al., 2001; Brown et al., 2002; Cunningham et al., 2008; Shimokawa and Shinomoto, 2009; Shimokawa et al., 2010). Therefore, the authors propose Gamma prior distribution on the precision parameter σ. Since Gamma distribution is the conjugate prior for the Gaussian distribution with precision parameter σ, the choice of Gamma prior will result in an analytical expression for the posterior. The Gamma prior distribution $\pi(\sigma)$ in terms of the precision parameter, can be transformed into a function of adaptive bandwidth $h(t)$ by the change of variable formula:

$$\pi(h(t)) = \pi(\sigma)\left|\frac{d\sigma}{\mathrm{dh}(t)}\right|. \quad (31)$$

The likelihood function is the probability density of the spike train conditional on the bandwidth parameter $\hat{f}(\mathbf{s}|h(t))$ which is approximated by

$$\hat{f}(\mathbf{s}|h(t)) = \frac{1}{N}\sum_{i=1}^{N} K_{h(t)}(t - s_i). \quad (32)$$

Using Bayes' theorem with Eq. (31) and (32), the posterior distribution of kernel bandwidth, $\pi(h(t)|\mathbf{s})$ is calculated and the adaptive bandwidth is then estimated under the squared error loss function with

$$\hat{h}(t) = \int h(t)\pi(h(t)|\mathbf{s})\mathrm{d}h(t). \quad (33)$$

A closed form expression for adaptive bandwidth is given in Ahmadi et al. (2018a) along with the derivation in the appendix. The derived Bayesian optimal bandwidth is used in Eq. (11) to estimate the firing rate

$$\hat{\lambda}(t) = \sum_{i=1}^{N} \frac{1}{\sqrt{2\pi}\hat{h}(t)} \exp\left\{-\frac{(t - s_i)^2}{2\hat{h}(t)^2}\right\}. \quad (34)$$

In Ahmadi et al. (2018a), the authors compare BAKS to optimized kernel smoothing, variable kernel smoothing, BARS and other established rate estimation approaches, through the measure of MISE and suggest that BAKS yields significantly lower MISE compared to the other methods while tested on 100 repetitions of a single trial. The comparison has been with a different number of trials and different underlying rate functions. The authors test the effectiveness of BAKS methods on real neural data recorded from the motor and visual cortex of non human primate and observe the performance. An added advantage of BAKS, as opposed to the other Bayesian methods, is its low computational complexity.

Ahmadi et al. (2018b) use BAKS for offline brain machine interface decoding and demonstrate the improvement against decoding with binning method due to the smoother estimate of the firing rate.

5. Conclusion

The development of the optimal firing rate estimation methods is an essential problem in theoretical neuroscience, which has received a lot of attention over the past decades. In this paper, we reviewed some of the existing firing rate estimation methods and briefly summarized the technical details concerning each of the methods. For an in-depth description of a particular technique, original papers are referred to. The list of the reviewed method is not exhaustive. It is important to note that, this paper does not offer a comparison of the mentioned methods since each method may have crucial applications in neuroscientific studies including, but not limited to, the ones mentioned here.

Conflict of interest

None declared.

Acknowledgments

I would like to thank Dr. Lubomir Kostal for his helpful suggestions and feedback during the preparation of the manuscript. This work was supported by the Institute of Physiology RVO:67985823 and by the Czech Science Foundation project 17-06943S.

References

Abramson, I.S., 1982. On bandwidth variation in kernel estimates – a square root law. Ann. Stat. 10, 1217–1223.
Adrian, E.D., 1928. Basis of Sensation. W. W. Norton and Co., New York.
Adrian, E.D., Zotterman, Y., 1926. The impulses produced by sensory nerve endings: Part 3. Impulses set up by Touch and Pressure. J. Physiol. 61, 465–483.
Ahmadi, N., Constandinou, T.G., Bouganis, C.-S., 2018a. Estimation of neuronal firing rate using Bayesian Adaptive Kernel Smoother (BAKS). PLOS ONE 13, e0206794.
Ahmadi, N., Constandinou, T.G., Bouganis, C.-S., 2018b. Spike rate estimation using Bayesian adaptive kernel smoother (BAKS) and its application to brain machine interfaces. Annual International Conference of the IEEE Engineering in Medicine and Biology Society (EMBC), vol. 40 2547–2550.
Baker, S.N., Lemon, R.N., 2000. Precise spatiotemporal repeating patterns in monkey primary and supplementary motor areas occur at chance levels. J. Neurophysiol. 84, 1770–1780.
Baker, S.N., Spinks, R., Jackson, A., Lemon, R.N., 2001. Synchronization in monkey motor cortex during a precision grip task. I. Task-dependent modulation in single-unit synchrony. J. Neurophysiol. 85, 869–885.
Barbieri, R., Quirk, M.C., Frank, L.M., Wilson, M.A., Brown, E.N., 2001. Construction and analysis of non-Poisson stimulus-response models of neural spiking activity. J. Neurosci. Methods 105, 25–37.
Berry II, M.J., Meister, M., 1998. Refractoriness and neural precision. Advances in Neural Information Processing Systems. pp. 110–116.
Bessou, P., Laporte, Y., Pages, B., 1968. Principles of neural science. J. Physiol. 196, 47–63.
Bowman, A.W., Azzalini, A., 1997. Applied Smoothing Techniques for Data Analysis: The Kernel Approach with S-Plus Illustrations. OUP, Oxford.
Breiman, L., Meisel, W., Purcell, E., 1977. Variable kernel estimates of multivariate densities. Technometrics 19, 135–144.
Britten, K.H., Shadlen, M.N., Newsome, W.T., Movshon, J.A., 2004. Responses of single neurons in macaque MT/V5 as a function of motion coherence in stochastic dot stimuli. Neural Signal Archive 1.
Brown, E.N., Barbieri, R., Ventura, V., Kass, R.E., Frank, L.M., 2002. The time-rescaling theorem and its application to neural spike train data analysis. Neural Comput. 14, 325–346.
Byron, M.Y., Afshar, A., Santhanam, G., Ryu, S.I., Shenoy, K.V., Sahani, M., 2006. Extracting dynamical structure embedded in neural activity. Neural Inform. Process Syst. 1545–1552.
Cherif, S., Cullen, K.E., Galiana, H.L., 2008. An improved method for the estimation of firing rate dynamics using an optimal digital filter. J. Neurosci. Methods 173, 165–181.
Cox, D.R., 1962. Renewal Theory. Methuen.
Cox, D.R., 1965. On the estimation of the intensity function of a stationary point process. J. R. Stat. Soc. B 27, 332–337.
Cox, D.R., 1966. The Statistical Analysis of Series of Events. John Wiley and Sons.
Cunningham, J.P., Byron, M.Y., Shenoy, K.V., Sahani, M., 2008. Inferring neural firing rates from spike trains using Gaussian processes. Adv. Neural Info. Processing Sys. 20, 329–336.
Cunningham, J.P., Gilja, V., Ryu, S.I., Shenoy, K.V., 2009. Methods for estimating neural firing rates, and their application to brain–machine interfaces. Neural Netw. 22, 1235–1246.
Dayan, P., Abbott, L.F., 2001. Theoretical Neuroscience: Computational and Mathematical Modeling of Neural Systems. MIT Press, Cambridge, MA.
Daley, D.J., Vere-Jones, D., 2002. An Introduction to the Theory of Point Processes. Springer, New York.
Denison, D.G.T., Mallick, B.K., Smith, A.F.M., 1998. Automatic Bayesian curve fitting. J. R. Stat. Soc. B 60, 333–350.
DiMatteo, I., Genovese, C.R., Kass, R.E., 2001. Bayesian curve-fitting with free-knot splines. Biometrika 88, 1055–1071.
Endres, D., Oram, M., 2010. Feature extraction from spike trains with Bayesian binning: 'Latency is where the signal starts'. J. Comput. Neurosci. 29, 149–169.
Endres, D., Oram, M., Schindelin, J., Foldiak, P., 2008. Bayesian binning beats approximate alternatives: estimating peri-stimulus time histograms. Advances in Neural Information Processing Systems 20, 393–400.
Gerstein, G.L., Kiang, N., 1960. An approach to the quantitative analysis of electrophysiological data from single neurons. Biophys. J. 1, 15–28.
Gerstein, G.L., Mandelbrot, B., 1964. Random walk models for the spike activity of a single neuron. Biophys. J. 4, 41–68.
Gerstner, W., Kistler, W.M., 2002. Spiking Neuron Models. Cambridge University Press.
Hardle, W., Abbott, L.F., 1991. Smoothing Techniques: With Implementation in S.

Springer.
Harris, C.M., Waddington, J., 2012. On the convergence of time interval moments: caveat sciscitator. J. Neurosci. Methods 205, 345–356.
Jamali, M., Sadeghi, S.G., Cullen, K.E., 2009. Response of vestibular nerve afferents innervating utricle and saccule during passive and active translations. J. Neurophysiol. 101, 141–149.
Johnson, D.H., 1978. The relationship of post-stimulus time and interval histograms to the timing characteristics of spike trains. Biophys. J. 22, 413–430.
Johnson, D.H., 1996. Point process models of single-neuron discharges. J. Comput. Neurosci. 3, 275–299.
Johnson, N.L., Kotz, S., 1971. Continuous Univariate Distributions – 1. Wiley, New York.
Jones, M.C., 1990. Variable kernel density estimates and variable kernel density estimates. Aust. J. Stat. 32, 361–371.
Kaiser, J.F., 1974. Nonrecursive digital filter design using the I-sinh window function. Proc. 1974 IEEE Symp. Circuits Syst. 20–23.
Kandel, E.R., Schwartz, J.H., Jessell, T.M., 1991. Principles of Neural Science. Appleton and Lange.
Kass, R.E., Ventura, V., Cai, C., 2003. Statistical smoothing of neuronal data. Network 14, 5–15.
Kass, R.E., Ventura, V., Brown, E.N., 2005. Statistical issues in the analysis of neuronal data. J. Neurophysiol. 94, 8–25.
Kaufman, C.G., Ventura, V., Kass, R.E., 2005. Spline-based non-parametric regression for periodic functions and its application to directional tuning of neurons. Stat. Med. 24, 2255–2265.
Knight, B.W., 1972. The relationship between the firing rate of a single neuron and the level of activity in a population of neurons: experimental evidence for resonant enhancement in the population response. J. Gen. Physiol. 59, 767–778.
Kohler, E., Keysers, C., Umilta, M.A., Fogassi, L., Gallese, V., Rizzolatti, G., 2002. Hearing sounds, understanding actions: action representation in mirror neurons. Science 297, 846–848.
Kostal, L., Lansky, P., Stiber, M., 2018. Statistics of inverse interspike intervals: the instantaneous firing rate revisited. Chaos 28, 106305.
Kostal, L., Lansky, P., 2006. Classification of stationary neuronal activity according to its information rate. Netw. Comput. Neural Syst. 17, 193–210.
Kostal, L., Lansky, P., Roaspars, J.P., 2007. Neuronal coding and spiking randomness. Eur. J. Neurosci. 26, 2693–2701.
Kostal, L., Shinomoto, S., 2016. Efficient information transfer by Poisson neurons. Math. Biosci. Eng. 13, 509–520.
Koyama, S., Kostal, L., 2014. The effect of interspike interval statistics on the information gain under the rate coding hypothesis. Math. Biosci. Eng. 11, 63–80.
Kuffler, S.W., Fitzhugh, R., Barlow, H.B., 1957. Maintained activity in the cat's retina in light and darkness. J. Gen. Physiol. 40, 683–702.
Lansky, P., Rodriguez, R., Sacerdote, L., 2004. Mean instantaneous firing frequency is always higher than the firing rate. Neural Comput. 16, 477–489.
Lee, D., Malpeli, J.G., 1998. Effects of saccades on the activity of neurons in the cat lateral geniculate nucleus. J. Neurophysiol. 79, 922–936.
Lemon, C.H., Smith, D.V., 2006. Influence of response variability on the coding performance of central gustatory neurons. J. Neurosci. 26, 7433–7443.
Levine, M.W., 1991. The distribution of the intervals between neural impulses in the maintained discharges of retinal ganglion cells. Biol. Cybern. 65, 459–467.
Loftsgaarden, D.O., Quesenberry, C.P., 1965. A nonparametric estimate of a multivariate density function. Ann. Math. Stat. 36, 1049–1051.
Lütkenhöner, B., Smith, R.L., 1986. Rapid adaptation of auditory-nerve fibers: fine structure at high stimulus intensities. Hear. Res. 24, 289–294.
Mandl, G., 1992. Coding for stimulus velocity by temporal patterning of spike discharges in visual cells of cat superior colliculus. Vis. Res. 33, 1451–1475.
Martinez-Conde, S., Macknik, S.L., Hubel, D.H., 2000. Microsaccadic eye movements and firing of single cells in the striate cortex of macaque monkeys. Nat. Neurosci. 3, 251–258.
Missal, M., De Brouwer, S., Lefevre, P., Olivier, E., 2000. J. Neurophysiol. 83, 2080–2092.
Mochizuki, Y., Shinomoto, S., 2014. Analog and digital codes in the brain. Phys. Rev. E 89, 022705.
Moore, G.P., Perkel, D.H., Segundo, J.P., 1966. Statistical analysis and functional interpretation of neuronal spike data. Annu. Rev. Physiol. 28, 493–522.
Movshon, J.A., Thompson, I.D., Tolhurst, D.J., 1978. Spatial summation in the receptive fields of simple cells in the cat's striate cortex. J. Physiol. 283, 53–77.
Mukamel, R., Ekstrom, A.D., Kaplan, J., Iacoboni, M., Fried, I., 2010. Single-neuron responses in humans during execution and observation of actions. Curr. Biol. 20, 750–756.
Nawrot, M., Aertsen, A., Rotter, S., 1999. Single-trial estimation of neuronal firing rates: from single-neuron spike trains to population activity. J. Neurosci. Methods 94, 81–92.
Omi, T., Shinomoto, S., 2011. Optimizing time histograms for non-Poissonian spike trains. Neural Comput. 23, 3125–3144.
Papoulis, A., Pillai, S.U., 2002. Probability, Random Variables, and Stochastic Processes. Tata McGraw-Hill Education.
Parzen, E., 1962. On estimation of a probability density function and mode. Ann. Math. Stat. 33, 1065–1076.
Paulin, M.G., 1992. Digital filters for firing rate estimation. Biol. Cybern. 66, 525–531.
Pauluis, Q., Baker, S.N., 2000. An accurate measure of the instantaneous discharge probability, with application to unitary joint-event analysis. Neural Comput. 12, 647–669.
Perkel, D.H., Bullock, T.H., 1968. Neural Coding. The MIT Press.
Perkel, D.H., Gerstein, G.L., Moore, G.P., 1967. Neuronal spike trains and stochastic point processes: I. The single spike train. Biophys. J. 7, 391–418.
Pillow, J.W., Paninski, L., Uzzell, V.J., Simoncelli, E.P., Chichilnisky, E.J., 2005. Prediction and decoding of retinal ganglion cell responses with a probabilistic spiking model. J. Neurosci. 25, 11003–11013.
Rad, K.R., Paninski, L., 2010. Efficient, adaptive estimation of two-dimensional firing rate surfaces via Gaussian process methods. Network 21, 142–168.
Richmond, B.J., Optican, L.M., Podell, M., Spitzer, H., 1987. Temporal encoding of two-dimensional patterns by single units in primate inferior temporal cortex. I. Response characteristics. J. Neurophysiol. 57, 132–146.
Rosenblatt, M., 1956. Remarks on some nonparametric estimates of a density function. Ann. Math. Stat. 27, 832–837.
Rospars, J.P., Lansky, P., Duchamp, A., Duchamp-Viret, P., 2003. Relation between stimulus and response in frog olfactory receptor neurons in vivo. Eur. J. Neurosci. 18, 1135–1154.
Rudd, M.E., Brown, L.G., 1997. Noise adaptation in integrate-and-fire neurons. Neural Comput. 9, 1047–1069.
Ruskin, D.N., Bergstrom, D.A., Kaneoke, Y., Patel, B.N., Twery, M.J., Walters, J.R., 1999. Multisecond oscillations in firing rate in the basal ganglia: robust modulation by dopamine receptor activation and anesthesia. J. Neurophysiol. 81, 2046–2055.
Sain, S.R., Scott, D.W., 1996. On locally adaptive density estimation. J. Am. Stat. Assoc. 91, 1525–1534.
Sanderson, A.C., 1980. Adaptive filtering of neuronal spike train data. IEEE Trans. Biomed. Eng. 27, 271–274.
Sanderson, A.C., Kozak, W.M., Calvert, T.W., 1973. Distribution coding in the visual pathway. Biophys. J. 13, 218–244.
Sawczuk, A., Powers, R.K., Binder, M.D., 1995. Spike frequency adaptation studied in hypoglossal motoneurons of the rat. J. Neurophysiol. 73, 1799–1810.
Scott, D.W., 1992. Multivariate Density Estimation: Theory, Practice, and Visualization. John Wiley and Sons.
Seal, J., Commenges, D., Salamon, R., Bioulac, B., 1983. A statistical method for the estimation of neuronal response latency and its functional interpretation. Brain Res. 278, 382–386.
Shadlen, M.N., Newsome, W.T., 1994. Noise, neural codes and cortical organization. Curr. Opin. Neurobiol. 4, 569–579.
Shadlen, M.N., Newsome, W.T., 1998. The variable discharge of cortical neurons: implications for connectivity, computation, and information coding. J. Neurosci. 18, 3870–3896.
Sheinberg, D.L., Logothetis, N.K., 2001. Noticing familiar objects in real world scenes: the role of temporal cortical neurons in natural vision. J. Neurosci. 21, 1340–1350.
Shimazaki, H., Shinomoto, S., 2007. A method for selecting the bin size of a time histogram. Neural Comput. 19, 1503–1527.
Shimazaki, H., Shinomoto, S., 2010. Kernel bandwidth optimization in spike rate estimation. J. Comput. Neurosci. 29, 171–182.
Shimokawa, T., Koyama, S., Shinomoto, S., 2010. A characterization of the time-rescaled gamma process as a model for spike trains. J. Comput. Neurosci. 29, 183–191.
Shimokawa, T., Shinomoto, S., 2009. Estimating instantaneous irregularity of neuronal firing. Neural Comput. 21, 1931–1951.
Shinomoto, S., 2010. Estimating the firing rate. Analysis of Parallel Spike Trains. Springer, pp. 21–35.
Silverman, B.W., 1986. Density Estimation for Statistics and Data Analysis. Routledge.
Stein, R.B., 1965. A theoretical analysis of neuronal variability. Biophys. J. 5, 173–194.
Stein, R.B., Gossen, E.R., Jones, K.E., 2005. Neuronal variability: noise or part of the signal? Nat. Rev. Neurosci. 6, 389–397.
Szucs, A., 1998. Applications of the spike density function in analysis of neuronal firing patterns. J. Neurosci. Methods 81, 159–167.
Terrell, G.R., Scott, D.W., 1992. Variable kernel density estimation. Ann. Stat. 20, 1236–1265.
Tilunaite, A., Croft, W., Russell, N., Bellamy, T.C., Thul, R., 2017. A Bayesian approach to modelling heterogeneous calcium responses in cell populations. PLoS Comput. Biol. 13, e1005794.
Tovee, M.J., Rolls, E.T., 1995. Information encoding in short firing rate epochs by single neurons in the primate temporal visual cortex. Vis. Cogn. 2, 35–58.
Tuckwell, H.C., 2005. Introduction to Theoretical Neurobiology: vol. 2, Nonlinear and Stochastic Theories. Cambridge University Press.
Val-Calvo, M., Álvarez-Sánchez, J.R., Alegre-Cortés, J., de la Paz-López, F., Ferrández-Vicente, M., Fernández-Jover, E., Val-Calvo, I., 2019. Frequency variation analysis in neuronal cultures for stimulus response characterization. Neural Comput. Appl. 1–6.
Van Horn, M.R., Waitzman, D.M., Cullen, K.E., 2013. Vergence neurons identified in the rostral superior colliculus code smooth eye movements in 3D space. J. Neurosci. 33, 7274–7284.
Ventura, V., Cai, C., Kass, R.E., 2005. Trial-to-trial variability and its effect on time-varying dependency between two neurons. J. Neurophysiol. 94, 2928–2939.
Vizuete, J.A., Pillay, S., Ropella, K.M., Hudetz, A.G., 2014. Graded defragmentation of cortical neuronal firing during recovery of consciousness in rats. Neuroscience 275, 340–351.
Waitzman, D.M., Ma, T.P., Optican, L.M., Wurtz, R.H., 1991. Superior colliculus neurons mediate the dynamic characteristics of saccades. J. Neurophysiol. 66, 1716–1737.
Wand, M.P., Jones, M.C., 1994. Kernel Smoothing. Chapman and Hall/CRC.
Wen, B., Wang, G., Dean, I., Delgutte, B., 2009. Dynamic range adaptation to sound level statistics in the auditory nerve. J. Neurosci. 29, 13797–13808.
Williams, C., Rasmussen, C.E., 2006. Gaussian Processes for Machine Learning. MIT Press, Cambridge, MA.
Yaksi, E., Friedrich, R.W., 2006. Reconstruction of firing rate changes across neuronal populations by temporally deconvolved Ca^{2+} imaging. Nat. Methods 3, 377–383.

Attachment II

Manuscript published in *Frontiers in Computational Neuroscience* **15**, 620410.
Published in June 2021
doi: 10.3389/fncom.2021.620410

frontiers in Computational Neuroscience

ORIGINAL RESEARCH
published: 07 June 2021
doi: 10.3389/fncom.2021.620410

Variability and Randomness of the Instantaneous Firing Rate

Rimjhim Tomar[1,2]* *and Lubomir Kostal*[1]

[1] *Department of Computational Neuroscience, Institute of Physiology, Czech Academy of Sciences, Prague, Czechia,*
[2] *Second Medical Faculty, Charles University, Prague, Czechia*

The apparent stochastic nature of neuronal activity significantly affects the reliability of neuronal coding. To quantify the encountered fluctuations, both in neural data and simulations, the notions of variability and randomness of inter-spike intervals have been proposed and studied. In this article we focus on the concept of the instantaneous firing rate, which is also based on the spike timing. We use several classical statistical models of neuronal activity and we study the corresponding probability distributions of the instantaneous firing rate. To characterize the firing rate variability and randomness under different spiking regimes, we use different indices of statistical dispersion. We find that the relationship between the variability of interspike intervals and the instantaneous firing rate is not straightforward in general. Counter-intuitively, an increase in the randomness (based on entropy) of spike times may either decrease or increase the randomness of instantaneous firing rate, in dependence on the neuronal firing model. Finally, we apply our methods to experimental data, establishing that instantaneous rate analysis can indeed provide additional information about the spiking activity.

Keywords: variability, randomness, firing rate, entropy, rate coding, neural coding, temporal coding, instantaneous firing rate

OPEN ACCESS

Edited by:
Mayank R. Mehta,
University of California, Los Angeles, United States

Reviewed by:
Ergin Yilmaz,
Bulent Ecevit University, Turkey
Charles Smith,
North Carolina State University, United States
Taro Tezuka,
University of Tsukuba, Japan
Cristina Zucca,
University of Turin, Italy

***Correspondence:**
Rimjhim Tomar
rimjhim.tomar@fgu.cas.cz

Received: *22 October 2020*
Accepted: *26 April 2021*
Published: *07 June 2021*

Citation:
Tomar R and Kostal L (2021) Variability and Randomness of the Instantaneous Firing Rate. Front. Comput. Neurosci. 15:620410. doi: 10.3389/fncom.2021.620410

1. INTRODUCTION

One of the primary research areas of computational neuroscience is dedicated to understanding the principles of neuronal coding, i.e., the way information is embedded into neuronal signals. It is generally understood that neurons use brief electrical impulses (called action potentials or spikes) to convey information. The way information is presented in the time sequence of spikes, however, is still a matter of debate (Shadlen and Newsome, 1994; Stein et al., 2005).

A widely accepted answer to the problem is the rate coding hypothesis, which says that the neurons transmit information through the average number of spikes sent along the axon per a certain time window (this is called the *mean firing rate*). The origin of this theory is credited to Edgar Adrian who found out that the firing rate of the stretch receptor of a frog's muscle changes as a function of stimuli (Adrian, 1926). However, since then, many studies have shown that neurons can encode information without necessarily changing the mean firing rate in response to a stimulus (Perkel and Bullock, 1968; Gerstner and Kistler, 2002; Rigotti et al., 2013; Dettner et al., 2016) prompting the temporal coding hypothesis, which states that the temporal structure of the ISIs is also employed in the embedding of neural information in the spike train (Theunissen and Miller, 1995). Theoretically, information can be encoded in the temporal pattern of the ISIs in an infinite number of ways (Thorpe and Gautrais, 1997; Jacobs et al., 2009; Ainsworth et al., 2012), therefore measures are needed to quantify the features of spiking neuronal signals from different perspectives

(Perkel and Bullock, 1968; Victor and Purpura, 1997; Buračas and Albright, 1999; Rieke et al., 1999; Nemenman et al., 2004). A possible way of looking at the role of temporal structures can be through variability coding hypothesis (Perkel and Bullock, 1968) which states that neuronal variability may not be entirely noise, and part of it might reflect the aspects of neural code that is not yet understood; whether it is the variability of the ISIs or of the firing rate. A standard measure for comparing variability in spike trains is through the coefficient of variation (C_V) which is defined as the ratio of standard deviation to the mean of ISIs (Barbieri and Brunel, 2007). Variability of the firing rate is measured by the Fano factor (Ditlevsen and Lansky, 2011; Rajdl and Lansky, 2013; Stevenson, 2016) which is defined as the ratio of variance to the mean number of spikes in a fixed time window.

Another concept that is similar to variability but not equivalent, is the notion of randomness (Kostal et al., 2007b). Variability and randomness both are used as a differentiating measure in the cases where spike trains might seem similar from the rate coding perspective. It is important to distinguish between the two quantities because highly variable data might not be random at all if it consists of relatively predictable values. For example multi-modal data with well separated peaks may have higher variability than uniformly distributed data where the outcomes are the least predictable. Shannon's entropy (Shannon and Weaver, 1949) is widely used to measure randomness (Steuer et al., 2001; McDonnell et al., 2011; Watters and Reeke, 2014), however it is not suitable for continuous distributions. Few other randomness measures based on entropy have been used in neural context recently. In Kostal et al. (2007a) and Kostal et al. (2013) the authors propose a randomness measure for ISIs, creating an alternative to C_V; whereas an entropy based randomness measure of spike counts is introduced in Rajdl et al. (2017), analogous to the Fano factor.

The instantaneous rate is often ambiguously defined as the inverse of a certain inter-spike interval, e.g., of the first complete ISI after stimulus onset, or of a combination of first n intervals, etc. (Bessou et al., 1968; Awiszus, 1988; Lansky et al., 2004). However, statistically consistent definition of the instantaneous rate (Kostal et al., 2018) cannot depend on the "intrinsic" timing given by the particular spike train realization (e.g., the first evoked spike). Instead, it must be evaluated with respect to the "external" time frame, consistently across trials, i.e., asynchronously with respect to individual spike train realizations. In this paper we consider models of spike trains described by renewal processes, and investigate the dependence between the ISI dispersion coefficients and instantaneous rate dispersion coefficients and emphasize that instantaneous rate provides another perspective in the evaluation of neuronal data.

The paper is divided as follows: first, the concept of instantaneous rate is introduced. Next, the concepts of variability and randomness are defined formally. In section 2, we derive the instantaneous rate distribution and the related dispersion measures for a few of the most commonly used models of steady-state neuronal activity. Included models are restricted to the framework of renewal spiking activity for the purpose of this paper. In section 3, we compare the dispersion characteristics of the neuronal models from rate coding and temporal coding perspectives. Upon comparison we find that for some neuronal models, the firing patterns have a different level of randomness in different settings whereas for others, the changed perspective of observation (from rate to temporal) does not affect the randomness of the data. More details on this is available in section 4.

2. MATERIALS AND METHODS

2.1. Instantaneous Rate

The class of stochastic processes whose realization consists of a sequence of point events in time is called *stochastic point processes* (Cox and Miller, 1965). Neuronal spike trains are often described as stochastic point processes, with spikes corresponding to events. There are essentially two ways of describing point processes, either in terms of the number of events occurring in a time window, or in terms of the intervals between these events. Consequently, a spike train can be described either by using a sequence of the occurrence times of its individual spikes, $X_1, X_2, ...$ (see **Figure 1A**) or through the ISIs defined as $T_i = X_{i+1} - X_i$. Generally, the point process is *stationary* if the underlying joint probability distribution of the numbers of the spikes in k time intervals $(t'_1 + h, t''_1 + h), (t'_2 + h, t''_2 + h), ...(t'_k + h, t''_k + h)$ does not depend on displacement variable h (Cox and Lewis, 1966, p. 59). In this paper, we consider an important class of stationary point processes, the renewal point processes, in which the length T of consequent ISIs is an independently and identically distributed random variable with the probability distribution function (pdf) f_T, $T \sim f_T(t)$. Renewal processes are often used to model the activity of spontaneously active cells (Tuckwell, 1988).

Let the number of spikes that occur in the time interval $[0, w]$ be denoted by $N(w)$. A natural way of calculating the firing rate is to divide the number of spikes $N(w)$ by the time window w. The mean of ISIs, $\mathbb{E}(T)$, satisfies the following relationship with the mean of the counting process $\mathbb{E}[N(w)]$ (Cox and Lewis, 1966; Rudd and Brown, 1997),

$$\lim_{w\to\infty} \frac{\mathbb{E}(N(w))}{w} = \frac{1}{\mathbb{E}(T)} = \lambda. \tag{1}$$

where λ is the point process intensity (Cox and Lewis, 1966).

For finite w, Equation (1) holds true for renewal processes only if time origin t_0 is arbitrary, i.e., it is not related to the renewal point process realization (**Figure 1B**). In this case, t_0 falls into some ISI, say T_k. Then the sequence of random variables $(W, T_{k+1}, T_{k+2}, ...)$, where W is the time to the first spike from the origin, is not stationary. Moreover, the point process intensity λ is equal to the mean firing rate. The corresponding renewal process is referred to as *equilibrium renewal process*, as opposed to the *ordinary renewal process* which starts from an arbitrary spiking event and all the ISIs follow the same renewal pdf (Cox and Miller, 1965).

The instantaneous firing rate is typically defined as the inverse of the ISIs $(1/T)$ (Pauluis and Baker, 2000). However, as proven in

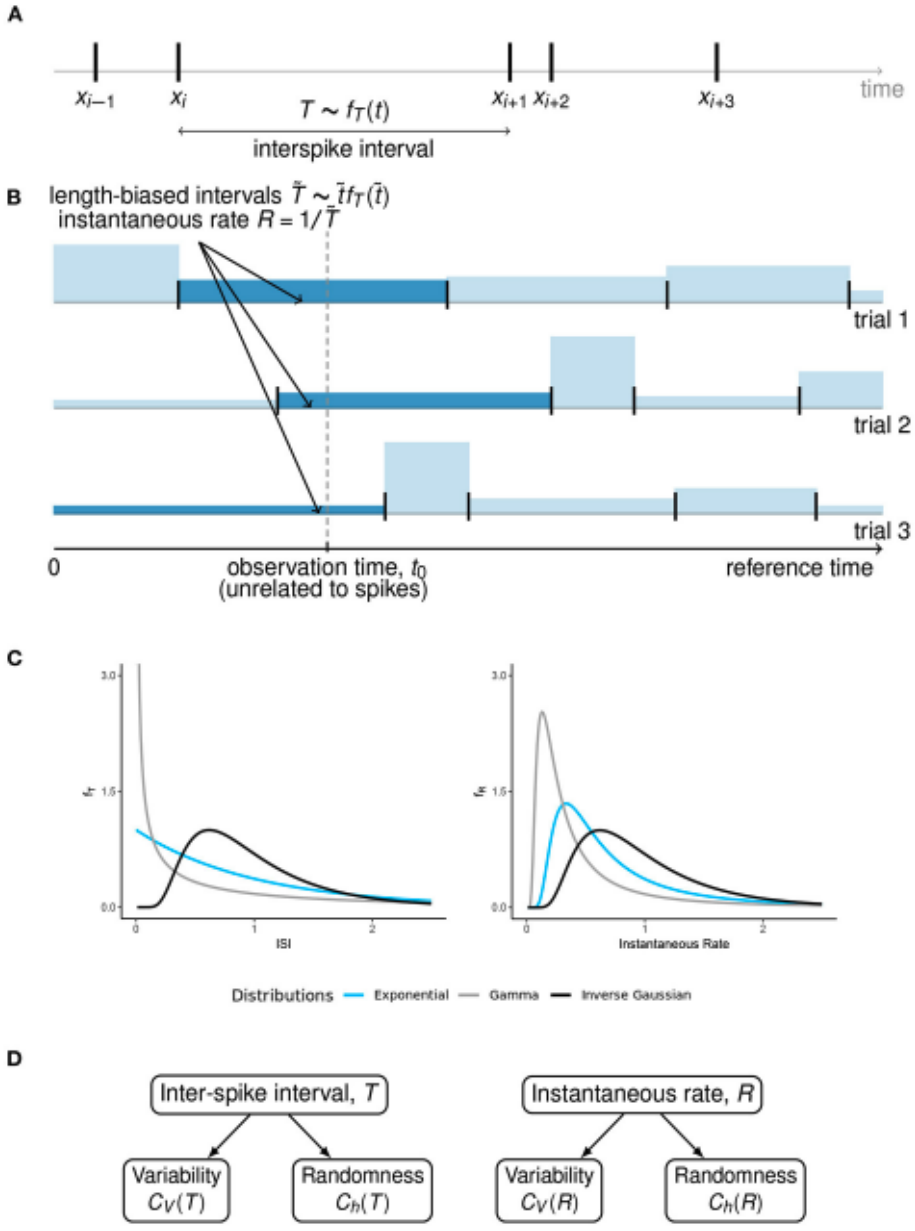

FIGURE 1 | Length-biased ISIs and instantaneous rate. **(A)** An overview of the ISIs when the spikes occur at times $X_{i-1}, X_i, X_{i+1}, \ldots$. We assume that the ISIs are independent and identically distributed with pdf $f_T(t)$, under steady state conditions. **(B)** When the observation time t_0 is fixed with respect to some reference time, unrelated to the spike times, the probability of observing a particular ISI is proportional to its length. These "length-biased" intervals ($\tilde{T}$) are used to define the instantaneous rate R with the property $\mathbb{E}(R) = 1/\mathbb{E}(T)$. **(C)** A graphical representation of how the ISI distributions can visually differ from the instantaneous rate distributions, for some well-known ISI models with equal mean firing rate. **(D)** A summary of the concepts of variability and randomness for the two ways of spike train description that we have considered in this article.

Lansky et al. (2004), the mean instantaneous firing rate is higher than or equal to the mean firing rate,

$$\mathbb{E}\left(\frac{1}{T}\right) \geq \frac{1}{\mathbb{E}(T)} \tag{2}$$

with equality if all the ISIs are of the same length.

The undesirable inequality in Equation (2) becomes equality once we realize that the "time instant" (at which the instantaneous rate is measured) does not generally coincide with a spike. As shown in Kostal et al. (2018), the instant is chosen with respect to the "external" time frame, across trials, i.e., asynchronously with respect to individual spike train realizations. Consequently, the probabilities of observed ISIs ($\tilde{T}$) are proportional to their length, $\tilde{T} \sim \lambda \tilde{t} f_T(\tilde{t})$ (**Figure 1B**). The mean inverse of these length-biased ISIs equals to the mean firing rate λ.

The instantaneous rate $R = 1/\tilde{T}$ observed, in this case, is a random variable described by the pdf,

$$f_R(r) = \frac{1}{\mathbb{E}(T)} \frac{f_T(1/r)}{r^3}, \tag{3}$$

For a detailed overview of the derivations, refer to Kostal et al. (2018).

An immediate consequence of Equation (3) is,

$$\mathbb{E}\left(\frac{1}{\tilde{T}}\right) = \mathbb{E}(R) = \frac{1}{\mathbb{E}(T)} = \lambda. \tag{4}$$

Hence, for the purpose of the derivation of instantaneous rate distributions for different models of steady-state firing (**Figure 1C**), we will restrict ourselves to the case of equilibrium renewal process. The variability of instantaneous rate is explored in the next section.

2.2. Quantification of Variability and Randomness

The most common method to measure statistical dispersion of ISIs, described by a continuous positive random variable T, is the standard deviation $\sigma(T)$, defined as

$$\sigma(T) = \sqrt{\mathbb{E}([T - \mathbb{E}(T)]^2)}. \tag{5}$$

The *relative* dispersion measure quantity is known as coefficient of variation $C_V(T)$,

$$C_V(T) = \lambda\sigma(T) \tag{6}$$

where $\lambda = 1/\mathbb{E}(T)$. The coefficient of variation $C_V(T)$ is a dimensionless quantity and its value does not depend on the choice of the units of ISIs or on linear scaling; hence it can be used to meaningfully compare the ISI distributions with different means, unlike $\sigma(T)$ (Softky and Koch, 1993; Doron et al., 2014).

From Equation (3), we can write the standard deviation for the instantaneous rate as

$$\sigma(R) = \sqrt{\lambda\mathbb{E}(1/T) - \lambda^2}, \tag{7}$$

which leads to the relative dispersion measure,

$$C_V(R) = \sqrt{\frac{\mathbb{E}(1/T)}{\lambda} - 1}. \tag{8}$$

From Equation (5), it follows that σ or C_V measure how much the probability distribution is "spread" with respect to the mean value but these quantities do not describe all possible differences between spike trains with equal rate coding characteristics. Spike trains of equal variability may still differ in higher than second statistical moments. Moreover, neither σ nor C_V quantifies how random or unpredictable the outcomes are Kostal et al. (2007a).

To quantify randomness as a further describing characteristic of a spike train, entropy based measures like differential entropy (Shannon and Weaver, 1949), h, have been proposed

$$h(f_X) = -\int f_X(x) \ln f_X(x) \mathrm{d}x. \tag{9}$$

where X is a continuous random variable with pdf f_X. However, $h(f_X)$ by itself can not be used as a measure of randomness since it can take both positive and negative values and depends on the scaling of the random variable X. Kostal and Marsalek (2010) proposed the entropy-based dispersion coefficient σ_h,

$$\sigma_h = \exp(h(f_X) - 1). \tag{10}$$

Entropy-based dispersion σ_h can be interpreted with the help of asymptotic equipartition property (Principe, 2010; Cover and Thomas, 2012), the details of which can be found in Kostal et al. (2013). Analogous to Equation (6), the relative entropy-based measure of dispersion, C_h is defined as

$$C_h = \lambda\sigma_h. \tag{11}$$

An immediate consequence of the above equation is that the maximum value of C_h is $C_h = 1$, which occurs only in the case of exponential f_T.

3. RESULTS

Among the different point process models of stationary neuronal activity, we have chosen the classically used Gamma, lognormal, inverse Gaussian, shifted exponential, and the mixture of exponential distributions (Tuckwell, 1988).

First three distributions are part of the scale family (Casella and Berger, 2002), i.e., their ISI pdfs $f_T(t;\lambda)$, explicitly parameterized by the intensity λ, satisfy the relationship

$$f_T(t,\lambda) = \lambda f_T(t\lambda, 1). \tag{12}$$

We explore these neuronal models in the following subsections (**Figure 1D**). Detailed derivations of the following results are provided in the **Supplementary Material** for better legibility.

3.1. Gamma Distribution

Gamma distribution is frequently used as a descriptor of ISIs in experimental data analysis (Levine, 1991; McKeegan, 2002; Reeke and Coop, 2004; Pouzat and Chaffiol, 2009), its pdf is

$$f_T(t) = \frac{b^a t^{a-1} e^{-bt}}{\Gamma(a)}, \tag{13}$$

where $\Gamma(z) = \int_0^\infty x^{z-1}e^{-x}\mathrm{d}x$ is the gamma function and $a > 0$, $b > 0$ are the parameters. The mean firing rate and the coefficient of variation are,

$$\lambda = \frac{b}{a}, \quad C_V(T) = \frac{1}{\sqrt{a}}. \tag{14}$$

Using Equation (9), the expression for the entropy of the ISI distribution is derived as

$$h(f_T) = \log\left(\frac{\Gamma(a)}{b} e^{a+(1-a)\psi(a)}\right), \tag{15}$$

where $\psi(x) = \Gamma'(x)/\Gamma(x)$ is the digamma function.

Substituting the values from Equations (14) and (15) into Equation (11), gives the dispersion coefficient of randomness,

$$C_h(T) = \frac{\Gamma(a)}{a} e^{a+(1-a)\psi(a)-1}. \tag{16}$$

The instantaneous rate distribution $f_R(r)$ is obtained through Equation (3) and it follows the inverted gamma distribution,

$$f_R(r) = \frac{b^{a+1} r^{-a-2} e^{-b/r}}{\Gamma(a+1)}. \tag{17}$$

Coefficient of variation $C_V(R)$ is evaluated through Equation (8),

$$C_V(R) = \sqrt{\frac{1}{a-1}}, \quad a > 1. \tag{18}$$

The differential entropy for $f_R(r)$ is,

$$h(f_R) = \log(\Gamma(a+1) b e^{(a+1)-(a+2)\psi(a+1)}), \tag{19}$$

and the dispersion coefficient of randomness is,

$$C_h(R) = a\Gamma(a+1) e^{a-(a+2)\psi(a+1)}. \tag{20}$$

The dispersion measures $C_V(T)$ and $C_V(R)$ are related through the following equation,

$$C_V(R) = \frac{C_V(T)}{\sqrt{1 - C_V(T)^2}}. \tag{21}$$

This relationship is illustrated in **Figure 2** and we see that $C_V(R) \to \infty$ as $C_V(T) \to 1$. For $C_V(T) = 1$, gamma distribution becomes exponential distribution with pdf,

$$f_T(t) = \lambda e^{-\lambda t}. \tag{22}$$

Note that the firing intensity λ completely characterizes the exponential distribution and that $C_V(T) = 1$, regardless of the value of λ. The entropy $h(f_T)$ of the exponential distribution is

$$h(f_T) = 1 - \ln \lambda. \tag{23}$$

One of the key features of the exponential distribution is that, for a fixed mean firing rate λ, it maximizes the differential entropy among all probability distributions on the real positive half line (Cover and Thomas, 2012). Deriving from Equation (11),

$$C_h(T) = 1. \tag{24}$$

The corresponding instantaneous rate distribution, follows from Equation (3),

$$f_R(r) = \frac{\lambda^2 e^{-\lambda/r}}{r^3} \tag{25}$$

which is the inverse gamma distribution mentioned in Equation (17) with $a = 1$ and $b = \lambda$. For the inverse gamma distribution, the second moment exists only when $a > 1$. In **Figure 3**, we can see where gamma distribution becomes exponential and has $C_h(T) = 1$.

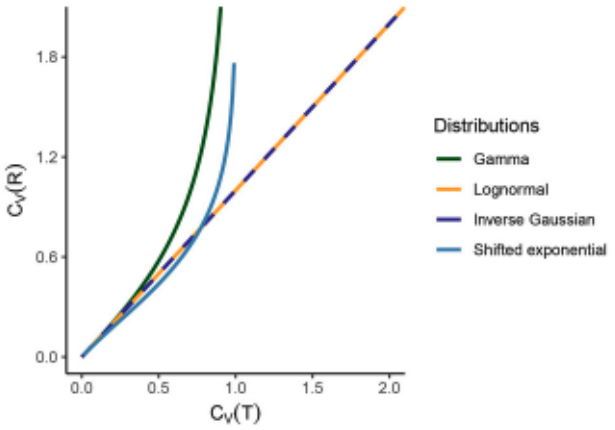

FIGURE 2 | Comparison of $C_V(T)$ and $C_V(R)$ for several standard statistical ISI models. For the gamma distribution, $C_V(R) \to \infty$ as $C_V(T) \to 1$, since gamma distribution becomes exponential for $C_V(T) = 1$. For lognormal and inverse Gaussian distribution, the relationship between the dispersion coefficients is an identity. For shifted exponential distribution, $C_V(T)$ and $C_V(R)$ depend on the mean firing rate λ and the refractory period τ. Hence, we vary the value of $C_V(T)$ and $C_V(R)$ (consequently of λ and τ) and we see that $C_V(R) > C_V(T)$ until $C_V(T) = 0.7715$ but then instantaneous rate distribution maintains a higher variability than ISIs. As $C_V(T) \to 1$, the shifted exponential becomes exactly exponential and therefore $C_V(R) \to \infty$.

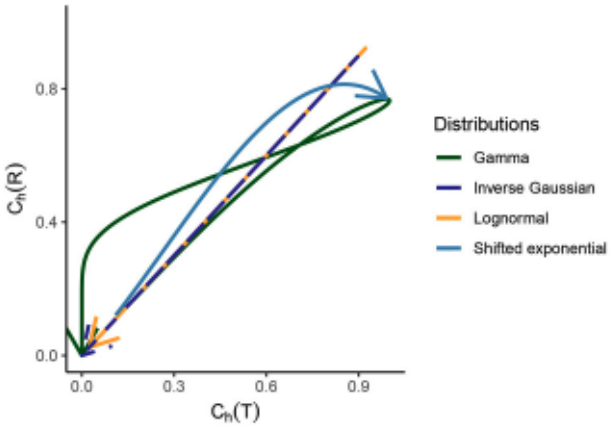

FIGURE 3 | Relationship between the dispersion coefficients of randomness for the gamma, lognormal, inverse Gaussian, and shifted exponential distribution of ISIs. Starting from the origin, the arrow indicated to the end corresponds to $C_V(T)$ values ranging from 0 to ∞. For the first three distributions, which are part of the scale family and for which we consider $\lambda = 1$ for a meaningful comparison, it holds that for $C_V(T) \to 0$, we see that $C_h(T) \to 0$ for $C_h(R) \to 0$. As $C_V(T)$ grows, the randomness grows for ISIs and instantaneous rate in the beginning. After a certain point, the randomness starts to decline and as $C_V(T) \to \infty$, we have $C_h(T) \to 0$ and $C_h(R) \to 0$. For the shifted exponential distribution where we have to consider a varying $C_V(T)$ and for that a varying mean firing rate λ and refractory period τ, $C_h(T)$ increases monotonously as a function of $C_V(T)$, whereas $C_h(R)$ obtains its maximum for $C_V(T) = 0.85$ and then declines.

3.2. Lognormal Distribution

The lognormal distribution represents a common ISI descriptor in experimental data analysis (Levine, 1991; Pouzat and Chaffiol, 2009), even though it is rarely presented as a result of any of the

neuronal models (Bershadskii et al., 2001). The pdf is,

$$f_T(t) = \frac{1}{\sigma t\sqrt{2\pi}} \exp\left\{ -\frac{(\ln t - \ln m)^2}{2\sigma^2} \right\}, \tag{26}$$

where m is the scale parameter and $\sigma > 0$ is the shape parameter. The mean firing rate and coefficient of variation are as follows,

$$\lambda = \frac{1}{me^{\sigma^2/2}}, \quad C_V(T) = \sqrt{e^{\sigma^2} - 1}. \tag{27}$$

We compute the differential entropy

$$h(f_T) = \frac{1}{2}\log(2\pi e\sigma^2 m^2), \tag{28}$$

and the dispersion coefficient of randomness,

$$C_h(T) = \sigma\sqrt{2\pi}e^{-(\sigma^2+1)/2}. \tag{29}$$

The instantaneous rate distribution follows the pdf,

$$f_R(r) = \frac{1}{me^{\sigma^2/2}} \frac{1}{r^2\sigma\sqrt{2\pi}} \exp\left\{ -\frac{(\ln r + \ln m)^2}{2\sigma^2} \right\}, \tag{30}$$

with

$$C_V(R) = \sqrt{e^{\sigma^2} - 1}. \tag{31}$$

The expression for the differential entropy is derived from Equation (11),

$$h(f_R) = \frac{1}{2}\log\left(\frac{2\pi e\sigma^2}{m^2 e^{2\sigma^2}}\right). \tag{32}$$

The dispersion coefficient is evaluated as,

$$C_h(R) = \sigma\sqrt{2\pi}e^{-(\sigma^2+1)/2}. \tag{33}$$

For the lognormal distribution, there is a "symmetric" relationship between $f_T(t)$ and $f_R(r)$ (Kostal et al., 2018),

$$f_R(r;\lambda) = f_T(r;1/\lambda), \tag{34}$$

i.e., the shape of the probability distributions of ISI and instantaneous rates are exactly the same for $\lambda = 1$. Furthermore, the relationship between $C_V(T)$ and $C_V(R)$ is that of an identity (**Figure 2**),

$$C_V(R) = C_V(T) \tag{35}$$

and from Equations (29) and (33), we have

$$C_h(T) = C_h(R). \tag{36}$$

For lognormal distribution, the randomness and variability of instantaneous rate and ISI are the same, regardless of the perspective, as seen in **Figures 2, 3**.

3.3. Inverse Gaussian Distribution

Inverse Gaussian distribution is often fitted to experimentally observed ISIs (Gerstein and Mandelbrot, 1964; Berger et al., 1990; Levine, 1991; Pouzat and Chaffiol, 2009). The time that a Weiner process with positive drift takes to reach the first passage time is distributed according to the inverse Gaussian distribution. The probability density of inverse Gaussian distribution can be expressed as a function of its mean $a > 0$ and scale parameter $b > 0$

$$f_T(t) = \sqrt{\frac{a}{2\pi bt^3}} \exp\left\{ -\frac{1}{2b}\frac{(t-a)^2}{at} \right\}, \tag{37}$$

with

$$\lambda = \frac{1}{a}, \quad C_V(T) = \sqrt{b}. \tag{38}$$

From Equation (9), the expression for differential entropy is,

$$h(f_T) = \frac{1}{2}\log(2\pi a^2 be) + \frac{3e^{1/b}}{\sqrt{2\pi b}} K^{(1,0)}\left(-\frac{1}{2}, \frac{1}{b}\right), \tag{39}$$

where $K_\nu^{(1,0)}(z)$ is the derivative of the modified Bessel function of the second kind (Abramowitz and Stegun, 1972).

$$K_\nu^{(1,0)}(z) = \frac{\partial}{\partial \nu} K_\nu(z). \tag{40}$$

Equation (11) gives,

$$C_h(T) = \sqrt{\frac{2\pi b}{e}} \exp\left\{ \frac{3e^{1/b}}{\sqrt{2\pi b}} K^{(1,0)}\left(-\frac{1}{2}, \frac{1}{b}\right) \right\}. \tag{41}$$

The instantaneous firing rate follows the distribution

$$f_R(r) = \sqrt{\frac{1}{2\pi abr^3}} \exp\left\{ -\frac{1}{2b}\frac{(1-ar)^2}{ar} \right\}. \tag{42}$$

From Equation (8),

$$C_V(R) = \sqrt{b}, \tag{43}$$

and from Equation (9), differential entropy is,

$$h(f_R) = \frac{1}{2}\log\left(\frac{2\pi be}{a^2}\right) + \frac{3e^{1/b}}{\sqrt{2\pi b}} K^{(1,0)}\left(-\frac{1}{2}, \frac{1}{b}\right). \tag{44}$$

The expression for the dispersion coefficient of randomness is as follows,

$$C_h(R) = \sqrt{\frac{2\pi b}{e}} \exp\left\{ \frac{3e^{1/b}}{\sqrt{2\pi b}} K^{(1,0)}\left(-\frac{1}{2}, \frac{1}{b}\right) \right\}. \tag{45}$$

Analogous to the lognormal distribution, we observe that the inverse Gaussian distribution also satisfies the "symmetrical" property (Equation 34) and,

$$C_V(T) = C_V(R), \quad C_h(T) = C_h(R). \tag{46}$$

Results from **Figures 2, 3** illustrate this curious property that the randomness and variability of this distribution is equal for ISIs and instantaneous rate perspective.

3.4. Distribution Involving a Refractory Period

The refractory period is a state of the neuron, occurring right after a spike, where it is impossible for another spike to be emitted. A shifted exponential distribution function is used as an ISI descriptor for neurons with refractory period τ (Reeke and Coop, 2004). The probability density function of the shifted exponential function with parameter $a > 0$ and refractory period $\tau \geq 0$ is

$$f_T(t) = \begin{cases} 0, & t \leq \tau \\ ae^{-a(t-\tau)}, & t > \tau \end{cases} \tag{47}$$

with

$$\lambda = \frac{a}{1+a\tau}, \quad C_V(T) = \frac{1}{1+a\tau}. \tag{48}$$

We observe that $C_V(T) < 1$ for $a > 0$ and $\tau > 0$. The differential entropy for the shifted exponential distribution is evaluated as

$$h(f_T) = \log\left(\frac{e}{a}\right), \tag{49}$$

and substituting these values into Equation (11), we arrive at

$$C_h(T) = \frac{1}{1+a\tau}. \tag{50}$$

The pdf of the instantaneous rate is,

$$f_R(r) = \begin{cases} 0, & r \geq 1/\tau \\ \frac{a^2}{r^3(1+a\tau)} e^{-a(\frac{1}{r}-\tau)}, & r < 1/\tau \end{cases} \tag{51}$$

with

$$C_V(R) = \sqrt{(1+a\tau)e^{a\tau}\Gamma(0, a\tau) - 1} \tag{52}$$

where $\Gamma(s,x) = \int_x^\infty t^{s-1}e^{-t}dt$ is the upper incomplete gamma function (Abramowitz and Stegun, 1972).

Evaluation of the differential entropy from Equation (9) yields,

$$h(f_R) = -\log\left(\frac{a^2}{1+a\tau}\right) - \frac{3(1+e^{a\tau}\Gamma(0,a\tau)+(1+a\tau)\log\tau)}{1+a\tau} + \frac{2+a\tau}{1+a\tau} \tag{53}$$

Expression for the dispersion coefficient is derived through Equation (11),

$$C_h(R) = \frac{1+a\tau}{a}\exp\left\{-\log\left(\frac{a^2}{1+a\tau}\right) - \frac{3(1+e^{a\tau}\Gamma(0,a\tau)+(1+a\tau)\log\tau)}{1+a\tau} + \frac{2+a\tau}{1+a\tau} - 1\right\}. \tag{54}$$

For the shifted exponential distribution, we observe that from Equation (48),

$$a = \frac{\lambda}{1-\lambda\tau}, \tag{55}$$

which leads to,

$$C_V(T) = 1 - \lambda\tau, \tag{56}$$

i.e., $C_V(T)$ depends on λ and τ. Hence, in order to analyze the relationship between $C_V(T)$ and $C_V(R)$ we have to vary the values of λ and τ (**Figure 2**).

Substituting the values from Equations (55) and (56) into Equation (54), we get

$$C_V(R) = \sqrt{\left(1+\frac{1-C_V(T)}{C_V(T)}\right)\exp\left(\frac{1-C_V(T)}{C_V(T)}\right)\Gamma\left(0, \frac{1-C_V(T)}{C_V(T)}\right) - 1} \tag{57}$$

The dispersion coefficient of randomness $C_h(R)$ increases until it attains its maximum value 0.8137 for $C_V(T) = 0.85$, whereas $C_h(T)$ keeps increasing monotonously. This behavior can be better understood by looking at the behavior of $C_h(R)$ while $C_V(T)$ increases in **Figure 6C**. It is observed that $C_h(R)$ attains its maximum value and then declines as $C_V(T) \to 1$, whereas $C_h(T)$ monotonously increases.

3.5. Mixture of Two Exponential Distributions With Refractory Period and Application to Experimental Data

Throughout the years, empirical studies have produced evidence of bimodal or multimodal trends in ISI data (Rodieck et al., 1962; Nakahama et al., 1968; Obeso et al., 2000; Dorval et al., 2008). The underlying assumption is that a neuron might be in one of the several "states," with each state being characterized by a different ISI distribution (Tuckwell, 1988). A mixture of two distributions is commonly used to modal such data, for example, Bhumbra and Dyball (2004) used a mixture of two lognormal distributions as an ISI descriptor of supraoptic nucleus neurons, and recently gamma-exponential mixture distribution has been used to characterize the ISI distribution in the auditory system (Heil et al., 2007; Neubauer et al., 2009).

In this section, we consider the mixture of two exponential distributions (Tuckwell, 1989), which is often used to describe the bursting activity in neurons, where a sequence of short ISIs is dispersed among comparatively longer ISIs. In 1965, Smith and Smith (1965) used the mixture of two exponential distributions to explain the bursting activity in the isolated cortical neurons of an unanesthetized cat. Thomas (1966) used mixed exponential distributions to describe the ISIs in their study of the clustered firing of cortical neurons. Trapani and Nicolson (2011) found that in the lateral line organs of a zebrafish, when the depolarizing currents were blocked, the ISI data of afferent neurons was best described by a mixture of exponential distributions.

The pdf of the mixed exponential distribution with refractory period $\tau \geq 0$ and mixture components with parameter $a > 0, b > 0, a \neq b$ is given by

$$f_T(t) = \begin{cases} 0, & t \leq \tau \\ pae^{-a(t-\tau)} + (1-p)be^{-b(t-\tau)}, & t > \tau \end{cases} \tag{58}$$

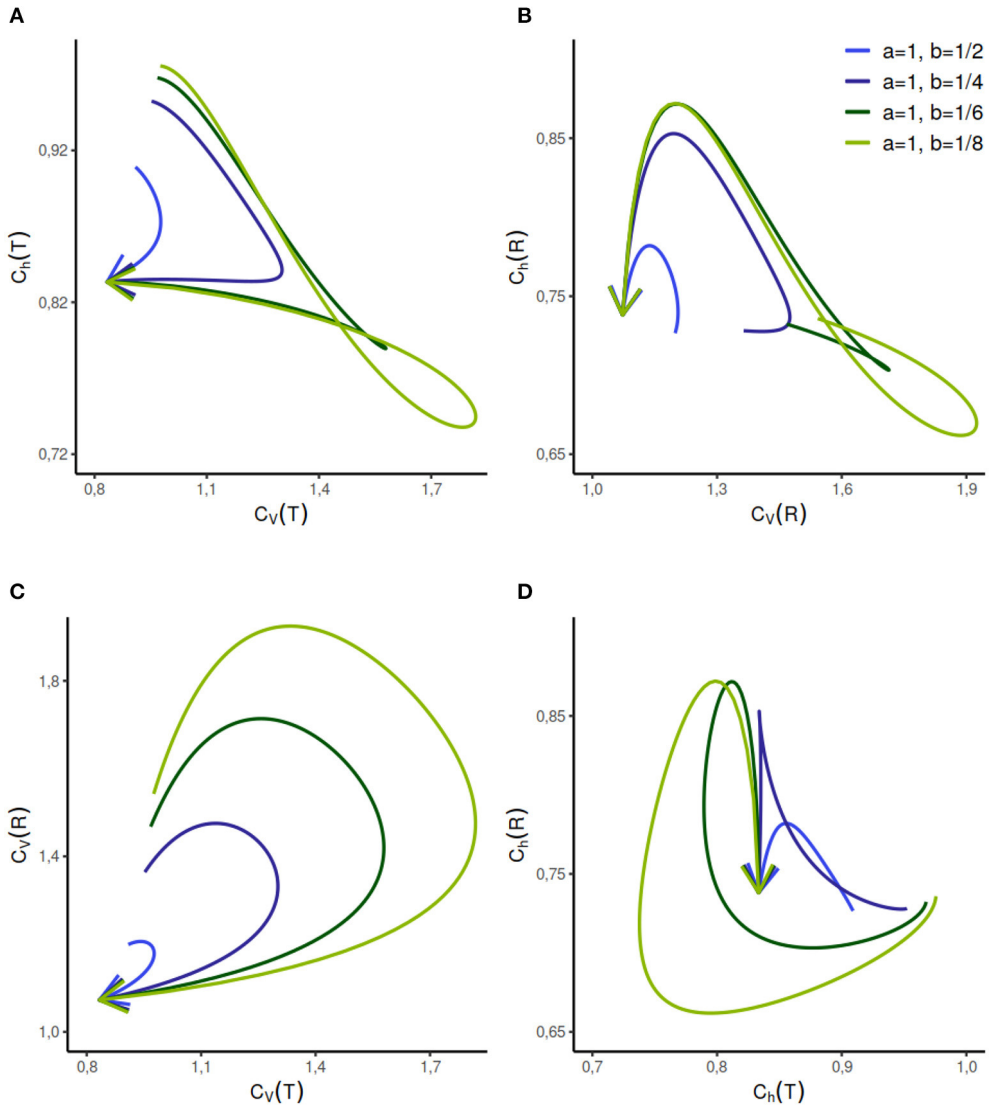

FIGURE 4 | Dispersion measures of the mixed exponential distribution with refractory period randomly set to $\tau = 0.2$ and variable weight of components as $p \in [0, 1]$ in the direction of the arrows. The rate parameter of one component is fixed at $a = 1$ whereas the rate parameter b of the second component varies. When $p = 0$ or $p = 1$, the distribution is shifted exponential with refractory period τ. The dispersion measure of randomness $C_h(T)$ describes $C_V(T)$ uniquely when the $a = 1, b = 1/2$, whereas the reverse is not true **(A)**. This relationship gets complicated with the increasing separation between the rate parameters of the components. As seen in **(B–D)**, the relationship between the other dispersion measures is relatively complicated and non-unique for the given set of parameters.

where $p \in (0, 1)$. In this case,

$$\lambda = \frac{ab}{pb(1 + a\tau) + (1 - p)a(1 + b\tau)}. \tag{59}$$

The analytical expressions for the C_Vs and C_hs are difficult to obtain, however, they can be calculated numerically for a given set of parameters (**Figure 4**). The parameter range for this distribution can be vast, we analyze the dispersion coefficients for a few different sets of component rate parameters a and b, given a value of τ and $p \in [0, 1]$. We study the change in randomness and variability as probability variable p increases in the direction of the arrows. The behavior of this model is relatively complicated but for selected cases, such as when $a = 1, b = 1/2$, or $a = 1, b = 1/4$, different firing regimes are uniquely described by $C_h(T)$ but not by $C_V(T)$.

Song et al. (2018) model the spike generation in the spontaneously active afferent neurons of the Zebrafish lateral line, as a renewal process. The authors propose that a spike is generated if the neuron is recovered from the refractory period *and* a synaptic release (excitatory input) from hair cells has arrived and thus ISI $T = \tau + T_E$ where τ is the absolute refractory period and T_E is the time to excitation (we omit the small relative refractory period used in the original paper,

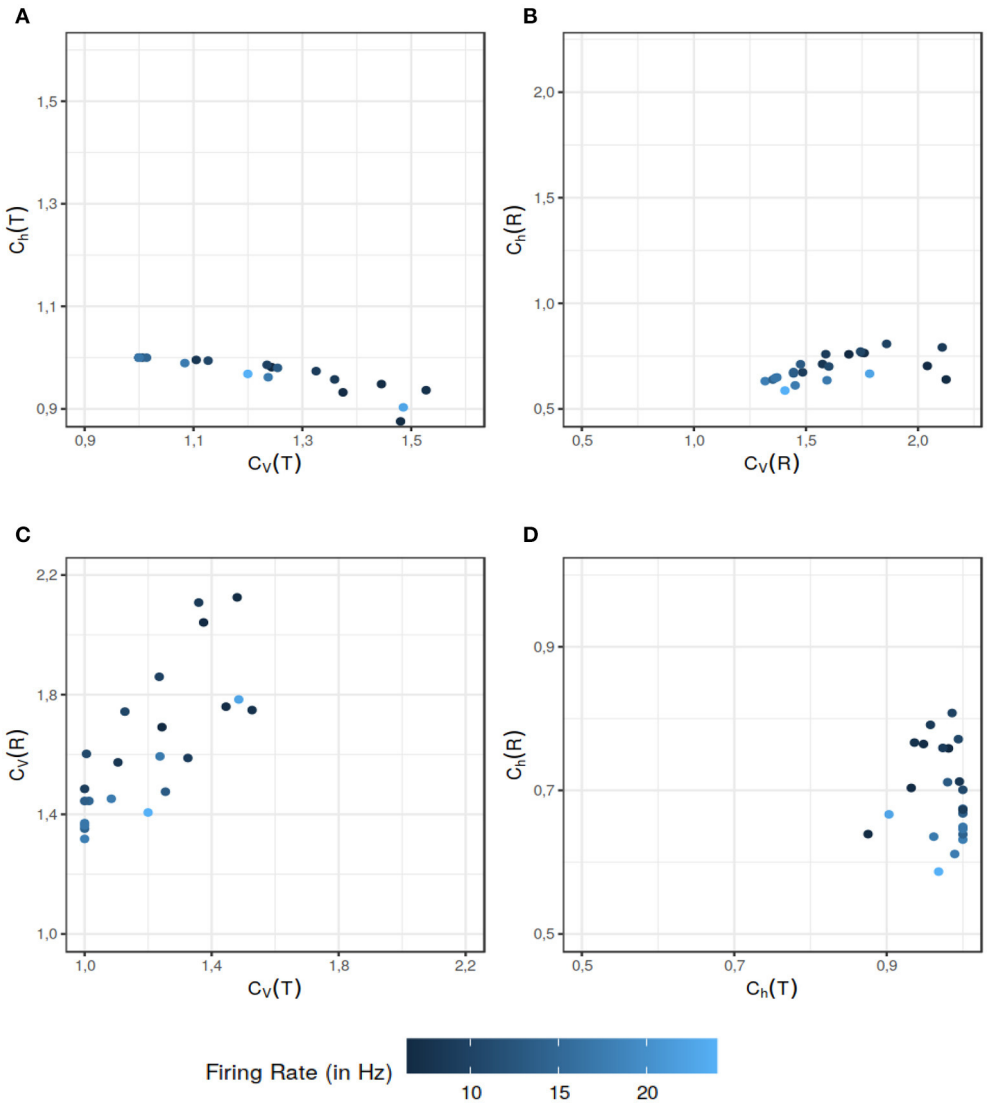

FIGURE 5 | Comparison between the dispersion coefficients of variability and randomness of the experimental data for the data sets used in Song et al. (2018). The ISI data has two components: the refractory period and the hair-cell synaptic release time (the time to excitation input). Latter is modeled by a mixture distribution of two exponentials. The color gradient indicates the mean firing rate of the particular data set. The comparison of various dispersion quantities reveal various aspect to differentiate the data sets. As seen in **(A)**, $C_h(T)$ classifies the data sets in a similar category from the randomness perspective even if their ISI variability are on a wider scale. The dispersion measure of variability $C_V(R)$ also does a better job of differentiating among the data sets in **(B)** when their randomness dispersion measure would put them in a similar category. In **(C)**, $C_V(T)$ and $C_V(R)$ reveal separate aspects of the data sets. Overall $C_V(R)$ helps differentiate among the data sets with similar $C_V(T)$ values. Finally in **(D)** we can see that $C_h(R)$ further differentiates the data sets with equal $C_h(T)$. The data sets which might have similar randomness on the ISI scale, can be differentiated on the basis of their instantaneous rate randomness. All of these figures support our assertion that dispersion measures of instantaneous rate provide additional information that can be helpful in distinguishing the data sets.

for computational simplicity). It is demonstrated in the paper that the mixture of exponential distributions used to model the hair cell synaptic release time T_E, yields the best fit for the ISI data. The pdf of the ISI, in this case is given by Equation (58). We calculated C_h and C_V for ISIs and the instantaneous rate of each data set fitted with a combination of absolute refractory period and mixture of exponential distributions. For the given data sets, $C_V(T)$ and $C_V(R)$ offer more information than their randomness counterparts $C_h(T)$ (**Figure 5A**) and $C_h(R)$ (**Figure 5B**) respectively. When it comes to the dispersion measures of variability, as seen in **Figure 5C**, in some situations $C_V(R)$ offers additional information to distinguish further nuances in the data. The data sets which might seem of similar ISI variability, differ when it comes to the variability of their instantaneous rate. Similar results follow for the randomness (**Figure 5D**). This example supports our assertion that the dispersion measures based on the instantaneous rate can provide additional information to help differentiate among the data sets.

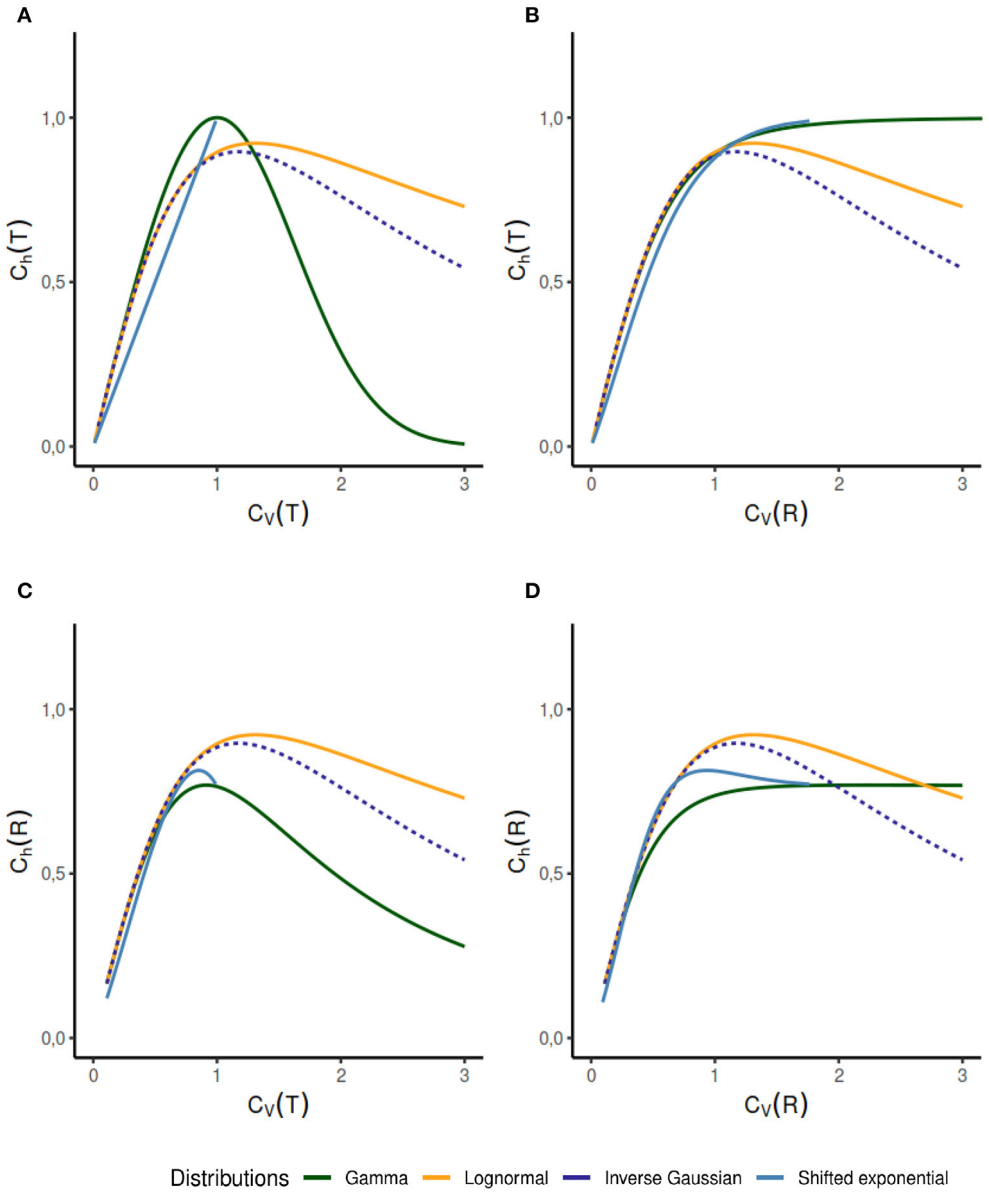

FIGURE 6 | Dispersion measures of the gamma, lognormal, inverse Gaussian, and shifted exponential distributions. Each randomness dispersion measure $C_h(R)$ and $C_h(T)$ is categorized by their dependence on ISI variability $C_V(T)$ and on instantaneous rate variability $C_h(T)$. Firing rate is fixed at $\lambda = 1$ for the scale family distributions. For the gamma distribution, $C_h(T)$ declines as a function of $C_V(T)$ **(A)** but increases as a function of $C_V(R)$ **(B)**. For lognormal and inverse Gaussian distribution $C_h(T) = C_h(R)$, regardless of the perspective change **(A–D)**. The shifted exponential distribution has a monotonously increasing $C_h(T)$, when it is a function of $C_V(T)$ or $C_V(R)$ **(A,B)**; whereas $C_h(R)$ attains its maximum for $C_V(T) = 0.85$ and $C_V(R) = 0.9282$ respectively, and then declines **(C,D)**.

4. DISCUSSION

We studied the spiking activity described by the renewal processes from two perspectives, the temporal point of view (in terms of ISIs) and the frequency point of view (in terms of instantaneous rate). We found that for a given spike train the temporal characteristics and the instantaneous rate characteristics, can either follow the same trend or opposite trends. This is due to the fact that the instantaneous rate distribution is obtained from length-biased sampling of ISIs (Equation 3). Spike trains described by non-renewal processes have been studied widely (Eden and Kass, 2016) but are beyond the scope of this paper. For the special case of serially correlated ISIs, the results of our analysis apply to marginal distributions and therefore remain unchanged (Kostal and Lansky, 2006).

1. We observe several different relationships between the variability from temporal and instantaneous rate perspectives

(**Figure 2**). For gamma distribution, the variability of instantaneous rate is higher than the variability in ISIs whereas for lognormal and inverse Gaussian distribution it stays the same, $C_V(T) = C_V(R)$. On the other hand, for shifted exponential distribution $C_V(R) < C_V(T)$ until $C_V(T) = 0.7715$ but after that $C_V(R)$ increases rapidly compared to $C_V(T)$.

2. In the case of gamma distribution, both the randomness measures $C_h(T)$ and $C_h(R)$ decline eventually as a function of $C_V(T)$ but they become constant as a function of $C_V(R)$ (**Figures 6A–D**). The randomness for gamma distribution differs in each particular case, and for small values of $C_V(T)$, $C_h(R) < C_h(T)$. Lognormal and inverse Gaussian distributions attain their maximum for $C_V(T)$ values close to 1 and then their randomness keeps declining (**Figures 6A,C**). For these two distributions, $C_h(T) = C_h(R)$ whether it is mapped against $C_V(T)$ or $C_V(R)$. For shifted exponential distribution, $C_h(T)$ increases as a function of $C_V(T)$ (**Figure 6A**) whereas $C_h(R)$ attains its maximum for $C_V(T) = 0.85$ and then declines fast as $C_V \to 1$ (**Figure 6C**).
3. We studied the case of mixed exponential distribution with a refractory period. Although the theoretical analysis is complicated, we use the experimental data obtained from Song et al. (2018) to inspect the temporal and instantaneous rate perspectives. The dispersion measures for instantaneous rate provide a novel outlook on the data, different from the one provided by the dispersion measures for the ISIs (**Figure 6**). In cases like these, the instantaneous rate may be helpful in distinguishing further nuances in the data.

DATA AVAILABILITY STATEMENT

Publicly available datasets were analyzed in this study. This data can be found at: https://static-content.springer.com/esm/art%3A10.1038%2Fs41598-018-33064-z/MediaObjects/41598_2018_33064_MOESM1_ESM.pdf.

AUTHOR CONTRIBUTIONS

LK proposed the concept of the article. RT and LK wrote the manuscript. RT performed the calculations, numerical simulations, and analysis. All authors contributed to the article and approved the submitted version.

FUNDING

This research was supported by the Czech Science Foundation project 20-10251S.

ACKNOWLEDGMENTS

We thank Prof. Josef Trapani from Amherst College, MA and Prof. Nessy Tania from Smith College, MA for their helpful discussions and for kindly providing the experimental data. We would also like to thank Joseph Farrow from Durham University for his useful insights.

SUPPLEMENTARY MATERIAL

The Supplementary Material for this article can be found online at: https://www.frontiersin.org/articles/10.3389/fncom.2021.620410/full#supplementary-material

REFERENCES

Abramowitz, M., and Stegun, I. (1972). *Handbook of Mathematical Functions*. New York, NY: American Association of Physics Teachers.

Adrian, E. D. (1926). The impulses produced by sensory nerve-ending. *J. Physiol.* 62, 33–51. doi: 10.1113/jphysiol.1926.sp002334

Ainsworth, M., Lee, S., Cunningham, M. O., Traub, R. D., Kopell, N. J., and Whittington, M. A. (2012). Rates and rhythms: a synergistic view of frequency and temporal coding in neuronal networks. *Neuron* 75, 572–583. doi: 10.1016/j.neuron.2012.08.004

Awiszus, F. (1988). Continuous functions determined by spike trains of a neuron subject to stimulation. *Biol. Cybern.* 58, 321–327. doi: 10.1007/BF00363941

Barbieri, F., and Brunel, N. (2007). Irregular persistent activity induced by synaptic excitatory feedback. *Front. Comput. Neurosci.* 1:5. doi: 10.3389/neuro.10.005.2007

Berger, D., Pribram, K., Wild, H., and Bridges, C. (1990). An analysis of neural spike-train distributions: determinants of the response of visual cortex neurons to changes in orientation and spatial frequency. *Exp. Brain Res.* 80, 129–134. doi: 10.1007/BF00228854

Bershadskii, A., Dremencov, E., Fukayama, D., and Yadid, G. (2001). Probabilistic properties of neuron spiking time-series obtained *in vivo*. *Eur. Phys. J. B Condens. Matter Complex Syst.* 24, 409–413. doi: 10.1007/s10051-001-8691-4

Bessou, P., Laporte, Y., and Pages, B. (1968). A method of analysing the responses of spindle primary endings to fusimotor stimulation. *J. Physiol.* 196:37. doi: 10.1113/jphysiol.1968.sp008492

Bhumbra, G., and Dyball, R. (2004). Measuring spike coding in the rat supraoptic nucleus. *J. Physiol.* 555, 281–296. doi: 10.1113/jphysiol.2003.053264

Buraças, G. T., and Albright, T. D. (1999). Gauging sensory representations in the brain. *Trends Neurosci.* 22, 303–309. doi: 10.1016/S0166-2236(98)01376-9

Casella, G., and Berger, R. L. (2002). *Statistical Inference*. Grove, CA: Duxbury Pacific.

Cover, T. M., and Thomas, J. A. (2012). *Elements of Information Theory*. New York, NY: John Wiley & Sons.

Cox, D., and Miller, H. (1965). *The Theory of Stochastic Processes*. New York, NY: John Wiley & Sons.

Cox, D. R., and Lewis, P. A. W. (1966). *The Statistical Analysis of Series of Events*. London: Methuen & Co Ltd. doi: 10.1007/978-94-011-7801-3

Dettner, A., Münzberg, S., and Tchumatchenko, T. (2016). Temporal pairwise spike correlations fully capture single-neuron information. *Nat. Commun.* 7:13805. doi: 10.1038/ncomms13805

Ditlevsen, S., and Lansky, P. (2011). Firing variability is higher than deduced from the empirical coefficient of variation. *Neural Comput.* 23, 1944–1966. doi: 10.1162/NECO_a_00157

Doron, G., Von Heimendahl, M., Schlattmann, P., Houweling, A. R., and Brecht, M. (2014). Spiking irregularity and frequency modulate the behavioral report of single-neuron stimulation. *Neuron* 81, 653–663. doi: 10.1016/j.neuron.2013.11.032

Dorval, A. D., Russo, G. S., Hashimoto, T., Xu, W., Grill, W. M., and Vitek, J. L. (2008). Deep brain stimulation reduces neuronal entropy in the MPTP-primate model of Parkinson's disease. *J. Neurophysiol.* 100, 2807–2818. doi: 10.1152/jn.90763.2008

Eden, U. T., and Kass, R. E. (2016). "Chapter 107: Statistical models of spike train data," in *Neuroscience in the 21st Century*, eds D. W. Pfaff and N. Volkow (New York, NY: Springer), 3137–3151. doi: 10.1007/978-1-4939-3474-4_167

Gerstein, G. L., and Mandelbrot, B. (1964). Random walk models for the spike activity of a single neuron. *Biophys. J.* 4, 41–68. doi: 10.1016/S0006-3495(64)86768-0

Gerstner, W., and Kistler, W. M. (2002). *Spiking Neuron Models: Single Neurons, Populations, Plasticity*. Cambridge: Cambridge University Press. doi: 10.1017/CBO9780511815706

Heil, P., Neubauer, H., Irvine, D., and Brown, M. (2007). Spontaneous activity of auditory-nerve fibers: insights into stochastic processes at ribbon synapses. *J. Neurosci*. 27, 8457–8474. doi: 10.1523/JNEUROSCI.1512-07.2007

Jacobs, A. L., Fridman, G., Douglas, R. M., Alam, N. M., Latham, P. E., Prusky, G. T., et al. (2009). Ruling out and ruling in neural codes. *Proc. Natl. Acad. Sci. U.S.A*. 106, 5936–5941. doi: 10.1073/pnas.0900573106

Kostal, L., and Lansky, P. (2006). Classification of stationary neuronal activity according to its information rate. *Network* 17, 193–210. doi: 10.1080/09548980600594165

Kostal, L., Lansky, P., and Pokora, O. (2013). Measures of statistical dispersion based on shannon and fisher information concepts. *Info. Sci*. 235, 214–223. doi: 10.1016/j.ins.2013.02.023

Kostal, L., Lansky, P., and Rospars, J. P. (2007a). Neuronal coding and spiking randomness. *Eur. J. Neurosci*. 26, 2693–2701. doi: 10.1111/j.1460-9568.2007.05880.x

Kostal, L., Lansky, P., and Stiber, M. (2018). Statistics of inverse interspike intervals: the instantaneous firing rate revisited. *Chaos* 28:106305. doi: 10.1063/1.5036831

Kostal, L., Lansky, P., and Zucca, C. (2007b). Randomness and variability of the neuronal activity described by the ornstein-uhlenbeck model. *Network* 18, 63–75. doi: 10.1080/09548980701243134

Kostal, L., and Marsalek, P. (2010). Neuronal jitter: can we measure the spike timing dispersion differently. *Chin. J. Physiol*. 53, 454–464. doi: 10.4077/CJP.2010.AMM031

Lansky, P., Rodriguez, R., and Sacerdote, L. (2004). Mean instantaneous firing frequency is always higher than the firing rate. *Neural Comput*. 16, 477–489. doi: 10.1162/089976604772744875

Levine, M. W. (1991). The distribution of the intervals between neural impulses in the maintained discharges of retinal ganglion cells. *Biol. Cybern*. 65, 459–467. doi: 10.1007/BF00204659

McDonnell, M. D., Ikeda, S., and Manton, J. H. (2011). An introductory review of information theory in the context of computational neuroscience. *Biol. Cybern*. 105:55. doi: 10.1007/s00422-011-0451-9

McKeegan, D. E. F. (2002). Spontaneous and odour evoked activity in single avian olfactory bulb neurones. *Brain Res*. 929, 48–58. doi: 10.1016/S0006-8993(01)03376-5

Nakahama, H., Suzuki, H., Yamamoto, M., Aikawa, S., and Nishioka, S. (1968). A statistical analysis of spontaneous activity of central single neurons. *Physiol. Behav*. 3, 745–752. doi: 10.1016/0031-9384(68)90146-7

Nemenman, I., Bialek, W., and Van Steveninck, R. D. R. (2004). Entropy and information in neural spike trains: progress on the sampling problem. *Phys. Rev. E* 69:056111. doi: 10.1103/PhysRevE.69.056111

Neubauer, H., Koppl, C., and Heil, P. (2009). Spontaneous activity of auditory nerve fibers in the barn owl (tyto alba): analyses of interspike interval distributions. *J. Neurophysiol*. 101, 3169–3191. doi: 10.1152/jn.90779.2008

Obeso, J. A., Rodriguez-Oroz, M. C., Rodriguez, M., Lanciego, J. L., Artieda, J., Gonzalo, N., et al. (2000). Pathophysiology of the basal ganglia in Parkinson's disease. *Trends Neurosci*. 23, S8–S19. doi: 10.1016/S1471-1931(00)00028-8

Pauluis, Q., and Baker, S. N. (2000). An accurate measure of the instantaneous discharge probability, with application to unitary joint-event analysis. *Neural Comput*. 12, 647–669. doi: 10.1162/089976600300015736

Perkel, D. H., and Bullock, T. H. (1968). Neural coding. *Neurosci. Res. Prog. Bull*. 6:221–348.

Pouzat, C., and Chaffiol, A. (2009). Automatic spike train analysis and report generation. an implementation with R, R2HTML and star. *J. Neurosci. Methods* 181, 119–144. doi: 10.1016/j.jneumeth.2009.01.037

Principe, J. C. (2010). *Information Theoretic Learning: Renyi's Entropy and Kernel Perspectives*. New York, NY: Springer Science & Business Media. doi: 10.1007/978-1-4419-1570-2

Rajdl, K., and Lansky, P. (2013). Fano factor estimation. *Math. Biosci. Eng*. 11:105. doi: 10.3934/mbe.2014.11.105

Rajdl, K., Lansky, P., and Kostal, L. (2017). Entropy factor for randomness quantification in neuronal data. *Neural Netw*. 95, 57–65. doi: 10.1016/j.neunet.2017.07.016

Reeke, G. N., and Coop, A. D. (2004). Estimating the temporal interval entropy of neuronal discharge. *Neural Comput*. 16, 941–970. doi: 10.1162/089976604773135050

Rieke, F., Warland, D., Van Steveninck, R., and Bialek, W. S. (1999). *Spikes: Exploring the Neural Code, Vol 7*. Cambridge: MIT Press.

Rigotti, M., Barak, O., Warden, M. R., Wang, X. J., Daw, N. D., Miller, E. K., et al. (2013). The importance of mixed selectivity in complex cognitive tasks. *Nature* 497:585. doi: 10.1038/nature12160

Rodieck, R., Kiang, N.-S., and Gerstein, G. (1962). Some quantitative methods for the study of spontaneous activity of single neurons. *J. Biophys*. 2, 351–368. doi: 10.1016/S0006-3495(62)86860-X

Rudd, M. E., and Brown, L. G. (1997). Noise adaptation in integrate-and-fire neurons. *Neural Comput*. 9, 1047–1069. doi: 10.1162/neco.1997.9.5.1047

Shadlen, M. N., and Newsome, W. T. (1994). Noise, neural codes and cortical organization. *Curr. Opin. Neurobiol*. 4, 569–579. doi: 10.1016/0959-4388(94)90059-0

Shannon, C. E., and Weaver, W. (1949). *The Mathematical Theory of Communication*. Urbana, IL: University of Illinois Press.

Smith, D. R., and Smith, G. K. (1965). A statistical analysis of the continual activity of single cortical neurones in the cat unanaesthetized isolated forebrain. *Biophys. J*. 5, 47–74. doi: 10.1016/S0006-3495(65)86702-9

Softky, W. R., and Koch, C. (1993). The highly irregular firing of cortical cells is inconsistent with temporal integration of random EPSPS. *J. Neurosci*. 13, 334–350. doi: 10.1523/JNEUROSCI.13-01-00334.1993

Song, S., Lee, J. A., Kiselev, I., Iyengar, V., Trapani, J. G., and Tania, N. (2018). Mathematical modeling and analyses of interspike-intervals of spontaneous activity in afferent neurons of the Zebrafish lateral line. *Sci Rep*. 8, 1–14. doi: 10.1038/s41598-018-33064-z

Stein, R. B., Gossen, E. R., and Jones, K. E. (2005). Neuronal variability: noise or part of the signal? *Nat. Rev. Neurosci*. 6:389. doi: 10.1038/nrn1668

Steuer, R., Ebeling, W., Russell, D. F., Bahar, S., Neiman, A., and Moss, F. (2001). Entropy and local uncertainty of data from sensory neurons. *Phys. Rev. E* 64:061911. doi: 10.1103/PhysRevE.64.061911

Stevenson, I. H. (2016). Flexible models for spike count data with both over-and under-dispersion. *J. Comput. Neurosci*. 41, 2-9-43. doi: 10.1007/s10827-016-0603-y

Theunissen, F., and Miller, J. P. (1995). Temporal encoding in nervous systems: a rigorous definition. *J. Comput. Neurosci*. 2, 149–162. doi: 10.1007/BF00961885

Thomas, E. (1966). Mathematical models for the clustered firing of single cortical neurones. *Br. J. Math. Stat. Psychol*. 19, 151–162. doi: 10.1111/j.2044-8317.1966.tb00365.x

Thorpe, S. J., and Gautrais, J. (1997). "Rapid visual processing using spike asynchrony," in *Advances in Neural Information Processing Systems*, Cambridge, 901–907.

Trapani, J., and Nicolson, T. (2011). Mechanism of spontaneous activity in afferent neurons of the Zebrafish lateral-line organ. *J. Neurosci*. 31, 1614–1623. doi: 10.1523/JNEUROSCI.3369-10.2011

Tuckwell, H. C. (1988). *Introduction to Theoretical Neurobiology: Vol. 2, Nonlinear and Stochastic Theories, Vol. 8*. Cambridge: Cambridge University Press.

Tuckwell, H. C. (1989). Stochastic processes in the neurosciences. *SIAM*. doi: 10.1137/1.9781611970159

Victor, J. D., and Purpura, K. P. (1997). Metric-space analysis of spike trains: theory, algorithms and application. *Network* 8, 127–164. doi: 10.1088/0954-898X_8_2_003

Watters, N., and Reeke, G. N. (2014). Neuronal spike train entropy estimation by history clustering. *Neural Comput*. 26, 1840–1872. doi: 10.1162/NECO_a_00627

Conflict of Interest: The authors declare that the research was conducted in the absence of any commercial or financial relationships that could be construed as a potential conflict of interest.

Attachment III

Manuscript published in *Biosystems* **222**, 104780. Published December 2022
doi: 10.1016/j.biosystems.2022.104780

Contents lists available at ScienceDirect

BioSystems

journal homepage: www.elsevier.com/locate/biosystems

A simple neuronal model with intrinsic saturation of the firing frequency

Rimjhim Tomar [a,b,*], Charles E. Smith [c], Petr Lansky [a]

[a] Institute of Physiology of the Czech Academy of Sciences, Videnska 1083, 14220 Prague 4, Czech Republic
[b] Second Medical Faculty, Charles University, V Uvalu 84, 15006 Prague 6, Czech Republic
[c] Department of Statistics, North Carolina State University, 2311 Stinson Drive, Raleigh, NC 27695-8203, United States of America

ARTICLE INFO

Keywords:
Rate coding
Temporal coding
Neuronal models
Leaky integrate-and-fire
Firing rate
Reversal potential

ABSTRACT

We present a comparison of the intrinsic saturation of firing frequency in four simple neural models: leaky integrate-and-fire model, leaky integrate-and-fire model with reversal potentials, two-point leaky integrate-and-fire model, and a two-point leaky integrate-and-fire model with reversal potentials. "Two-point" means that the equivalent circuit has two nodes (dendritic and somatic) instead of one (somatic only). The results suggest that the reversal potential increases the slope of the "firing rate vs input" curve due to a smaller effective membrane time constant, but does not necessarily induce saturation of the firing rate. The two-point model without the reversal potential does not limit the voltage or the firing rate. In contrast to the previous models, the two-point model with the reversal potential limits the asymptotic voltage and the firing rate, which is the main result of this paper. The case of excitatory inputs is considered first and followed by the case of both excitatory and inhibitory inputs.

1. Introduction

Frequency coding is one of the basic forms of information transfer within the nervous system. It assumes that the frequency of uniformly sized action potentials varies with stimulation intensity (Adrian, 1928). As the stimulus intensity is increased, an increase in neuronal activity follows. A survey of the role of the mean firing rate of neuronal models was presented by Gerstner and van Hemmen (1992).

No saturation frequency exists as an intrinsic part of common simple neuronal models, which means that with increasing stimulation the firing frequency increases without any limit. Of course, this feature of the models is in contrast with observed neuronal behavior. The common way to solve this problem is by adding a dead time (absolute refractory period) to each interspike interval (ISI) calculated from the model (e.g., Tuckwell, 1988; Bugmann et al., 1997; Tal and Schwartz, 1997; Fusi and Mattia, 1999). Some other methods are: by considering a negative feedback (Barbi et al., 1975), by adaptation (Ermentrout, 1998), or both (Pakdaman et al., 1999). Relative refractory periods, either due to a time varying threshold or a time varying conductance, can also produce a saturation in firing rate (Jack et al., 1983; Schaette et al., 2005). Here we present a simple two-point, reversal potential model that inherently has a saturation frequency. The transfer function of this model is compared with the simple leaky integrate-and-fire (LIF) model, the LIF model with reversal potentials, and the two-point LIF model. Numerical simulations illustrate the differences among the transfer functions of these three models and the two-point LIF model with reversal potentials for typical values of the parameters.

2. Methods and results

2.1. Neuronal models

2.1.1. Leaky integrate-and-fire (LIF) model

The LIF model is the simplest realistic neuronal model (Lapicque, 1907). In this model the behavior of the depolarization $V(t)$ of the neuronal membrane is described by the differential equation

$$dV(t) = \left(-\frac{V(t)}{\tau} + \mu\right)dt, \quad V(t_j) = v_0, \tag{1}$$

where $\tau > 0$ is the membrane time constant ($\tau = RC$, where R is the membrane resistance and C is its capacitance); $\mu \in \mathbb{R}$ is measured in mV per unit time, which reflects the input signal resulting from the dendritic currents generated by the sensory stimulation or action of other neurons; t_j is the moment of the last firing of an action potential and $t > t_j$. The relaxation time constant τ includes several recovery processes — the decay of the transmitter substance generating postsynaptic potentials, the filtering action of the membrane impedance and also the passive propagation of the somato-dendritic depolarization

Abbreviations: ISI, Interspike interval; LIF, Leaky integrate-and-fire

* Corresponding author at: Institute of Physiology of the Czech Academy of Sciences, Videnska 1083, 14220 Prague 4, Czech Republic.
E-mail address: rimjhim.tomar@fgu.cas.cz (R. Tomar).

https://doi.org/10.1016/j.biosystems.2022.104780
Received 28 April 2022; Received in revised form 1 September 2022; Accepted 13 September 2022

to the trigger zone. The solution for Eq. (1) is given by,

$$V(t) = \exp\left(-\frac{1}{\tau}(t-t_j)\right)v_0 + \mu\tau\left[1-\exp\left(-\frac{1}{\tau}(t-t_j)\right)\right]. \tag{2}$$

The asymptotic voltage is,

$$V(\infty) := \lim_{t\to\infty} V(t) = \mu\tau. \tag{3}$$

The firing of an action potential in this kind of model is identified with the first crossing of V through a firing threshold S, where $S > v_0$. At these instants, the membrane potential is reset to its initial value v_0, which is typically taken to be the resting potential 0 mV. If $s = t_{j+1} - t_j$ is the ISI length, then the voltage at firing threshold S is

$$V(t_{j+1}) = \exp\left(-\frac{s}{\tau}\right)v_0 + \mu\tau\left[1-\exp\left(-\frac{s}{\tau}\right)\right], \tag{4}$$

Due to the constancy of the input signal, the ISIs are constant. The firing frequency $f(\mu)$, expressed as a function of the input signal μ such that $\mu > S/\tau$, is the inverse of the ISI length s. From Eq. (4), it follows that

$$f(\mu) = 1/s = \frac{1}{\tau\ln\left(\frac{\mu\tau}{\mu\tau - S}\right)}, \tag{5}$$

note that we have set $v_0 = 0$. This relationship is also known as the gain function (Gerstner and van Hemmen, 1992) or transfer function (Tal and Schwartz, 1997). With increasing μ, $f(\mu) \to \infty$. The (oblique) asymptote of $f(\mu)$ is

$$f_a = -\frac{1}{2\tau} + \frac{\mu}{S}. \tag{6}$$

As expected, the slope decreases with increasing threshold S and does not depend on τ. It starts abruptly at the rheobase $\mu_0 = S/\tau$ (rheobase is the minimal injected current required to elicit an action potential) and grows monotonically towards a linear asymptote. If we rescale Eq. (6) by dividing it by the rheobase level, i.e. the excitation that just produces firing, then Eqs. (5) and (6) become

$$f(\mu/\mu_0) = \frac{1}{\tau\ln\left(\frac{\mu/\mu_0}{\mu/\mu_0 - 1}\right)}, \tag{5a}$$

$$f_a = -\frac{1}{2\tau} + \frac{1}{\tau}\frac{\mu}{\mu_0}, \tag{6a}$$

which now has a slope of $1/\tau$ (Tal and Schwartz, 1997). The shapes of the input–output frequency curves for model (1) and its modifications have been studied for a long time (e.g., Knight, 1972; Fohlmeister, 1979; Scharstein, 1979). Fig. 1 shows the shape of the transfer function and its asymptote for a particular set of parameters (specified in Section 2.2).

2.1.2. Leaky integrate-and-fire model with reversal potentials

Stein's stochastic neuronal model (Stein, 1970) that takes into account reversal potentials (e.g. Hanson and Tuckwell, 1983; Smith and Smith, 1994; Lanska and Lansky, 1987) is

$$d\mathrm{V(t)} = -\frac{V(t)}{\tau}d\mathrm{t} + a(V_E(t) - V(t))d\mathrm{N(t)} + i(V(t) - V_I(t))d\mathrm{M(t)}, \quad V(t_j) = v_0, \tag{7}$$

where $\tau > 0$ plays the same role as in (1), $-1 < i < 0 < a < 1$ are constants, $V_I < v_0 = 0 < S < V_E$ are the excitatory and inhibitory reversal potentials, $N(t)$, $M(t)$ are two independent homogeneous Poisson processes with intensities λ^+ and λ^-, respectively. The assumed Poissonian character of the input follows from pooling of many relatively independent inputs. Intensities λ^+ and λ^- reflect the input signal in model (7), the values a and i reflect the fractional change of the membrane potential in response to the input pulse as they contribute to the membrane potential at the trigger zone. The depolarization of the membrane caused by an excitatory postsynaptic potential decreases with decreasing distance of the membrane potential from the excitatory reversal potential, V_E. In the same manner, the hyperpolarization caused by an inhibitory postsynaptic potential is smaller if the membrane potential is closer to the inhibitory reversal potential, V_I. Hence the process remains confined within these boundaries. To derive a deterministic counterpart of model (7), a sequence of models given by (7) and characterized by the quadruplet $\{\lambda_n^+, \lambda_n^-, a_n, i_n\}$ is needed such that $\lambda_n^+ \to +\infty$, $\lambda_n^- \to +\infty$, $a_n \to 0_+$, $i_n \to 0_-$ fulfilling the condition $\lambda_n^+ a_n \to \mu_E > 0$ and $\lambda_n^- i_n \to \mu_I < 0$. Then (7) can be replaced by

$$dV(t) = \left(-\left(\frac{1}{\tau} + \mu_E - \mu_I\right)V(t) + \mu_E V_E(t) - \mu_I V_I(t)\right)dt. \tag{8}$$

The main difference between models (1) and (8) is that in (8) the leakage time constant of the model also depends on the inhibitory and excitatory inputs. For model (8) the asymptotic voltage is

$$V(\infty) = \frac{\mu_E V_E - \mu_I V_I}{\frac{1}{\tau} + \mu_E - \mu_I}, \tag{9}$$

which in contrast to the LIF model is finite even when the excitation, μ_E, increases to infinity. Denoting by $\tau_{ef} = \tau/(1 + \tau\mu_E - \tau\mu_I)$ the effective time constant and $\mu_{ef} = \mu_E V_E - \mu_I V_I$ the effective input of model (8), the firing frequency is given by Eq. (5) where μ and τ are replaced by μ_{ef} and τ_{ef}. The asymptote as a function of the excitatory input μ_E is

$$f_a = \frac{S(V_E - \tau\mu_I(V_E - V_I))}{\tau V_E(V_E - S)\ln^2(V_E/(V_E - S))} + \frac{(1/\tau - \mu_I)}{\ln(V_E/(V_E - S))} + \frac{\mu_E}{\ln(V_E/(V_E - S))}, \tag{10}$$

from which we can see that again the frequency grows without limit with increasing excitation. We would like to compare the slope in Eq. (10) with that in Eq. (6), however, μ and μ_E are in different units, mV/ms and 1/ms respectively. Normalizing by the rheobase level of μ_E calculated from Eq. (9), namely $\mu_{E0} = (S/\tau - \mu_I S + \mu_I V_I)/(V_E - S)$, allows for a meaningful comparison. Eq. (10) becomes

$$f_a = \frac{S(V_E - \tau\mu_I(V_E - V_I))}{\tau V_E(V_E - S)\ln^2(V_E/(V_E - S))} + \frac{(1/\tau - \mu_I)}{\ln(V_E/(V_E - S))} + \frac{S(\mu_I - 1/\tau) - \mu_I V_I}{(S - V_E)\ln(V_E/(V_E - S))}\frac{\mu_E}{\mu_{E0}}, \tag{10a}$$

and after some calculation, we can see that the asymptotic slope of the reversal potential model is higher than that of the LIF model. Fig. 2 shows the profile of the firing frequency and its asymptote for this model.

2.1.3. Two-point integrate-and-fire model

In Lansky and Rodriguez (1999) the coding properties of a two-point neuronal model based on two LIF models were studied. The model is formally defined in the following way:

$$dV_1(t) = \left(-\frac{V_1(t)}{\tau} + \frac{V_2(t) - V_1(t)}{\tau_r} + \mu\right)dt \tag{11}$$

and

$$dV_2(t) = \left(-\frac{V_2(t)}{\tau} + \frac{V_1(t) - V_2(t)}{\tau_r}\right)dt, \tag{12}$$

where $\tau > 0$ is the same time constant as in Eq. (1) and $\tau_r > 0$ is a junctional time constant derived from the conductance between the compartments. The first terms on the right-hand sides represent the transmembrane leakage, the second terms the electrical coupling between the compartments, and the last term in Eq. (11) represents the input. For simplicity, in Eqs. (11) and (12), we assume that the parameters of the membrane are the same in both compartments. The initial conditions for Eqs. (11) and (12) follow from the firing of the model. In accordance with the integrate-to-threshold scenario, when the membrane potential $V_2(t)$ at the trigger zone reaches the firing threshold S, the value of the function $V_2(t)$ is reset to zero while the function $V_1(t)$ continues its evolution, that is we assume no antidromic spike propagation into the dendrite. Therefore, we need to solve the

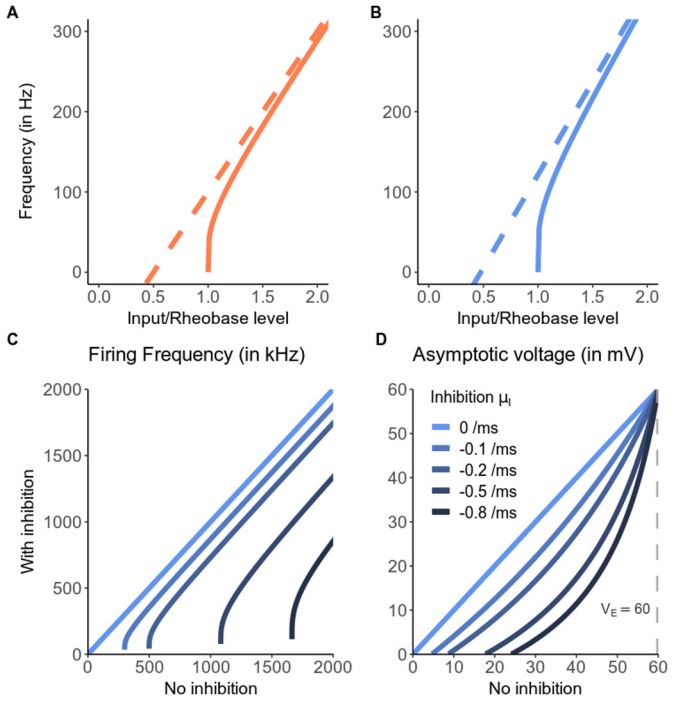

Fig. 1. *Transfer function of the leaky integrate-and-fire (LIF) model and LIF model with reversal potential, and the effect of reversal potentials on the firing frequency and asymptotic voltage of the latter.* **A** Transfer function of the LIF model with input normalized to rheobase. **B** Transfer function of the LIF model with reversal potentials. Input is normalized to rheobase and μ_I is set to 0. **C** Firing frequency of the LIF model with reversal potentials with different inhibitory inputs. The excitatory input increases from left to right. All the other parameters are the same as in the previous figures. Reversal potentials do not limit the firing rate. **D** Asymptotic voltage of the LIF model with reversal potentials with different inhibitory input. Reversal potentials limit the asymptotic voltage to the value of $V_E = 60$ mV.

first-passage-time problem for $V_2(t)$ under the initial conditions $V_1(t_j) = v_{10}$ and $V_2(t_j) = 0$, where v_{10} is the value of the dendritic potential at the time of the last spike.

The asymptotic solutions $V_1(\infty)$ and $V_2(\infty)$ are

$$V_1(\infty) = \frac{\tau(\tau + \tau_r)\mu}{2\tau + \tau_r} \tag{13}$$

and

$$V_2(\infty) = \frac{\tau^2 \mu}{2\tau + \tau_r}. \tag{14}$$

The firing is achieved under the condition that the stimulation is sufficiently strong, in other words, that the firing threshold is lower than the asymptotic depolarization at the trigger zone compartment, $V_2(\infty) > S$. Thus from Eq. (14), the condition for the rheobase stimulation, which determines the model sensitivity, is

$$\mu_0 = \frac{S}{\tau}\frac{\tau_r + 2\tau}{\tau}. \tag{15}$$

The general solutions of Eqs. (11) and (12) are

$$V_1(t) = V_1(\infty) + \frac{1}{2}\exp\left(-\frac{1}{\tau}(t - t_j)\right)\left(-\mu\tau + V_1(t_j)\right) - \frac{1}{2}\exp\left(-\frac{\tau_r + 2\tau}{\tau_r \tau}(t - t_j)\right)\left(\frac{\tau_r \tau \mu}{\tau_r + 2\tau} - V_1(t_j)\right) \tag{16}$$

and

$$V_2(t) = V_2(\infty) + \frac{1}{2}\exp\left(-\frac{1}{\tau}(t - t_j)\right)\left(-\mu\tau + V_1(t_j)\right) + \frac{1}{2}\exp\left(-\frac{\tau_r + 2\tau}{\tau_r \tau}(t - t_j)\right)\left(\frac{\tau_r \tau \mu}{\tau_r + 2\tau} - V_1(t_j)\right), \tag{17}$$

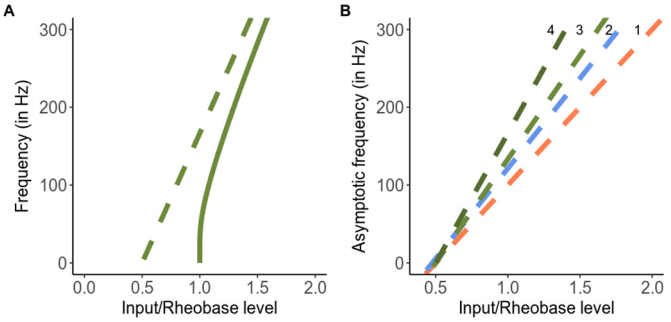

Fig. 2. *Transfer function of the two-point leaky integrate-and-fire (LIF) model and a comparison of the asymptotic slopes of the first three discussed models.* **A** Transfer function of the two-point LIF model, with parameter values set at $\tau = 5$ ms, $\tau_r = 2.5$ ms and $S = 15$ mV. **B** Asymptotic slopes of the LIF model [1], LIF model with reversal potentials as $\mu_I = 0$ [2], two-point model with $\tau_r = 10$ ms [3] and $\tau_r = 5$ ms [4]. Parameters are set as $\tau = 5$ ms, $S = 15$ mV, $V_E = 60$ mV and $V_I = -10$ mV.

where t_j is the time instant of the last spike emission, $t > t_j$. Solving Eqs. (16) and (17) for long-lasting suprathreshold stimulation, the system achieves its steady-state characterized by a constant $V_1(t_j)$ for each j and consequently constant ISIs. Therefore, under the conditions $V_1(t_j) = V_1(t_{j+1})$, $V_2(t_j + 0) = 0$ and $V_2(t_{j+1} - 0) = S$, where t_j and t_{j+1} are two consecutive instants of neuronal firing ans $s = t_{j+1} - t_j$ is the ISI length, we obtain an equation for the firing frequency $f = 1/s = 1/(t_{j+1} - t_j)$,

$$1 - \frac{\mu}{\mu_0} = \left(e^{-\frac{1}{\tau f}} + e^{-\frac{\tau_r + 2\tau}{\tau_r \tau f}}\right)\left(\frac{1}{2} - \frac{\mu}{\mu_0}\right) + \frac{\mu}{\mu_0}e^{-\frac{2(\tau_r + \tau)}{\tau_r \tau f}}, \tag{18}$$

where the dependence on S is through the value of μ_0 given by Eq. (15). Solving this equation for f, we achieve the input–output transfer function. The firing frequency tends again to infinity with increasing μ with the asymptote

$$f_a = -\frac{1}{2\tau}\frac{\tau_r + 2\tau}{\tau_r + \tau} + \frac{\tau}{S(\tau_r + \tau)}\mu. \tag{19}$$

This can be seen in Fig. 2A, through the profile of the transfer function. The asymptotic slope of the two-point model is higher than that of the LIF model with reversal potentials and the LIF model, as shown in Fig. 2B.

2.1.4. Two-point leaky integrate-and-fire model with reversal potentials

To avoid this infinite firing rate feature of the previous three neuronal models, let us incorporate model (8) into the two-point model (11) and (12). The resulting model is given by equations

$$\mathrm{d}V_1(t) = \left(-(\frac{1}{\tau} + \mu_E - \mu_I)V_1(t) + \frac{V_2(t) - V_1(t)}{\tau_r} + \mu_E V_E(t) - \mu_I V_I(t)\right)\mathrm{d}t \tag{20}$$

and

$$\mathrm{d}V_2(t) = \left(-\frac{V_2(t)}{\tau} + \frac{V_1(t) - V_2(t)}{\tau_r}\right)\mathrm{d}t. \tag{21}$$

Using the notation $\tau_{ef} = \tau/(1 + \tau\mu_E - \tau\mu_I)$ and $\mu_{ef} = \mu_E V_E - \mu_I V_I$, the asymptotic solutions $V_1(\infty)$ and $V_2(\infty)$ are

$$V_1(\infty) = \frac{\mu_{ef}(\tau_r + \tau)}{1 + \tau_{ef}(\tau_r + \tau)}, \tag{22}$$

$$V_2(\infty) = \frac{\mu_{ef}\tau}{1 + \tau_{ef}(\tau_r + \tau)}. \tag{23}$$

The analytical expression for firing rate is difficult to obtain for this model, but the firing rate can be calculated numerically for a given set of parameters. For Fig. 3, Eqs. (20) and (21) were used to determine the firing frequency for a fixed set of μ_E values. Linear regression was

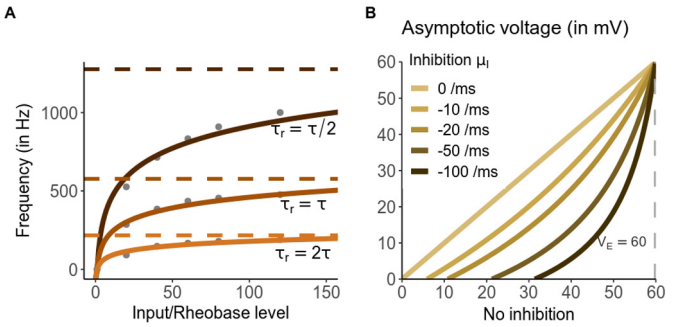

Fig. 3. *Effect of reversal potentials on the firing frequency and asymptotic voltage of the two-point leaky integrate-and-fire (LIF) model with reversal potentials.* **A** Transfer function of the two-point LIF model with reversal potentials, with parameter values set at $\tau = 5$ ms, $S = 15$ mV, $V_E = 60$ mV, $V_I = -10$ mV and τ_r is 2.5 ms, 5 ms and 10 ms for the different cases. **B** Asymptotic voltage of the two-point model with reversal potentials with different inhibitory inputs. Reversal potential limits asymptotic voltage as well as the firing rate.

used to fit a logarithmic curve to the frequency points and the predicted values from the model fit were used to generate the lines that represent the frequency curve in Fig. 3.

For increasing μ_E the depolarization V_1 at the dendritic compartment is limited by V_E, using this with Eq. (21) yields the maximum firing frequency,

$$f_{max} = \frac{\tau + \tau_r}{\tau\tau_r \ln\left(\frac{V_E\tau}{V_E\tau - S(\tau+\tau_r)}\right)}, \tag{24}$$

which is represented by the dashed lines in Fig. 3.

2.2. Numerical example

For numerical illustration of the derived results, the parameters of the models must be specified. We assume the value $S = 15$ mV of the firing threshold and $\tau = 5$ ms for all the models. These parameters completely define the LIF model and the input–output transfer function is illustrated in Fig. 1A.

Several other parameters appear in (8). First of all, we can specify the reversal potentials with respect to the resting depolarization as $V_E = 60$ mV and $V_I = -10$ mV. To specify the input parameters of model (8) we have to realize that in contrast to (1), in (8) the influence of inhibition and excitation is separated. Let $\mu_I = 0$ (no inhibition), and the input–out transfer function is presented in Fig. 1B. Increasing inhibition has a divisive (rather than subtractive) effect on the transfer function. Figs. 1D and 1C illustrate that for the LIF model, reversal potentials limit the asymptotic voltage but not the firing frequency.

To estimate the junctional time constant τ_r for the two-point models is not a simple task, as it reflects not only electrical but also spatial properties of that particular neuron. We select the values $\tau_r = 2.5$ ms, $\tau_r = 5$ ms and $\tau_r = 10$ ms, namely $\tau/2$, τ and 2τ. The input–output transfer function for the two-point LIF model is presented in Fig. 2A and for the two-point LIF model with reversal potentials in Fig. 3A. Only in Fig. 3A the limiting firing frequency is finite.

3. Discussion

The saturation of firing frequency can be induced by including a dead time or absolute refractory period (Indiveri, 2003; Hampel and Lansky, 2008). In the absence of dead time, the simplest neuronal model to allow the intrinsic saturation of the firing frequency is the two-point model with reversal potentials.

We have concentrated on the role of excitatory input on high firing frequency with the value of μ_I fixed. The role of inhibition could be examined more closely as it may have either a subtractive or divisive effect (Holt and Koch, 1997), and may be critical to increasing the regularity of spiking in high conductance states (e.g. Barta and Kostal, 2021; Destexhe, 2010; Denève and Machens, 2016). Additionally, this analysis can be extended to integrate-and-fire models with stochastic synaptic input (Burkitt, 2006). As stochasticity in the input increases, the firing frequency transfer function becomes more linear around the rheobase input level, providing a noisy, but single neuron temporal alternative to population averaging of neurons. For nonlinear models, the effect of noise can also be to switch between domains of attraction for appropriate types of noise input, such as Poisson vs white noise (e.g. Smith, 1992). Noise can also increase the bandwidth for transmission and minimize distortion as noted by Stein (1970).

The transition from a one to two-point model aims to include some aspects of the spatial structure of the dendritic tree. This could be further extended by multiple compartments and partial-differential-equation membrane models, (e.g. Dayan and Abbott, 2001; Tuckwell, 1988's chapter on spatial models) however, the firing rate saturation already occurs with two compartments provided reversal potentials were added. The reversal potentials characterize different types of synapses, typically negative for the potassium ions in inhibitory synapses and positive for sodium ions in excitatory synapses. If the neuron has a short electrotonic length, then the synaptic input and trigger site are close together and can be regarded as one compartment. However, if the synaptic input is further away with respect to the length constant of the neuron then a second (or higher) compartment is needed to accurately represent the electrical properties of the synapse (Jack et al., 1983; Gerstner and Kistler, 2002). The analysis presented in this article serves as a benchmark to compare other models and experimental results using current injection. The asymptotic forms of the transfer function for firing frequency, presented in this article allow comparison with the mean firing frequencies obtained after stochastic modifications, as well as point process estimation approaches (Cox and Lewis, 1966; Johnson, 1996; Kass et al., 2005).

Declaration of competing interest

The authors declare that they have no known competing financial interests or personal relationships that could have appeared to influence the work reported in this paper.

Data availability

No data was used for the research described in the article.

Acknowledgments

This work was supported by the Czech Science Foundation project 20-10251S, Charles University project GA UK 373121, and by North Carolina State University.

References

Adrian, E.D., 1928. The Basis of Sensation. WW Norton & Co, New York.
Barbi, M., Carelli, V., Frediani, C., Petracchi, D., 1975. The self-inhibited leaky integrator: Transfer functions and steady state relations. Biol. Cybernet. 20, 51–59.
Barta, T., Kostal, L., 2021. Regular spiking in high-conductance states: The essential role of inhibition. Phys. Rev. E 103, 022408.
Bugmann, G., Christodoulou, C., Taylor, J.G., 1997. Role of temporal integration and fluctuation detection in the highly irregular firing of a leaky integrator neuron model with partial reset. Neural Comput. 9, 985–1000.
Burkitt, A., 2006. A review of the integrate-and-fire neuron model: II. Inhomogeneous synaptic input and network properties. Biol. Cybernet. 95, 97–112.
Cox, D.R., Lewis, P.A.W., 1966. The Statistical Analysis of Series of Events. Springer, Netherlands.
Dayan, P., Abbott, L.F., 2001. Theoretical Neuroscience. MIT Press, Cambridge, Mass.
Denève, S., Machens, C.K., 2016. Efficient codes and balanced networks. Nat. Neurosci. 19, 375–382.
Destexhe, A., 2010. Inhibitory noise. Front. Cell. Neurosci. 4.

Ermentrout, B., 1998. Linearization of F-I curves by adaptation. Neural Comput. 10, 1721–1729.

Fohlmeister, J., 1979. A theoretical study of neural adaptation and transient responses due to inhibitory feedback. Bull. Math. Biol. 41, 257–282.

Fusi, S., Mattia, M., 1999. Collective behavior of networks with linear (VLSI) integrate-and-fire neurons. Neural Comput. 11, 633–652.

Gerstner, W., van Hemmen, J.L., 1992. Universality in neural networks: the importance of the 'mean firing rate'. Biol. Cybernet. 67, 195–205.

Gerstner, W., Kistler, W.M., 2002. Spiking Neuron Models: Single Neurons, Populations, Plasticity. Cambridge University Press, Cambridge.

Hampel, D., Lansky, P., 2008. On the estimation of refractory period. J. Neurosci. Methods 171, 288–295.

Hanson, F.B., Tuckwell, H.C., 1983. Diffusion approximation for neuronal activity including synaptic reversal potential. J. Theor. Neurobiol. 2, 127–153.

Holt, G.R., Koch, C., 1997. Shunting inhibition does not have a divisive effect on firing rates. Neural Comput. 9, 1001–1009.

Indiveri, G., 2003. A low-power adaptive integrate-and-fire neuron circuit. In: Proceedings of the 2003 International Symposium on Circuits and Systems, 2003 4, IV–IV. IEEE.

Jack, J.J.B., Noble, D., Tsien, R.W., 1983. Electric Current Flow in Excitable Cells. Claredon Press, Oxford.

Johnson, D.H., 1996. Point process models of single-neuron discharges. J. Comput. Neurosci. 3, 275–299.

Kass, R.E., Ventura, V., Brown, E.N., 2005. Statistical issues in the analysis of neuronal data. J. Neurophysiol. 94, 8–25.

Knight, B.W., 1972. Dynamics of encoding in a population of neurons. J. Gen. Physiol. 59, 734–766.

Lanska, V., Lansky, P., 1987. Diffusion approximations of the neuronal model with synaptic reversal potentials. Biol. Cybernet. 56, 19–26.

Lansky, P., Rodriguez, R., 1999. The spatial properties of a model neuron increase its coding range. Biol. Cybernet. 81, 161–167.

Lapicque, L., 1907. Sur l'excitation electrique des nerfs traitée comme une polarisation. J. Physiol. Pathol. Génér 9.

Pakdaman, K., Alvarez, F., Segundo, J.P., Diez-Martinez, O., Vibert, J.-F., 1999. Adaptation prevents discharge saturation in models of single neurons with recurrent excitation. Int. J. Mod. Simul. 22, 260–269.

Schaette, R., Gollisch, T., Herz, A.V.M., 2005. Spike-train variability of auditory neurons in vivo: dynamic responses follow predictions from constant stimuli. J. Nuerophysiol. 93, 3270–3281.

Scharstein, H., 1979. Input–output relationship of the leaky-integrator neuron model. J. Math. Biol. 8, 403–420.

Smith, C.E., 1992. A heuristic approach to stochastic models of single neurons. In: Single Neuron Computation. Academic Press, Boston, pp. 561–588.

Smith, C.E., Smith, M.V., 1994. Moments of voltage trajectories for stein's model with synaptic reversal potentials. J. Theor. Neurobiol. 3, 67–77.

Stein, R.B., 1970. The role of spike trains in transmitting and distorting sensory signals. In: The Neurosciences. The Rockefeller University Press, New York, pp. 597–604.

Tal, D., Schwartz, E.L., 1997. Computing with the leaky integrate-and-fire neuron: Logarithmic computation and multiplication. Neural Comput. 9, 305–318.

Tuckwell, H.C., 1988. Introduction To Theoretical Neurobiology, 2: Nonlinear and Stochastic Theories. Cambridge University Press, Cambridge.

Attachment IV

Unpublished manuscript

Plant odor background may increase coding efficiency of moth pheromone receptor neurons

Rimjhim Tomar[1, 2*], Paul Clemencon[3, 4], Christelle Monsempes[3], Elodie Demondion [3], Philippe Lucas[3**], Lubomir Kostal[1***]

1 Institute of Physiology of the Czech Academy of Sciences, Prague, Czech Republic
2 Charles University, Second Medical Faculty, Prague, Czech Republic
3 Institute of Ecology and Environmental Sciences, INRA, Versailles, France
4 Institut de Recherche sur la Biologie de l'Insecte, UMR7261, CNRS, University of Tours, Tours, France

* rimjhim.tomar@fgu.cas.cz ** philippe.lucas@inrae.fr *** kostal@biomed.cas.cz

Abstract

Insects detect odorants with olfactory receptor neurons (ORNs) located on their antennae. Male moths specifically depend on pheromone-responding neurons (Phe-ORNs) to find females for reproduction purposes, using sex pheromones emitted by their conspecific females. These sex pheromones are a small part of a complex chemical world and some of the volatile plant compounds (VPCs) found in the environment interfere with the Phe-ORNs. Male moths use VPCs to locate food sources, potential habitats of female moths, and oviposition sites. Insect olfactory tracking behavior generally results from the integration of multiple information sources, however, the effects of VPCs as they naturally appear in the environment have not been studied extensively yet. To this end, we stimulated the ORNs of male *Agrotis ipsilon* with intermittent puffs of pheromone against VPC backgrounds of different concentrations, to mimic the natural environment. We found that the response of ORNs to pheromones is affected by the presence of VPC. In particular, we found that higher VPC concentration facilitates the encoding efficiency of the pheromone signal by ORNs in terms of information per evoked spike. Using regression analysis and other statistical methods, we confirmed that the accuracy of the stimulus prediction is consistently higher with a VPC background. While it has been often reported that VPCs alter the detection of pheromones in moths, we show here that some VPCs at high concentration increase the information efficiency in Phe-ORNs.

Keypoints

1. We measured the response of olfactory receptor neurons (ORNs) of the male moth of the *Agrotis ipsilon* species to pheromone while being exposed to volatile plant compound (VPC) backgrounds. Linalool and (Z)-3-hexenyl acetate were used as VPC background.

2. Logistic regression analysis and mutual information per spike analysis show that the efficiency of encoding performance improves under certain high concentrations of VPCs.

3. High concentrations of VPC improve the information transmitted per spike about the pheromone despite suppressing the firing rate in ORNs.

1 Introduction

Moths rely on olfaction to find food sources, mates, or enemies. The male moth's olfactory system contains specific olfactory receptor neurons (ORNs) to detect the sex pheromones emitted by the female moths. The detection of these pheromones by ORNs triggers an oriented flight along the pheromone plume toward the source of the pheromone. Volatile plant compounds (VPCs) also play a huge role in this olfactory world since insects depend on plants for food (Knudsen et al., 1993, 2006). The male moth olfactory system has evolved to detect pheromones and process relevant neural information efficiently, yet VPCs have been shown to interfere with pheromone detection (Chang et al., 2016). Insect olfaction is a complex sensory process that runs from the specific detection of odorants by binding onto olfactory receptors expressed in ORNs to neural encoding, blend perception (integration in higher centers), and behavior. Herbivore species can discriminate potential host-plant species based on their volatile emissions (Conchou et al., 2017). Since they live in a complex olfactory world (Conchou et al., 2019), the moth olfactory system is well developed (Hansson and Stensmyr, 2011). Considering the hundreds of different VPCs released by plants (Knudsen et al., 1993, 2006), the ability of the insect olfactory system to extract ecologically relevant information from that very complex chemical environment is remarkable (Riffell et al., 2013, 2014). Male moths can detect the sex pheromone emitted by a female located hundreds of meters away and navigate upwind towards the odor plume (Horst et al., 2001). Male moths rely on their ORNs capability to process information rapidly about the chemical nature and proportion of the pheromone constituents, and despite having an evolved system for that, general odorants have been shown to interfere with pheromone detection in a dose-dependent manner (Conchou et al., 2021). VPCs in the background have been shown to alter the quality and intensity of the coding of the pheromone signal. Plant and insect species live in close intimacy with each other. The standing biodiversity of both taxa is to a large extent the result of their ancient co-evolution. Insects depend on plants as food sources either directly for phytophagous and pollinator species or indirectly for parasitoids and predators. This explains the importance of the VPCs for insect ecology. Almost all of the plant tissues (leaves, flowers, fruits, roots, etc.) and types of vegetation (trees, grasses, shrubs, etc.) release VPC albeit with different profiles and in different amounts.

There is no clear relationship between the chemical structure of the VPC and the effect of the VPCs on pheromone detection. In fact, the effects of a single VPC can vary, depending on the moth species. Linalool is an antagonist of pheromone reception in *Spodoptera littoralis* (Party et al., 2009), but a weak agonist in *A. ipsilon*. The dispersion of the pheromone response intensity was generally greater in the presence of a plant volatile background compared to a non-odorized air (Renou et al., 2015). Thus, plant volatiles can either synergize or antagonize the response of ORNs to pheromone (Dickens et al., 1990; Hatano et al., 2015; Light et al., 1993; Schmidt-Büsser et al., 2009; Trona et al., 2013; Yang et al., 2004).

It's been concluded that the pheromone-VPC interactions only occur at supra-natural concentrations of VPCs (Badeke et al., 2016). Our findings, however, suggest that certain high VPC concentrations might improve encoding efficiency in *A. ipsilon*, while suppressing the neuronal response to pheromones. The next step in this direction might be to use a temporally dynamic odor background as well as a mixture of plant odors to better mimic the odor landscape (Conchou et al., 2020) to better understand the adaptation of the olfactory system of moths to the detection of specific stimuli in a complex and changing chemical environment.

2 Materials and Methods

2.1 Animal care

Larvae were reared on an artificial diet. Males were separated from females at the pupal stage to prevent them from being exposed to the pheromone before the stimulation started. New adults were collected every day, kept under an inverted light-dark cycle (16 : 8 photoperiod light: dark photoperiod), and fed *ad libitum* with a sucrose solution. After 4 to 5 days, males of *Agrotis ipsilon* were tested for the experiments. All experiments were performed during the scotophase.

2.2 Chemicals

One of the main constituents of the sex pheromone blend of *Agrotis ipsilon* is the (Z)-7-dodecenyl acetate, and was bought from Pherobank (purity $> 99\%$). For the VPCs, we bought (Z)-3-hexenyl acetate (CAS 3681-71-8) and linalool (CAS 78-70-6) from Sigma-Aldrich. These VPCs with different physicochemical properties are ecologically relevant for a male moth seeking a female in a French agroecosystem. All delivered VPC concentrations were defined relatively to an arbitrary unit (AU) where one AU is the molar concentration delivered on the antenna from a source containing 1% (Z)-3-HAC in mineral oil (CAS 8012-95-1). Mineral oil was used as a control background odor.

2.3 Odor stimulus delivery

The device is similar to the one used by (Clémençon, Tomar et al., in prep.). Briefly, a system of PFTE tubing (internal diameter 1.32 mm) and 3-way electro valves (Lee Company LHDA1233215H) allowed a low dead-volume 4-way-manifold (MPP-8, Warner Instruments, Holliston, MA, USA) whose distal end was located close to the antenna to deliver a computer-controlled specific pattern of VPC and pheromone with a 50 ms precision. Pheromone delivery consisted in a 3cm long capillary containing a piece of filter paper with 0.1ng of Z7-12Ac diluted in 1uL of hexane connected to the tubing system. This dose has been already described as an electrophysiologically active concentration. VPC delivery consisted in 4mL glass vials containing a background odor. Vials were connected to the tubing with hypodermic needles inserted into the Teflon septum vial lids in order to avoid the adsorption of odors. The vials were kept at 23°C using a Thermo Mixer (ThermoMixer TM C Eppendorf, fisher scientific) to avoid temporal variations in headspace concentrations. Airflow compensation systems ensured that the flow delivered to the antenna was constant and that the delivered pheromone concentration was not affected by the opening of the microvalves delivering the odor. A permanent humidified airflow was continuously delivered to prevent the antenna from drying. Contaminated air was removed thanks to an exhaust fan. We have wrapped the manifold with an aluminum shield connected to the ground to minimize electrical artifacts during the opening and closing of the valves.

2.4 Calibration and maintenance

Pheromone and odor sources were changed between each recording. We ensured every day that the airflow at the distal end of the manifold in different valve configurations was equal to 200mL/min (+- 10mL/min) with an electronic flowmeter. We decontaminate the tubing and the valves connected to the manifold at 80°C during 4 hours.

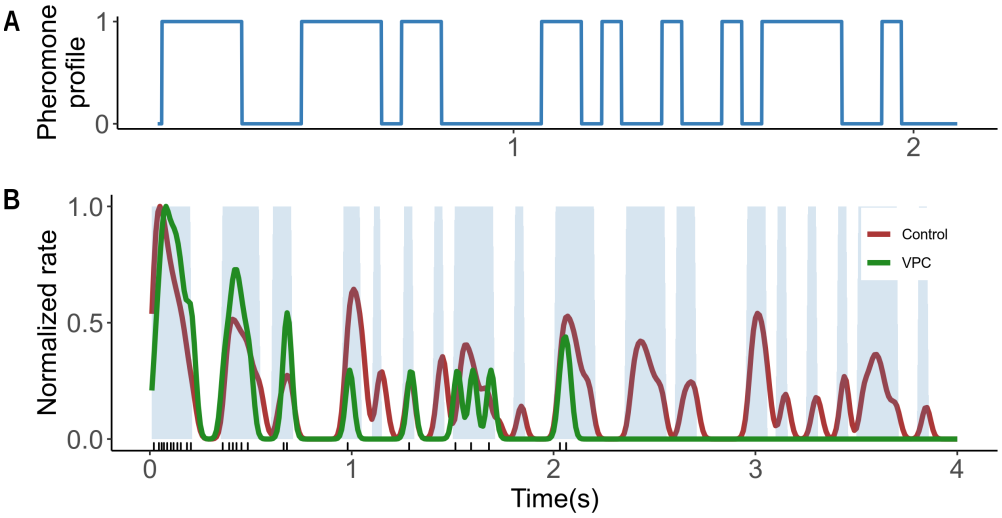

Fig 1. *Pheromone plume profile and the muting effect of a high VPC concentration* **A** The profile of the pheromone plume delivered to the olfactory receptor neurons. The $2s$ plume was delivered repeatedly during the $40s$ stimulation. **B** During high concentrations of the VPC background (e.g., in 10^{-2} of (Z)-3-hexenyl acetate) some neurons stopped responding to the odor stimuli. The spikes elicited during the VPC background are shown on the x-axis.

2.5 Single Sensillum Recordings

For electrophysiological recordings, we used tungsten electrodes shaped electrolytically (TW5-6, Science Products, Hofheim, Germany). Male moths were quickly anesthetized with CO_2 and restrained in a Styrofoam folder with their head protruding. Once one antenna was immobilized with adhesive tape, a reference electrode was inserted in the main branch of the antenna and the recording electrode was inserted at the base of a trichoid sensillum. The antennae of *Agrotis ipsilon* present a strong odotopy, the ORNs located on the branches are mostly Phe-ORNs. The signal was amplified (x1000), band-pass filtered and sampled at 10kHz with a Digidata 1440A acquisition board (Molecular Devices). The recordings were acquired thanks to the pCLAMP10 software (Molecular Devices, San Jose, CA, USA). We have recorded one sensillum per insect.

2.6 Stimulation sequences

We recorded each Phe-ORN during a 8 minute recording sequence consisting of the presentation of two distinct 40-second stimulations separated by a 2 minute gap. Each stimulation lasted 40 seconds. For the pheromone, it consisted of the repetition (20 times) of the same 2-seconds-trial, a sequence of short pheromone puffs/blanks of random durations generated randomly (white noise pattern: durations of puffs and blanks have an exponential distribution). In the meanwhile, the background was either (1) absent (control stimuli), or (2) delivered continuously. The background onset started 2 ms before the pheromone stimulation to assess the response of Phe-ORNs to individual VPCs. The order of presentation of the 2 distinct stimulations: Pheromone + No Background, Pheromone+ Continuous Background was randomized. In addition, we also designed a protocol to assess spike-frequency adaptation (called the “adaptation protocol”). It consisted of the same random presentation of the 40-s of the background, either constant or absent, but we have only kept the first and the last (20th) 2-seconds-pheromone-trial.

2.7 Statistical Analyses

The analysis includes 186 ORNs recorded over two distinct 40-second stimulations per ORN, one with pheromone and no background and another with pheromone and the background of (Z)-3-hexenyl acetate or linalool. The minimum and maximum number of neurons per VPC concentration were 11 and 21 respectively. During the high concentration of the VPC background, some neurons stopped responding altogether (Fig. 1B), and those have been excluded from the analysis.

Neural response The firing rate of ORN was estimated with kernel density estimation using a Gaussian kernel (Shimazaki and Shinomoto, 2010; Tomar, 2019)

$$\lambda_t = \sum_{i=1}^{N} K_w(t - t_i) \tag{1}$$

where t_i is the spike time and $K_w(s)$ is the normal distribution bandwidth $w = 20ms$, defined as

$$K_w(s) = \frac{1}{\sqrt{2\pi}w} \exp -\left(\frac{s^2}{2w^2}\right). \tag{2}$$

The firing rate shown in figure 2 was sampled at every $10ms$.

For individual concentrations of VPC, the average firing rate of neurons was calculated for the duration of the trial (figure 2A and 2F). To look at the neural response adaptions (figures 2C and 2H), we averaged the population firing rate for each trial.

For the relative change in the firing rate (figures 2D and 2E), we took the mean firing rate during 20 trials of each neuron (with and without VPC background) and calculated the population mean firing rate. The relative change in the mean firing rate is

$(\lambda_{vpc} - \lambda_{air})/\lambda_{air}$

where λ_{vpc} is the mean firing rate of the neuron population with a VPC background and λ_{air} is without the VPC background (the box-plots of the mean relative change are shown in the figures). Inactive neurons were excluded from the analysis.

Response model fitting and AUC-ROC performance evaluation In order to understand to which extent the presence of a VPC background modulates or influences the ORNs' encoding of pheromones we have trained two separate models: one capturing the neural response to the pheromone alone, and another reflecting the combined impact of the pheromone and a VPC background. Through model fitting, we aim to understand which of these models best describes the experimental binary data (the absence/presence of pheromone).

The first model was constructed to capture the neuronal response when exposed solely to the pheromone. As independent variables, we used the firing rate estimated by a Gaussian kernel specified in the previous section and a weighted history function which accounts for the firing rate in the past 200ms. Specifically, the weighting function considers an exponentially decreasing influence of past firing rates up to four-time points (or bins) in the past. For a given firing rate of a neuron in the time bin j, we modeled the probability of the stimulus being present as:

$$\text{prob}_j = \frac{e^{\beta_0 + \beta_1 * \lambda_j + \beta_2 * w_j}}{1 + e^{\beta_0 + \beta_1 * \lambda_j + \beta_2 * w_j}} \tag{3}$$

where λ_j is the firing rate in the respective time bin, w_j is the calculated weighted history for that time bin, β_0, β_1 and β_2 are the regression beta coefficients which are estimated on the available training data with maximum likelihood estimation. Using the

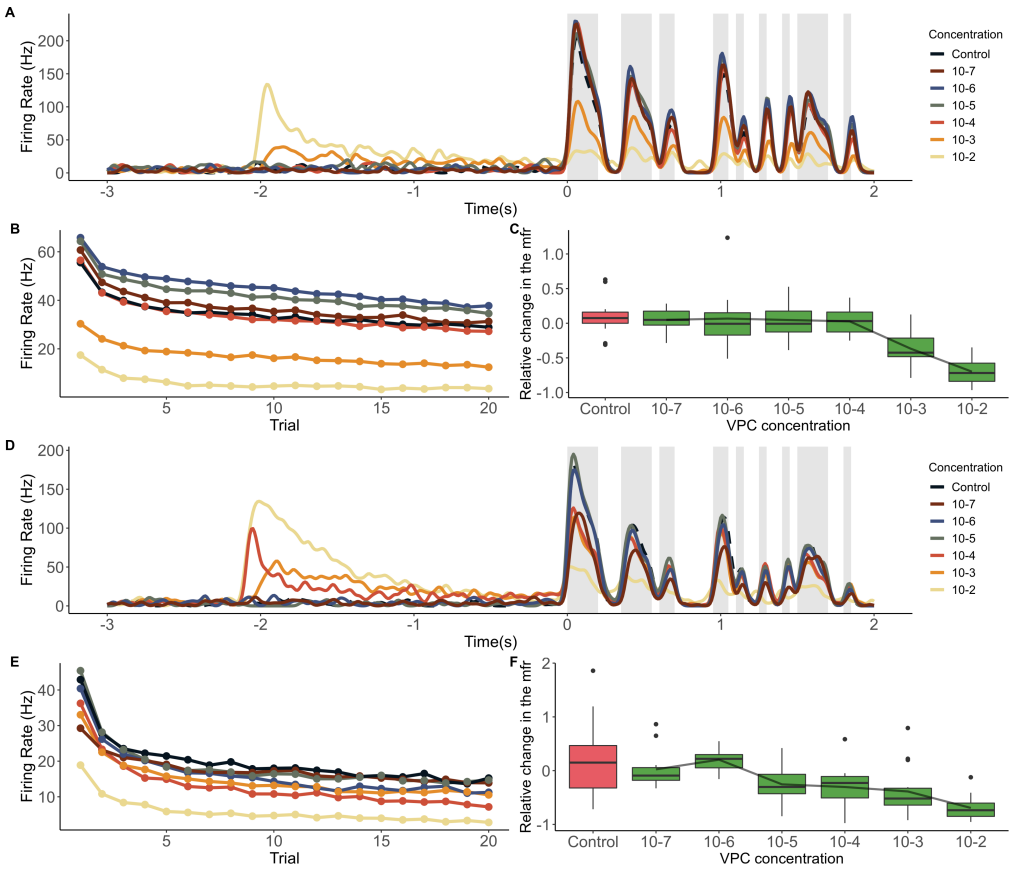

Fig 2. *High concentrations of VPCs activate the neural response in ORNs and suppress the subsequent neural response to pheromones.* **A** Average firing rate of Phe-ORNs when exposed to VPCs introduced at -2s and pheromone introduced at 0s (indicated by the grey shaded area). The control is represented by a dashed line. We tested different concentrations of (Z)-3-hexenyl acetate. **B** Here, the 40s pheromone stimulation period is composed of the repetition of 20 trials, each lasting 2s. This segmentation helps us examine the adaptation of the ORNs' response over time. As the trials progress, the average firing rate of the neuron population decreases, indicating a diminished response. **C** This panel shows the relative change in the mean firing rate of ORNs when VPCs are present, presented as box plots. For these measurements, we use (Z)-3-hexenyl acetate as the VPC background. The relative change is calculated using the formula: $(\lambda_{vpc}$ - $\lambda_{air})/\ \lambda_{air}$ where λ_{vpc} is the mean firing rate during VPC background and λ_{air} is the mean firing rate without the VPC background. **D, E, & F** Linalool was used as the VPC background and analyses were the same as in the panels **A**, **B**, and **C**.

independent variables, we predicted the presence or absence of the pheromone. This model serves as a baseline, providing insights into the natural encoding of the pheromone without any external influences.

The second model aimed to take into account the potential modulatory effects of a VPC background. Again, using the firing rate and weighted history as independent variables, this model predicts the absence or presence of pheromone, but now in the context of a VPC background. This model helps us grasp the potential interactions between the pheromone and VPCs in shaping neuronal responses.

After fitting both models to the observed data, we used the Area Under the Receiver Operating Characteristic Curve (AUC) as a performance metric to assess the models' performances (Bradley, 1997). The AUC provides a robust measure of a model's ability to discriminate between classes—in this case, the presence or absence of the pheromone. An AUC score close to 1.0 indicates a near-perfect ability to differentiate, while a score near 0.5 suggests no better performance than random guessing.

By comparing the AUC scores of both models, we could ascertain which model represents the observed neuronal responses with the best accuracy. An appreciable difference in the AUC values between the two models would underscore the significance of VPCs in influencing the encoding process. Conversely, comparable AUC values would hint at the resilience of the encoding process against the background of VPCs.

If the AUC value in the trial k for a neuron n is denoted as $a_{k,n}$, then the mean AUC value for the kth trial is obtained by averaging $a_{k,n}$ across all the neurons in the group (categorized according to the VPC type and its concentration),

$$a_k = \frac{1}{m}\sum_{i=1}^{m} a_{k,i}. \tag{4}$$

The results of our model fitting and the corresponding AUC evaluations for both (Z)-3-hexenyl acetate and linalool are depicted in figures 3 and 4, respectively.

Logistic regression analysis on ORN response To quantify to which extent the background of VPCs impacted the neuronal ability to encode the pheromone efficiently, we used logistical regression to predict the absence or presence of pheromone. Using the same predictor variables as in the previous section, the logistic model for each background was trained on the first three trials and then used to predict the stimulus in the remaining 16 trials. To train the predictive model for each background, we divided the 2 second trials into 200 bins of 10ms and calculated the firing rate λ_{air} or λ_{vpc} according to the background condition. To quantify the performance of the predictors, we compared the model's predicted stimulus condition (absent/present) to the neuron's measured stimulus condition. The proportion of predictions that are correctly classified is called the "prediction accuracy" (Sohil et al., 2022). If the model prediction accuracy in the trial k for a neuron n is denoted as $p_{k,n}$ then the average prediction accuracy for the kth trial is obtained by averaging $p_{k,n}$ across all the neurons in the group (defined by the VPC type and its concentration),

$$p_k = \frac{1}{m}\sum_{i=1}^{m} p_{k,i} \tag{5}$$

and if the number of spikes fired by the neuron n in the trial k is $a_{k,n}$, then the average prediction accuracy per spike r is calculated as,

$$p_k^* = \frac{1}{m}\sum_{i=1}^{m} \frac{p_{k,i}}{a_{k,i}} \tag{6}$$

The ratio of average prediction accuracies for ORNs exposed to pheromone with VPC background vs. pheromone alone is plotted on the $\log_{10}$ scale in figure 5.

Mutual information between the stimulus and the response Information theory has been historically used to quantify the information transfer among neurons and answer questions like how much information can a spike train of a neuron provide about the external stimulus (Dimitrov et al., 2011; Fuller and Williams, 1983; Jacobson, 1950; Kostal et al., 2013; Quian Quiroga and Panzeri, 2009; Timme et al., 2014; Wibral et al., 2015). The fundamental information-theoretic quantity is called *entropy* (Shannon, 1948), which measures the uncertainty of a discrete random variable X as

$$H(X) = \sum_x P(x) \log_2 P(x) \tag{7}$$

where X is distributed according to $P(X)$. The corresponding unit for entropy is *bits* when logarithm is taken on base 2 and *nats* when natural logarithm is used.

In the case of two discrete random variables X and Y, conditional entropy is defined as the entropy of a random variable conditional on the knowledge of another random variable (Cover and Thomas, 2006),

$$H(X|Y) = \sum_y P(y) H(X|Y = y) \tag{8}$$

where $H(X|Y = y)$ can be obtained from equation 7 with replacing $P(x)$ with $P(x|y)$.

Let's consider two variables, S representing a set of stimuli and R representing a set of responses. The *mutual information* $I(R, S)$ is the reduction in uncertainty about a random variable (in this case, about the stimulus) due to another random variable being known (in this case, due to the response being known). It can be defined in terms of entropies as (Cover and Thomas, 2006)

$$I(R, S) = H(S) - H(S|R) \tag{9}$$

Mutual information can be interpreted as an average reduction in uncertainty about the absence/presence of stimulus, based on the response.

For the given analysis, we pooled the spiking data of the neuron population during the delivery of a given VPC concentration (and its control category). We divided the 2s trials into 50ms bins. Using this binned data, we computed the mutual information between the stimulus and the response for a particular trial k of a given concentration d, denoted as $I_{k,d}(R_{k,d}, S_{k,d})$. This computation was performed using the *entropy* package in the statistical software **R**. Additionally, the mutual information per spike was obtained by dividing the $I_{k,d}(R_{k,d}, S_{k,d})$ with the number of spikes $a_{k,d}$ in that trial. Given the VPC type and concentration, the average mutual information per spike during a trial k is calculated as

$$I_k(R_k, S_k) = \frac{I_{k,d}(R_{k,d}, S_{k,d})}{a_{k,d}}. \tag{10}$$

To demonstrate the change in the mutual information per spike as the background changes to VPC, we plotted the ratio of the mutual information per spike on the $\log_{10}$ scale as the neurons were exposed to pheromone with VPC background vs. pheromone alone for figure 6.

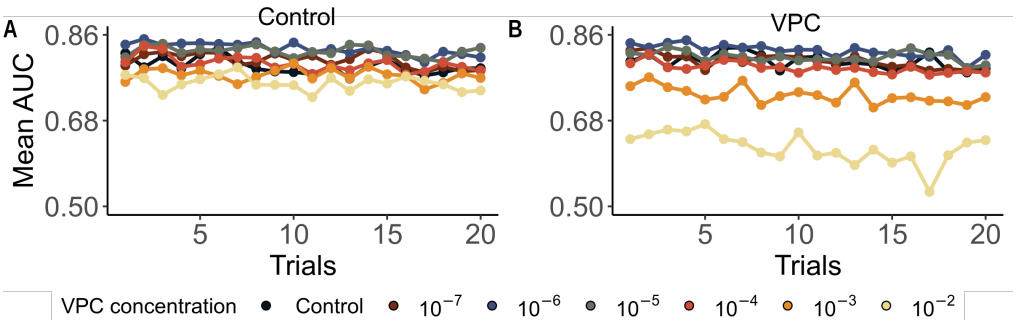

Fig 3. *Mean AUC values for the logistic models fit for (Z)-3-hexenyl acetate background* **A** Represents the mean AUC values across 20 trials for the model trained on neuronal responses to pheromone alone. The values consistently fluctuate between 0.80 and 0.85, indicating a stable performance of the model across the trials. **B** Mean AUC values for the model trained on neuronal responses to pheromone in the presence of a (Z)-3-hexenyl acetate background. While the AUC values largely remain comparable to those in **A**, falling within the 0.8 to 0.85 range for most trials, there's a discernible dip in the performance at the concentration 10^{-2}, where the AUC values consistently range from 0.55 to 0.65. This suggests an improvement in the ORNs' encoding capability at this specific concentration of (Z)-3-hexenyl acetate.

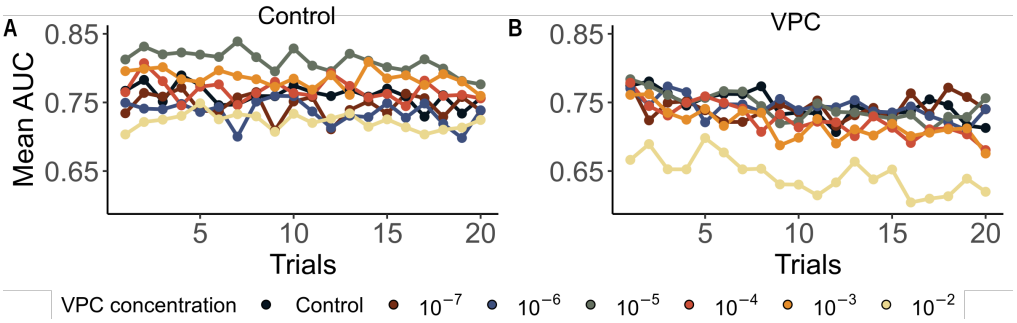

Fig 4. *Mean AUC values for the logistic models for linalool background* **A** Represents the mean AUC values across 20 trials for the model trained on neuronal responses to pheromone alone. The values reflect a consistent performance of the model and vary between 0.70 and 0.85. **B** Mean AUC values for the model trained on neuronal responses to pheromone in the presence of a linalool background.

3 Results

3.1 High VPC concentrations activate the neuronal firing and suppress the response to the pheromone

(Z)-3-hexenyl acetate activated the neuronal firing at the threshold of 10^{-3} (Fig. 2A) whereas linalool activated it at 10^{-4} (Fig. 2F). Both of the VPC backgrounds evoked the strongest response at 10^{-2}. As the pheromone plume was released, the neuronal response was observed to be suppressed by these high concentrations. Pooling the response of neurons for the 20 trials of $2s$ shows that for the concentrations above the threshold, the firing rate does not recover to the control level (Fig. 2B, Fig. 2E).

To highlight the "adaptation effect", we averaged the neuronal response per trial, for each background concentration. The response to pheromone is comparably high in the first trial, then the firing activity decreases slowly (Fig. 2A and 2C). The effect of the high VPC concentrations is visible in (Z)-3-hexenyl acetate background (Fig. 2C) as

well as linalool background (Fig. 2F). The relative change in the mean firing rate is shown in figure 2D and E, and as the VPC concentration increases we see a downward trend in the change, demonstrating that on average the high concentrations of the VPCs suppress the neuronal response.

3.2 Logistic regression model performance declines during high concentration of odor background

In this section, we introduce logistic regression models to decipher the presence or absence of pheromone stimuli from the firing rate. In terms of the mean AUC values, which measure the model's discriminatory power between the presence and absence of the pheromone, both models demonstrate consistent performances across trials. However, notable variations emerge with the introduction of VPC backgrounds.

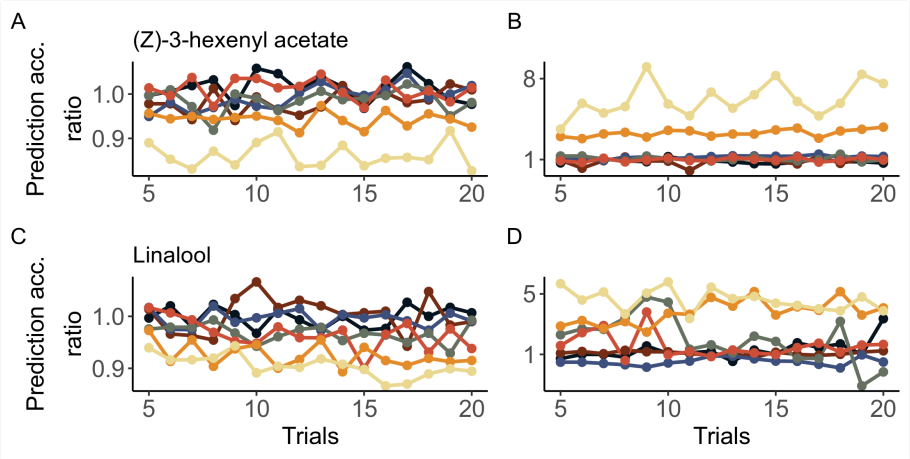

Fig 5. *High VPC background concentrations improve per spike pheromone encoding efficiency in ORNs.* The y-axis is represented on a base 10 logarithmic scale. **A** Ratio of the prediction accuracies of the models when exposed to a (Z)-3-hexenyl acetate background relative to the accuracy without a VPC background. Regardless of the concentration variations of the VPC, the ratio remains approximately equal to 1 throughout all trials, indicating that the presence of (Z)-3-hexenyl acetate does not significantly alter the model's performance. **B** Contrary to panel A, this panel shows that the prediction accuracy per spike ratio consistently exceeds the baseline for VPC concentrations of 10^{-3} and 10^{-2}. **C** Similarly to panel A, when the model is subjected to a linalool background, the prediction accuracy ratio is close to 1 across various trials, implying a minimal effect of linalool on the model's predictive capabilities. **D** Similar to B, the model displays an augmented prediction accuracy per spike, especially for high concentrations around 10^{-3} and 10^{-2}.

For (Z)-3-hexenyl acetate, as shown in Figure 3, the performance remains largely uniform across most trials for both the pheromone-only and the VPC background models. However, a pronounced dip in AUC values is observable specifically at the 10^{-2} concentration for the latter model. This decrease in AUC values at this specific concentration suggests an alteration in the neuronal encoding process. In contrast, for

linalool, as visualized in Figure 4, while the performance for the pheromone-only model remains stable across trials, the model trained with the linalool background starts showing variations at specific concentrations. For the low VPC concentrations, the AUC values remain in a range similar to subfigure A, around 0.75. However, as the concentration of linalool in mineral oil increases, at the concentration 10^{-2}, there's a pronounced dip in performance, with AUC values ranging between 0.6 and 0.65, suggesting a significant modulation in the ORNs' encoding capability at this specific concentration of linalool. The model's discriminative capability slightly decreases as the linalool concentration increases, especially around concentrations of 10^{-2}.

In essence, the AUC values derived from our logistic regression models not only validate the encoding capability of ORNs towards pheromone stimuli but also emphasize the modulatory influence of VPCs at particular concentrations. These findings, along with the previously observed suppression in firing rates (refer to Figure 2), highlight the nuanced interactions between pheromone stimuli and VPC backgrounds.

3.3 Stimulus prediction per spike increases with high concentration of odor background

In this section, we introduce the logistic prediction models designed for discerning the presence or absence of pheromone stimuli based on firing rate measurements. The ratios of prediction accuracies under different background conditions of VPCs compared to control are depicted on a logarithmic scale in figure 5 for the VPCs (Z)-3-hexenyl acetate and linalool, respectively. Model performances are comparable for both control and VPC backgrounds. Upon calculating the prediction accuracy per spike, obtained by dividing the prediction accuracy for a given trial by the count of spikes occurring within that trial, we observe a trend in the coding efficiency. Notably, under high VPC concentrations, the ratio is consistently higher. For (Z)-3-hexenyl acetate this change is visible in the VPC concentration 10^{-3} and strongly present for 10^{-2}.

Parallel findings are observed for linalool, with the ratio of prediction accuracy per spike consistently and substantially higher at both 10^{-3} and 10^{-2} concentrations. It is worth highlighting that the concentrations of VPCs with heightened ratios of prediction accuracies per spike align with those concentrations demonstrated to suppress firing rates, as illustrated in Figure 2.

3.4 Mutual information per spike is higher for the high concentrations of the VPC

The ratio of the average mutual information per spike in different background conditions (VPC vs. control) confirms that for the higher concentrations of the VPC, the mutual information per spike between the stimulus and the response increases. The impact of the background VPC concentrations can be seen in Fig. 6, where each tile represents the difference between the logarithm of mutual information per spike under the VPC background and the logarithm of the mutual information per spike without VPC background. For both (Z)-3-hexenyl acetate and linalool, it is the highest for 1%. For linalool, the contrast is stronger at 0.1% than (Z)-3-hexenyl acetate. This corresponds with the behavior observed in Fig. 2 and 5.

3.5 The VPCs facilitate the ORN coding efficiency independently of spike-frequency adaptation

Our results suggest that ORNs have an increased efficiency in terms of information encoded per spike in the presence of high VPC concentrations even though their firing

rate decreases. In this section, we also consider the potential impact of neural adaptation of consecutive trials. We compare neurons exposed to varying concentrations of VPC with near identical average firing rates during the 40s stimulation period. This approach allows us to isolate the impact of VPC from the effect of neural adaptation over time.

Fig. 7A shows the comparative analysis of ORNs' response to varying VPC levels, highlighting a reduction in overall firing rate as the VPC concentration level increases. The increased efficiency gain during the background of high concentrations of VPC is not a result of neural adaptation to repeated stimuli, but the levels of VPC concentrations also play a role. We compare the prediction accuracy per spike of neurons that maintain the same average firing rate during the stimulus period. The analysis shown in Fig. 7B reveals that among the neurons with the same average firing rate, the majority (about 70%) exhibited higher prediction accuracy per spike at the high VPC concentration backgrounds of 10^{-2} and 10^{-3}. This highlights that the high VPC concentrations enhance neural processing capabilities and that the benefits derived from VPCs are not just a consequence of neural adaptation to repeated stimuli but rather an independent factor contributing to the increased efficiency in ORNs.

4 Discussion

4.1 High concentrations of plant volatiles alter the firing response of Phe-ORNs

In this study, we investigated the impact of volatile plant compounds (VPCs) on the encoding of pheromone signals by the olfactory receptor neurons (Phe-ORNs) of male *Agrotis ipsilon*.

Our experimental approach consisted of stimulating ORNs with a dynamic pheromone pattern that emulated natural plume conditions while varying the concentrations of VPC backgrounds. Various studies have concluded that the presence of a VPC background can modify the response of Phe-ORNs to pheromones. For instance, Deisig et al. (2012) examined how different concentrations of heptanal and its combination with a sex pheromone affect the mean spike frequency of Phe-ORNs. Rouyar et al. (2011) compared the informational content of the firing activity in Phe-ORNs when exposed to pheromone pulses with or without a VPC background. Further studies by Renou et al. (2015) and Dupuy et al. (2017) investigated the maximum firing rates of Phe-ORNs under various background conditions, Conchou et al. (2021) used the pheromone salience in addition to the firing frequency comparisons. The metric used in our study for performance assessment covers all these aspects. Our results show that the impact of the VPC background on the response of Phe-ORNs is dose-dependent with the most significant decrease in neural response to pheromones observed at the highest VPC concentration.

4.2 Information per spike increases with increasing VPC concentration

While most ORNs exhibited similar responses when solely exposed to pheromones (control group), a notable shift in coding efficiency was observed under elevated concentrations of VPCs. ORNs exhibited improved coding efficiency when exposed to high VPC concentrations. Specifically, ORNs demonstrated enhanced coding efficiency in the presence of high VPC concentrations, a phenomenon that was apparent with both (Z)-3-hexenyl acetate and linalool, albeit at different concentration thresholds.

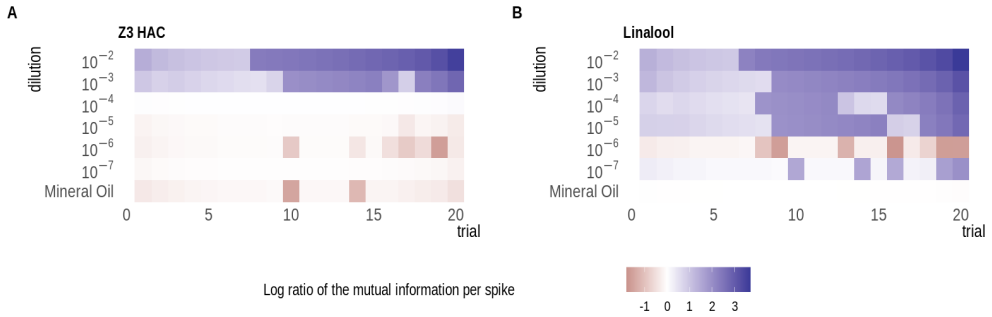

Fig 6. The ratio of the average mutual information per spike in different background conditions from no to high VPC background concentration, plotted on a $\log_{10}$ scale.

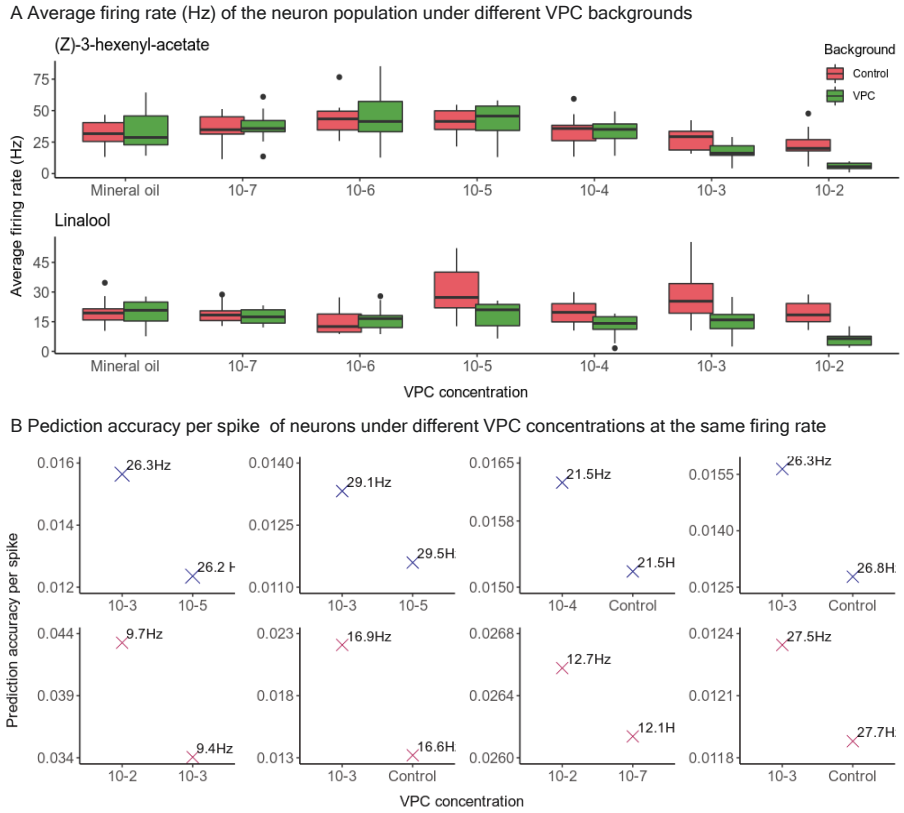

Fig 7. A Differential impact of VPC on the average firing rate (Hz) of neuron populations when exposed to (Z)-3-hexenyl acetate and linalool over varying concentrations. The boxplots represent the distribution of neurons' responses, with individual data points indicating unique neuron activity. The firing rate demonstrates a compound- and concentration-dependent response, with notable variation between the control and VPC-exposed groups. **B** Comparative analysis of VPC effects on neuron firing rates across varied concentrations. Neurons with identical baseline firing rates are shown side by side to underscore the differential impact of VPC. The first row (blue) represents neurons under (Z)-3-hexenyl acetate, while the second row (red) corresponds to those under linalool. This selection of neurons, despite having equal firing rates at different VPC concentrations, reveals a notable enhancement in prediction accuracy per spike at higher VPC concentrations.

Despite the reduction in firing response triggered by VPC backgrounds, an increase in the amount of information conveyed per spike was recorded.

The dynamics of sensory noise-altering information processing across different modalities further contextualizes our findings. For instance, intrinsic noise can alter the way speech sounds are processed by the auditory system (Schilling et al., 2022). In the locusts' brain neuron DNI, the added noise increased both the firing rate and the information content carried by the spike train, however, the information content carried per spike was reduced by half (Simmons and van Steveninck, 2010). Even though the information content per spike was reduced, the neurons were able to fire spikes with precise timing in response to the changes in the light intensity, suggesting that the neurons can reliably respond to important sensory cues even in the cases of increased spiking activity due to noise. This study highlights the importance of precise spike timing for efficient information transfer in sparse spiking regimes. Another example of this is observed in the olfactory system of locusts where precise spike timing is found to carry information about odor identity Gupta and Stopfer (2014).

These observations are in agreement with the efficient neural coding principle which suggests that the sensory neural system has evolved to encode stimuli in the most energy-efficient way possible, encoding the most amount of information at the lowest cost (Attneave, 1954; Yu and Yu, 2017). Several studies estimate that the brain spends a significant amount of energy on spike generation and spiking activity (Attwell and Laughlin, 2001; Lennie, 2003). Since each spike is expensive, encoding more information in fewer spikes can be an optimization strategy (Sengupta et al., 2013). Examples of this can be seen in the visual cortex (Olshausen and Field, 1996; Vinje and Gallant, 2000; Yu and Ferster, 2013), auditory cortex (Willmore and Tolhurst, 2001; Zhang et al., 2019), and the olfactory system (Stopfer, 2007; Theunissen, 2003).

4.3 Ecological implications

It has been suggested that the pheromone-VPC interactions only occur at supra-natural concentrations of VPCs (Badeke et al., 2016). However, the release of VPCs into the atmosphere is susceptible to modification due to climate change and other environmental factors that affect plant metabolism (Holopainen et al., 2018). For instance, Chan et al. (2024) discusses how anthropogenic pollutants degrade floral scents and reduce flower visitation by moths, and Nataraj et al. (2022) investigates how the plant species *Artemisia brevifolia* produces increasing amounts of VPC with increasing elevation, potentially as a response to increased stress or as part of its adaptive optimization strategies to harsh environmental conditions

In our study, the observed dual effect of certain high VPC concentrations—simultaneously enhancing pheromone encoding efficiency while suppressing pheromone responses—suggests a nuanced strategy employed by ORNs to optimize information transmission under challenging sensory conditions. This adaptability implies the existence of coding mechanisms that adjust in the presence of heightened VPC levels. The next step in this direction might be to use a temporally dynamic odor background as well as a mixture of plant odors to further investigate how the "odorant" background influences the encoding of the signal cues.

ACKNOWLEDGMENTS

This work was supported by the Czech Science Foundation project 20-10251S and Charles University project GA UK 373121.

References

F. Attneave. Some informational aspects of visual perception. *Psychol. Rev.*, 61(3): 183–193, May 1954. ISSN 0033-295X. doi: 10.1037/h0054663.

D. Attwell and S. B. Laughlin. An energy budget for signaling in the grey matter of the brain. *J. Cereb. Blood Flow Metab.*, 21(10):1133–1145, Oct. 2001. ISSN 0271-678X. doi: 10.1097/00004647-200110000-00001.

E. Badeke, A. Haverkamp, B. S. Hansson, and S. Sachse. A challenge for a male noctuid moth? discerning the female sex pheromone against the background of plant volatiles. *Front. Physiol.*, 7:143, Apr. 2016. ISSN 1664-042X. doi: 10.3389/fphys.2016.00143.

A. P. Bradley. The use of the area under the ROC curve in the evaluation of machine learning algorithms. *Pattern Recognit.*, 30(7):1145–1159, July 1997. ISSN 0031-3203. doi: 10.1016/S0031-3203(96)00142-2.

J. K. Chan, S. Parasurama, R. Atlas, R. Xu, U. A. Jongebloed, B. Alexander, J. M. Langenhan, J. A. Thornton, and J. A. Riffell. Olfaction in the anthropocene: NO3 negatively affects floral scent and nocturnal pollination. *Science*, 383(6683):607–611, Feb. 2024. ISSN 0036-8075, 1095-9203. doi: 10.1126/science.adi0858.

H. Chang, M. Guo, B. Wang, Y. Liu, S. Dong, and G. Wang. Sensillar expression and responses of olfactory receptors reveal different peripheral coding in two helicoverpa species using the same pheromone components. *Sci. Rep.*, 6:18742, Jan. 2016. ISSN 2045-2322. doi: 10.1038/srep18742.

L. Conchou, P. Anderson, and G. Birgersson. Host plant species differentiation in a polyphagous moth: Olfaction is enough. *J. Chem. Ecol.*, 43(8):794–805, Aug. 2017. ISSN 0098-0331, 1573-1561. doi: 10.1007/s10886-017-0876-2.

L. Conchou, P. Lucas, C. Meslin, M. Proffit, M. Staudt, and M. Renou. Insect odorscapes: From plant volatiles to natural olfactory scenes. *Front. Physiol.*, 10:972, Aug. 2019. ISSN 1664-042X. doi: 10.3389/fphys.2019.00972.

L. Conchou, P. Lucas, N. Deisig, E. Demondion, and M. Renou. Effects of an odor background on moth pheromone communication: constituent identity matters more than blend complexity. Sept. 2020.

L. Conchou, P. Lucas, N. Deisig, E. Demondion, and M. Renou. Effects of Multi-Component backgrounds of volatile plant compounds on moth pheromone perception. *Insects*, 12(5):409, May 2021. ISSN 2075-4450. doi: 10.3390/insects12050409.

T. M. Cover and J. A. Thomas. *Elements of Information Theory*. John Wiley & Sons, July 2006. ISBN 9780471241959.

N. Deisig, J. Kropf, S. Vitecek, D. Pevergne, A. Rouyar, J.-C. Sandoz, P. Lucas, C. Gadenne, S. Anton, and R. Barrozo. Differential interactions of sex pheromone and plant odour in the olfactory pathway of a male moth. *PLoS One*, 7(3):e33159, Mar. 2012. ISSN 1932-6203. doi: 10.1371/journal.pone.0033159.

J. C. Dickens, E. B. Jang, D. M. Light, and A. R. Alford. Enhancement of insect pheromone responses by green leaf volatiles. *Sci. Nat.*, 77(1):29–31, Jan. 1990. ISSN 0028-1042, 1432-1904. doi: 10.1007/bf01131792.

A. G. Dimitrov, A. A. Lazar, and J. D. Victor. Information theory in neuroscience. *J. Comput. Neurosci.*, 30(1):1–5, Feb. 2011. ISSN 0929-5313, 1573-6873. doi: 10.1007/s10827-011-0314-3.

F. Dupuy, A. Rouyar, N. Deisig, T. Bourgeois, D. Limousin, M.-A. Wycke, S. Anton, and M. Renou. A background of a volatile plant compound alters neural and behavioral responses to the sex pheromone blend in a moth. *Front. Physiol.*, 8:79, Feb. 2017. ISSN 1664-042X. doi: 10.3389/fphys.2017.00079.

M. S. Fuller and W. J. Williams. A continuous information theoretic approach to the analysis of cutaneous receptor neurons. *Biol. Cybern.*, 47(1):13–16, 1983. ISSN 0340-1200. doi: 10.1007/BF00340064.

N. Gupta and M. Stopfer. A temporal channel for information in sparse sensory coding. *Curr. Biol.*, 24(19):2247–2256, Oct. 2014. ISSN 0960-9822, 1879-0445. doi: 10.1016/j.cub.2014.08.021.

B. S. Hansson and M. C. Stensmyr. Evolution of insect olfaction. *Neuron*, 72(5): 698–711, Dec. 2011. ISSN 0896-6273, 1097-4199. doi: 10.1016/j.neuron.2011.11.003.

E. Hatano, A. M. Saveer, F. Borrero-Echeverry, M. Strauch, A. Zakir, M. Bengtsson, R. Ignell, P. Anderson, P. G. Becher, P. Witzgall, and T. Dekker. A herbivore-induced plant volatile interferes with host plant and mate location in moths through suppression of olfactory signalling pathways. *BMC Biol.*, 13:75, Sept. 2015. ISSN 1741-7007. doi: 10.1186/s12915-015-0188-3.

J. K. Holopainen, V. Virjamo, R. P. Ghimire, J. D. Blande, R. Julkunen-Tiitto, and M. Kivimäenpää. Climate change effects on secondary compounds of forest trees in the northern hemisphere. *Front. Plant Sci.*, 9:1445, Oct. 2018. ISSN 1664-462X. doi: 10.3389/fpls.2018.01445.

R. Horst, F. Damberger, P. Luginbühl, P. Güntert, G. Peng, L. Nikonova, W. S. Leal, and K. Wüthrich. NMR structure reveals intramolecular regulation mechanism for pheromone binding and release. *Proc. Natl. Acad. Sci. U. S. A.*, 98(25):14374–14379, Dec. 2001. ISSN 0027-8424. doi: 10.1073/pnas.251532998.

H. Jacobson. The informational capacity of the human ear. *Science*, 112(2901):143–144, Aug. 1950. ISSN 0036-8075. doi: 10.1126/science.112.2901.143.

J. T. Knudsen, L. Tollsten, and L. G. Bergström. Floral scents—a checklist of volatile compounds isolated by head-space techniques. *Phytochemistry*, 33(2):253–280, May 1993. ISSN 0031-9422. doi: 10.1016/0031-9422(93)85502-I.

J. T. Knudsen, R. Eriksson, J. Gershenzon, and B. Ståhl. Diversity and distribution of floral scent. *Bot. Rev.*, 72(1):1, Jan. 2006. ISSN 0006-8101, 1874-9372. doi: 10.1663/0006-8101(2006)72[1:DADOFS]2.0.CO;2.

L. Kostal, P. Lansky, and M. D. McDonnell. Metabolic cost of neuronal information in an empirical stimulus-response model. *Biol. Cybern.*, 107(3):355–365, June 2013. ISSN 0340-1200, 1432-0770. doi: 10.1007/s00422-013-0554-6.

P. Lennie. The cost of cortical computation. *Curr. Biol.*, 13(6):493–497, Mar. 2003. ISSN 0960-9822. doi: 10.1016/s0960-9822(03)00135-0.

D. M. Light, R. A. Flath, R. G. Buttery, F. G. Zalom, R. E. Rice, J. C. Dickens, and E. B. Jang. Host-plant green-leaf volatiles synergize the synthetic sex pheromones of the corn earworm and codling moth (lepidoptera). *Chemoecology*, 4(3):145–152, Sept. 1993. ISSN 0937-7409, 1423-0445. doi: 10.1007/BF01256549.

N. Nataraj, M. Hussain, M. Ibrahim, A. E. Hausmann, S. Rao, S. Kaur, J. Khazir, B. A. Mir, and S. B. Olsson. Effect of altitude on volatile organic and phenolic compounds of artemisia brevifolia wall ex dc. from the western himalayas. *Frontiers in Ecology and Evolution*, 10, 2022. ISSN 2296-701X. doi: 10.3389/fevo.2022.864728.

B. A. Olshausen and D. J. Field. Emergence of simple-cell receptive field properties by learning a sparse code for natural images. *Nature*, 381(6583):607–609, June 1996. ISSN 0028-0836. doi: 10.1038/381607a0.

V. Party, C. Hanot, I. Said, D. Rochat, and M. Renou. Plant terpenes affect intensity and temporal parameters of pheromone detection in a moth. *Chem. Senses*, 34(9): 763–774, Nov. 2009. ISSN 0379-864X, 1464-3553. doi: 10.1093/chemse/bjp060.

R. Quian Quiroga and S. Panzeri. Extracting information from neuronal populations: information theory and decoding approaches. *Nat. Rev. Neurosci.*, 10(3):173–185, Mar. 2009. ISSN 1471-003X, 1471-0048. doi: 10.1038/nrn2578.

M. Renou, V. Party, A. Rouyar, and S. Anton. Olfactory signal coding in an odor background. *Biosystems.*, 136:35–45, Oct. 2015. ISSN 0303-2647, 1872-8324. doi: 10.1016/j.biosystems.2015.06.001.

J. A. Riffell, H. Lei, L. Abrell, and J. G. Hildebrand. Neural basis of a pollinator's buffet: olfactory specialization and learning in manduca sexta. *Science*, 339(6116): 200–204, Jan. 2013. ISSN 0036-8075, 1095-9203. doi: 10.1126/science.1225483.

J. A. Riffell, E. Shlizerman, E. Sanders, L. Abrell, B. Medina, A. J. Hinterwirth, and J. N. Kutz. Sensory biology. flower discrimination by pollinators in a dynamic chemical environment. *Science*, 344(6191):1515–1518, June 2014. ISSN 0036-8075, 1095-9203. doi: 10.1126/science.1251041.

A. Rouyar, V. Party, J. Prešern, A. Blejec, and M. Renou. A general odorant background affects the coding of pheromone stimulus intermittency in specialist olfactory receptor neurones. *PLoS One*, 6(10):e26443, Oct. 2011. ISSN 1932-6203. doi: 10.1371/journal.pone.0026443.

A. Schilling, R. Gerum, C. Metzner, A. Maier, and P. Krauss. Intrinsic noise improves speech recognition in a computational model of the auditory pathway. *Front. Neurosci.*, 16:908330, June 2022. ISSN 1662-4548, 1662-453X. doi: 10.3389/fnins.2022.908330.

D. Schmidt-Büsser, M. von Arx, and P. M. Guerin. Host plant volatiles serve to increase the response of male european grape berry moths, eupoecilia ambiguella, to their sex pheromone. *J. Comp. Physiol. A Neuroethol. Sens. Neural Behav. Physiol.*, 195(9): 853–864, Sept. 2009. ISSN 0340-7594, 1432-1351. doi: 10.1007/s00359-009-0464-1.

B. Sengupta, A. A. Faisal, S. B. Laughlin, and J. E. Niven. The effect of cell size and channel density on neuronal information encoding and energy efficiency. *J. Cereb. Blood Flow Metab.*, 33(9):1465–1473, Sept. 2013. ISSN 0271-678X, 1559-7016. doi: 10.1038/jcbfm.2013.103.

C. E. Shannon. A mathematical theory of communication. *The Bell System Technical Journal*, 27(3):379–423, July 1948. ISSN 0005-8580. doi: 10.1002/j.1538-7305.1948.tb01338.x.

H. Shimazaki and S. Shinomoto. Kernel bandwidth optimization in spike rate estimation. *J. Comput. Neurosci.*, 29(1-2):171–182, Aug. 2010. ISSN 0929-5313, 1573-6873. doi: 10.1007/s10827-009-0180-4.

P. J. Simmons and R. R. d. R. van Steveninck. Sparse but specific temporal coding by spikes in an insect sensory-motor ocellar pathway. *J. Exp. Biol.*, 213(Pt 15): 2629–2639, Aug. 2010. ISSN 0022-0949, 1477-9145. doi: 10.1242/jeb.043547.

F. Sohil, M. U. Sohali, and J. Shabbir. An introduction to statistical learning with applications in R. *Statist. Decisions*, 6(1):87–87, Jan. 2022. ISSN 0721-2631, 2475-4269. doi: 10.1080/24754269.2021.1980261.

M. Stopfer. Olfactory processing: massive convergence onto sparse codes. *Curr. Biol.*, 17(10):R363–4, May 2007. ISSN 0960-9822. doi: 10.1016/j.cub.2007.03.019.

F. E. Theunissen. From synchrony to sparseness. *Trends Neurosci.*, 26(2):61–64, Feb. 2003. ISSN 0166-2236. doi: 10.1016/s0166-2236(02)00016-4.

N. Timme, W. Alford, B. Flecker, and J. M. Beggs. Synergy, redundancy, and multivariate information measures: an experimentalist's perspective. *J. Comput. Neurosci.*, 36(2):119–140, Apr. 2014. ISSN 0929-5313, 1573-6873. doi: 10.1007/s10827-013-0458-4.

R. Tomar. Review: Methods of firing rate estimation. *Biosystems.*, 183:103980, Sept. 2019. ISSN 0303-2647. doi: 10.1016/J.BIOSYSTEMS.2019.103980.

F. Trona, G. Anfora, A. Balkenius, M. Bengtsson, M. Tasin, A. Knight, N. Janz, P. Witzgall, and R. Ignell. Neural coding merges sex and habitat chemosensory signals in an insect herbivore. *Proc. Biol. Sci.*, 280(1760):20130267, June 2013. ISSN 0962-8452, 1471-2954. doi: 10.1098/rspb.2013.0267.

W. E. Vinje and J. L. Gallant. Sparse coding and decorrelation in primary visual cortex during natural vision. *Science*, 287(5456):1273–1276, Feb. 2000. ISSN 0036-8075, 1095-9203. doi: 10.1126/science.287.5456.1273.

M. Wibral, J. T. Lizier, and V. Priesemann. Bits from brains for biologically inspired computing. *Frontiers in Robotics and AI*, 2, 2015. ISSN 2296-9144. doi: 10.3389/frobt.2015.00005.

B. Willmore and D. J. Tolhurst. Characterizing the sparseness of neural codes. *Network*, 12(3):255–270, Aug. 2001. ISSN 0093-3341, 0954-898X.

Z. Yang, M. Bengtsson, and P. Witzgall. Host plant volatiles synergize response to sex pheromone in codling moth, cydia pomonella. *J. Chem. Ecol.*, 30(3):619–629, Mar. 2004. ISSN 0098-0331. doi: 10.1023/b:joec.0000018633.94002.af.

J. Yu and D. Ferster. Functional coupling from simple to complex cells in the visually driven cortical circuit. *J. Neurosci.*, 33(48):18855–18866, Nov. 2013. ISSN 0270-6474, 1529-2401. doi: 10.1523/JNEUROSCI.2665-13.2013.

L. Yu and Y. Yu. Energy-efficient neural information processing in individual neurons and neuronal networks. *J. Neurosci. Res.*, 95(11):2253–2266, Nov. 2017. ISSN 0360-4012, 1097-4547. doi: 10.1002/jnr.24131.

Q. Zhang, X. Hu, B. Hong, and B. Zhang. A hierarchical sparse coding model predicts acoustic feature encoding in both auditory midbrain and cortex. *PLoS Comput. Biol.*, 15(2):e1006766, Feb. 2019. ISSN 1553-734X, 1553-7358. doi: 10.1371/journal.pcbi.1006766.

Attachment V

Unpublished manuscript

Effects of spike frequency adaptation on neural response variability

Rimjhim Tomar[1, 2*] Tomas Barta[3**], Lubomir Kostal[1***]

1 Institute of Physiology of the Czech Academy of Sciences, Prague, Czech Republic
2 Charles University, Second Medical Faculty, Prague, Czech Republic
3 Okinawa Institute of Science and Technology, Okinawa, Japan

* rimjhim.tomar@fgu.cas.cz ** tomas.barta@oist.jp *** kostal@biomed.cas.cz

Abstract

Neural variability quenching is a decrease in the trial-to-trial variability of neural activity evoked by a stimulus. This phenomenon has been observed across different levels of neural activity in the brain including the membrane potential of individual cells (Monier et al., 2003) and firing activity (Churchland et al., 2010). Monier et al. (2003) suggested that the decrease of membrane potential variability is due to an increase in inhibitory activity associated with the stimulus onset. However, the origins of the decrease of firing activity variability (measured by Fano factor) as well as its utility are still unclear. Cortical models consisting of balanced excitatory and inhibitory neuron subpopulations with recurrent architecture reproduce the stimulus induced trial-to-trial variability quenching observed in cortical neurons (Litwin-Kumar and Doiron, 2012).

We explore the effect of spike frequency adaptation (SFA) on the trial-to-trial variability quenching evoked by stimulus onset. We use a cortical model with excitatory and inhibitory subpopulations, where the feedforward input is purely excitatory and the inhibitory input is determined by the network properties. We employ exponential integrate-and-fire neurons with SFA (Zerlaut et al., 2018). Each neuron responded to a stimulus with a different intensity, mitigating the effect of preferred and non-preferred stimuli. When the SFA was implemented by after-hyperpolarization current, the Fano factor increased after the stimulus onset, while in networks with SFA implemented by voltage-gated sodium channel inactivation (dynamic firing threshold), the Fano factor decreased, even for neurons whose firing rate did not change upon stimulus onset. Next, we analyze to which extent the differences between the SFA mechanisms affect information transmission properties.

Our work provides a potential mechanism that can lead to neural variability quenching and analyzes its possible utility by evaluating information transmission capabilities.

1 Introduction

Neural variability refers to the fluctuations in neural responses observed across time and trials (Faisal et al., 2008; Shadlen and Newsome, 1998; Tomko and Crapper, 1974). It is a fundamental characteristic of cortical neural activity, influenced by both intrinsic neural noise (Carandini, 2004; Moreno-Bote et al., 2014) and the dynamic nature of neural circuits (van Vreeswijk and Sompolinsky, 1996; Vogels and Abbott, 2005). Studies have shown that the trial-to-trial variability of neural response to identical

stimuli is significantly quenched at the onset of the stimulus. Monier et al. (2003) explored the variability of membrane potentials in cat visual cortex neurons and observed a quenching effect. Their study demonstrated that membrane potential variability also decreases upon visual stimulus presentation, suggesting that the reduction in variability extends to subthreshold membrane potential dynamics. Churchland et al. (2010) investigated firing rate variability in macaque monkeys and found that the variability of neural responses decreases at the onset of a stimulus. This reduction in variability was shown to be a general feature across different cortical areas and sensory modalities, indicating its fundamental role in sensory processing. Goris et al. (2014) further showed that variability quenching is associated with a reduction in noise correlations between neurons, highlighting its role in enhancing the signal-to-noise ratio during sensory processing.. This phenomenon is observed in the membrane potential recordings (Finn et al., 2007; Orbán et al., 2016), in spiking activity (Chang et al., 2012; Churchland et al., 2006), in human electroencephalography (EEG)/electrocorticography (ECOG) (Arazi et al., 2017, 2019; He and Zempel, 2013; Schurger et al., 2015), and in functional magnetic resonance imaging (fMRI) recordings (Ferri et al., 2015; He, 2013; Huang et al., 2017).

Cortical neurons are known to exhibit significant variability in their spike emission patterns (Azouz and Gray, 2000; Shadlen and Newsome, 1998), as well as firing rate fluctuations over long timescales (Kohn and Smith, 2005), both of which contribute to trial-to-trial variability (Arieli et al., 1996; Churchland et al., 2006; Luczak et al., 2009; Tsodyks et al., 1999). Cortical models with balanced excitatory and inhibitory populations capture high spike time variability and asynchronous firing due to balanced inputs. Still, these models fail to fully capture long-timescale fluctuations and the complete spectrum of trial-to-trial variability observed in cortical neuron (Brunel, 2000; Renart et al., 2010; van Vreeswijk and Sompolinsky, 1998). In contrast, models with recurrent architecture and clustered connections accurately capture both fast spiking variability and slow firing rate fluctuations, producing richer dynamics and higher trial-to-trial variability, closely aligning with experimental observations of cortical activity (Deco and Hugues, 2012; Litwin-Kumar and Doiron, 2012).

Doiron and Litwin-Kumar (2014) concluded that to reproduce the quenching of trial-to-trial variability upon stimulus onset, it is necessary for the feedforward inputs to be coherent with the recurrent network architecture. Experimental data (noa) indicate that a significant portion of excitatory neurons display spike frequency adaptation (SFA), which is a phenomenon in which a neuron's firing rate decreases over time in response to a sustained or constant input. SFA mechanisms have already been utilized to create more realistic neural network models, as they account for activity-dependent changes in neuronal firing rates and enhance the biological plausibility of these models (Ganguly et al., 2024; Salaj et al., 2021). The biophysical mechanisms of SFA involve the inactivation of depolarizing currents and the activation of hyperpolarizing currents (Benda and Herz, 2003). In our article, we present a cortical model with recurrent architecture with excitatory feedforward input and examine the effect of different SFA mechanisms on neural variability after the onset of stimulus. We compare two different SFA mechanisms: adaptation through after-hyperpolarizing currents and adaptation through the inactivation of sodium channels. We demonstrate that although SFA mechanisms similarly influence neural activity, their impact on trial-to-trial variability differs.

2 Methods

2.1 Spike frequency adaptation

Spike frequency adaptation (SFA) is a phenomenon observed in many neurons where the firing rate decreases progressively during sustained input to the neuron, and it plays a crucial role in stabilizing neuronal network dynamics (Barranca et al., 2019). The mechanisms behind SFA can be either spike-dependent or voltage-dependent and can be categorized into two types:

1. Inactivation of depolarizing currents,
2. Activation of hyperpolarizing currents.

In this article, we explore both mechanisms of adaptation. The inactivation of depolarizing currents is modeled through the inactivation of voltage-gated sodium channels. For the adaptation via activation of hyperpolarizing currents, we incorporate after-hyperpolarizing (AHP) currents.

To capture these adaptation mechanisms in our model, we use the adaptive exponential integrate-and-fire (AdEx) model, which we modify to include the adaptation mechanisms.

2.2 Single neuron dynamics

To model the single neuron dynamics, we used the AdEx model (Brette and Gerstner, 2005), which we modified to incorporate dynamic threshold by adding slow gating variable s to the term with the exponential function:

$$C_m \frac{\mathrm{d}V^i}{\mathrm{d}t} = g_L(E_L - V^i) + I^i_{\mathrm{syn}}(V^i, t) + (1 - s^i)k_a e^{\frac{V^i - V_{\mathrm{thr}}}{k_a}} - I^i_w + I^i_{\mathrm{bcg}} + I^i_{\mathrm{stim}}, \quad (1)$$

$$\tau_w \frac{\mathrm{d}I^i_w}{\mathrm{d}t} = -I^i_w + a \cdot (V^i - E_L) + \sum_{t_s \in \{t_{\mathrm{spike}}\}^i} b\delta(t - t_s), \quad (2)$$

$$\tau_s \frac{\mathrm{d}s^i}{\mathrm{d}t} = -s^i + \sum_{t_s \in \{t_{\mathrm{spike}}\}^i} c(1 - s^i)\delta(t - t_s), \quad (3)$$

with an action potential recorded when membrance potential of the ith neuron V^i crosses the threshold 0 mV and reset at the leak reversal potential E_L. $\{t_{\mathrm{spike}}\}^i$ is the set of all action potentials fired by the i-th neuron. C_m is the membrane capacitance, g_L represents the leak conductance. I^i_{syn} represents the synaptic current for the ith neuron, k_a is the scaling factor for the exponential term. I_w is the adaptation current, which is parametrized by a in the case of voltage-dependent adaptation and b in the case of spike-dependent adaptation. I^i_{bcg} and I^i_{stim} represent the background and stimulus current respectively. τ_w is the time constant for the adaptation current, τ_s is the time constant for the slow gating variable s^i, and c is the scaling factor for s^i.

The exponential term represents the conductance of the voltage-gated Na^+ channels and the gating variable s represents the ratio of inactivated Na^+ channels. We used the model parameters as in (Zenke and Ganguli, 2018), with the exception of the adaptation parameters, in order to compare different adaptation mechanisms. The parameters are provided in the Table 1.

As in (Zerlaut et al., 2018), adaptation was only applied to excitatory neurons. In the case of dynamic threshold adaptation $b = 0$ and $c = 0.15$, meaning that 15% of all open channels become blocked with every fired action potential. In the case of after-hyperpolarization currents (AHP), we set $c = 0$ and $b = 20\,\mathrm{pA}$.

Table 1. Parameters of the LIF model

Membrane capacitance	C_m	150 pF
Leak conductance	g_L	10 nS
Resting potential	E_L	−80 mV
	V_{thr}	−50 mV
	k_a	2 mV for exc.
		0.5 mV for inh.
Exc. reversal potential	E_{e}	0 mV
Inh. reversal potential	E_{i}	−80 mV
Exc. synapse decay	τ_{exc}	5 ms
Inh. synapse decay	τ_{inh}	5 ms
Exc. synapse strength	w^0_{exc}	1 nS
Inh. synapse strength	w^0_{inh}	5 nS

2.3 Network properties

The network consists of 10000 neurons, out of which 7500 are excitatory and 2500 are inhibitory. We consider two different variants of the connection matrix. In the first case, regardless of the neuron type, the connection probability is 5% (Zerlaut et al., 2018). In the second case, we consider more realistic, proximity-based probabilities of synaptic connections between neurons. Neurons in the visual cortex often have a preferred orientation, which is the specific angle of a visual stimulus to which a neuron responds most strongly. Studies have shown that the synaptic connections among cortical neurons are not random but exhibit functional specificity, with functionally similar neurons forming synaptically coupled subnetworks (Ko et al., 2011). This concept is used to model the probability of synaptic connections between neurons based on their preferred orientations.

If α_i and α_j are the preferred orientation of neurons i and j respectively, then the similarity factor is calculated using the absolute difference between the preferred orientations (Dalva et al., 1997),

$$d_{ij} = |\alpha_i - \alpha_j|, \tag{4}$$

Stepanyants et al. (2008) showed that the probability of potential connectivity and the expected number of potential synapses can be modeled based on the spatial separation and geometric properties of neurons. Following that, the probability of a synaptic connection is modeled using a Gaussian distribution:

$$p_{ij} = e^{-\frac{d_{ij}^2}{2\sigma^2}}, \tag{5}$$

where σ represents the standard deviation, or spread, of the Gaussian distribution. This approach ensures that neurons with similar preferred orientations are more likely to connect, reflecting realistic patterns observed in cortical networks where functionally similar neurons are more densely interconnected (Harris et al., 2015; Ko et al., 2011).

The synaptic current I^i_{syn} is the current from conductance-based recurrent synapses:

$$I^i_{\text{syn}} = -g^i_{\text{exc}}(V^i - E_{\text{exc}}) - g^i_{\text{inh}}(V^i - E_{\text{inh}}), \tag{6}$$

$$\frac{\mathrm{d}g^i_{\text{exc}}}{\mathrm{d}t} = -\frac{g^i_{\text{exc}}}{\tau_{\text{exc}}} + \sum_{j=1}^{N} \sum_{t_s \in \{t_{\text{spike}}\}^j} w^{ji}_{\text{exc}} \delta(t - t_s), \tag{7}$$

$$\frac{\mathrm{d}g^i_{\text{inh}}}{\mathrm{d}t} = -\frac{g^i_{\text{inh}}}{\tau_{\text{inh}}} + \sum_{j=1}^{N} \sum_{t_s \in \{t_{\text{spike}}\}^j} w^{ji}_{\text{inh}} \delta(t - t_s), \tag{8}$$

where g^i_{exc} and g^i_{inh} are the excitatory and inhibitory conductances for the ith neurons and E_{exc} and E_{inh} are the reversal potentials for the excitatory and inhibitory synapses respectively. $\tau_{\text{exc}} = \tau_{\text{inh}} = 5\,\text{ms}$ are synaptic decay time constants, w^{ji}_{exc} and w^{ji}_{inh} the synaptic weights. $w^{ji}_{\text{exc}} = 0$ if the j-th neuron is inhibitory, $w^{ji}_{\text{inh}} = 0$ if the j-th neuron is excitatory and otherwise for any connection the probability of the weight being non-zero is 5% in the case of the fixed connectivity matrix and then $w^{ji}_{\text{exc}} = w^0_{\text{exc}} = 1\,\text{nS}$ and $w^{ji}_{\text{inh}} = w^0_{\text{inh}} = 5\,\text{nS}$.

2.4 External input

The external excitatory input is modeled as an Ornstein-Uhlenbeck process (Destexhe et al., 2001; Uhlenbeck and Ornstein, 1930):

$$I^i_{\text{ext}} = -g^i_{\text{ext}}(V^i - E_{\text{ext}}) \tag{9}$$

$$\frac{\mathrm{d}g^i_{\text{ext}}}{\mathrm{d}t} = -\frac{g^i_{\text{ext}} - \mu^i_{\text{ext}}(t)}{\tau_{\text{exc}}} + \sqrt{2\tau_{\text{exc}}}\sigma^i_{\text{ext}}(t)\eta^i(t), \tag{10}$$

where $\eta^i(t)$ is white noise, μ^i_{ext} and σ^i_{ext} are set so that the stationary mean and standard deviation of g^i_{ext} match those of a Poisson shot noise with an exponential kernel with a time constant τ_{exc}, amplitude w^0_{exc} and intensity λ^i_{ext}:

$$\mu^i_{\text{ext}}(t) = w^0_{\text{exc}}\lambda^i_{\text{ext}}(t)\tau_{\text{exc}}, \tag{11}$$

$$\sigma^i_{\text{ext}}(t) = \sqrt{\frac{\tau_{\text{exc}}\lambda^i_{\text{ext}}(t)}{2}}w^0_{\text{exc}}. \tag{12}$$

During the 12 s simulation, we modelled λ^i_{ext} as

$$\lambda^i_{\text{ext}} = \begin{cases} \lambda_{\text{bcg}} & \text{for } t < 6\,\text{s}, \\ \lambda_{\text{bcg}} + \lambda_{\text{stim}}\sin(\alpha_i - \alpha_{\text{stim}}) & \text{for } t \geq 6\,\text{s}, \end{cases} \tag{13}$$

where α_i is the preferred orientation of the i-th neuron and α_{stim} is the stimulus orientation, $\lambda_{\text{bcg}} = 1\,\text{kHz}$ and $\lambda_{\text{stim}} = 6\,\text{kHz}$.

We assume that neurons $1, \ldots, N_{\text{exc}}$, where $N_{\text{exc}} = 7500$ are excitatory and neurons $N_{\text{exc}}, \ldots, N$, where $N = 10000$ are inhibitory. We then set the preferred orientations as

$$\alpha_i = \begin{cases} \frac{\pi}{2}\frac{i}{N_{\text{exc}}} & \text{for } i \leq N_{\text{exc}}, \\ \frac{\pi}{2}\frac{i - N_{\text{exc}}}{N - N_{\text{exc}}} & \text{for } i > N_{\text{exc}}. \end{cases} \tag{14}$$

2.5 Variability quantification

To compare the trial-to-trial variability of two neurons with the same mean spike count, $\mathrm{E}[N(w)]$, where $N(w)$ is the number of spikes in the time window $(0, w)$, we can use the variance of the observed spikes, $\mathrm{Var}[N(w)]$. A relative dispersion measure, known as the Fano Factor, quantifies this trial-to-trial variability by scaling the variance with the mean spike count:

$$\mathrm{FF} = \frac{\mathrm{Var}[N(w)]}{\mathrm{E}[N(w)]}. \tag{15}$$

A Fano Factor of one indicates that the spike counts follow a Poisson distribution, where the variance equals the mean, which is typical of random processes. Additionally, trial-to-trial variability can be estimated using the coefficient of variation of the interspike intervals (ISIs), $C_V(T) = \sigma(T)/\mathbb{E}(T)$ or a steady-state spike train where ISIs are described by a continuous random variable T. In this context,

$$FF_0 = C_V^2 \tag{16}$$

where FF_0 is the Fano factor calculated from infinite length time window ($w \to +\infty$) and $\sigma(T)$ is the standard deviation of the ISIs.

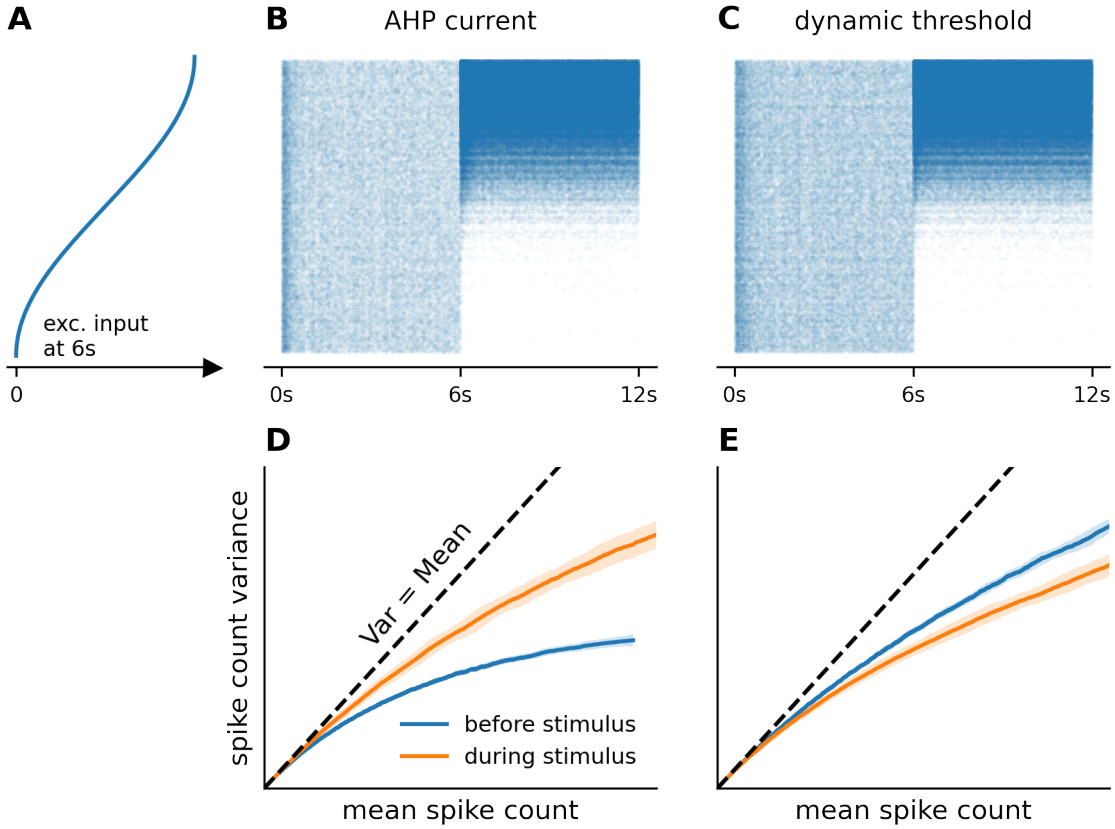

Fig 1. Trial-to-trial variability after stimulus onset depends on spike frequency adaptation mechanism: fixed connection probability A: The curve illustrates the strength of the external input on top of the background input that each neuron starts receiving after 6 s. Each neuron receives a different input due to a different preferred stimulus. **B-C:** Raster plots of the 8000 excitatory neurons from one trial of the simulation with AHP (**B**) and dynamic threshold (**C**). **D-E:** With each spike frequency adaptation (SFA) mechanism we ran the simulation 3600 times. For each neuron, we calculated the mean number of spikes and their variance before the stimulus onset (in the interval between 1 s and 5 s after the simulation start) and after the stimulus onset (interval between 7 s and 12 s after the simulation start). With the AHP SFA, the trial-to-trial variability of the neurons increased after the stimulus onset, while with the dynamic threshold SFA the trial-to-trial variability decreased after the stimulus onset.

3 Results and discussion

We ran the simulation 3600 times for each SFA mechanism - AHP and dynamic threshold. Raster plots from a sample simulation are shown in Fig. 1A-C. In the case of a fixed connectivity matrix, the neurons show transient activity at the beginning of the simulation and after the stimulus onset. After the stimulus onset, the activity of neurons receiving strong input increases, while the activity of neurons receiving only weak external input is attenuated. For some neurons, the steady state activity remains

approximately the same as before the stimulus onset. We calculated the spiking

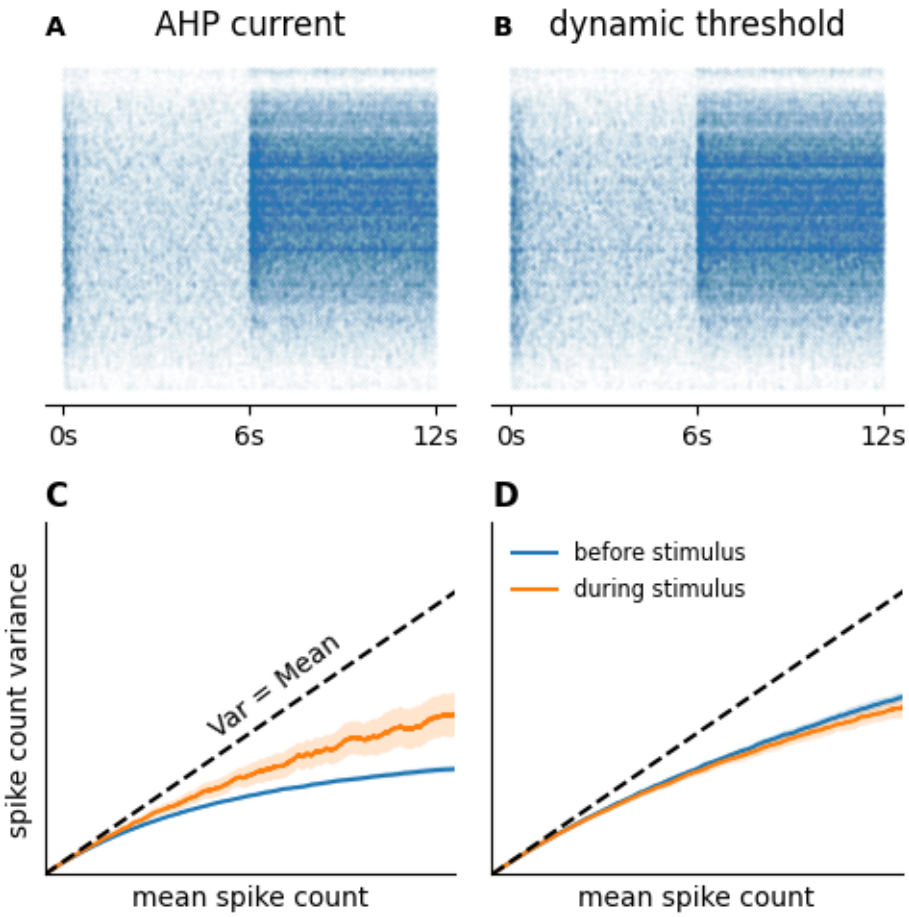

Fig 2. Trial-to-trial variability after stimulus onset depends on spike frequency adaptation mechanism (proximity based connection probability) A-B: Raster plots of the 8000 excitatory neurons from one trial of the simulation with connection probability based on proximity, with AHP (**A**) and dynamic threshold (**B**) spike frequency adaptation (SFA). **C-D:** The simulation was run 3600 times to calculate and the graph illustrates the mean number of spikes and their variance before and after the stimulus onset for each neuron. Like in the case of constant connection probability, the trial-to-trial variability of the neurons increased after the stimulus onset in the case of AHP SFA whereas the trial-to-trial variability decreased after the stimulus onset in the case of dynamic threshold SFA.

statistics—the mean number of spikes and the variance of the number of spikes before and after the stimulus onset. We left out the transient periods 1 s after the simulation start and 1 s after the stimulus onset. We plotted the spike count variance against the mean spike count (Fig. 1D-E). In each situation (AHP / dynamic threshold + before/after stimulus onset) the mean count - count variance formed a continuous curve with very little variance and the trial-to-trial variability of a neuron is essentially determined by its firing rate. Comparing this curve before and after stimulus onset shows us whether trial-to-trial variability increased or decreased after the stimulus onset. For AHP SFA, the trial-to-trial variability increased after the stimulus onset, while with dynamic threshold the trial-to-trial variability decreased after the stimulus onset.

In the second case where synaptic connections are probability-based, influenced by the similarity in preferred stimuli between neurons, the raster plots (Fig. 2A-B) show a pronounced increase in activity within certain clusters of neurons immediately following the stimulus onset at 6s. These clusters are likely composed of neurons with similar preferred orientations, which are interconnected with a higher probability. This structural connectivity results in localized areas of intense activity, as these neurons are more likely to receive and propagate excitatory inputs amongst each other. Neurons at the beginning and the end of the network exhibit less pronounced changes in activity in response to the stimulus onset. This phenomenon can be attributed to the edge effects within the network's structural framework. Given the connectivity matrix is based on proximity-based probabilities where synaptic connections are more likely between neurons with similar stimulus preferences, neurons at the extremes edges of the network (beginning and end) might be less active due to fewer connections with other active neurons in the network.

The spiking statistics (Fig. 2C-D) shows an increase in the trial-to-trial variability after the stimulus onset in the case of AHP SFA, whereas dynamic threshold quenches the trial-to-trial variability after the stimulus onset.

4 Conclusion

Cortical neurons exhibit a high degree of variability in neural responses in spontaneous and evoked states (Churchland et al., 2006; Litwin-Kumar and Doiron, 2012). This variability decreases when a stimulus is presented. To understand how neural populations encode information, it is important to study the mechanisms underlying stimulus-induced trial-to-trial variability (Averbeck et al., 2006; Josić et al., 2009; Ponce-Alvarez et al., 2013). In this study, we explored the potential underlying mechanisms of these phenomena within a realistic neural network. Doiron and Litwin-Kumar (2014) concluded that feedforward input that's coherent with the recurrent network architecture is necessary to produce the trial-to-trial variability quenching. We showed that variability quenching further depends on the SFA mechanisms employed by the network. Adaptation by inactivation of sodium channels leads to a reduced trial-to-trial variability whereas adaptation by after-hyperpolarizing currents yields an increased trial-to-trial response variability. The reduction in trial-by-trial variability under the dynamic threshold adaptation regime confirms previous results obtained across different brain areas (Arazi et al., 2017; Broday-Dvir et al., 2018; Churchland et al., 2010; Goris et al., 2014; He, 2013), which were reproduced by several spiking neuron models (Doiron and Litwin-Kumar, 2014; Litwin-Kumar and Doiron, 2012). Our study reveals that the specific SFA mechanism employed can significantly influence trial-to-trial variability upon stimulus onset, leading to either an increase or decrease in variability. This finding emphasizes the critical role of SFA mechanisms in shaping neural response dynamics and underscores their importance in accurately modeling and understanding neural variability in cortical networks.

References

Cell features :: Allen brain atlas: Cell types. https://celltypes.brain-map.org/data. Accessed: 2024-5-15.

A. Arazi, N. Censor, and I. Dinstein. Neural variability quenching predicts individual perceptual abilities. *J. Neurosci.*, 37(1):97–109, Jan. 2017. ISSN 0270-6474, 1529-2401. doi: 10.1523/JNEUROSCI.1671-16.2016.

A. Arazi, Y. Yeshurun, and I. Dinstein. Neural variability is quenched by attention. *J. Neurosci.*, 39(30):5975–5985, July 2019. ISSN 0270-6474, 1529-2401. doi: 10.1523/JNEUROSCI.0355-19.2019.

A. Arieli, A. Sterkin, A. Grinvald, and A. Aertsen. Dynamics of ongoing activity: explanation of the large variability in evoked cortical responses. *Science*, 273(5283): 1868–1871, Sept. 1996. ISSN 0036-8075. doi: 10.1126/science.273.5283.1868.

B. B. Averbeck, P. E. Latham, and A. Pouget. Neural correlations, population coding and computation. *Nat. Rev. Neurosci.*, 7(5):358–366, May 2006. ISSN 1471-003X. doi: 10.1038/nrn1888.

R. Azouz and C. M. Gray. Dynamic spike threshold reveals a mechanism for synaptic coincidence detection in cortical neurons *in vivo*. *Proc. Natl. Acad. Sci. U. S. A.*, 97 (14):8110–8115, July 2000. ISSN 0027-8424. doi: 10.1073/pnas.130200797.

V. J. Barranca, H. Huang, and S. Li. The impact of spike-frequency adaptation on balanced network dynamics. *Cogn. Neurodyn.*, 13(1):105–120, Feb. 2019. ISSN 1871-4080. doi: 10.1007/s11571-018-9504-2.

J. Benda and A. V. M. Herz. A universal model for spike-frequency adaptation. *Neural Comput.*, 15(11):2523–2564, Nov. 2003. ISSN 0899-7667. doi: 10.1162/089976603322385063.

R. Brette and W. Gerstner. Adaptive exponential integrate-and-fire model as an effective description of neuronal activity. *J. Neurophysiol.*, 94(5):3637–3642, Nov. 2005. ISSN 0022-3077. doi: 10.1152/jn.00686.2005.

R. Broday-Dvir, S. Grossman, E. Furman-Haran, and R. Malach. Quenching of spontaneous fluctuations by attention in human visual cortex. *Neuroimage*, 171:84–98, May 2018. ISSN 1053-8119, 1095-9572. doi: 10.1016/j.neuroimage.2017.12.089.

N. Brunel. Dynamics of sparsely connected networks of excitatory and inhibitory spiking neurons. *J. Comput. Neurosci.*, 8(3):183–208, May 2000. ISSN 0929-5313, 1573-6873. doi: 10.1023/A:1008925309027.

M. Carandini. Amplification of trial-to-trial response variability by neurons in visual cortex. *PLoS Biol.*, 2(9):E264, Sept. 2004. ISSN 1544-9173, 1545-7885. doi: 10.1371/journal.pbio.0020264.

M. H. Chang, K. M. Armstrong, and T. Moore. Dissociation of response variability from firing rate effects in frontal eye field neurons during visual stimulation, working memory, and attention. *J. Neurosci.*, 32(6):2204–2216, Feb. 2012. ISSN 0270-6474, 1529-2401. doi: 10.1523/JNEUROSCI.2967-11.2012.

M. M. Churchland, B. M. Yu, S. I. Ryu, G. Santhanam, and K. V. Shenoy. Neural variability in premotor cortex provides a signature of motor preparation. *J. Neurosci.*, 26(14):3697–3712, Apr. 2006. ISSN 0270-6474, 1529-2401. doi: 10.1523/JNEUROSCI.3762-05.2006.

M. M. Churchland, B. M. Yu, J. P. Cunningham, L. P. Sugrue, M. R. Cohen, G. S. Corrado, W. T. Newsome, A. M. Clark, P. Hosseini, B. B. Scott, D. C. Bradley, M. A. Smith, A. Kohn, J. A. Movshon, K. M. Armstrong, T. Moore, S. W. Chang, L. H. Snyder, S. G. Lisberger, N. J. Priebe, I. M. Finn, D. Ferster, S. I. Ryu, G. Santhanam, M. Sahani, and K. V. Shenoy. Stimulus onset quenches neural variability: a widespread cortical phenomenon. *Nat. Neurosci.*, 13(3):369–378, Mar. 2010. ISSN 1097-6256, 1546-1726. doi: 10.1038/nn.2501.

M. B. Dalva, M. Weliky, and L. C. Katz. Relationships between local synaptic connections and orientation domains in primary visual cortex. *Neuron*, 19(4):871–880, Oct. 1997. ISSN 0896-6273. doi: 10.1016/s0896-6273(00)80968-x.

G. Deco and E. Hugues. Neural network mechanisms underlying stimulus driven variability reduction. *PLoS Comput. Biol.*, 8(3):e1002395, Mar. 2012. ISSN 1553-734X, 1553-7358. doi: 10.1371/journal.pcbi.1002395.

A. Destexhe, M. Rudolph, J. M. Fellous, and T. J. Sejnowski. Fluctuating synaptic conductances recreate in vivo-like activity in neocortical neurons. *Neuroscience*, 107 (1):13–24, 2001. ISSN 0306-4522. doi: 10.1016/s0306-4522(01)00344-x.

B. Doiron and A. Litwin-Kumar. Balanced neural architecture and the idling brain. *Front. Comput. Neurosci.*, 8:56, May 2014. ISSN 1662-5188. doi: 10.3389/fncom.2014.00056.

A. A. Faisal, L. P. J. Selen, and D. M. Wolpert. Noise in the nervous system. *Nat. Rev. Neurosci.*, 9(4):292–303, Apr. 2008. ISSN 1471-003X. doi: 10.1038/nrn2258.

F. Ferri, M. Costantini, Z. Huang, M. G. Perrucci, A. Ferretti, G. L. Romani, and G. Northoff. Intertrial variability in the premotor cortex accounts for individual differences in peripersonal space. *J. Neurosci.*, 35(50):16328–16339, Dec. 2015. ISSN 0270-6474, 1529-2401. doi: 10.1523/JNEUROSCI.1696-15.2015.

I. M. Finn, N. J. Priebe, and D. Ferster. The emergence of contrast-invariant orientation tuning in simple cells of cat visual cortex. *Neuron*, 54(1):137–152, Apr. 2007. ISSN 0896-6273. doi: 10.1016/j.neuron.2007.02.029.

C. Ganguly, S. S. Bezugam, E. Abs, M. Payvand, S. Dey, and M. Suri. Spike frequency adaptation: bridging neural models and neuromorphic applications. *Communications Engineering*, 3(1):1–13, Feb. 2024. ISSN 2731-3395, 2731-3395. doi: 10.1038/s44172-024-00165-9.

R. L. T. Goris, J. A. Movshon, and E. P. Simoncelli. Partitioning neuronal variability. *Nat. Neurosci.*, 17(6):858–865, June 2014. ISSN 1097-6256, 1546-1726. doi: 10.1038/nn.3711.

J. J. Harris, R. Jolivet, E. Engl, and D. Attwell. Energy-Efficient information transfer by visual pathway synapses. *Curr. Biol.*, 25(24):3151–3160, Dec. 2015. ISSN 0960-9822, 1879-0445. doi: 10.1016/j.cub.2015.10.063.

B. J. He. Spontaneous and task-evoked brain activity negatively interact. *J. Neurosci.*, 33(11):4672–4682, Mar. 2013. ISSN 0270-6474, 1529-2401. doi: 10.1523/JNEUROSCI.2922-12.2013.

B. J. He and J. M. Zempel. Average is optimal: an inverted-u relationship between trial-to-trial brain activity and behavioral performance. *PLoS Comput. Biol.*, 9(11): e1003348, Nov. 2013. ISSN 1553-734X, 1553-7358. doi: 10.1371/journal.pcbi.1003348.

Z. Huang, J. Zhang, A. Longtin, G. Dumont, N. W. Duncan, J. Pokorny, P. Qin, R. Dai, F. Ferri, X. Weng, and G. Northoff. Is there a nonadditive interaction between spontaneous and evoked activity? Phase-Dependence and its relation to the temporal structure of Scale-Free brain activity. *Cereb. Cortex*, 27(2):1037–1059, Feb. 2017. ISSN 1047-3211, 1460-2199. doi: 10.1093/cercor/bhv288.

K. Josić, E. Shea-Brown, B. Doiron, and J. de la Rocha. Stimulus-dependent correlations and population codes. *Neural Comput.*, 21(10):2774–2804, Oct. 2009. ISSN 0899-7667. doi: 10.1162/neco.2009.10-08-879.

H. Ko, S. B. Hofer, B. Pichler, K. A. Buchanan, P. J. Sjöström, and T. D. Mrsic-Flogel. Functional specificity of local synaptic connections in neocortical networks. *Nature*, 473(7345):87–91, May 2011. ISSN 0028-0836, 1476-4687. doi: 10.1038/nature09880.

A. Kohn and M. A. Smith. Stimulus dependence of neuronal correlation in primary visual cortex of the macaque. *J. Neurosci.*, 25(14):3661–3673, Apr. 2005. ISSN 0270-6474, 1529-2401. doi: 10.1523/JNEUROSCI.5106-04.2005.

A. Litwin-Kumar and B. Doiron. Slow dynamics and high variability in balanced cortical networks with clustered connections. *Nat. Neurosci.*, 15(11):1498–1505, Sept. 2012. ISSN 1097-6256. doi: 10.1038/nn.3220.

A. Luczak, P. Barthó, and K. D. Harris. Spontaneous events outline the realm of possible sensory responses in neocortical populations. *Neuron*, 62(3):413–425, May 2009. ISSN 0896-6273. doi: 10.1016/j.neuron.2009.03.014.

C. Monier, F. Chavane, P. Baudot, L. J. Graham, and Y. Frégnac. Orientation and direction selectivity of synaptic inputs in visual cortical neurons: a diversity of combinations produces spike tuning. *Neuron*, 37(4):663–680, Feb. 2003. ISSN 0896-6273. doi: 10.1016/s0896-6273(03)00064-3.

R. Moreno-Bote, J. Beck, I. Kanitscheider, X. Pitkow, P. Latham, and A. Pouget. Information-limiting correlations. *Nat. Neurosci.*, 17(10):1410–1417, Oct. 2014. ISSN 1097-6256, 1546-1726. doi: 10.1038/nn.3807.

G. Orbán, P. Berkes, J. Fiser, and M. Lengyel. Neural variability and Sampling-Based probabilistic representations in the visual cortex. *Neuron*, 92(2):530–543, Oct. 2016. ISSN 0896-6273, 1097-4199. doi: 10.1016/j.neuron.2016.09.038.

A. Ponce-Alvarez, A. Thiele, T. D. Albright, G. R. Stoner, and G. Deco. Stimulus-dependent variability and noise correlations in cortical MT neurons. *Proc. Natl. Acad. Sci. U. S. A.*, 110(32):13162–13167, Aug. 2013. ISSN 0027-8424, 1091-6490. doi: 10.1073/pnas.1300098110.

A. Renart, J. de la Rocha, P. Bartho, L. Hollender, N. Parga, A. Reyes, and K. D. Harris. The asynchronous state in cortical circuits. *Science*, 327(5965):587–590, Jan. 2010. ISSN 0036-8075, 1095-9203. doi: 10.1126/science.1179850.

D. Salaj, A. Subramoney, C. Kraisnikovic, G. Bellec, R. Legenstein, and W. Maass. Spike frequency adaptation supports network computations on temporally dispersed information. *Elife*, 10, July 2021. ISSN 2050-084X. doi: 10.7554/eLife.65459.

A. Schurger, I. Sarigiannidis, L. Naccache, J. D. Sitt, and S. Dehaene. Cortical activity is more stable when sensory stimuli are consciously perceived. *Proceedings of the National Academy of Sciences*, 112(16):E2083–E2092, 2015. doi: 10.1073/pnas.1418730112.

M. N. Shadlen and W. T. Newsome. The variable discharge of cortical neurons: implications for connectivity, computation, and information coding. *J. Neurosci.*, 18 (10):3870–3896, May 1998. ISSN 0270-6474. doi: 10.1523/JNEUROSCI.18-10-03870.1998.

A. Stepanyants, J. A. Hirsch, L. M. Martinez, Z. F. Kisvárday, A. S. Ferecskó, and D. B. Chklovskii. Local potential connectivity in cat primary visual cortex. *Cereb. Cortex*, 18(1):13–28, Jan. 2008. ISSN 1047-3211, 1460-2199. doi: 10.1093/cercor/bhm027.

G. J. Tomko and D. R. Crapper. Neuronal variability: non-stationary responses to identical visual stimuli. *Brain Res.*, 79(3):405–418, Oct. 1974. ISSN 0006-8993. doi: 10.1016/0006-8993(74)90438-7.

M. Tsodyks, T. Kenet, A. Grinvald, and A. Arieli. Linking spontaneous activity of single cortical neurons and the underlying functional architecture. *Science*, 286(5446): 1943–1946, Dec. 1999. ISSN 0036-8075. doi: 10.1126/science.286.5446.1943.

G. E. Uhlenbeck and L. S. Ornstein. On the theory of the brownian motion. *Phys. Rev.*, 36(5):823–841, Sept. 1930. ISSN 0959-8472. doi: 10.1103/PhysRev.36.823.

C. van Vreeswijk and H. Sompolinsky. Chaos in neuronal networks with balanced excitatory and inhibitory activity. *Science*, 274(5293):1724–1726, Dec. 1996. ISSN 0036-8075. doi: 10.1126/science.274.5293.1724.

C. van Vreeswijk and H. Sompolinsky. Chaotic balanced state in a model of cortical circuits. *Neural Comput.*, 10(6):1321–1371, Aug. 1998. ISSN 0899-7667. doi: 10.1162/089976698300017214.

T. P. Vogels and L. F. Abbott. Signal propagation and logic gating in networks of integrate-and-fire neurons. *J. Neurosci.*, 25(46):10786–10795, Nov. 2005. ISSN 0270-6474, 1529-2401. doi: 10.1523/JNEUROSCI.3508-05.2005.

F. Zenke and S. Ganguli. SuperSpike: Supervised learning in multilayer spiking neural networks. *Neural Comput.*, 30(6):1514–1541, June 2018. ISSN 0899-7667, 1530-888X. doi: 10.1162/neco_a_01086.

Y. Zerlaut, S. Chemla, F. Chavane, and A. Destexhe. Modeling mesoscopic cortical dynamics using a mean-field model of conductance-based networks of adaptive exponential integrate-and-fire neurons. *J. Comput. Neurosci.*, 44(1):45–61, Feb. 2018. ISSN 0929-5313, 1573-6873. doi: 10.1007/s10827-017-0668-2.